UNIVERSITY OF ICELAND

Ph.D. Dissertation

in Civil Engineering

Multi-Hazard Assessment of Long-Span Bridges, Considering the Effects of Seismic and Wind Action

Abdul Matin Jami

June 2025

FACULTY OF CIVIL AND ENVIRONMENTAL ENGINEERING

Multi-Hazard Assessment of Long-Span Bridges, Considering the Effects of Seismic and Wind Action

Abdul Matin Jami

Dissertation submitted in partial fulfillment of a
Philosophiae Doctor degree in Civil Engineering

Ph.D. Committee
Professor Rajesh Rupakhety
Professor Bjarni Bessason
Professor Jónas Þór Snæbjörnsson

Examiner/Opponents
Professor Tatjana Isaković
Professor Christian Málaga-Chuquitaype

Faculty of Civil and Environmental Engineering
School of Engineering and Natural Sciences
University of Iceland
Reykjavik, June 2025

Multi-Hazard Assessment of Long-Span Bridges, Considering the Effects of Seismic and Wind Action

Dissertation submitted in partial fulfillment of a *Ph.D.* degree in Civil Engineering

Faculty of Civil and Environmental Engineering
School of Engineering and Natural Sciences
University of Iceland
Sæmundargatu 2
102 Reykjavik
Iceland

Telephone: 525 4000

Bibliographic information:
Abdul Matin Jami, 2025, Multi-Hazard Assessment of Long-Span Bridges, Considering the Effects of Seismic and Wind Action, Ph.D. dissertation, Faculty of Civil and Environmental Engineering, University of Iceland, 191 pp.

Author ORCID: 0000-0001-7053-1278

Abstract

This PhD research project focuses on the multi-hazard evaluation of long-span bridges and the development of novel solutions to improve the effectiveness of structural control schemes. In particular, the study investigates seismic response mitigation using passive devices such as tuned mass dampers and lead rubber bearings. The research aims to examine the response of both uncontrolled and passively controlled long-span bridges, specifically suspension and cable-stayed types, subjected to near-fault earthquake excitations and strong wind forces. A key objective is to quantify the probabilities of exceeding various performance limit states and to establish fragility functions for these structures under combined seismic and wind hazards. The project further explores the feasibility and efficiency of passive control systems in reducing structural fragility.

These objectives are motivated by several core research questions. First, due to their considerable length and inherent flexibility, suspension and cable-stayed bridges are especially vulnerable to long-period and impulsive motions characteristic of near-fault earthquakes. The study seeks to understand the extent to which near-fault effects compromise the safety of such bridges and whether their fragility under these conditions is significantly greater than under ordinary ground motions. It also evaluates the effectiveness and practicality of using passive control devices, such as tuned mass dampers, to mitigate this fragility. In addition, the research addresses how the combined effects of stochastic wind and seismic loads can be integrated into fragility analysis and the implications for design practice.

To investigate these questions, detailed finite element models were developed using SAP2000, MATLAB, and OpenSees. The models include a three-span concrete bridge, multiple five-span concrete bridges, a 300-meter span cable-stayed bridge in Iceland (Ölfusá River), and a 1500-meter span suspension bridge in China (Runyang River). Wind forces were simulated using stochastic processes based on the spectral representation method, while seismic input was derived from real ground motion records from past earthquakes. A novel simulation methodology was also implemented to generate over 55,000 pulse-type near-fault ground motions for comprehensive evaluation of their effects.

The findings indicate that well-optimized passive control systems can significantly reduce structural responses under both seismic and wind loading. Fragility analyses confirm the effectiveness of tuned mass dampers in decreasing structural vulnerability and, in certain cases, enhancing pier moment capacity, particularly when vertical seismic components are considered. The study also identifies bridge bearings as critical elements influencing overall seismic performance, underscoring the importance of post-earthquake inspection and design strategies that facilitate their replacement. Given Iceland's proximity to active fault lines, the results highlight the importance of accounting for near-fault effects in the seismic design and long-term resilience of critical infrastructure.

Table of Contents

List of Figures

List of Publications

This dissertation draws upon research contributions featured in the following papers, either published in reputable International Scientific Indexing journals or currently under submission.

1. Jami, M., Rupakhety, R., Elias, S., Bessason, B., & Snæbjörnsson, J. T. (2022). Recent Advancement in Assessment and Control of Structures under Multi-Hazard. Applied Sciences, 12(10), 5118.
2. Jami, M., Rupakhety, R., Bessason, B., & Snæbjörnsson, J. T. (2023). Multimode Vibration Control Strategies of LSBs Subjected to Multi-hazard: A Case Study of the Runyang Suspension Bridge. Journal of Vibration Engineering & Technologies, 1-14.
3. Jami, M., Rupakhety, R., Elias, Domenico, D., (2025). Reliability of Bridges Under Near-Fault Pulse-Type Ground Motions with Vertical Component Consideration. Elsevier, STRUCTURES-D-25-02305R1.
4. Jami, M., Rupakhety, R., Bessason, B., & Snæbjörnsson, J. T. (2025). Fragility of long-span bridges to near-fault pulse-like ground motions. (Manuscript in preparation).
5. Jami, M., Rupakhety, R., Elias, Ólafsson S. (2020). Seismic Response Mitigation of Bridges with Tuned Mass Dampers. 17th World Conference on Earthquake Engineering (17WCEE), Japan.
6. Jami, M., Rupakhety, R., Elias, Domenico, D., Falsone G., Ricciardi G. (2021). Are bridges safe under near-fault pulse-type ground motions considering the vertical component? 1st European Conference of the European Association on Quality Control of Bridges and Structures EUROSTRUCT 2021.
7. Jami M., and Rupakhety R. (2022). Multi-Hazard Consideration in Control of Structures with Low Fundamental Frequency (Long-Span Bridges & Tall Buildings). 3rd European conference on earthquake engineering and seismology, Sep 4-9.2022.
8. Jami M., and Rupakhety R. (2025). The Impact of Near-Fault Ground Motion Pulses on Long-Span Bridges and Mitigation Strategies. The 19th World Conference on Seismic Isolation, Energy Dissipation and Active Vibration Control of Structures, Sep 15-19, 2025 (accepted).

Acknowledgements

The completion of my doctoral project demanded extensive effort, and without the cooperation and support of several individuals, it would not have been possible. First and foremost, my sincere gratitude to Professor Rajesh Rupakhety. Without his unwavering support and guidance, I would not have been able to accomplish any of my research projects throughout my PhD journey. I am also deeply indebted to Bjarni Bessason and Professor Jónas Þór Snæbjörnsson for their invaluable support and guidance. Their insightful feedback and suggestions significantly enhanced the quality of my research work.

I want to extend my heartfelt appreciation to the Earthquake Engineering Research Center in Selfoss for providing the necessary resources and a conducive environment for research. Particularly thankful to Professor Simon Olafsson for his valuable suggestions and guidance, which were instrumental in my work. Special thanks go to Elínborg Gunnarsdóttir for her assistance with all the paperwork and her efforts to ensure my family, and I could live in Iceland without any problems. Her support made our stay smooth and worry-free, and I will always remember her efforts with deep gratitude. I am also grateful to Dr. Elias Rahimi for his assistance throughout my research. His expertise and insights were incredibly helpful. To all the PhD candidates at the Centre, thank you for your support. I wish you the best of luck.

A special thank you to my wife, Razia Jami, whose unwavering support, love, and understanding have been a constant source of strength. Her encouragement and patience made this journey possible. I would also like to extend my gratitude to my mother, my brother, and my entire family. Their support and encouragement strengthened my resolve to complete this vital work.

I gratefully acknowledge the research grants provided by the University of Iceland, which enabled me to pursue and advance my career in my chosen field of research.

The start of my doctoral studies coincided with the COVID-19 pandemic and the adverse developments that led to catastrophic conditions in my home country, Afghanistan. Bringing my wife and child out of the dire situation in Afghanistan and having them join me in Iceland significantly alleviated many of my worries. The years we spent in Selfoss were incredibly joyful for me and my family, and we will never forget them. I want to express my deepest gratitude once again to everyone at the University of Iceland, especially the Earthquake Engineering Research Center, for their support in this matter. I also sincerely thank the warm-hearted people of Selfoss, who provided my family and me with fantastic living conditions during our time in Selfoss. Your assistance was crucial in helping me navigate those challenging times successfully.

1 Introduction

Bridges are fundamental to the functioning of modern societies, facilitating connectivity and supporting economic and social activity. Long-span bridges (LSBs), in particular, serve as vital links across wide rivers, deep valleys, and coastal inlets, often situated in regions subject to diverse and challenging environmental conditions. While their elegant forms and structural efficiency enable them to span considerable distances, these same characteristics make them especially vulnerable to dynamic loads. Among the many hazards that civil infrastructure may face, earthquakes and strong wind events stand out as particularly disruptive, each capable of inducing significant structural responses. Moreover, these hazards may interact in complex ways, potentially compounding the risks to structural stability, functionality, and long-term serviceability.

Traditional engineering approaches have predominantly treated hazards as isolated events. However, growing research indicates that this perspective may not adequately reflect the complex risk landscape that structures face in real-world conditions. For instance, long-span bridges located near active fault zones are particularly vulnerable to near-fault ground motions, which are characterized by high-energy pulses and abrupt velocity changes. These impulsive motions, especially when accompanied by strong vertical components, have been shown to trigger failure mechanisms that are often overlooked in conventional seismic design frameworks. At the same time, structures optimized primarily for seismic resistance may exhibit diminished performance under prolonged wind loading, highlighting critical trade-offs inherent in traditional single-hazard design strategies.

Motivated by these considerations, this dissertation examines the behavior of long-span bridges under multi-hazard conditions and investigates effective strategies for reducing their vulnerability. Particular emphasis is placed on developing realistic modeling approaches that capture the complex interaction between hazards such as strong winds and near-fault seismic events. The study highlights the critical role of control technologies, specifically passive devices such as Tuned Mass Dampers (TMDs) and Lead Rubber Bearings (LRBs), in enhancing structural performance under dynamic loading conditions. Through a combination of numerical simulations, representative case studies, and optimization techniques, the research explores both the susceptibility of long-span bridges to extreme events and the potential for improving their resilience. Ultimately, this work aims to advance the design of infrastructure capable of maintaining reliable performance amidst complex and uncertain hazard scenarios.

1.1 Objectives and Scope of Research

The primary objective of this research is to advance understanding of the behavior of long-span bridges (LSBs) under the combined influence of multiple hazards, with particular emphasis on seismic and wind-induced loads. Due to their inherent flexibility and extended spans, LSBs are especially susceptible to dynamic excitation. Among the various hazards, near-fault ground motions pose a critical threat, often characterized by intense velocity

pulses and abrupt force reversals that can severely impact structural performance. Similarly, wind-induced forces, though different in origin, can excite comparable vibration modes, compounding the dynamic demands on these structures. This study investigates how such hazards affect bridge performance and explores practical strategies for mitigating vulnerability through passive control mechanisms.

A central focus is placed on assessing the response of various bridge types, including cable-stayed, suspension, and multi-span concrete bridges, to near-fault earthquakes and strong wind events. Detailed numerical models are developed to simulate the dynamic responses of these structures under realistic loading scenarios, incorporating both horizontal and vertical seismic components as well as stochastically generated wind fields. The research constructs fragility functions to quantify the probability of damage or failure across varying hazard intensities. These functions offer a probabilistic framework essential for performance-based design and risk-informed decision-making.

Beyond response analysis, the study evaluates the effectiveness of passive control devices,specifically Tuned Mass Dampers (TMDs) and Lead Rubber Bearings (LRBs), in enhancing structural resilience. Comparative simulations between controlled and uncontrolled bridge models are used to assess the potential of these devices to reduce displacements and accelerations during extreme events. Case studies based on real-world structures, including a long-span cable-stayed bridge in Iceland and a suspension bridge in China, are used to validate the models and demonstrate practical relevance.

The research integrates structural modeling, hazard simulation, fragility assessment, and control system evaluation to provide comprehensive and actionable insights. Its findings aim to inform engineers, researchers, and infrastructure planners engaged in the design of safer and more resilient bridges, especially in regions where seismic activity and high winds present significant design challenges. More broadly, this work contributes to the advancement of performance-based engineering and multi-hazard risk assessment for critical infrastructure.

1.2 Dissertation organization

This dissertation is structured around the four key issues outlined earlier. The core findings of the research have been disseminated through publications in peer-reviewed journals within the fields of earthquake engineering and engineering seismology. These journal articles, along with a submitted manuscript and several conference papers, are included as self-contained sections in the appendices. The first three chapters of the dissertation provide the necessary background for these contributions, including literature reviews relevant to the addressed challenges and practical applications that contextualize the findings. Below is a list of the associated scientific papers.

1.2.1 Scientific papers

Paper 1: Jami, M., Rupakhety, R., Elias, S., Bessason, B., & Snæbjörnsson, J. T. (2022). Recent Advancement in Assessment and Control of Structures under Multi-Hazard. Applied Sciences, 12(10), 5118.

Paper 2: Jami, M., Rupakhety, R., Bessason, B., & Snæbjörnsson, J. T. (2023). Multimode Vibration Control Strategies of LSBs Subjected to Multi-hazard: A Case Study of the Runyang Suspension Bridge. Journal of Vibration Engineering & Technologies, 1-14.

Paper 3: Jami, M., Rupakhety, R., Elias, Domenico, D., (2025). Reliability of Bridges Under Near-Fault Pulse-Type Ground Motions with Vertical Component Consideration. STRUCTURES-D-25-02305R1.

Paper 4: Jami, M., Rupakhety, R., Bessason, B., & Snæbjörnsson, J. T. (2025). Fragility of long-span bridges to near-fault pulse-like ground motions. (Manuscript in preparation).

Paper 5: Jami, M., Rupakhety, R., Elias, Ólafsson S. (2020). Seismic Response Mitigation of Bridges with Tuned Mass Dampers. 17th World Conference on Earthquake Engineering (17WCEE), Japan.

Paper 6: Jami, M., Rupakhety, R., Elias, Domenico, D., Falsone G., Ricciardi G. (2021). Are bridges safe under near-fault pulse-type ground motions considering the vertical component?. 1st European Conference of the European Association on Quality Control of Bridges and Structures EUROSTRUCT 2021.

Paper 7: Jami M., and Rupakhety R. (2022). Multi-Hazard Consideration in Control of Structures with Low Fundamental Frequency (Long-Span Bridges & Tall Buildings). 3rd European conference on earthquake engineering and seismology, Sep 4-9.2022.

Paper 8: Jami M., and Rupakhety R. (2025). The Impact of Near-Fault Ground Motion Pulses on Long-Span Bridges and Mitigation Strategies. The 19th World Conference on Seismic Isolation, Energy Dissipation and Active Vibration Control of Structures, Sep 15-19, 2025.

1.2.2 Dissertation chapters

Chapter 1

This chapter provides an overview of the dissertation, outlining its structure and the key issues it addresses.

Chapter 2

Chapter 2 establishes the essential background for the research by introducing fundamental concepts in multi-hazard risk assessment and emphasizing the need for integrated approaches to enhance bridge resilience. It explains how hazards, exposure, and vulnerability interact, thereby laying the foundation for the challenges tackled in this study. Additionally, the chapter offers concise summaries of the four scientific papers that form the core contributions of the dissertation, presenting an overview of their methodologies and principal findings to prepare the reader for the detailed analyses in the subsequent chapters.

Chapter 3

Chapter 3 synthesizes the key results of the research, discusses the assumptions and limitations encountered, and outlines recommendations for future work. It reflects on the broader insights obtained from the investigation into the multi-hazard resilience of bridge structures and examines how the proposed strategies advance performance-based design

principles. This chapter also identifies potential avenues for further research to address emerging challenges and enhance the long-term safety and sustainability of critical infrastructure.

2 Background and summary of appended papers

This chapter provides background information on hazard vulnerability and risk within the context of multi-hazard assessment and performance enhancement for long-span bridges (LSBs). It begins with an introduction to the fundamental components of risk, including hazard, exposure, and vulnerability, and explains their relevance to LSBs. Following this, the chapter presents a summary of the research papers that form the core contributions of the dissertation, highlighting their methodologies, key findings, and their role in addressing the challenges outlined in this study.

2.1 Introduction

Civil infrastructure, such as bridges, roads, and buildings, is exposed to various hazards throughout its lifespan. Among these, earthquakes and strong winds are major risks to public safety and comfort. With rapid urban expansion, structures are becoming larger and more complex, making them more vulnerable to these natural hazards. As a result, understanding and evaluating the impact of natural events on infrastructure has become a crucial field of research. Statistics presented in Jami et al. (2022) underscore the significant effects that natural disasters have had over the past 25 years, including economic damage, casualties, and widespread disruptions to populations.

Natural events affect structures in numerous ways. While it is rare for multiple hazards to occur simultaneously, certain events can trigger secondary hazards or amplify their destructive potential. For example, earthquakes often lead to secondary hazards such as fires or landslides (Ravankhah et al., 2017).

Throughout the lifespan of any infrastructure, it is likely to encounter different types of hazards, each requiring specific safety measures. A design optimized to withstand just one hazard may not offer sufficient protection against others, highlighting the need for multi-hazard mapping that considers the interactions between various threats (Jami et al., 2022).

Infrastructures such as dams, tunnels, bridges, and highways are essential for modern life. While assessing multi-hazard risks can be complex, it is vital for ensuring that these infrastructures remain safe and operational after disasters (Ettouney et al., 2005; García, 2010). Several studies have explored this issue. For instance, Ettouney and Alampalli (2016) examined the effects of multiple hazards on infrastructure performance and costs, while Ardebili (2017) and Bodda (2018) analyzed the resilience of floodwalls and dams under multi-hazard conditions.

Risk assessment in civil engineering combines hazard analysis, exposure, and vulnerability to estimate the likelihood and impact of adverse events on infrastructure. This chapter compiles significant published research on multi-hazard risk assessment, summarizing key findings and insights. The following sections discuss essential background concepts of risk:

hazards, exposure, and vulnerability. This review was originally based on the keywords "Risk assessment" and "Multi-hazard" and was published in *Recent Advancements in Assessment and Control of Structures under Multi-Hazard*. For further details, refer to Appendix A, Jami et al. (2022).

2.2 Risk

Risks associated with natural disasters can result in significant loss of life, economic downturns, and environmental damage. In a broader context, risk refers to the uncertainty surrounding the potential consequences of a particular event or action. While risk can be linked to various fields such as business, finance, or insurance, in the context of engineering, it is closely associated with structural vulnerability, hazard, and physical exposure. In the following sections, the roles of each of these risk components, hazard, exposure, and vulnerability, are briefly reviewed, as they form the foundation for assessing the risk posed to infrastructure by natural disasters. By understanding how these elements interact, engineers can better predict and mitigate the potential impacts of various hazards on structures.

2.2.1 Hazard and multi-hazard definition

The term "hazard" typically refers to any event or process that has the potential to cause harm to people, property, or the environment. According to Ettouney and Alampalli (2017), "hazard is any external or internal process or event that might degrade the performance of the system at hand." The United Nations General Assembly (UNGA, 2017) defines a hazard as "a process, phenomenon, or human activity that may cause loss of life, injury, or other health impacts, property damage, social and economic disruption, or environmental degradation."

While these definitions encompass various types of hazards, this study focuses on those that have the potential to impact the performance of civil engineering structures. Of the three components that constitute disaster risk, hazard, exposure, and vulnerability, hazard is the one most often beyond human control. However, a proper understanding of the intensity, frequency, and spatiotemporal distribution of hazards can significantly help reduce the associated disaster risk. Thanks to advancements in data collection, sensing technologies, and modelling tools, our ability to predict and understand the effects of hazards on infrastructure has improved dramatically.

Hazards can be categorized in many ways, based on their nature and consequences. Broadly, hazards can be classified into two major categories:

1. **Natural Hazards**: These are classified based on their origin into subcategories such as atmospheric, shallow Earth processes, hydrological, biophysical, and geophysical hazards (for further details, see Jami et al., 2022).

2. **Man-made Hazards**: These include events like fires and explosions.

In addition to these categories, certain slow processes, such as corrosion, fatigue, and aging, can also affect the performance of structures over time and should be considered in a multi-

hazard framework. These processes may amplify the impacts of other hazards and need to be addressed accordingly.

The principle of retrofitting structures to withstand multiple hazards over their lifespan is well-established in civil engineering and is reflected in standards and design codes. These codes often incorporate the impact of multiple hazards through the concept of load combinations. However, it remains a question whether these load combinations sufficiently account for multi-hazard interactions. In response, Jami et al. (2022) provide a definition of multi-hazard: "Multi-hazard generally refers to a scenario where two or more hazards interact through structural performance. A multi-hazard interaction, for example, can impact risk due to a hazard when a decision regarding structural exposure and vulnerability to the frequency, location, and amplitude of another hazard is made. For example, a change in design wind load and/or structural capacity can impact structural vulnerability to earthquake forces. Multi-hazard interactions may result in common or conflicting design solutions. For example, provision of structural ductility is beneficial for both blast and seismic loads."

In classifying multi-hazard risks, Jami et al. (2022) reviewed various studies and concluded by categorizing the consequences of multi-hazard risks into three groups:

1. **Based on hazard occurrence**: Focuses on how the timing and occurrence of multiple hazards influence risk.

2. **Based on influence on design parameter selection**: Investigates how different hazards may affect the selection of design parameters.

3. **Based on influence on fragility and risk**: Examines how the interaction of multiple hazards affects the fragility and overall risk of a structure.

These categories provide a comprehensive framework for understanding and addressing the complexities of multi-hazard risks in infrastructure design and assessment.

2.2.2 Exposure, multi-hazard mapping and planning

In the context of multi-hazard assessment, “Exposure” refers to the degree to which infrastructures, buildings, or people are at risk from different hazards, either sequentially or simultaneously. The United Nations Office for Disaster Risk Reduction (UNDRR) defines exposure as “the situation of people, infrastructure, housing, production capacities, and other tangible human assets located in hazard-prone areas.”

As noted earlier, exposure is a key determinant of risk, and while it is largely influenced by external factors, it can be mitigated to some extent through better planning and strategy development. Improving exposure management requires enhancing emergency response capabilities and strengthening the resilience of structures to withstand various hazards.

A critical first step in reducing exposure is identifying hazards and mapping their spatial distributions. While significant progress has been made in mapping individual hazards, multi-hazard mapping remains a complex challenge. This is due to the variety of hazards involved, each characterized by different measures of amplitude, frequency, physical phenomena, and impacts on structures (Jami et al., 2022). The difficulty of combining these

diverse hazard types into a single map lies in the need to account for their interactions and compounded effects.

Several studies have explored multi-hazard mapping approaches. Barua et al. (2016) presented a multi-hazard map for Bangladesh, which combined various natural hazards, including floods, tornadoes, cyclones, and earthquakes, based on a database of historical disaster data. The study also considered a weighting scheme for combining these hazards, acknowledging their differing impacts.

Similarly, Pourghasemi et al. (2020) and Pourghasemi et al. (2019) developed multi-hazard maps for the Fars province and the western region of Iran. These studies focused on hazards such as landslides, floods, and fires. Using historical data, they trained machine learning algorithms to predict hazard distributions. The importance of multi-hazard mapping in these studies was emphasized through their incorporation of watershed management, sustainable development, and land-use planning considerations.

In addition to machine learning and statistical methods, an alternative approach proposed by Bathrellos et al. (2017) involves the use of the Analytical Hierarchy Process (AHP) for multi-hazard mapping in moderately small regions. Rather than relying purely on statistical data, this approach identifies the relationship between hazards and influencing factors, offering a framework for decision-making. Multi-hazard maps developed using the AHP method can be found in studies by Khatakho et al. (2021), Bathrellos et al. (2017), and Karaman (2015), demonstrating the versatility and utility of this approach for integrating various hazard types.

The integration of multi-hazard mapping and planning into infrastructure development and risk management is essential for enhancing resilience and minimizing exposure to potential disasters. By understanding hazard distributions and their interactions, decision-makers can better allocate resources, design safer structures, and implement more effective mitigation measures.

2.2.3 Vulnerability

Vulnerability refers to the inherent characteristics of structures that make them susceptible to damage from hazards (Jami et al., 2022). According to the United Nations General Assembly (UNGA, 2017), vulnerability is the conditions determined by physical, social, economic, and environmental factors that increase the susceptibility of individuals, communities, assets, or systems to the effects of hazards. In risk assessment, vulnerability is one of the most manageable factors through human intervention, making it a critical target for mitigation efforts. Reducing vulnerability, therefore, plays a central role in minimizing overall risk.

However, assessing the vulnerability of civil engineering structures, especially against a single hazard like earthquakes, can be complex and involves significant uncertainties (Bessason et al., 2022; Thorvaldsdottir et al., 2021; Ferreira et al., 2021). In the case of multi-hazard scenarios, overall vulnerability may differ from vulnerability to individual hazards, which adds another layer of complexity to risk assessments. This complexity arises from various factors, including variations in structural materials, design, environmental conditions, hazard exposure, usage, age, and maintenance.

The study of structural vulnerability to multiple hazards is an evolving research field. Vulnerability is often represented using fragility or vulnerability curves, which provide a probabilistic estimate of the likelihood that certain damage thresholds will be exceeded, given a specific hazard intensity. On a broader scale, vulnerability classification relies on general information about structures, their function, and their exposure to hazards, a method commonly used for buildings. For example, Nassirpour et al. (2018) applied this approach to rank school infrastructure in the Philippines, considering risks from flood, wind, and earthquakes.

Schwarz et al. (2018) developed a methodology for assessing building vulnerability under both single and multiple hazards by incorporating principles from the European Macroseismic Scale 1998 (EMS-98, Grünthal et al., 1998). Their methodology included vulnerability tables for hazards like wind, flood, and earthquakes, and established a framework for developing multi-dimensional vulnerability models. These models were applied in several cities in Germany, highlighting the practical application of multi-hazard assessments.

Real-world applications of multi-hazard assessments also contribute significantly to this field. For instance, Gautam and Dong (2018) examined the structural damage caused by the 2015 Gorkha Earthquake and the 2017 Chhatiune Khola flash flood in central Nepal. Ayala et al. (2006) proposed a conceptual model for evaluating the vulnerability of historic buildings, focusing on English parish churches as a case study. Julia and Ferreira (2021) provided a comprehensive review of single and multi-hazard vulnerability and risk in historic urban areas, demonstrating how multi-hazard risk analysis can help preserve cultural heritage.

These studies underscore the importance of understanding and evaluating vulnerability in multi-hazard contexts, as the interaction of various hazards can have cumulative and compounded effects on infrastructure. Through the development of vulnerability models and multi-hazard assessments, the resilience of structures can be better evaluated, and more effective strategies for risk reduction can be implemented.

2.3 Summary of appended papers

2.3.1 Paper 1, Recent advancement in assessment and control of structures under multi-hazard.

This paper presents a comprehensive review of recent advancements in the multi-hazard assessment and control of civil engineering structures. Drawing from over 260 peer-reviewed studies and technical reports, the literature has been thematically organized based on structure type (e.g., bridges, buildings, wind turbines) and the types of hazards considered.

For this research, an extensive search was carried out across major scholarly databases using keywords such as “multi-hazard,” “vibration control,” “seismic fragility,” and “life-cycle assessment.” The studies were further classified by structural systems and performance goals, resulting in a rich overview of both theoretical developments and practical applications in the field. Two main themes emerge from this synthesis: assessment and

control. The assessment theme covers topics such as hazard mapping, structural fragility, life-cycle cost evaluation, and performance reliability under different hazard combinations. The control theme focuses on technologies used to reduce vibrations and enhance structural resilience, ranging from traditional passive systems, such as base isolators and TMDs, to emerging hybrid and semi-active control solutions. Each approach is discussed in terms of its effectiveness against various hazards, cost implications, and adaptability to existing structures.

One of the major insights from this review is that evaluating hazards independently is no longer sufficient for reliable design. Structures often undergo cumulative damage, where one hazard weakens the system, increasing its vulnerability to subsequent events. For example, an earthquake can induce minor damage that compromises a bridge's ability to withstand wind, flooding, or traffic loads that follow. Despite this, many existing control systems and retrofit strategies are still designed with a single hazard in mind, which can lead to unintended consequences when multiple hazards interact.

The review classifies a wide range of hazard combinations relevant to bridges, including:

- Earthquake and Corrosion
- Earthquake and Floods
- Earthquake, Floods, and Ground-Failures
- Earthquake and Scour
- Earthquake, Scour, and Corrosion
- Earthquake, Scour, Corrosion, and Traffic-Load
- Earthquake, Scour, Corrosion, Wind, Traffic-Load and Liquefaction
- Earthquakes, Corrosion, Surge, and Wave
- Earthquakes, Wind, Tsunami, Flood, Surge, and Wave
- Earthquakes, Blast and Fire
- Earthquake and traffic loads
- Earthquake, Traffic-Load, and Deterioration
- Earthquakes and High water
- Wind and traffic Load
- Storm Surge and wave

The review also draws attention to a noticeable gap in current research: most control solutions and retrofit strategies are still developed with a single hazard in mind. This is especially problematic for bridges, which are critical lifelines in any infrastructure network. There is an urgent need for retrofit techniques and control systems specifically designed to

handle the complex interactions of multiple hazards, whether they act concurrently or sequentially. By recognizing these challenges and filling these knowledge gaps, engineers can move closer to designing truly resilient structures capable of withstanding a wide range of extreme events. To illustrate the broader framework for integrating these insights into engineering practice, Figure 2.1 presents a flowchart that outlines the sequential steps in multi-hazard consideration and risk assessment for bridge structures.

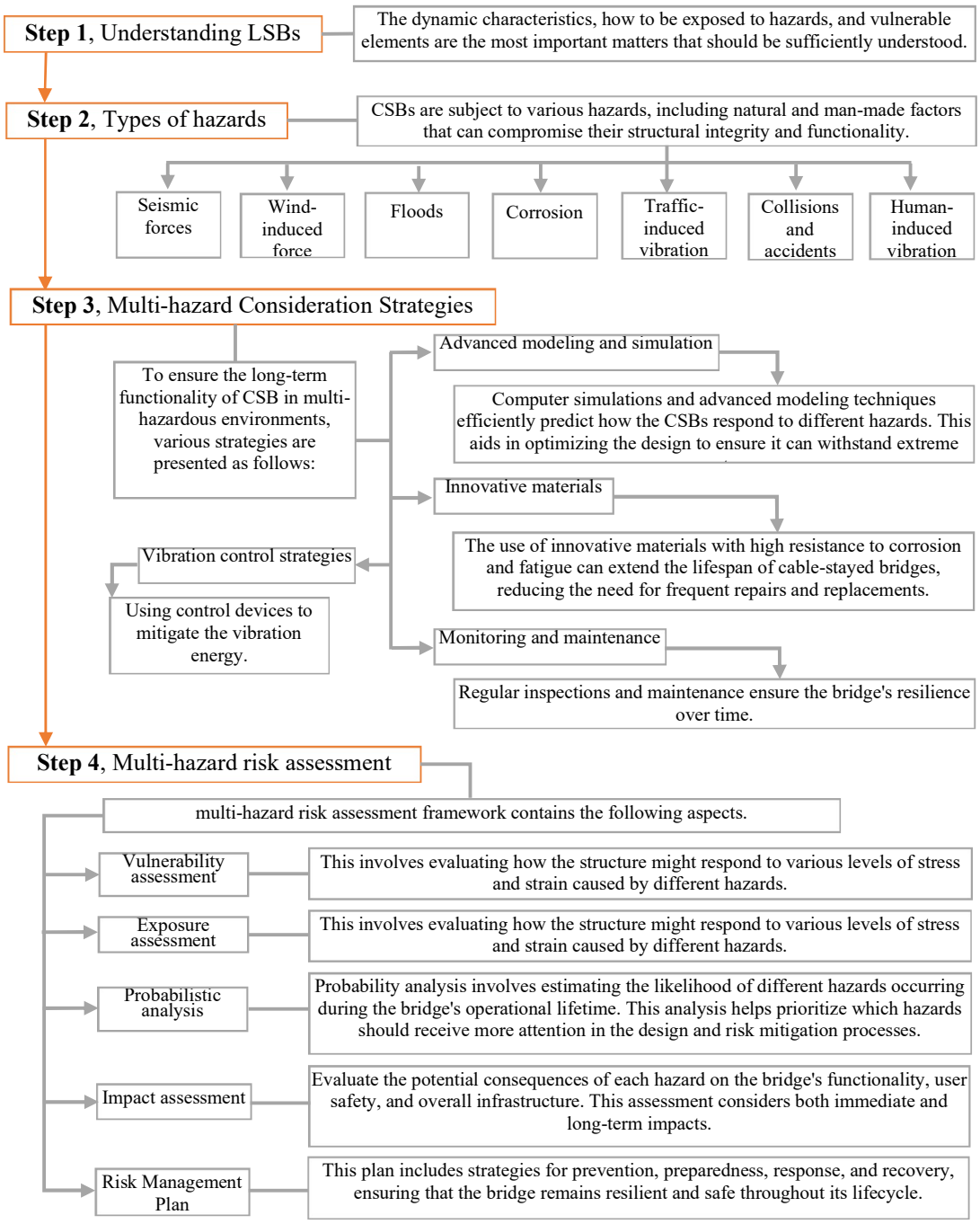

Figure 2.1. Flowchart to explore the multi-hazard consideration and risk assessment for bridges.

Figure 2.1 presents a structured flowchart outlining the essential steps in evaluating multi-hazard considerations and performing risk assessments for bridge structures. The chart begins with a foundational understanding of LSBs, emphasizing their dynamic characteristics, typical vulnerabilities, and exposure to various hazards. This initial step is critical for identifying which elements of the bridge are most susceptible to failure under different loading conditions. Next, the chart categorizes the primary types of hazards that can impact bridges throughout their lifespan. These include natural hazards such as earthquakes and wind, environmental processes like corrosion and fatigue, operational loads from traffic, and accidental impacts or collisions. Recognizing the nature and frequency of these hazards enables engineers to prioritize design and mitigation strategies accordingly.

The third component highlights the implementation of multi-hazard mitigation strategies. These strategies include advanced numerical modelling to simulate structural response under multiple hazard scenarios, the use of innovative materials for durability, vibration control systems to reduce dynamic responses, and proactive maintenance and monitoring protocols to extend service life. Ultimately, the flowchart presents a comprehensive risk assessment framework that combines vulnerability and exposure analysis, probabilistic hazard modelling, and consequence evaluation. This step supports the development of targeted risk management plans, enabling decision-makers to prepare for, respond to, and recover from hazardous events more effectively.

This review aims to provide both a foundation for new researchers and a practical resource for engineers, helping bridge the gap between theory and application in multi-hazard structural engineering. By identifying what has been done and what still needs to be addressed, it encourages a shift toward more integrated, future-focused approaches to safeguarding our built environment.

2.3.2 Paper 2, Multi-mode vibration control strategies of long-span bridges subjected to multi-hazard: a case study of the Runyang suspension bridge.

This section presents a detailed summary of the study published by Jami et al. (2023), which focuses on the Runyang Suspension Bridge (RSB), a long-span bridge in China, used as a benchmark structure to explore the performance of multi-mode vibration control strategies under earthquake and wind hazards. The motivation behind the study stems from the fact that long-span bridges are not only dynamically sensitive due to their size and flexibility but are also often exposed to multiple types of hazards over their lifespan. The primary objective of the study was to assess and enhance the bridge's dynamic performance when subjected to seismic ground motions, stochastic wind fields, and their combined action, utilising TMDs as the control mechanism.

Methodology and Framework

The study followed a multi-step analytical process illustrated in Figure 3.2, which outlines the overall methodology for evaluating multi-hazard-induced structural responses and optimising vibration control schemes. First, a detailed finite element model (FEM) of the RSB was developed using SAP2000. The model was carefully calibrated using parameters and validation data from prior studies. Two types of hazard inputs were considered: A set of seismic ground motions, including near-fault records with pulse-type characteristics, and a

spatially correlated wind velocity field, generated stochastically to represent realistic turbulent wind behaviour across the bridge span.

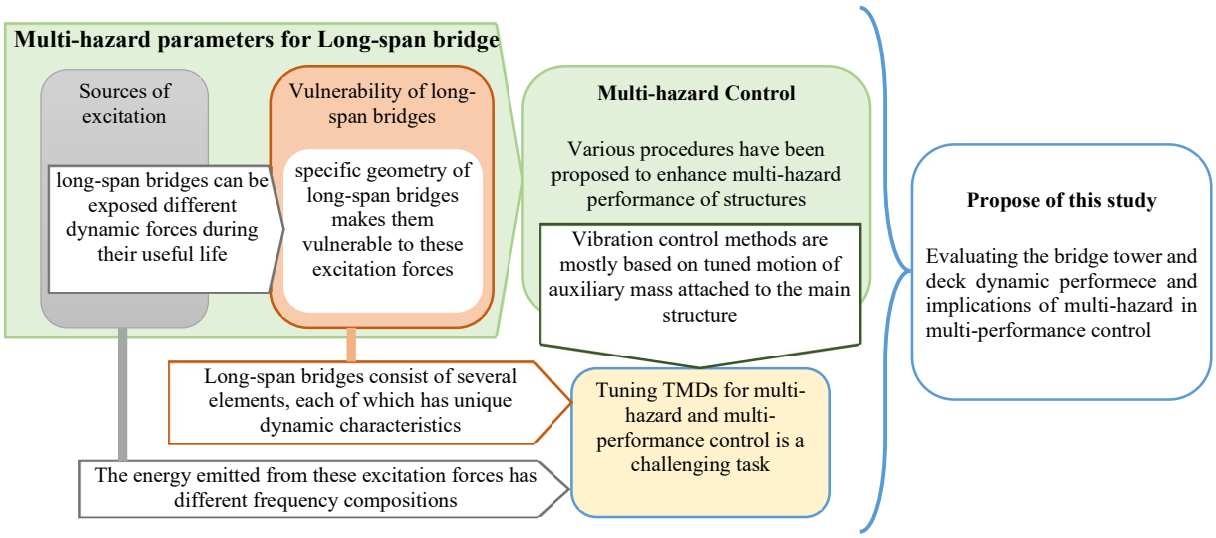

Figure 2.2. Flowchart for overview of the multi-hazard assessment and control of the long-span bridge.

The bridge's response, particularly acceleration and displacement, was studied at both the tower tops and the mid-span deck, under individual and combined hazard scenarios. Several TMD configurations were tested, with varying placement and tuning strategies to target specific vibration modes relevant to different structural components.

Main Findings and Results

The analysis revealed that seismic loads primarily controlled the acceleration response, especially at the towers, while wind loads had a more significant impact on the displacement response, particularly at the mid-span deck. These findings highlighted a mode-dependent and location-specific vulnerability of the bridge to different types of dynamic excitations. In simple terms, optimizing a vibration control system for one hazard (e.g., earthquakes) could unintentionally worsen the bridge's response to another (e.g., wind), unless a multi-performance objective is adopted.

To address this, a range of TMD configurations were tested: TMDs targeting deck acceleration (for seismic loads) were found to be ineffective or even detrimental when wind loads were dominant. Conversely, TMDs tuned for wind-induced displacement did not reduce seismic-induced accelerations at the towers and could even amplify them. The best performance was achieved using a multi-mode control strategy, where TMDs were installed on both the deck and towers, each tuned to different vibration modes. This configuration reduced both seismic and wind-induced responses without introducing undesirable trade-offs. The findings demonstrate the importance of integrating hazard characteristics and structural behaviour into the design of vibration mitigation systems.

An additional scenario was explored to assess how the bridge behaves under the simultaneous action of wind and earthquake forces. The results, presented in Figure 3.3, show that the structural response under combined hazards is not simply additive. Instead,

interaction effects between the two hazards result in complex response patterns, sometimes amplifying, and sometimes attenuating, the bridge's motion compared to individual hazard scenarios. These findings underscore the nonlinear and coupled nature of structural responses under multi-hazard conditions, further validating the need for a multi-objective control approach.

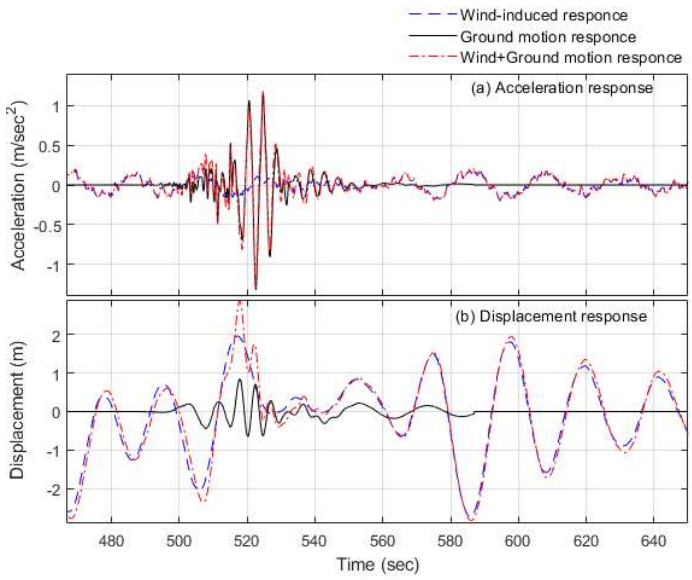

Figure 2.3. Mid-span acceleration (a), and displacement (b) response in transverse direction due to wind-induced force, ground motion (Chi-Chi Taiwan), and their combination

This case study demonstrates that vibration control of long-span bridges under multi-hazard conditions requires a carefully tailored, mode-specific strategy. TMDs can be highly effective, but only when tuned with consideration for both the frequency content of the hazards and the vibration characteristics of the structural components they are meant to protect. The multi-performance framework presented in this study provides a practical path forward for designing resilient bridges that can withstand multiple extreme events throughout their lifetime.

In conclusion, the study by Jami et al. (2023) offers valuable insights into the complex interplay between structural dynamics and multiple hazards in long-span bridges. By demonstrating the limitations of single-objective control systems and highlighting the benefits of a multi-mode, multi-objective vibration control strategy, the research advances the state of practice in bridge resilience design. It reinforces the need for integrated hazard-response frameworks that consider both the spatial distribution and dynamic nature of hazards, paving the way for safer and more adaptable infrastructure.

It is important to note that the RSB, due to its exceptionally long span and flexible design, demonstrates a very low natural frequency in the transverse direction. Identification studies have shown that the fundamental transverse period can range from 16 to 20 seconds (see Reference 20 in Paper 2). This is largely due to the bridge's suspension system, where lateral stiffness is governed by cables and hangers that offer minimal resistance. Furthermore, the tall and slender towers contribute to the overall flexibility. These aspects are reflected in the

mode shape illustrated in Figure 4 of Paper 2, which accurately depicts the first lateral vibration mode of the bridge.

2.3.3 Paper 3, Reliability of bridges under near-fault pulse-type ground motions with vertical component consideration.

The study emphasizes the significance of vertical ground motion, which is often neglected in traditional seismic design approaches that primarily focus on horizontal motions. The aim is to highlight how vertical ground motion can significantly impact the performance and reliability of bridges, especially those located near seismic faults, where ground motion is more pronounced and complex.

The analysis involves two types of bridges: an ordinary beam bridge, representing a typical bridge design, and the Runyang Suspension Bridge (RSB), which serves as a benchmark for long-span bridges. A database of 100 carefully selected near-fault pulse-type ground motions (NFPTGMs) was used to simulate the seismic loads. These ground motions are known for their unique characteristics, including large amplitude pulses and long-duration shaking, which can lead to higher seismic demands on structures.

The study explores the differential effects of vertical and horizontal ground motions on the dynamic behaviour of both bridge types. It also examines the interaction between these two components of ground motion, assessing how the inclusion of vertical motion influences the predicted seismic responses and vulnerability of the bridges. The findings aim to refine current seismic design practices by emphasizing the need to consider both horizontal and vertical motions in the assessment of bridge performance under near-fault seismic conditions.

Analytical Framework and Fragility Method

The analytical framework for evaluating the seismic behaviour of both bridge types involved a detailed 3D model that accounted for the nonlinearity of materials by incorporating plastic hinges at key points, such as piers and towers. This approach allows for more accurate simulation of the bridge's response under seismic loading, as it captures the progression of damage and potential failure mechanisms.

To develop fragility curves, the researchers followed a systematic process, outlined in Figure 2.4. These curves are crucial for assessing the likelihood that a bridge will reach or exceed a particular damage state under increasing levels of earthquake intensity. The steps involved in generating the fragility curves are as follows:

Selection of Ground Motions: A set of ground motions, specifically near-fault pulse-type ground motions, was selected to represent various seismic scenarios. These motions were chosen based on their ability to capture the characteristics of strong, pulse-like shaking near fault zones.

Nonlinear Simulations: For each selected ground motion, nonlinear dynamic simulations were run to capture the structural response of the bridges. This process involved applying the ground motions to the 3D model of the bridges, considering the material properties and plastic hinge behaviour at critical points.

Damage State Definition: Several damage states were defined, ranging from slight damage (e.g., cracks in concrete) to complete failure (e.g., collapse). These damage states served as thresholds for assessing the severity of the bridge's response under different levels of seismic intensity.

Statistical Fitting: After running the simulations, the collapse probabilities for each damage state were statistically fitted to produce fragility curves. These curves plot the probability of reaching or exceeding each damage state as a function of earthquake intensity.

The fragility curves generated in this analysis provide a probabilistic measure of the bridge's vulnerability to different levels of earthquake shaking. They help engineers assess the likelihood of various damage states under different seismic scenarios, providing a more comprehensive understanding of the structural risks posed by vertical and horizontal ground motions in near-fault regions.

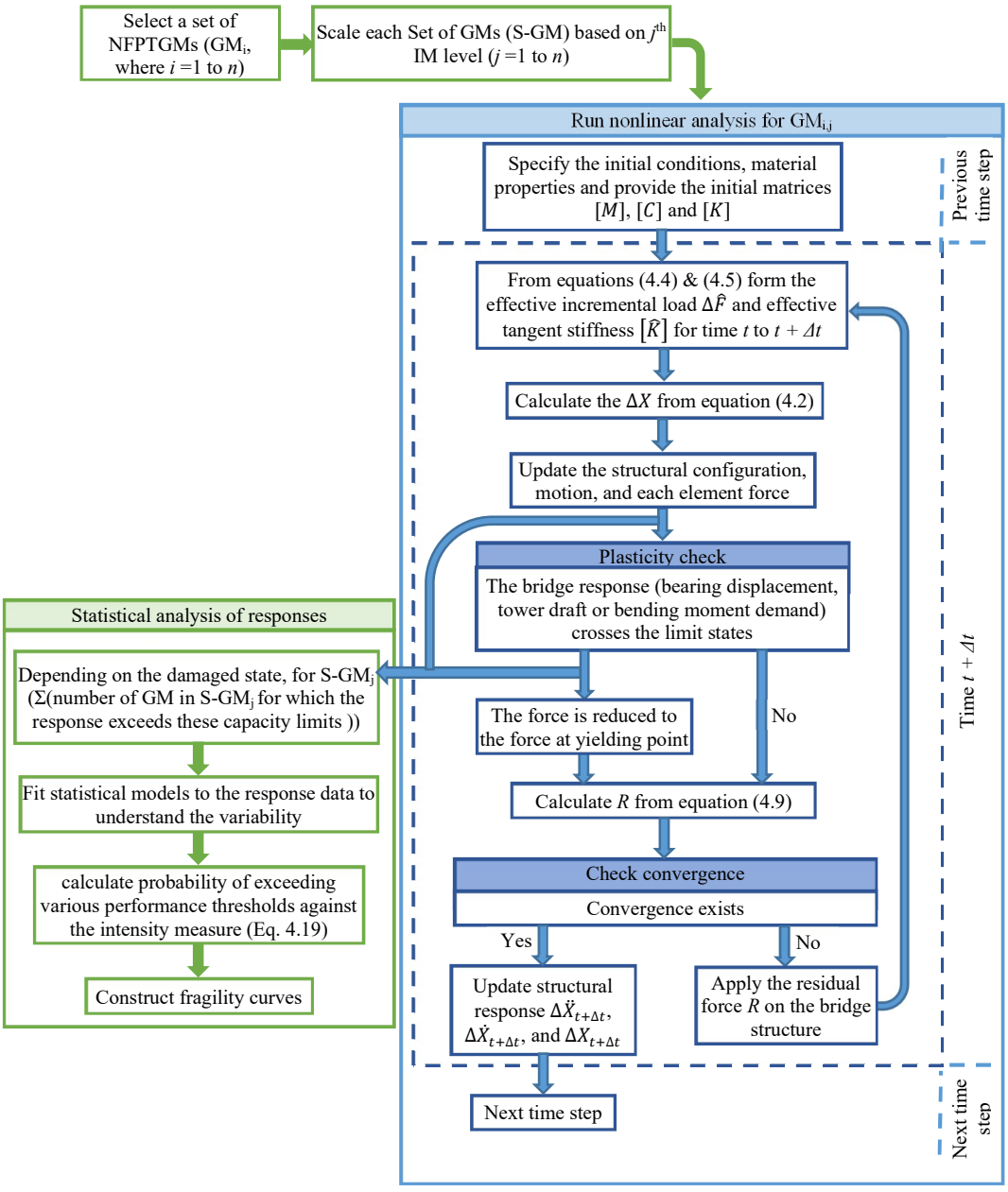

Figure 2.4. Flowchart for fragility analysis of bridge structures.

To address the challenges posed by vertical ground motion, the study introduced a novel 3D-Tuned Mass Damper (TMD) system designed specifically to mitigate the adverse effects of such motion on the bridge's performance. The 3D-TMD system was conceived to target not only horizontal vibrations but also the vertical vibrations, which are often overlooked in traditional seismic designs.

The optimal parameters for the TMD, including damping ratios and tuning frequencies, were determined through an optimization process using a Genetic Algorithm (GA). This computational technique is particularly effective for solving complex optimization problems by simulating the process of natural selection. In this case, the GA was used to efficiently search for the best TMD parameters that would simultaneously reduce the bridge's overall vibration and enhance the moment capacity of key structural components, particularly the piers and towers, under vertical shaking.

The key advantage of this approach lies in its ability to tailor the TMD system for both horizontal and vertical seismic responses. By optimizing the TMD's tuning and damping characteristics, the system not only reduced the bridge's vibratory response to seismic events but also contributed to improving the structural capacity of critical elements under combined shaking forces. This ensures that the bridge performs better during seismic events that involve both vertical and horizontal ground motions, which is particularly important in near-fault regions where vertical motions can be substantial.

This study offers several important insights that challenge common assumptions in seismic bridge engineering, particularly regarding the effects of near-fault earthquakes with strong vertical ground motion.

Main Findings and Results

The analysis demonstrated that the vertical component not only significantly contributes to the overall structural response but also causes a dynamic reduction in moment capacity, especially in bridge piers and towers. Specifically, the moment capacity of critical bridge elements was found to decrease by up to 19% when vertical ground motion was included in the analysis. Furthermore, fragility analysis revealed that the probability of collapse was notably underestimated in traditional horizontal-only analysis, highlighting the risk of overestimating structural safety. This means that structures deemed "safe" under conventional seismic assessments may actually be much more vulnerable in real-world seismic events.

To address these issues, the research introduced a 3D-Tuned Mass Damper (TMD) system, optimized to control vibrations in longitudinal, transverse, and vertical directions. Unlike conventional TMDs, which are typically tuned to lateral motion only, the 3D-TMD was shown to be highly effective in reducing seismic demand and improving moment capacity. Specifically, the use of 3D-TMDs resulted in:

- A reduction of up to 68% in peak moment responses for the Runyang Suspension Bridge (RSB)
- A reduction of up to 61% in moment responses for the beam bridge
- An increase of up to 19% in moment capacity for the RSB's tower columns

- An increase of up to 13% in capacity for the beam bridge's critical pier

These improvements were particularly significant under near-fault pulse-type ground motions (NFPTGMs). The 3D-TMD not only reduced the structural response but also stabilized axial forces, helping the columns resist higher moment demands when vertical shaking was present.

The results also indicate that the RSB bridge is more fragile in the longitudinal direction, primarily due to its greater stiffness and associated mass participation in that direction. In contrast, the transverse direction of the RSB is highly flexible, with a fundamental period of approximately 20 seconds, well beyond the dominant frequency range of most earthquakes. As a result, the transverse response is less sensitive to horizontal excitation, and the effect of vertical ground motion is also limited due to the weak coupling with that mode. For the concrete girder bridge, the fundamental frequencies in both directions are similar, and the fragility trends reflect this symmetry. Slightly higher fragility in the transverse direction is attributed to the bridge's single-pier configuration, which amplifies moment demand under lateral loads.

In conclusion, the findings strongly support a shift towards more realistic, multi-directional seismic design and assessment frameworks. Including vertical motion in seismic analysis is not merely a refinement, it is essential for accurately predicting bridge performance in near-fault zones. Furthermore, the deployment of advanced control strategies like 3D-TMDs offers a practical and effective means of enhancing both safety and resilience for existing and future bridge structures. This study adds to the growing body of evidence that seismic risk cannot be fully addressed without considering the complex, three-dimensional nature of earthquake ground motion.

2.3.4 Paper 4, Fragility of long-span bridges to near-fault pulse-like ground motions.

This section presents a study focused on understanding how long-span bridges behave when subjected to the unique and demanding conditions created by near-fault earthquakes. The Ölfusá Cable-Stayed Bridge (OCSB) in Selfoss, Iceland, was chosen as the case study due to its critical role in the region's infrastructure and its location near active fault lines. Given the strong seismic activity in Iceland, gaining a clearer picture of how this bridge would perform during a major earthquake is essential for ensuring its long-term safety and functionality.

The goal of the research was to develop a realistic and detailed assessment of the bridge's seismic performance under near-fault ground motions, particularly focusing on the effects of velocity pulses that often accompany such events. By developing a nonlinear model and simulating a wide range of possible earthquake scenarios, the study aimed to capture the key factors that influence the bridge's behaviour. In particular, the research explored how the design and optimization of isolation devices, specifically Lead Rubber Bearings (LRBs), could improve the bridge's ability to withstand these demanding seismic conditions and maintain its performance after strong shaking.

Methodology
The bridge was modelled using the OpenSees platform, which allowed for detailed nonlinear dynamic analyses. To accurately capture the inelastic behaviour of the structure, plastic

hinges were assigned to the bridge tower elements. Meanwhile, the deck was isolated from the substructure by LRBs, designed to absorb seismic energy and limit the displacement demands on the superstructure.

Two types of seismic input were used in the analysis: a database of 106 recorded near-fault ground motions provided by EERC, and a large set of 55,200 simulated pulse-type ground motions created to explore a wider range of possible future events. The simulation procedure for generating these synthetic ground motions, which involves developing the Peak Ground Velocity (PGV), pulse signal, and combining them with residual ground motion components, is summarised in Figure 2.5. This flowchart provides an overview of the systematic steps taken to replicate realistic near-fault seismic effects.

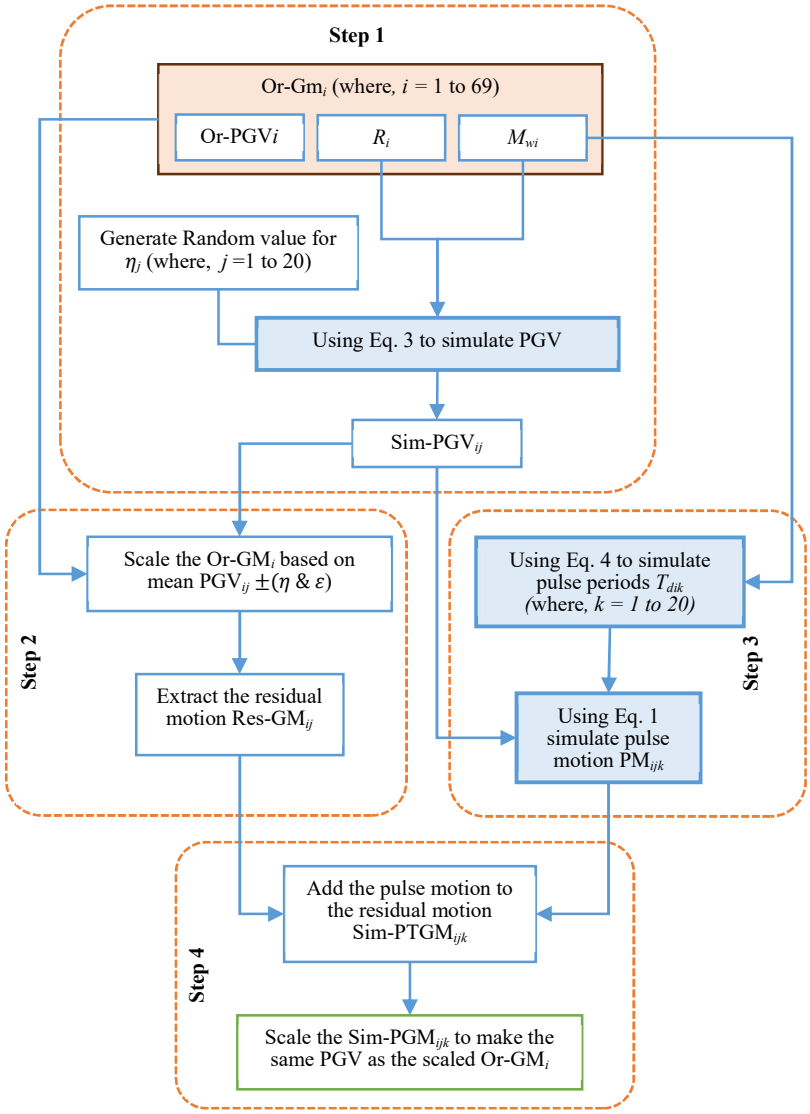

Figure 2.5. Flowchart summarizing steps for simulation of PTGMs.

The research also involved optimizing the LRB parameters, focusing particularly on the lead core diameter. Several diameters ranging from 10 cm to 70 cm were tested to find the most effective size for minimizing mid-span displacement. Nonlinear time history analyses were

performed on both recorded and simulated ground motions, and fragility curves were developed based on bearing shear strain, using a lognormal distribution to characterize different damage states.

Main Findings and Results

The results highlighted several important aspects of bridge behaviour under near-fault seismic loading. One of the most significant findings was that the bridge's seismic response was highly sensitive to the characteristics of the incoming ground motions, particularly the velocity pulse period. When the pulse period aligned with the bridge's fundamental periods, ranging between 0.6 and 2.0 seconds, the structural demands were notably amplified. This resonance effect significantly increased displacements and internal forces, especially in the bearings. The results also indicated that the pulse period of the near-fault ground motion is an important predictor of seismic fragility, suggesting that fragility curves based on amplitude-based intensity measures alone are not reliable for capturing the true risk. This underscores the need to consider the dynamic interaction between the bridge and the specific characteristics of near-fault ground motions when assessing seismic vulnerability.

The LRBs proved effective in controlling seismic demands, but their performance depended heavily on the tuning of their parameters. For moderate-intensity ground motions, a lead core diameter of 0.4 metres provided the best balance between flexibility and energy dissipation. For higher-intensity seismic inputs, a larger 0.5-metre core was more effective in maintaining bridge stability. This indicates that isolation systems should be carefully adapted to the specific seismic risk profile of each bridge, rather than relying on generalised design solutions. The fragility curves confirmed that, without proper tuning, the bearings would be the first elements to reach critical damage states under strong seismic excitation.

Overall, this research reinforces the importance of explicitly considering near-fault pulse effects in the seismic design of cable-stayed bridges. It also demonstrates that advanced modelling techniques, combined with intelligent optimisation of isolation devices like LRBs, can significantly enhance structural resilience. By addressing the unique demands posed by NFPTGMs, the study contributes to the broader goal of advancing performance-based design practices for critical infrastructure in seismic regions.

3 Conclusions and Future Research

This doctoral dissertation focused on advancing the understanding and resilience of bridge structures exposed to complex multi-hazard conditions, with particular attention to near-fault seismic effects and the interplay between earthquake and wind loads. The research combined a comprehensive review of current multi-hazard assessment methods with detailed numerical simulations and optimization studies aimed at improving structural performance through advanced control strategies. Therefore, it can be acknowledged that the central finding of this work is the critical importance of adopting a multi-hazard and multi-performance perspective in bridge engineering. The most important of these findings will be briefly mentioned below.

A key insight from the seismic vulnerability assessments was the substantial impact of near-fault pulse-type ground motions on bridge structures. When the pulse periods of seismic ground motions aligned closely with the natural vibration periods of bridges, the resulting structural responses were amplified considerably. The period of near-fault ground motion pulses is a key parameter affecting the seismic fragility of long-span bridges. Seismic fragility curves based solely on amplitude-based intensity measures are therefore not adequate. These traditional methods fail to capture the full complexity of near-fault ground motions, particularly their frequency characteristics, such as the pulse period. A more comprehensive approach is needed, one that incorporates both amplitude and frequency (pulse period) as intensity parameters in the fragility assessment. This would provide a more accurate representation of a bridge's vulnerability, especially under the unique conditions of near-fault seismic events.

One of the case studies revealed that the vertical component of ground motion had a profound effect, resulting in reductions in pier and tower moment capacities of up to 19%. This reduction significantly increased the probability of structural failure compared to assessments based solely on horizontal shaking (see paper 3).

In a novel contribution of this research, a new methodology is proposed, where the performance of a 3D-TMD is evaluated not only based on its ability to reduce dynamic responses, but also on its influence on the moment capacity of bridge piers during seismic events (see paper 3). In a case study, this dual focus revealed that 3D-TMDs not only decreased peak seismic demands, achieving up to a 62% reduction in moments, but also helped stabilize axial forces, effectively improving the structural capacity of critical bridge elements in real-time. This more holistic evaluation approach provides a deeper understanding of how vibration control devices contribute to overall structural resilience under extreme loading conditions.

In evaluating the performance of LRBs, it was found that the lead core is the key component responsible for absorbing the energy from horizontal pulse motions. A case study focused on optimizing the lead core diameter for a cable-stayed bridge revealed important trends (see paper 4). Bearings with a smaller diameter (less than 0.4 m) lacked sufficient stiffness, leading to excessive deformation and larger mid-span displacements. In contrast, larger diameters (greater than 0.4 m) made the bearings overly stiff, reducing their ability to dissipate seismic energy and increasing force transmission to the structure. The results indicated that a 0.4-meter lead core provided the best balance, offering enough flexibility to absorb energy without causing instability, while optimizing the bearing’s hysteretic

behaviour for efficient energy dissipation. It was also observed that the choice of lead diameter should depend on the expected ground motion characteristics: for moderate pulse intensities and excitation periods close to the bridge's natural period, a 0.4-meter lead diameter performed better, while for stronger pulses with higher peak ground velocities, a 0.5-meter diameter yielded improved results.

Also, the fragility analyses conducted in this research further revealed that bearings are often the most vulnerable components of isolated bridge systems under near-fault seismic excitation. Special attention must therefore be given to the design, monitoring, and potential post-event replacement of these critical elements to ensure long-term bridge functionality and safety.

Beyond individual bridge responses, this research highlights the broader need to integrate life-cycle resilience considerations into bridge design, particularly for seismically controlled or base-isolated long-span bridges, which were the exclusive focus of this work. The conclusions drawn throughout the dissertation are valid for these types of structures, where damage states are defined based on moment capacity or system performance under passive control. It is essential to note that these findings may not directly apply to conventional bridge systems that rely on ductile detailing and allow for controlled flexural damage. In such cases, damage states are typically defined based on ductility criteria. It is worth noting that the multi-hazard framework adopted in this research is particularly relevant to regions like Iceland, where both seismic activity and strong wind events are frequent and significant. In areas where only one of these hazards is dominant, such detailed multi-hazard analysis may not be necessary or justified. Within the defined scope, however, the study demonstrates that multi-hazard-informed strategies, combining advanced numerical modelling, intelligent vibration control systems, and probabilistic risk assessments, can substantially reduce the likelihood of catastrophic failures and contribute to the creation of more sustainable and disaster-resilient infrastructure.

3.1 Assumptions and Limitations

Several assumptions and simplifications were made throughout this research to allow for practical modeling and analysis while focusing on the primary objectives. Structural models of bridges were developed using different platforms, including SAP2000, MATLAB, and OpenSees. These tools enabled detailed finite element modeling and nonlinear dynamic analyses. However, certain idealizations were necessary. The models generally assumed elastic behavior for some components, while nonlinearities were concentrated in specific elements such as plastic hinges at pier and tower bases.

During optimization of control systems such as TMDs and isolation devices, the tuning was based on the initial dynamic properties of the structure, without accounting for potential period shifts under severe nonlinear behavior. This should be considered a limitation of the methodology, and future studies could benefit from incorporating adaptive tuning strategies that account for period changes during strong seismic events.

The ground motion datasets used in the analyses, while extensive, were based on available records and simulated near-fault pulse-type ground motions. Although care was taken to select a wide range of realistic seismic inputs, actual future earthquakes could present

characteristics that differ from the selected records. To create fragility surfaces using peak ground velocity (PGV) and pulse periods (Tp) as intensity parameters, may more ground motions than what is available are needed. Such motions need to cover a wide range of pulse period for different PGVs. A simple method was introduced in this work (Paper 4) to simulate artificial ground motions with near-fault characteristics. Although this method attempts to preserve the characteristics of recorded ground motion by using realistic scaling laws and attenuation models, it lacks a sound theoretical basis. Additionally, while the focus was on the interaction between seismic and wind hazards, other potential threats, such as scour, flooding, or operational loads, were not explicitly modeled.

Finally, the performance of control devices like TMDs and LRBs was evaluated assuming ideal conditions, including perfect installation, consistent material properties, and no degradation over time. In real-world applications, factors such as manufacturing variability, environmental exposure, and aging could influence the long-term effectiveness of these systems. Detuning effects of the control devices were not examined in detail in this work.

3.2 Recommendations for Future Work

Building on the findings of The importance, several directions for future research are proposed to further enhance the resilience and performance of bridge structures under multi-hazard conditions. One promising area is the expanded use of artificial intelligence (AI) techniques across different stages of structural analysis and design. AI could be applied to predict structural responses under a wide variety of loading scenarios with greater speed and accuracy, providing faster insights during both design and post-event assessments. Furthermore, AI could play a major role in optimizing control systems, enabling adaptive tuning strategies that respond to changes in structural behavior during extreme events. Although not implemented in this dissertation, a hybrid Artificial Neural Network–Genetic Algorithm (ANN-GA) approach is suggested as an example of how AI could be effectively applied for optimization tasks, such as improving the design parameters of seismic isolation systems or vibration control devices. Future work could expand on these ideas, optimizing full structural systems while balancing cost, performance, and environmental impacts over the life cycle of a bridge.

Another important direction for future research is the expansion of multi-hazard considerations beyond just seismic and wind actions. Integrating additional hazards such as flooding, scour, traffic loading, and blast impacts into the multi-hazard assessment framework would allow for a more comprehensive understanding of risks affecting bridges over their service life. Developing unified fragility models that account for the cumulative effects of multiple hazards, including sequential and simultaneous occurrences, would also significantly advance the reliability and applicability of risk assessments.

Another interesting area for further investigation is the generation of artificial ground motions representative of near-fault conditions. Several simple models for the strong pulse in such ground motions are available in the literature. While such pulses are important, they are narrow-band, and lack higher frequencies present in real ground motions. It is important to develop a robust methodology to simulate broadband ground motions in the near-fault area. One potential way to achieve this is to simulate the long-period shaking using physics-based three-dimensional wave propagation analysis. Such simulations can then be infused

with high frequency components. The way the high frequency components are related to the simulated low frequency pulses and how these components are to be mixed is not very clear. A potential approach to understand this problem is to train artificial neural networks with real near-fault ground motion data.

Further research is needed into active and semi-active control strategies, which could offer more efficient and adaptive responses to multi-hazard loading compared to purely passive systems. Exploring technologies like semi-active dampers or real-time control mechanisms could open new possibilities for reducing structural responses dynamically as hazard characteristics change during an event.

Long-term performance and degradation effects should also be incorporated into future resilience assessments. Factors such as material aging, corrosion, fatigue, and cumulative damage from multiple hazard events over time could greatly influence structural capacity and control system effectiveness. Incorporating these aspects will help develop more realistic life-cycle models for bridge infrastructure.

Finally, future research should expand beyond single-bridge assessments and move toward network-level analyses. Understanding how the degradation or failure of a few critical structures could impact broader transportation systems is essential for developing truly resilient infrastructure networks. This would require multi-hazard modeling at regional scales, incorporating the interdependence and cascading effects that occur during extreme events. Overall, by combining advanced numerical modeling, AI-driven tools, and expanded multi-hazard and multi-scale perspectives, future work can significantly contribute to designing safer, more adaptable, and more sustainable bridge infrastructure that can meet the challenges of an evolving natural and built environment.

References

Ardebili, M.A.H.; Saouma, V.E. Single and multi-hazard capacity functions for concrete dams. Soil Dyn. Earthq. Eng. 2017, 101, 234–249.

Barua, U., Akhter, M. S., & Ansary, M. A. (2016). District-wise multi-hazard zoning of Bangladesh. Natural Hazards, 82(3), 1895-1918.

Bathrellos, G. D., Skilodimou, H. D., Chousianitis, K., Youssef, A. M., & Pradhan, B. (2017). Suitability estimation for urban development using multi-hazard assessment map. Science of the Total Environment, 575, 119–134.

Bessason, B., Rupakhety, R., & Bjarnason, J. Ö. (2022). Comparison and modelling of building losses in South Iceland caused by different size earthquakes. Journal of Building Engineering, 46, 103806.

Bodda, S. S. (2018). Multi-Hazard Risk Assessment of a Flood Defense Structure. Master's Theses, North Carolina State University, Raleigh, NC, USA.

D'Ayala, D.; Copping, A.; Wang, H. A conceptual model for multi-hazard assessment of the vulnerability of historic buildings. In Proceedings of the Fifth International Conference, Structural Analysis of Historical Constructions: Possibilities of Numerical and Experimental Techniques, New Delhi, India, November 9-11. 2006; pp. 121–140.

Ettouney, M. M., & Alampalli, S. (2016). Multihazard considerations in civil infrastructure. CRC Press.

Ettouney, M. M., Alampalli, S., & Agrawal, A. K. (2005). Theory of multihazards for bridge structures. Bridge Structures, 1(3), 281-291.

Ferreira, M.; Meroni, F.; Azzaro, R.; Musacchio, G.; Rupakhety, R.; Bessason, B.; Thorvaldsdottir, S.; Lopes, M.; Oliveira, C.S.; Solarino, S. What scientific information on non-structural elements seismic risk people need to know? Part 1: Compiling an inventory on damage to non-structural elements. Ann. Geophys. 2021. Series/Report no.: 3/64 (2021), Istituto Nazionale di Geofisica e Vulcanologia (INGV), 23-Jul-2021, DOI: 10.4401/ag-8412

García, H. J. J. (2010). Multi-Hazard Risk Assessment: An Interdependency Approach. Ph.D. Thesis, The University of British Columbia, Vancouver, BC, Canada.

Gautam, D., & Dong, Y. (2018). Multi-hazard vulnerability of structures and lifelines due to the 2015 Gorkha earthquake and 2017 central Nepal flash flood. Journal of Building Engineering, 17, 196–201.

Grünthal, G., Musson, R., Schwarz, J., & Stucchi, M. (1998). European Macroseismic Scale 1998. Cahiers du Centre Européen de Geodynamique et de Seismologie, Volume 15, Luxembourg.

Jami, A. M., Elias, S., Matsagar, V., & Datta, T. K. Effectiveness of distributed tuned mass dampers in seismic response control of bridge with soil-structure interaction.

Jami, M., Elias, S., Rupakhety, R., & Ólafsson, S. (2021). Seismic response mitigation of bridges with tuned mass dampers. In The 17th World Conference on Earthquake Engineering. Sendai: International Association for Earthquake Engineering.

Jami, M., Rupakhety, R., Bessason, B., & Snæbjörnsson, J. T. (2023). Multimode Vibration Control Strategies of Long-Span Bridges Subjected to Multi-hazard: A Case Study of the Runyang Suspension Bridge. Journal of Vibration Engineering & Technologies, 1-14.

Jami, M., Rupakhety, R., Elias, S., Bessason, B., & Snæbjörnsson, J. T. (2022). Recent advancement in assessment and control of structures under multi-hazard. Applied Sciences, 12(10), 5118.

Julià, P.B.; Ferreira, T.M. From single-to multi-hazard vulnerability and risk in Historic Urban Areas: A literature review. Nat. Hazards 2021, 108, 93–128.

Karaman, H. (2015). Integrated multi-hazard map creation by using AHP and GIS. Geomatics Engineering Department, Istanbul Technical University, Recent Advances on Environmental and Life Science.

Khatakho, R., Gautam, D., Aryal, K. R., Pandey, V. P., Rupakhety, R., Lamichhane, S., ... & Adhikari, R. (2021). Multi-hazard risk assessment of Kathmandu Valley, Nepal. Sustainability, 13(10), 5369.

Nassirpour, A., Galasso, C., & D'ayala, D. (2018, June). Multi-hazard physical vulnerability prioritization of school infrastructure in the Philippines. In 11th US National Conference on Earthquake Engineering (11NCEE), Los Angeles,

OpenSeesWiki. Command Manual. Retrieved from https://opensees.berkeley.edu/wiki/index.php/Command_Manual.

Pourghasemi, H. R., Gayen, A., Edalat, M., Zarafshar, M., & Tiefenbacher, J. P. (2020). Is multi-hazard mapping effective in assessing natural hazards and integrated watershed management? Geoscience Frontiers, 11(4), 1203-1217.

Pourghasemi, H. R., Gayen, A., Panahi, M., Rezaie, F., & Blaschke, T. (2019). Multi-hazard probability assessment and mapping in Iran. Science of the Total Environment, 692, 556-571.

Ravankhah, M., Schmidt, M., & Will, T. (2017). Multi-hazard disaster risk identification for World Cultural Heritage sites in seismic zones. Journal of Cultural Heritage Management and Sustainable Development, 7, 272–289.

Schwarz, J., Maiwald, H., Beinersdorf, S., & Kaufmann, C. (2018). Evaluation of the vulnerability of existing building stocks under single and Multi-Hazard impact. In 16th European Conference on Earthquake Engineering (ECEE).

Thorvaldsdottir, S., Bessason, B., & Rupakhety, R. (2021). Non-structural earthquake risk management for residential buildings. Annals of Geophysics, 64(3), SE323-SE323.

Zahrai, S. M., & Froozanfar, M. (2019). Performance of passive and active MTMDs in seismic response of Ahvaz cable-stayed bridge. Smart Structures and Systems, 23(5), 449-466.

Appendix A

Paper 1

Jami, M., Rupakhety, R., Elias, S., Bessason, B., & Snæbjörnsson, J. T. (2022). Recent Advancement in Assessment and Control of Structures under Multi-Hazard. Applied Sciences, 12(10), 5118.

applied sciences

MDPI

Review

Recent Advancement in Assessment and Control of Structures under Multi-Hazard

Matin Jami [1], Rajesh Rupakhety [1,*], Said Elias [2], Bjarni Bessason [3] and Jonas Th. Snæbjörnsson [4]

[1] Earthquake Engineering Research Centre, Faculty of Civil and Environmental Engineering, School of Engineering and Natural Science, University of Iceland, Austurvegur 2a, 800 Selfoss, Iceland; amj38@hi.is
[2] Department of Construction Management and Engineering (CME), Faculty of Engineering Technology (ET), University of Twente (UTWENTE), 7522 NB Enschede, The Netherlands; elias.rahimi@utwente.nl
[3] Faculty of Civil and Environmental Engineering, School of Engineering and Natural Science, University of Iceland, 102 Reykjavík, Iceland; bb@hi.is
[4] Department of Engineering, School of Technology, Reykjavik University, 101 Reykjavík, Iceland; jonasthor@ru.is
* Correspondence: rajesh@hi.is; Tel.: +354-5254129

Abstract: This review presents an up-to-date account of research in multi-hazard assessment and vibration control of engineering structures. A general discussion of the importance of multi-hazard consideration in structural engineering, as well as recent advances in this area, is presented as a background. In terms of performance assessment and vibration control, various hazards are considered with an emphasis on seismic and wind loads. Although multi-hazard problems in civil engineering structures are generally discussed to some extent, the emphasis is placed on buildings, bridges, and wind turbine towers. The scientific literature in this area is vast with rapidly growing innovations. The literature is, therefore, classified by the structure type, and then, subsequently, by the hazard. Main contributions and conclusions from the reported studies are presented in summarized tables intended to provide readers with a quick reference and convenient navigation to related publications for further research. Finally, a summary of the literature review is provided with some insights on knowledge gaps and research needs.

Keywords: multi-hazard; earthquake; wind; flood; hazards; hurricane; mitigation; resilience; risk assessment; bridge; building; wind turbine; control system

Citation: Jami, M.; Rupakhety, R.; Elias, S.; Bessason, B.; Snæbjörnsson, J.T. Recent Advancement in Assessment and Control of Structures under Multi-Hazard. *Appl. Sci.* **2022**, *12*, 5118. https://doi.org/10.3390/app12105118

Academic Editors: Miguel Llorente Isidro, Ricardo Castedo and David Moncoulon

Received: 21 March 2022
Accepted: 13 May 2022
Published: 19 May 2022

1. Introduction

Natural hazards, such as earthquakes and wind forces, pose a challenge for human safety and comfort. Forces generated by these natural processes can damage, or even collapse, vulnerable civil engineering structures. The risk to lives and properties posed by natural hazards increases with urbanization, where large cities and metropolitan areas get more and more densely populated. Increasing urbanization and shortage of land results in the need to build taller and more complex structures which can be more vulnerable to lateral forces created by wind and earthquakes. Effects of natural hazards on civil engineering structures is, therefore, an important field of research.

Between 1998 and 2017, natural disasters affected 4.4 billion people worldwide, caused 1.3 million casualties [1], and resulted in economic loss of 2900 billion USD. During this 20-year period, floods, storms, and earthquakes were the most frequent hazards, accounting for 43.4, 28.2, and 7.8% of all natural disasters, respectively. Although floods were the most frequent hazard during this time, earthquakes and storms have been the deadliest and the costliest, respectively. Floods and earthquakes, combined, killed nearly one million people and resulted in an economic loss of almost 2000 billion USD during this 20-year period. The frequencies, casualties, and economic losses, caused by different types of natural hazards

between 1998 and 2017, are shown in Figure 1. The numbers in Figure 1, which are based on CRED report [1], clearly show that earthquakes and storms are the most damaging natural hazards. It is interesting to note that earthquakes have killed more people than all other hazards combined.

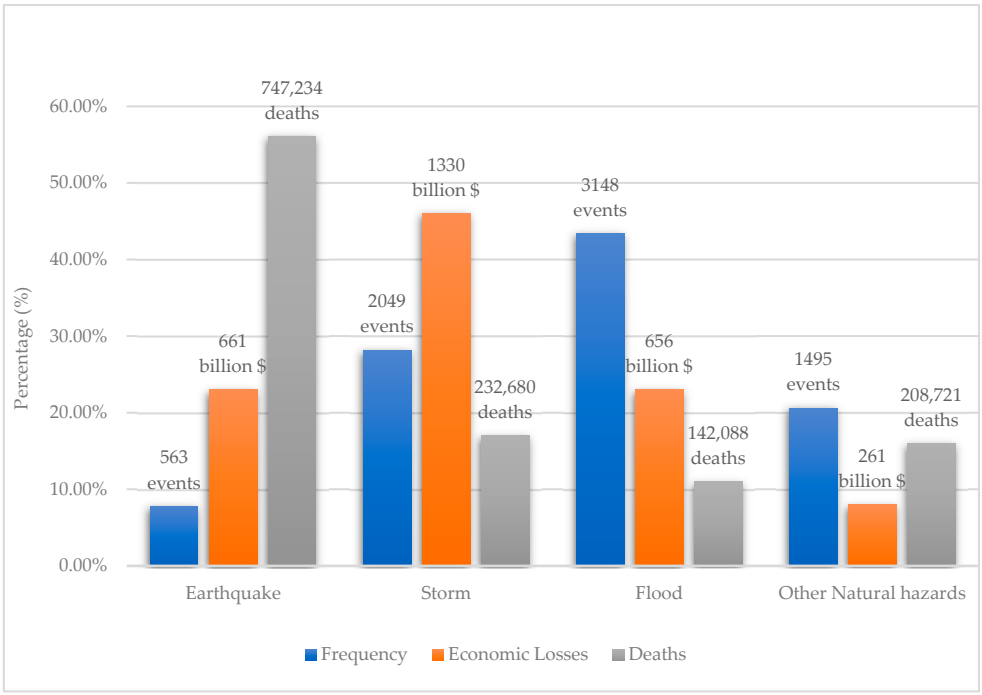

Figure 1. Frequencies of different natural hazards and their effects during 1998–2017 (based on CRED report, [1]).

Different natural processes affect structures and people in different ways. While the simultaneous occurrence of two different types of damaging hazards, such as strong wind and earthquake, is rare, some natural processes can induce secondary hazards. For example, fire and landslides are known to occur after strong earthquakes (see, for example, Ravankah et al. [2]). Moreover, a structure may be exposed to different types of natural hazards, albeit not simultaneously, during its lifetime. Therefore, it needs to be resistant to forces and damage mechanisms imposed by more than one natural process. Structures optimally designed for actions from one type of natural hazard may not necessarily be well equipped to deal with actions from all types of hazards. This leads to the need for hazard mapping, considering different types of natural processes and their interdependencies.

Consideration of multiple hazards in urban development is gaining popularity in the research community. For example, Bathrellos et al. [3] studied probabilities of incidence of floods, landslides, and earthquakes, in a specific area in Northeastern Greece, to map multiple hazards and identify areas suitable for urban development. Hicks et al. [4] explore disaster risk reduction from a multi-hazard perspective. Regional multi-hazard mapping for urban development is gaining popularity in research (e.g., [5]). Vulnerability and design of structures against multiple hazards is also gaining popularity in research. As an example, Aly [6], as well as Aly and Abburu [7], discuss some fundamental differences between wind and earthquake-resistant designs of high-rise buildings. A review of studies on the vulnerability of buildings subjected to wind and earthquake forces is presented by Indirli et al. [8]. A framework for life-cycle loss estimation in tall buildings subjected to wind and seismic forces is presented by Venanzi et al. [9]. Civil engineering infrastructure, such as dams, bridges, roads etc., are lifelines of modern society. Although multi-hazard risk assessment of infrastructure is challenging [10,11], it is an important tool to improve their safety and operability following natural disasters, which is instrumental for social resilience. Various factors affecting costs and performance of infrastructure in a multi-hazard environment is

discussed in Ettouney and Alampalli [12]. Performance and fragilities of special structures, such as dams and floodwalls exposed to multiple hazards, are studied in Ardebili and Saouma [13] and Bodda [14].

Natural events, such as wind and earthquakes, impose dynamic forces on buildings and other civil engineering structures. Damage caused by such forces depends on the dynamic properties of the structure, as well as the characteristics of the wind forces and ground motion. In most cases, structural damage is a result of excessive vibration. Vibration control, which refers to reducing oscillations of structures exposed to dynamic forces, can, therefore, be used as a protective measure. Vibration control makes use of active, passive, or hybrid secondary devices that are installed on the structure and designed/tuned/actuated for optimal reduction in structural responses such as displacement, acceleration, etc. Base-isolation, for example, has been a popular and effective protection against earthquakes (see, for example, [15–19]). Tuned mass dampers (TMD) and other supplemental damping devices of different designs and configurations have also been known to effectively reduce wind and earthquake-induced vibrations of different types of structures (see, for example, [20–22]). Vibration control systems can provide an alternative protection for existing structures where retrofitting or strengthening is considered too costly or not feasible, due to factors such as aesthetics, cultural aspects, etc. Control devices that are effective against the forces generated by one type of natural hazard might not be effective against other hazards. For example, base isolation systems, which are effective for seismic protection of structures, might cause an adverse response during strong wind [23]. Due to the uncertainties in the amplitude and frequency content of dynamic forces, induced by wind and earthquakes, and their relationship with the properties of the affected structures, consideration of a multi-hazard scenario is especially important when designing vibration control systems.

This work is an attempt to bring together and synthesize valuable information and conclusions presented in a vast body of research literature on multi-hazard effects and control of civil engineering structures. The work is based on a review and synthesis of published literature. Relevant studies were searched through scholarly databases such as Web of Science, Google Scholar, and Scopus. The keywords used for searching were "multi-hazard", "vibration-control", "seismic control", "tuned mass dampers", "seismic fragility", and "life-cycle assessment". The search results were then narrowed first by scanning the titles of articles to include only those that indicated relevance in the multi-hazard problem, addressing one or more of the criteria: (a) hazard mapping/quantification, (b) performance assessment, (c) design and/or optimization, (c) fragility assessment, (d) life-cycle and/or cost-benefit analysis, and (e) vibration control. This resulted in more than 400 articles. The Abstract and Conclusion sections of these articles were then studied to further filter out studies that did not address the multi-hazard problem. This resulted in 220 articles. The references listed in these articles were then checked to search for more relevant articles. Special attention was given to state-of-the art review studies. References listed in studies were checked in detail to search for additional relevant articles. In total, 263 articles were studied and are referenced to in this work. Among these, there are 210 journal articles, 17 books/reports, 11 theses, 14 book chapters, and 11 conference papers. These include 18 state-of-the art reviews.

Initial thematic development of the work was, first and foremost, based on the keywords listed in these articles. The keywords in these articles were extracted, and their frequencies were counted. In total, 699 unique keywords were found. Multi-word keywords were then replaced by a single word (called, here, a reduced keyword) that is representative of the scope of the work. For example, "vibration control" was reduced to "control", "risk assessment" was reduced to "risk", and so on. In some cases, such as "wind turbines", both words were retained. This resulted in 117 keywords. Similar keywords were then grouped together to identify themes/scopes. For example, "seismic", "ground motion", and "earthquakes" were placed under the theme of "Seismic". The number of occurrences of these themes were then counted, and the themes were ranked. Frequency distribution of the most frequent themes is presented in Figure 2. Some reduced keywords

with a low frequency of occurrence are therefore not considered useful in creating an overall theme of the subject being studied and are not shown in the figure. Control is the most frequent theme, and multi-hazard is the third most frequent theme. Seismic and wind loads are the most frequently considered hazards. In terms of structures, bridges, buildings, and wind turbines are frequent themes, while only a few (less than 10) occurrences of other infrastructure and lifelines were encountered. This thematic distribution of the studied articles was used to prepare the main structure of this paper, which is schematically presented in Figure 3.

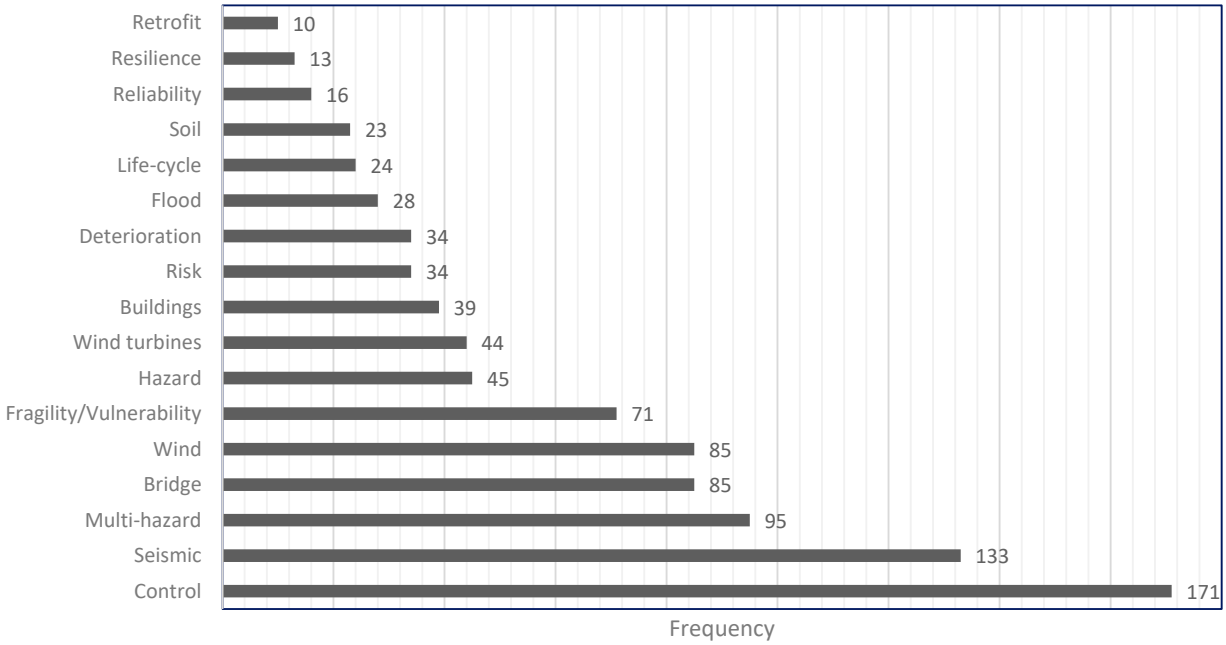

Figure 2. Frequency distribution of the most relevant themes extracted from reduced keywords.

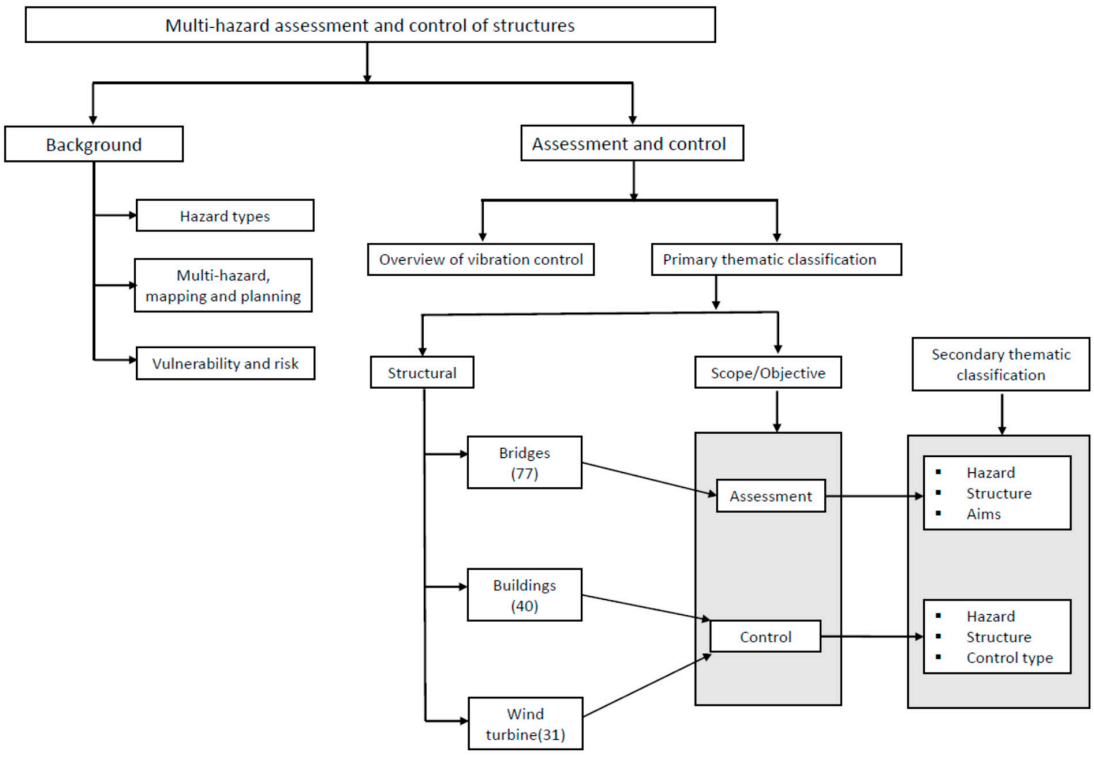

Figure 3. Schematic representation of thematic classification and organization of the paper.

Background information about different types of hazards, multi-hazard scenarios, and associated vulnerability and risk is provided in Section 2. This section is not a state-of-the-art review of these topics but rather background information for the rest of the paper (see Figure 3). The main part of the paper, which is the state-of-the-art review part of the paper, is briefly termed as assessment and control (see Figure 3). The review is based on the themes encountered in the studied literature. Topics such as fragility/vulnerability assessment, life-cycle assessment, multi-hazard assessment, and reliability assessment are covered under the assessment theme, while the control theme mainly deals with vibration suppression. As vibration control is the most dominant theme of the studied papers (see Figure 2), a brief literature review of different control systems is provided in Section 3. The review is primarily classified by two themes: namely, structure and scope of work. Bridges, buildings, and wind turbines are covered in Sections 4–6, respectively. Each of these sections is sub-divided into assessment and control sub-sections. The literature on bridges is dominated by the assessment theme, which is classified into secondary themes such as hazard type, type of bridge, and the main aims of the study. The literature on buildings and wind turbines contains several studies of multi-hazard vibration control. For each of these structures, the studies reviewed here are sub-classified into secondary themes of hazard, type of building/wind turbine, and the type of control device.

2. Risk: Hazard, Exposure, and Vulnerability

Risk related to disasters (disaster risks) can include loss of lives, disrupted economy, damages to the environment, etc. Risk is linked to the combination of hazard, physical exposure, and vulnerability of the infrastructure. The roles of each of these factors are briefly reviewed in the following sections.

2.1. Hazard

The definition of "hazard" in a broader sense is "any external or internal process or event that might degrade the performance of the system on hand" [12]. The United Nations General Assembly [24] defines hazard as "a process, phenomenon or human activity that may cause loss of life, injury or other health impacts, property damage, social and economic disruption or environmental degradation".

Natural events, such as storms, earthquakes, or floods, are well-known hazards with widespread potential to turn into disasters. While these events are mostly sudden and occur in a relatively short time window, slower processes, such as fatigue, corrosion, ageing, etc., can also impact structural performance over their life span.

Among the three elements that constitute disaster risk, hazard is the one that is mostly beyond human control. Nevertheless, a proper understanding of the occurrence frequency, spatio-temporal distribution, and intensity of the hazard is important for disaster risk reduction. Recent advances in sensing technology: data collection, processing, storage, sharing capabilities; and modelling/computational tools have improved our understanding how different hazards affect civil engineering structures. Hazards can be of different types. For example, they can be natural events, such as earthquakes, or man-made ones, such as explosions.

Different classifications of hazard have been proposed for multi-hazard studies. For example, Ettouney and Alampalli [12] discuss the classification of hazards based on Temporal, Frequency, and Newtonian characteristics. Temporal characterization distinguishes between simultaneous occurrence, segregation in time, and cascading effects. Frequency characterization distinguishes continuous processes, such as corrosion, from intermittent processes such as earthquakes. Intermittent processes can be further classified as frequent, intermediate, or rare. Newtonian characterization is another useful approach for hazard classification that is generally used in design codes. In design codes, hazards are generally quantified in terms of loads, such as wind load, earthquake load, etc. The impact of these loads can be quantified by different metrics, such as stress, deformation, etc., and are evaluated based on Newtonian mechanics. Such hazards have been termed as Newto-

nian [12]. Other processes, such as corrosion, wear and tear, fatigue, etc., are termed as non-Newtonian [12]. Natural hazards can also be classified based on their origin and the geo-atmospheric processes associated with them, such as

1. Biophysical (wildfire).
2. Atmospheric (wind or thunderstorms, lightning, hail, snow, and climate change).
3. Hydrological (drought and flood).
4. Shallow Earth Processes (erosion, subsidence and uplift, and mass movement).
5. Geophysical (volcanic eruption, tsunami, landslide, earthquake, and snow avalanche).

The idea that a structure needs to resist different types of hazards during its service life is well-established in civil engineering. For example, design codes and standards have provisions for different types of actions such as dead load, live load, wind load, seismic load, etc. Simultaneous occurrence of multiple actions is addressed in design codes through load combinations. Such recognition of multiple actions and load combinations does not encompass the real extent of multi-hazard effects and interactions. Multi-hazard generally refers to the concept where two or more hazards interact through structural performance. A multi-hazard interaction, for example, can impact risk due to a hazard when a decision regarding structural exposure and vulnerability against frequency, location, and amplitude of another hazard is made. For example, a change in design wind load and/or structural capacity can impact structural vulnerability to earthquake forces. Multi-hazard interactions may result in common or conflicting design solutions. For example, provision of structural ductility is beneficial for both blast and seismic loads.

Padgett and Kameshwar [25] present a comprehensive classification of multi-hazard combinations for bridges. Although their classification was intended for bridges, it can be generalized for most civil engineering structures, as is presented in Figure 4. Classification of hazard, according to Figure 4, helps to understand potential interactions between different hazards through their effects on structures.

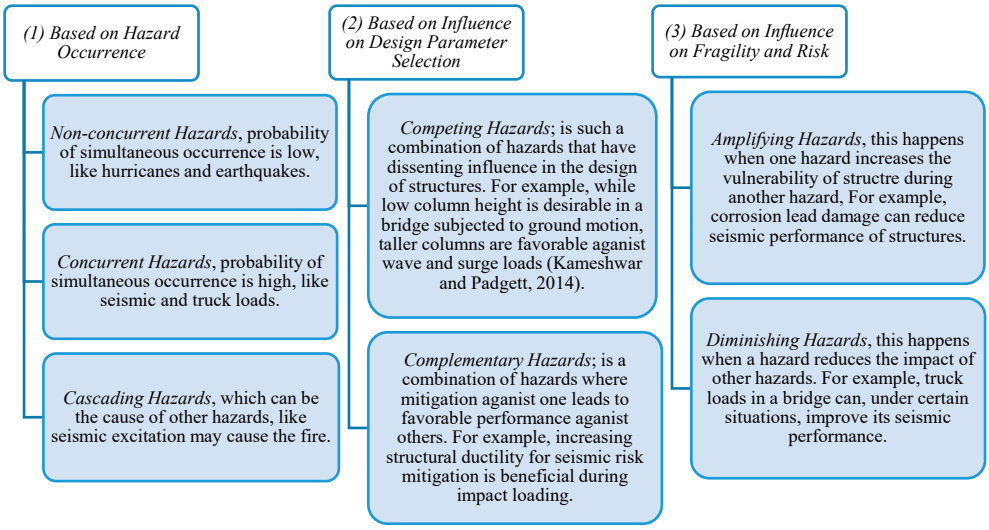

Figure 4. Classification of multi-hazard combinations [26] (modified from Padgett and Kameshwar [25]).

Multi-hazard consideration is important for structural safety and reliability. Duthinh and Simiu [27] present an interesting point regarding the traditional practice of treating different hazards independently and designing structural components based on the more demanding hazards. Taking an example of wind and earthquakes, they show that the ASCE Standard 7 provisions are not risk-consistent in the sense that, in regions affected by both strong wind and earthquakes, risks of exceedance of limit states can be up to twice as high as those in regions where only one of these hazards dominates. Kappes et al. [28] discuss the challenges of analyzing multi-hazard risk and existing frameworks to address those challenges. Zaghi et al. [29] presents the limitations of modern design codes in adequately

addressing multi-hazard risk and emphasizing the need for common nomenclature for multi-hazard design. They also mention several problems and challenges in the multi-hazard design of structures. Different aspects of multi-hazard approaches, to mitigate risk to civil engineering infrastructure, are further discussed in Gardoni and Lafave [30]. The implications of considering potential multi-hazard effects in the life cycle cost analysis of an infrastructure is addressed by Jalayer et al. [31] and Fereshtehnejad and Shafieezadeh [32].

2.2. Exposure, Multi-Hazard Mapping and Planning

In the context of disaster risk, the UNDRR (United Nations Office for Disaster Risk Reduction) defines exposure as "the situation of people, infrastructure, housing, production capacities and other tangible human assets located in hazard-prone areas" [33]. Exposure is a necessary factor for disaster risk. Exposure is one of the risk determinants that can be controlled, to some extent, by proper planning. Such decisions are, however, not feasible in cases of existing risk: for example, large cities already built-in hazardous space. Reducing exposure to multi-hazards is more challenging than if only a single hazard is considered. Urban planning, land-use policy-making, environmental protection decisions, etc., need to rely on, and benefit from, multi-hazard considerations.

Local and regional scale mapping of different types of hazards is essential in multi-hazard considerations when analyzing exposure. Although significant advancements have been made in mapping individual hazards, mapping multi-hazard is challenging due to the differences in their physical phenomena, measures of frequency/amplitude, impact on structures, etc.

Barua et al. [34] present a multi-hazard map for different districts of Bangladesh based on local historical disaster database and comparison of scenario hazard scales with those in other countries. Their study includes earthquakes, tornadoes, floods, and cyclones, which are combined through a weighing scheme. Pourghasemi et al. [35] present multi-hazard mapping of Fars Province in southern Iran. They consider floods, fires, and landslides. They test two different machine learning algorithms in predicting distribution of these hazards based on historical data, and make use of different conditioning factors such as aspect, elevation, drainage, annual mean rainfall, etc. They highlight the importance of multi-hazard mapping in land-use planning, sustainable development, and watershed management in the study region. A similar study for the western region of Iran is presented in Pourghasemi et al. [36].

For multi-hazard mapping of relatively small areas, the Analytical Hierarchy Process (AHP) has been proposed as a suitable method (see, for example, [3]). It is a class of Multi-Criteria Decision Analysis (MCA) and relies on the connection between influencing factors and hazards rather than statistics from historical databases. In this sense, the method is subjective in assigning intensities and weights of different hazards. Some examples of AHP application in multi-hazard mapping can be found in Bathrellos et al. [3], Karaman [37], and Khatakho et al. [5].

2.3. Vulnerability and Risk

Vulnerability lies within the characteristics or properties of the elements (structures) at risk, making them susceptible to impacts of hazards. The UNGA [24] defines vulnerability as "the conditions determined by physical, social, economic and environmental factors or processes which increase the susceptibility of an individual, a community, assets or systems to the impacts of hazards". The concept of vulnerability is used in a broad sense and with different meanings in different fields. Vulnerability is the risk determinant that is the most feasible one to manage/control/reduce through human action or interference. Vulnerability reduction is, therefore, one of the most effective forms of risk reduction. However, the quantification of vulnerability of civil engineering structures even to individual hazards, such as earthquakes, is a challenging task with many uncertainties (see, for example, [38–40]). In a multi-hazard scenario, the overall vulnerability can be different from the vulnerability to a single hazard, which makes the definition of vulnerability especially challenging. Its

complexity is due to the variations in structural material types, geometries, environments, exposure to hazards, usage, age, maintenance, and many other factors. Quantification of structural vulnerability to different types of hazards is a popular and growing research field. Structural vulnerability is mostly expressed in terms of fragility or vulnerability curves, which quantify, in a probabilistic sense, the chance of exceeding undesired states of damage conditioned to a given intensity of hazard. On a larger geographical scale, vulnerability classification of structures relies on general information about the structures, their usage, and exposure to hazards. Such classifications are commonly used for buildings. This method of vulnerability assessment was used by Nassirpour et al. [41] to rank school infrastructure in the Philippines, considering flood, wind, and earthquake hazards. A vulnerability assessment methodology for building, subjected to both single and multi-hazards, was presented by Schwarz et al. [42]. By following the principles of the European Macroseismic Scale 1998 (EMS-98, [43]), they developed vulnerability tables for different hazards (wind, flood, and earthquake). A framework to create multi-dimensional vulnerability models from vulnerability tables was also presented and applied in a few test cities in Germany. Gautam and Dong [44] present multi-hazard damage to structures in central Nepal caused by the 2015 Gorkha Earthquake and the 2017 Chhatiune Khola flash flood. A conceptual model for multi-hazard assessment of the vulnerability of historic buildings is presented by Ayala et al. [45] (2006) with an example application considering English parish churches. A comprehensive review of single and multi-hazard vulnerability and risk in historic urban areas is presented by Julia and Ferreira [46]. They also present interesting examples of the use of multi-hazard risk analysis in historic urban areas.

An interesting methodology for the risk evaluation of offshore structures subjected to ocean waves, wind, and ground motion is proposed by Bhartia and Vanmarcke [47]. They consider failure probabilities under short-term loads, as well as overall risks, due to loads of different intensities. Their results show that limit states (of failure), structural characteristics, as well as features of different types of loads interact in a complex way, controlling the relative importance of different hazards. Aggravating effects in a multi-hazard scenario are clearly demonstrated in their case-study example of ambient (ever-present wind over the sea) and seismic loads. An outline for identification of different hazards and subsequent risk assessment has been introduced by the United States Federal Emergency Management Agency, 1997, [48]. Ciurean et al. [49] present a comprehensive report of recent developments in multi-hazard processes and risks related to research, policy, and industry.

3. Vibration Control of Structures

Most of the structural damage caused by natural forces can be attributed to excessive vibrations. For static loads, vulnerability reduction can be achieved at the design stage by increasing stiffness and/or strength of structural elements. For existing structures, retrofitting strategies also aim to improve strength and/or stiffness of the structural elements. Similar strategies can also be used for dynamic forces such as wind and earthquakes, but newer and potentially more cost-effective solutions emerging in the scientific research are percolating to practical applications. These new solutions are not necessarily about increasing structural stiffness and/or strength. They fundamentally rely on changing the dynamic properties of the structures to make them less vulnerable to natural forces. This can, contrary to retrofitting in the traditional sense, even make the overall structure more flexible. A notable example is the well-established base-isolation technology for reducing earthquake-induced vibrations of buildings and bridges. Vibration reduction, also known as vibration control, makes use of different types of devices installed on the structure to reduce vibrations caused by different types of forces. While base-isolation, supplemental damping, and bracing systems to increase lateral stiffness and ductility have been researched and used for a long time, newer control strategies that rely mainly on dynamic devices installed on the primary structure are emerging. Depending on their mode of operation and need for external energy and/or internal feedback mechanism,

vibration control devices can be broadly classified as passive, active, semi-active, or hybrid systems. The following list gives a few examples of these different types of control systems

1. Passive: energy dissipation, base isolation, tuned mass dampers (TMD), and tuned liquid dampers.
2. Active: adaptive control, active bracing, and active mass damping.
3. Semi-active: semi-active energy dissipation, semi-active isolation, and semi-active mass damping.
4. Hybrid: hybrid bracing and hybrid mass damping.

Detailed definitions and the basic theory behind these different classes of structural control devices can be found in the seminal work of Housner et al. [50]. Most of these control concepts have been extensively investigated, and many of these systems are already installed in different types of structures.

Passive control devices are the ones most frequently used, as they don't require external energy supply. Tuned mass dampers (TMDs), fluid viscous dampers (FVD), tuned liquid dampers (TLD), and seismic base isolation (BI) are the most popular passive control systems.

An early state-of-the art review of seismically base isolated buildings is presented by Kelly [51], Buckle and Mayes [52], and Jangid and Datta [17]. They discuss different types of base isolation systems and summarize findings of the contemporary literature about their performance in seismic response control in addition to presenting a parametric study of crucial design parameters for optimal reduction in seismic performance. Patil and Reddy [19] present a state-of-the-art review of base isolation systems in seismic response mitigation. They focus on design code provisions for isolated structures and discuss effects of soft-soil and near-fault ground motions. Kunde and Jangid [18] present a state-of-the art review of seismically isolated bridges and identify some knowledge gaps in the contemporary literature. Soong and Spencer [21] discuss different types of supplemental energy dissipation systems, including passive and active dampers for structural control. They provide an informative timeline of the development of these control technologies and describe the state-of-the-art review in the context of seismic-resistant design and the retrofitting of structures. A review on the behavior of structures with passive control systems exposed to seismic loads is presented by Buckle [52]. This study discusses the advantages of passive systems in a seismic design and provides several examples of their successful applications. It also highlights limitations of passive control, considering uncertainties in seismic forces and limit states induced by unexpectedly demanding events, and points towards the need for better practical guidelines in their design and implementation.

A comprehensive review on the response control of structures by TMDs is reported by Elias and Matsagar [22]. They review different configurations of dampers, involving one or more tuned masses, installed at different locations of the structure. They report that the findings in the literature support effectiveness of TMDs in reducing wind and earthquake-induced vibrations of certain types of structures. They also identify potential obstacles, such as robustness and reliability, across different levels of loading, especially those that exceed the yield limit, causing inelastic deformations in the structure.

A state-of-the-art review of different types of structural control systems was presented by Saeed et al. [53]. Their review includes different control technologies that can be classified as active, semi-active, passive, or hybrid. They conclude that control systems have a huge potential and importance in modern structures.

Symans and Constantinou [54] present a detailed review of semi-active control systems for the seismic protection of structures and conclude that different solutions, such as stiffness control devices, electrorheological dampers, friction control dampers, fluid viscous dampers, etc., have the potential of practical feasibility in full-scale structures. Spencer and Nagarajaiah [55] also report on the state of the art of semi-active technologies for structural vibration control. They report that smart damping devices, such as Magnetorheological (MR) dampers, appear to combine desirable features of both passive and active control solutions, and they offer a viable control solution against wind and earthquake forces.

The literature on control of structures against wind or seismic forces is vast. As explained above, the state-of-the-art and recent findings, in the structural control of different kinds, have been presented in many works. As an example, one of the first comprehensive state-of-the-art reviews of structural control systems was published more than two decades ago by Housner et al. [50]. Although performance of different control schemes in a single hazard scenario, such as wind or an earthquake, is well-known and summarized in many works, structural control in multi-hazard scenario is an emerging field of research. While some interesting research has been published in this field, there is a lack of an overview of the state-of-the-art, ongoing progress, and future directions. Most of the literature in this regard is on seismic and/or wind-induced response reduction in bridges, buildings, and wind turbines. These topics are dealt with separately in the following sections.

4. Multi-Hazard Assessment and Control of Bridges

Bridges are lifelines of modern society. They are vulnerable to different hazards, as evidenced by several failures in the past. On 19 August 2016, a suspension railway bridge in Tolten-Chile collapsed due to train-induced vibrations [56]. On 29 August, during hurricane Katrina, the Twin Spans Bridge connecting New Orleans to Slidell, Louisiana, United States, suffered extensive damage [57]. On 21 July 2003, Kinzua Bridge in Pennsylvania, United States, was hit by a tornado with 100 mph (45 m/s) winds and collapsed [58]. On 14 January 2003, Sgt. Aubrey Cosens VC Memorial Bridge in Ontario, Canada collapsed [59] due to fatigue-induced failure of the steel hanger rods supporting the deck. On 17 January 1995, a bridge on Hanshin Expressway in Kobe, Japan collapsed during the Kobe Earthquake [60]. During the Loma Prieta earthquake in 1989, two famous bridges (Cypress Street Viaduct and San Francisco—Oakland Bay Bridge) in California, USA were heavily damaged [61,62]. The collapse of these two bridges killed forty-one persons.

Safety and reliability of bridges are controlled by a diverse set of factors related to the structural form, function, maintenance, and the hazards they are exposed to. Multi-hazard consideration is, therefore, emerging as an important topic in bridge design and safety assessment. Some of the recent advancements in this field are discussed in the following.

4.1. Multi-Hazard Assessment of Bridges

To understand the consequences of multi-hazard effects on the safety/reliability of bridges, a wide range of experimental and analytical studies have been conducted and reported in the literature. One of the most studied scenarios is the interaction of earthquakes with other actions: for example, traffic-load. The interaction between these hazards, when they occur concurrently, can be amplifying or diminishing (see, for example, [63,64]). Cascading effects might also be observed when bridges, partly damaged by earthquakes, are exposed to traffic (see, for example, [65,66]). Ground shaking and liquefaction induced by earthquakes can have complex interactions in bridge response, both amplifying and diminishing (see, for example, [67,68]). Another multi-hazard scenario for bridges is the simultaneous occurrence of high waves and hurricane surge (see, for example, [69–73]). Another scenario is foundation scour due to floods, which may increase the seismic vulnerability of bridges [74–81].

Aging and corrosion of bridge elements causes structural deterioration that can amplify the effect of other hazards, such as earthquakes or wind forces. The effect of deterioration caused by seismic and traffic loads on a reinforced concrete bridge is addressed by Deco and Frangopol [82], Choe et al. [83], Kumar et al. [84], Choe et al. [85], Gardoni and Rosowsky [86], Choine et al. [87], Rokneddin et al. [88], and Biondini et al. [89]. Long-span bridges are especially sensitive to wind forces, but they can also be affected by seismic excitation. A framework for the assessment of vulnerability of long-span bridges subjected to multi-hazards (seismic and wind excitation) is presented by Martin et al. [90]. A summary of recent advances in wind effects on long-span bridges, with a multi-hazard perspective, is presented in Chen et al. [91]. Studies on the multi-hazard effects and performance of bridges is summarized in Table 1.

Table 1. A summary of published works on bridges subjected to multi-hazard.

Type of Hazards	Reference	Type of Bridge Structure	Aims	Main Contribution/Conclusion
Multi-Hazard in General				
	Ettouney et al. [10]	Different type of bridges	Theoretical formulation	A general theory and application to structural analysis, design, life cycle costing, risk assessment, and health monitoring
Earthquake and Wind				
	Martina et al. [90]	suspension bridges	Fragility analysis	Fragility surfaces for bridges exposed to multiple extreme events
Earthquake and Corrosion				
	Choe et al. [85],	RC bridges	Fragility assessment	Fragility increment functions of corroding bridge columns and their application in life cycle cost and risk analysis
	Choe et al. [83]	RC bridges	Fragility assessment	Probabilistic models of seismic demand and fragility of corroding bridges, and their application in reliability analysis
	Kumar et al. [84]	RC bridges	Life-cycle cost assessment	Probabilistic model of life cycle cost considering cumulative damage, case studies highlighting dominance of cumulative seismic damage in reducing reliability
	Gardoni and Rosowsky [86]	RC bridges	Fragility assessment	Fragility increment functions and an example application
	Ghosh and Padgett [92]	Multi-span continuous highway bridges,	Fragility assessment	Time-dependent seismic fragility curves considering ageing and deterioration
	Simon et al. [93]	RC bridges	Fragility assessment	Losses in strength and stiffness due to corrosion have marginal effects on seismic fragilities of the case-study bridge
	Alipour, et al. [94]	Highway RC bridges	Fragility assessment	Time-dependent fragility models, and life cycle cost assessment
	Ghosh and Padgett [95]	Highway RC bridges	Loss assessment	Probabilistic framework for loss assessment using component-level cost estimates, case studies highlighting the impacts of deterioration
	Sung and Su [96]	RC bridge columns	Capacity, fragility, and loss estimation	Capacity models of deteriorated columns and resulting time-dependent fragility curves
	Zhong et al. [97]	RC bridges	Fragility assessment	Component and system level fragility curves, and a case study application
	Ou et al. [98]	RC bridges	Long-term performance assessment	Case studies of several bridges highlighting the need to increase design PGA to ensure adequate performance through the design life

Table 1. *Cont.*

Type of Hazards	Reference	Type of Bridge Structure	Aims	Main Contribution/Conclusion
	Rokneddin et al. [88]	RC bridges	Reliability assessment	Time-dependent fragility models of selected bridge classes, and an algorithm for reliability assessment, case studies highlight the need for accounting network-level importance in retrofit programs
	Akiyama and Frangopol [99]	RC bridges	Life cycle reliability assessment	Modelling spatial variability of rebar corrosion using X-ray, and a computational framework to incorporate corrosion hazard in seismic reliability
	Biondini et al. [89]	RC bridges	Life cycle performance assessment	Probabilistic modelling of capacities of corroding critical sections, case study highlighting undesirable effect of corrosion in seismic performance
	Ni et al. [100]	RC bridges	Modelling impact of corrosion on seismic performance	A new constitutive model for corroded reinforcing steel, and fragility curves at various time intervals
	Shekhar et al. [101]	Highway bridges	Study of realistic corrosion models and their impacts on life-cycle cost.	Framework for seismic life cycle costs from generic corrosion measures, case study demonstrating relevance of pitting versus uniform corrosion model
	Ghosh and Sood [102]	Highway bridges	Assessment of time-dependent capacities and more realistic degradation models in seismic fragility	A methodology for seismic fragility assessment incorporating pitting corrosion models and time-dependent capacity models, predictive equations for seismic reliability assessment over the service life
	Thanapol et al. [103]	RC bridges	Incorporation of spatial distribution of corrosion in seismic reliability assessment	Models to estimate steel weight loss at critical sections using spatially variable corrosion images using X-ray technology, followed by an illustrative case study
	Rao et al. [104]	RC bridges	Fragility assessment	Framework for seismic vulnerability assessment of deteriorating RC columns
	Alipour and Shafei [105]	Highway bridges	Network resilience assessment	Computational framework for risk assessment which emphasis on effect of ageing in seismic resilience
	Ghosh et al. [106], Rokneddin et al. [107],	Highway bridge network	Network reliability analysis	Methodology to estimate bridge fragilities using deterioration parameters from instrumented bridges in the network, and an example application
Earthquake and Floods				
	Dong and Frangopol [78]	Highway bridges	Life-cycle performance assessment	A framework for time-variant loss and resilience assessment, and effect of climate change

Table 1. *Cont.*

Type of Hazards	Reference	Type of Bridge Structure	Aims	Main Contribution/Conclusion
Earthquake, Floods, and Ground-Failures				
	Gehl and D'Ayala [108]	RC bridges	Fragility assessment	A Bayesian Networks based fragility surfaces
Earthquake and Scour				
	Wang et al. [109]	RC bridge	Estimation of load factors	Risk-consistent load factors based on case studies
	Wang et al. [77]	Bridge with pile foundation	Performance assessment	Experimental evidence for effects of scour depth on failure mechanisms of piers and piles
	Guo et al. [110]	RC bridges	Study of the effect of time-dependent scour hazard on seismic vulnerability	Fragility surfaces and time-dependent loss estimates with two case study bridges
	Alipour et al. [111]	RC bridges	Investigation of scour-load modification factors in seismic assessment	Reliability-based load and resistance factors
	Yilmaz [112]	Highway bridges	Risk and reliability assessment	Framework for risk assessment and uncertainty analysis
	Chandrasekaran and Banerjee [113]	RC Bridge	Optimal retrofitting	An approach for retrofit optimization, case study results showing that column jacketing is effective
	Guo and Chen [114]	RC bridges	Lifecycle assessment	A framework for lifecycle assessment, case study highlighting the need for a time-sensitive assessment
	Han et al. [74]	High-rise pile cap foundation	Performance assessment	Seismic capacity of foundation is significantly affected by scour depth
Earthquake, Scour, and Corrosion				
	Dong et al. [115]	RC bridges	Sustainability assessment	A framework for time-varying sustainability, and an illustrative application
	Asadi et al. [116]	RC bridge	Performance assessment	A framework for performance assessment and life cycle cost analysis
Earthquake, Scour, Corrosion, and Traffic-Load				
	Deco and Frangopol [117]	Highway bridges	Risk assessment	Framework for time-varying total risk and effect of structural redundancy
Earthquake, Scour, Corrosion, Wind, Traffic-Load and Liquefaction				
	Banerjee et al. [118]	Highway bridges	Review	Summary of state-of-the-art in different aspects of resilience: loss assessment, recovery actions, and maintenance
Earthquakes, Corrosion, Surge, and Wave				
	Kameshwar, and Padgett [119]	RC Coastal bridges	Lifecycle risk assessment and design	Object oriented consequence-based framework for lifecycle risk assessment considering structural deterioration

Table 1. *Cont.*

Type of Hazards	Reference	Type of Bridge Structure	Aims	Main Contribution/Conclusion
Earthquakes, Wind, Tsunami, Flood, Surge, and Wave				
	Gidaris et al. [120]	Highway bridges	Review	Summary of the state-of-the art in fragility and restoration models
Earthquakes, Blast and Fire				
	Echevarria, et al. [121]	Concrete-filled fiber reinforced polymer tube (CFFT) bridge columns	Experimental investigation of lightly reinforced CFFT columns	Experimentally validated design equations and a formulation for displacement-based seismic design including fire protection provisions
Earthquake and traffic loads				
	Sun et al. [122]	Bridges in Southeast Coastal areas of China	Study combinations of seismic and truck loads	Probabilistic methodology to combine earthquake and truck load
	Ghosh et al. [64]	Highway bridges	Studying effect of traffic loads on seismic reliability	Framework for joint fragility assessment, fragility surfaces, and case study application
Earthquake, Traffics-Load, and Deterioration				
	Deco and Frangopol [82]	Bridges in general	Life-cycle risk assessment	Probabilistic framework for life cycle risk assessment of spatially distributed group of bridges
Earthquakes and High water				
	Nikellis et al. [123]	Generic	Risk assessment	An analysis of risk metrics, stakeholder perceptions, and impact on retrofit strategies
Traffic Load and Wind				
	Chen et al. [91]	Long span bridges	Review	Summary of recent advances.
Wave and Storm Surge				
	Ataei, and Padgett [70]	Costal RC bridges	Capacity assessment	Probabilistic approach to global limit state capacities
	Ataei et al. [71]	Costal RC bridges	Fragility assessment	Development of surrogate models and uncertainty analysis

4.2. Multi-Hazard Vibration Control of Bridges

Although the literature on multi-hazard vulnerability and the risk assessment of bridges is vast, retrofitting bridges for multi-hazard protection is an emerging research topic that is gaining interest. Chandrasekaran and Banerjee [113] consider three different retrofit strategies to enhance bridge performance under the multi-hazard. Wang et al. [76] note that increasing foundation stiffness can be more beneficial than increasing foundation depth in reducing seismic vulnerability of bridges subjected to scour. Sung and Su [96] use time-dependent fragility curves to estimate the total direct costs of neutralized RC bridges as a function of ground motion intensity and service time and propose it as a tool to time retrofit campaigns. Benefits of the base isolation system, as a control/retrofit solution for increasing the reliability of steel bridges subjected to ground shaking and liquefaction hazards, is demonstrated in Wang et al. [124].

To the best of our knowledge, multi-hazard considerations in vibration control of bridges has not been reported in the literature yet.

5. Multi-Hazard Assessment and Vibration Control of Buildings

This section provides a review of studies related to building response to multi-hazard, with emphasis on wind and seismic forces. Building response to seismic forces is controlled

by various factors, such as amplitude, duration, and frequency content of ground shaking. It also depends on the characteristics of the building itself and the underlying soil properties. Larger earthquakes produce ground motion with more energy at lower frequencies than smaller earthquakes. Large earthquakes are hazardous to all buildings, particularly to those that have natural frequencies close to the dominant frequency of ground shaking. Such a phenomenon has been observed in ground shaking and building response during past earthquakes (see, for example, [125,126]).

Wind loads contain energy at lower frequencies than seismic ground motions. Low to mid-rise buildings with relatively low vibration frequencies are therefore more susceptible to dynamic vibrations caused by seismic forces than those due to wind. Wind forces on such structures could, nevertheless, have undesired effects on components such as roofs, windows, chimneys, etc. Damage to light and improperly anchored roofs in low-rise buildings during strong wind is, therefore, of concern. In super tall buildings, wind generally induces stronger displacement response than earthquakes. Seismic loads, however, might excite higher vibration modes of such structures, resulting in high floor accelerations. This implies low inter-story drift and, therefore, lower risk of structural damage, but high floor acceleration can be critical for non-structural components [6,9,127,128]. From a structural point of view, wind loads are, therefore, critical for flexible structures, while seismic loads are more demanding on stiff structures. Occupant comfort and safety is another consideration when it comes to the response of buildings to wind and earthquake loads. Large floor accelerations can cause discomfort to occupants and may pose a safety threat due to moving objects. Floor accelerations in tall buildings are typically higher during moderate to strong ground shaking than during strong wind. Strong seismic loading is, however, typically less frequent than strong wind. From a serviceability point of view, wind action is, therefore, more critical for occupant comfort. Multi-hazard effects in buildings also need to be looked at from a life-cycle cost perspective and accumulation of damage due to multiple events: for example, wind response of a structure partially damaged by an earthquake or vice versa. Damage accumulation and fatigue due to repeated loading from frequent actions, such as moderate to strong wind, is also an important consideration.

5.1. Multi-Hazard Assessment of Buildings

Huang [129] provides a comprehensive account of the dynamic responses of high-rise buildings under multiple hazards. It presents performance assessment methods and case study investigations using high-rise buildings in Hong Kong. Various factors, such as seismic source-to-site distance, recurrence periods, ground shaking amplitude, building height, damping ratios, properties of wind forces, etc., were considered in the analysis. The results show that seismic loads result in a higher floor acceleration response and lateral forces but weaker torsional forces and a lower displacement response compared to wind forces. The height of the buildings was also found to be an important parameter, with wind response being more sensitive to variation in height than seismic response. The results also showed that wind response is more strongly influenced by the level of damping of the building than seismic response.

Chen [127], and Rasigha and Neeladharan [128] report differences in the seismic and wind responses of mid-rise to high-rise buildings. Aly [6], as well as Aly and Abburu [7] present the responses of tall buildings subjected to wind and seismic forces. In these assessments, two tall buildings (76-story and 54-story) were considered for finite element analysis. They found that ground motions excite higher vibration modes in buildings, resulting in lower inter-story drift than wind forces, but higher floor accelerations last for a shorter time. Wind actions are, therefore, critical from an occupant comfort and serviceability consideration. Tall structures designed for strong wind may possess an adequate capacity against moderate ground shaking, but they might suffer non-structural losses due to high floor accelerations. A framework for life-cycle loss estimation, of non-structural damage in tall buildings under wind and seismic loads, is presented by Venanzi et al. [9]. Their framework assumes that damaged structures are restored to their

original condition after each hazardous event. Hazardous events are not simultaneous, and small maintenance costs are neglected. Their results show that for drift-dependent damages, wind forces are costlier than seismic forces. Seismic forces are costlier, in terms of non-structural damage, due to high floor accelerations. These observations are consistent with results reported in other studies, [6,7]. Antoun [130] studied the performance of a 74-story building located in Miami to evaluate the expected losses associated with a multi-hazard (wind and earthquake forces). Performance-based approaches were used for earthquake, wind, and hurricane forces. Monetary losses corresponding to structural and non-structural damage, as well as occupant discomfort, was estimated. They report that losses due to façade damage are dominant for high probabilities of exceedance, whereas structural damage becomes dominant at lower probabilities of exceedance.

Zhang et al. [131] proposed a framework for the damage risk assessment of high-rise buildings exposed to wind and seismic forces acting separately and concurrently. They used recorded earthquake and wind data, over a period of about 47 years, to estimate hazard curves for wind and seismic forces as well as copula-based bi-hazard surfaces. They then performed multi-hazard fragility assessment and estimated damage probabilities for separate and concurrent hazard models. Their results show that damage probability due to bi-hazards dominates the total damage probability in most damage states. They highlight the need for multi-hazard considerations in the design and evaluation of tall structures subjected to wind and seismic forces. Damage risk assessment and cost-benefit analysis of mitigation strategies, in residential buildings subjected to hurricane and seismic forces, are discussed in Li [132], giving a comprehensive overview of factors that are important in risk assessment, as well as their roles and impacts in hazard mitigation. The risk-cost-benefit framework, based on life-cycle and scenario-case analyses presented by Li [132], incorporate probabilistic modelling of hazards, structural fragility, and expected costs during different service intervals.

Multi-hazard consideration in performance-based engineering and performance-based design criteria, addressing wind and seismic forces, has been researched extensively in the literature. Chiu and Chock [133] present one of the first applications of the performance-based engineering approach in a multi-hazard scenario.

A probabilistic framework, for the multi-hazard risk assessment of reinforced concrete buildings subjected to seismic and blast loads, is discussed in Asprone et al. [134]. Annual risk of structural collapse, considering seismic action and progressive collapse due to blast forces, is formulated in this study. They conclude that the Monte Carlo (MC) simulation is suitable for calculating probability of progressive collapse, as well as for identifying critical blast scenarios.

Multi-hazard performance of different structural elements, such as columns, frames, plates, walls, etc., have been reported by many researchers. Resistance capacity of precast segmental columns, subjected to impact and cyclic loading, is investigated experimentally by Zhang et al. [135]. They found that, compared to monolithic columns, segmental columns (precast segments joined together, often with pre-stressed tendons) possess better ductility and sustain lower residual drift under cyclic loading. Under impact loading, segmental columns were found to have better self-centering capacity. They showed that shear resistance of such columns can be significantly improved by introducing concrete shear keys, but it comes at some cost related to stress-concentration and potential damage to concrete segments.

Rachel [136] presents a methodology for the resilience assessment of buildings subjected to seismic, wind, fire, and various post-earthquake scenarios. The results of this study showed that post-earthquake fire resilience in moment frame buildings is independent of seismic damage if frame connections are intact. The results also showed that multi-hazard resilience of moment resisting frame buildings can be improved by strengthening and/or fire-proofing gravity columns. Shin [137] presents multi-hazard performance evaluation matrices for retrofitted non-ductile reinforced concrete buildings subjected to seismic and blast loads.

Unnikrishnan and Barbato [138] investigated multi-hazard interaction on the performance of low-rise wood-frame buildings. Chulahawat and Mahmoud [139] present an algorithm to optimize building systems, with suspended floor slabs subjected to wind and seismic hazards, and observe that tall buildings with such systems are effectively optimized for both wind and seismic forces without a significant trade-off on performance to individual hazards.

5.2. Multi-Hazard Vibration Control of Buildings

Vibration control of buildings subjected to wind or seismic forces has been extensively researched. Vibration control of buildings in multi-hazard scenarios is, on the other hand, not as extensively studied. Some important studies in this area are summarized in Table 2. Performance assessment of control devices, their optimization, and life-cycle cost analysis are the main issues that have been addressed in these studies. Wind and earthquake forces are the most considered hazard in these studies. Most of these studies present traditional control systems such as passive TMDs, passive energy dissipation devices, viscous fluid dampers, multiple tuned passive TMDs, etc. Some recent advances in this area include inerter-based TMDs (Djerouni et al., [140]; Djerouni et al. [141]; Djerouni et al. [142]; Marian and Giaralis [143]), glass curtain wall TMDs (Bedon and Amadio [144]), and sliding floor isolators (Chulahwat and Mahmoud [139]; Mahmoud and Chulahwat [145]).

Table 2. A summary of published works on vibration control of the building subjected to multi-hazard.

Reference	Hazards	Structure	Control System	Main Contribution/Conclusion
Cao et al. [146]	Wind, Blast and Earthquake.	5- and 39-story benchmark buildings	Semi-active friction damper	A new controller called input space dependent controller (ISDC) which is more effective than sliding mode controller.
Mahmoud and Chulahwat [145] and Chulahqat and Mahmoud [139]	Wind and Earthquake	7- and 10-story steel frame buildings.	Sliding floor isolation.	A modified covariance matrix adaptation evolution strategy (CMA-ES) algorithm
Dogruel and Dargush [147]	Wind and Earthquake	16-story steel frame building.	Passive Energy Dissipation (PED).	Methodology for optimal life-cycle cost estimation, and optimal design of retrofitting
Shalom et al. [148]	Wind and Earthquake	76-storey building.	Multiple Tuned Mass Dampers (MTMDs)	Life-cycle cost-based optimization framework
Roy and Matsagar [149,150]	Wind and Earthquake	9-, 20-, and 25-story steel frame buildings.	PED	Optimal retrofits for earthquakes result in undesirable effects on wind response, and vice versa; damper performance is sensitive to site-specific hazard
Chapain and Aly [151]	Wind and Earthquake	76-story building	Viscous Fluid Dampers (VFDs)	VFDs are effective in multi-hazard control
Elias and Matsagar [152]	Wind and Earthquake	76-story and 20-story building	TMD	Optimally placed and tuned TMDs are effective in multi-hazard control
Elias et al. [153]	Wind and Earthquake	76-story building	MTMDs	MTMDs with equal stiffness are better than those with equal masses.
Bedon and Amadio [144]	Earthquake and blast	4-storey steel frame building	Glass curtain walls as passive TMD	Glass curtain walls can be utilized as distributed TMD for vibration mitigation
Gong [154]	Wind and Earthquake	5-,9-, and 20-story buildings	Variable Friction Cladding Connection (VFCC)	Experimental and analytical evidence demonstrating effectiveness of VFCC.

6. Multi-Hazard Assessment and Control of Wind Turbines

The tall and slender geometry of wind turbine towers and the large top mass of the turbine and the rotors make wind turbines sensitive to both wind and seismic excitation.

Wind and seismic loading have been the two most common environmental actions considered for research on the performance assessment of wind turbine towers. For offshore turbines, wave loading is also an important factor.

6.1. Multi-Hazard Assessment of Wind Turbines

Maryam [155], as well as Maryam and Gardoni [156] highlight the importance of multi-hazard consideration in site-selection and design of wind turbines. They present a multi-hazard probabilistic framework to evaluate the structural reliability of offshore wind turbines. Considering wind and seismic action, their results show that annual probabilities of failure are higher when seismic action is considered. Comparing two identical wind turbines, one in the Gulf of Mexico and the other off the coast of California, they conclude that, although the latter location is more favorable in terms of power production, annual probabilities of failure are higher due to higher seismicity. Avossa et al. [157] present a Monte Carlo simulation-based framework for the estimation of multi-hazard fragility curves of wind turbine structures. They provide an example application of the framework, to derive failure probabilities of a prototype wind turbine structure, conditioned on wind velocity and peak ground acceleration for different operational states of the turbine. Their results show that aerodynamic damping plays an important role in the seismic fragility. Fragility in an operational state, for seismic action in the fore-aft direction, increases with wind speed up to the rated wind speed, after which it starts to decrease. When the rotor is operating at the rated condition or is parked, the probability of failure is larger than 50% and the peak ground acceleration exceeds about 70% of the acceleration of gravity. Campo and Estrada [158] present similar conclusions regarding the importance of aerodynamic damping, stating that, while wind action is more damaging at the operational state, seismic action can be more threatening when the rotor is parked. Katsanos et al. [159] report, for a 5 MW offshore wind turbine, that seismic action contributes more than wind and wave action to structural demands such as base moment and tower-top displacement. They also report on the fragility of sensitive equipment located in the nacelle, which are found to be prone to severe damage at moderate ground shaking intensity. Zuo et al. [160] investigated the fragility of a prototype 5 MW offshore wind turbine structure subjected to aerodynamic forces and wave loading. They considered different operational states of the rotor and derived fragility curves for both the supporting tower and the rotor blades. Their results show that, when the wind speed is between the cut-in and cut-out range, exceedance probability of the blade failure is much higher than that of the tower failure. They also highlight the impact of aerodynamic damping in reducing wind-induced vibrations of the tower. Zuo et al. [161] studied the effect of soil structure interaction (SSI) on the 5 MW offshore prototype model. Their results show that the fore-aft displacement demand on the tower is significantly affected by SSI. Asareh et al. [162] investigated the fragility of a 5 MW wind turbine prototype subjected to wind and seismic action. Their results show that failure due to exceedance of tower-tip displacement and rotation is more likely than yielding or buckling of the tower.

6.2. Multi-Hazard Vibration Control of Wind Turbines

Vibration control of wind turbine structures, subjected to the combined actions of wind, waves, and earthquake ground motions, is extensively reported in the literature. These studies are mostly aimed at the optimization and performance assessment of control systems. A summary of relevant studies on the vibration control of wind turbine structures subjected to multi-hazard is presented in Table 3.

Table 3. A summary of published works on vibration control of wind turbine structures subjected to multi-hazard.

Reference	Hazard	Structure	Control System	Main Contribution/Conclusion
Xie et al. [163]	Wind and Waves	Offshore, 5 MW, barge-type floating	TMD on the platform	Modelling of drivetrain dynamics, optimization of TMD parameters, simulation results confirm the importance of drivetrain dynamics and that TMDs are effective in vibration suppression
He et al. [164]	Wind and Waves	Offshore, 5 MW, barge-type floating	TMD in the nacelle	TMDs are effective in reducing standard deviation of tower-top displacements, with upto 50% reduction for TMD mass ratio of 2%
Stewart and Lackner [165]	Wind and Waves	Offshore, 5 MW, monopile	TMD in the nacelle	Misalignment of wind and wave load significantly increases base moment in the side-side direction, which can be reduced by 40% with a TMD
Zhao et al. [166]	Wind, wave and seismic	Offshore, scaled model, monopile	TMD in the nacelle	Shake table tests for modal identification and estimation of aerodynamic damping, results show that TMDs are effective in reducing seismic response, effectiveness increases with rotation speed of blades
Sun and Jahangiri [167]	Misaligned wind-wave and seismic	Offshore, 5 MW, monopile	Pendulum tuned TMD(PTMD) in the nacelle	PTMDs are slightly more effective than two linear TMDs with equivalent mass and their stroke is smaller
Sun and Jahangiri [168]	Misaligned wind-wave	Offshore, 5 MW, monopile	PTMD in the nacelle	Increase in fatigue life due to PTMD is 50% higher than that due to dual linear TMDs.
Sun et al. [169]	Misaligned wind-wave and Seismic load	Offshore, 5 MW, monopile	PTMD in the nacelle	PTMD is more robust than dual linear TMDs, and with a mass ratio of 2% reduction in short-term fatigue damage is reduced by up to 90%.
Hu et al. [170]	Wind and waves	Offshore, 5 MW, barge-type floating	Tune Mass Damper Inerter (TMDI) in the nacelle	TMDI are more effective than TMD but there is a trade-off between fore-aft load control and device stroke; performance superior to TMD can be achieved for comparable device stroke
Zuo et al. [171]	Wind and Waves	Offshore, 5 MW, monopile	MTMD	MTMDs are efficient and robust in reducing the out-of-plane vibration of blades and the tower in parked and operational conditions.
Zuo et al. [172]	Wind, Waves and Earthquake	Offshore, 5 MW, monopile	MTMD	Multi-mode control using MTMDs are more efficient than STMDs in multi-hazard scenarios
Hussan et al. [173]	Wind, Waves and Earthquake	Offshore 5 MW with standard jacket foundation	MTMD	SSI plays important role in MTMD performance, often over-estimates it
Altay et al. [174]	Wind and Earthquake	Onshore 5 MW	TMD and Tuned Liquid Column Damper TLCD	Resonant tower vibrations at lower wind speeds are effectively reduced by TMDs and TLCDs, transient tower vibrations at higher wind speeds are less effectively reduced, only nominal control of seismic-induced vibrations
Colwell and Basu [175]	Wind and Waves	Offshore, monopile	TLCD	TLCDs are effective in reducing peak response and increasing fatigue life
Dezvareh et al. [176]	Wind and Waves	Offshore, 5 MW, jacket type	Tuned Liquid Column Gas Dampers (TLCGD)	Effective in reducing nacelle displacement and acceleration protecting the tower structure and acceleration-sensitive nacelle devices

Table 3. *Cont.*

Reference	Hazard	Structure	Control System	Main Contribution/Conclusion
Bargi et al. [177]	Wind, Waves and Earthquake	Offshore, 5 MW, jacket tupe	Tuned Liquid Column Gas Dampers (TLCGD)	Nacelle acceleration is better controlled under wind-wave excitation while nacelle displacement is better controlled under seismic load, heavier devices are more efficient but less robust against detuning
Sun [178]	Wind, Waves and Earthquake	Offshore, 5 MW, monopile	Semi-active TMD (S-TMD)	Semi-active TMDs are more efficient than passive TMDs
Hemmati and Oterkus [179]	Wind, Waves and Earthquake	Offshore, 5 MW, monopile	S-TMD	S-TMD provide better control than passive TMDs with as much as 4 times lower mass
Rezaee and Aly [180]	Wind, Wave, Earthquake,	Land based and offshore, 5 MW	MR damper-used as S-TMD and with outer bracing	The dampers are efficient in reducing strong vibrations and its duration during seismic loading. While displacement control starts early during ground shaking, acceleration control lags behind by a few seconds
Xie and Aly [181]	Wind and Earthquake	Various	TMD, TLD, VD, A-TMD, S-TMD, and TLCD,	A state-of-the-art review for evaluating the performance of the various types of control systems
Rezaee and Aly [182]	Wind and Waves	On-land 5 MW	TMD, TLCD, VD, and tuned sloshing damper (TSD)	Comparative study of different dampers show that VDs are the most robust, and that TSDs are effective at a wider range of frequencies
Zhao et al. [183]	Wind and Earthquake	On-land, 1.5 MW	Scissor-Jack Braced Viscous Damper (VD-SJB)	VD-SJB is effective and practical in reducing vibrations, seismic-vibration reduction in fore-aft direction is lower in operating condition than in parked condition
Zuo et al. [184]	Wind, Waves and Earthquake	Various	Various	State-of-the-art review
Rahman et al. [185]	Wind, Waves and Earthquake	Various	Various	Literature review

7. Concluding Remarks

This work is an attempt to summarize a vast body of research literature on multi-hazard effects on structures and their vibration mitigation measures. Aspects such as performance assessment, fragility modelling, life-cycle cost assessment, and vibration control in a multi-hazard scenario are covered. The main emphasis is on wind and seismic actions on major infrastructure, such as bridges, buildings, and wind turbine towers. Understanding of multi-hazard scenarios in a probabilistic sense and mapping them out for engineering design is an evolving field. At a local scale, multi-hazard mapping using the Analytical Hierarchy Process (AHP) is gaining popularity. Multi-hazard mapping at regional scales remains a challenging task, demanding more research on unifying frameworks that standardize and unify existing probabilistic hazard assessment methods used for different natural actions. Some recent advances in multi-hazard vulnerability of buildings include multi-dimensional vulnerability modelling. Fragility modelling in a multi-hazard scenario is still a growing field of knowledge, with many unresolved questions. Some examples of such unresolved issues relate to: (i) definition of intensity measures of hazards that might interact with each other, resulting in overall effects that are of different nature than those due to individual hazards; (ii) definition of joint probabilities of exceedances of intensities of different types of hazards; (iii) lack of empirical data on actual damage recorded in multi-hazard scenario, etc.

Multi-hazard assessment of bridges is a widely studied topic. Most studies in this area focus on seismic loads and corrosion. Other effects, such as wind loads, scour, traffic loads, etc., in conjunction with seismic loads, have also been reported. Published literature on

bridges subjected to seismic loads and corrosion focus on the fragility assessment. Multi-hazard effects in such assessments are generally modelled through fragility increment functions, damage accumulation, and time-dependent fragility curves. Probabilistic load and resistance factors, for different hazards affecting bridges, is another widely reported research theme. In most cases, such fragility models are intended for a life-cycle cost and risk analysis. While multi-hazard fragility of individual bridges is widely reported, there are only a few deals with bridge networks. More research is needed in capacity modelling, risk metrics, stakeholder perceptions, and load combinations.

The literature on multi-hazard effects on buildings is dominated by wind and earthquake loads. Performance-based engineering frameworks, progressive damage and collapse modelling, resilience assessment, multi-hazard performance evaluation metrices, etc., are some of the recent advances in damage risk and life cycle cost analysis of buildings. A variety of control systems such as passive TMDs, passive energy dissipation devices, viscous fluid dampers, multiple tuned passive TMDs, have been investigated in control of buildings subjected to wind and seismic forces. Some recent advances in this area seem promising and practically appealing: for example, sliding floor isolators, glass curtain wall TMDs, and variable friction cladding connections [VFCC]. While the literature on the vibration control of buildings subjected to wind or seismic action is vast, relatively few studies have addressed their simultaneous occurrence. More research is needed on probabilistic treatment of multi-hazard load cases, robustness of control devices against uncertainties in structural properties, as well as loading the feasibility of control from a life-cycle perspective.

Seismic and wind forces are the two most considered environmental actions in the performance assessment and vibration control of wind turbine structures. Wave action, and effects of wave/wind misalignment in offshore wind turbines is also widely researched. Multi-hazard probabilistic framework for reliability assessment of offshore wind turbines is relatively well-established. Monte Carlo simulation-based frameworks for multi-hazard fragility assessment are recently emerging. For land-based wind turbines, several studies have highlighted the role of aerodynamic damping in response to combined action of wind and earthquakes. Most of the published work on vibration control of wind turbines focuses on structural fragility of the supporting tower. Offshore wind turbines subjected to wind and waves is the most investigated scenario. The most reported control device is passive TMD placed on the nacelle, although use of TMD on the platform of a barge-type floating turbine has also been reported to be effective. Most of the studies conclude that control devices are effective in reducing multi-hazard fragility. Recent advances in multi-hazard control of wind turbines include interesting innovations such as braced viscous dampers, and semi-active control systems. Effect of ground motion variability on control performance is an area that needs to be studied better. Control performance against impulsive loads caused by, for example, near-fault ground motions (see, for example, Rupakhety et al. [186]; Elias et al. [187]; Sigurðsson et al. [188], Jami et al. [189]) also need to be investigated better. In addition, fragility of rotor blades and effects of drivetrain dynamics need more attention.

In most of structural vibration control studies reported in the literature, the structure is assumed to remain elastic, which may not be realistic in extreme loading conditions. Inelastic deformations of the structure can result in de-tuning of the control device resulting in lower performance. Control optimization and performance assessment of yielding structures subjected to multi-hazard scenarios, as well as damage accumulation due to multiple hazards occurring over the useful life of a structure, need to be investigated and better understood to facilitate practical applications of control systems in actual engineering projects.

Author Contributions: M.J.: Conceptualization, research, literature study, writing, and review; R.R.: methodology, writing, and review; S.E.: review; B.B.: writing, and review; J.T.S.: writing and review. All authors have read and agreed to the published version of the manuscript.

Funding: Matin Jami is supported by a doctoral grant from the University of Iceland. RR acknowledges support from the University of Iceland Research Fund.

Institutional Review Board Statement: Not applicable.

Informed Consent Statement: Not applicable.

Data Availability Statement: Not applicable.

Conflicts of Interest: The authors declare no conflict of interest.

References

1. Wallemarq, P.; Below, R.; McClean, D. *UNISDR and CRED Report: Economic Losses, Poverty & Disasters (1998–2017)*; United Nations Office for Disaster Risk Reduction: Geneva, Switzerland, 2018; Available online: https://www.cred.be/sites/default/files/CRED_Economic_Losses_10oct.pdf (accessed on 12 May 2022).
2. Ravankhah, M.; Schmidt, M.; Will, T. Multi-hazard disaster risk identification for World Cultural Heritage sites in seismic zones. *J. Cult. Herit. Manag. Sustain. Dev.* **2017**, *7*, 272–289. [CrossRef]
3. Bathrellos, G.D.; Skilodimou, H.D.; Chousianitis, K.; Youssef, A.M.; Pradhan, B. Suitability estimation for urban development using multi-hazard assessment map. *Sci. Total Environ.* **2017**, *575*, 119–134. [CrossRef] [PubMed]
4. Hicks, A.; Barclay, J.; Chilvers, J.; Armijos, M.T.; Oven, K.; Simmons, P.; Haklay, M. Global mapping of citizen science projects for disaster risk reduction. Citizen Science: Reducing Risk and Building Resilience to Natural Hazards. *Front. Earth Sci.* **2020**, *7*, 226. [CrossRef]
5. Khatakho, R.; Gautam, D.; Aryal, K.R.; Pandey, V.P.; Rupakhety, R.; Lamichhane, S.; Liu, Y.C.; Abdouli, K.; Talchabhadel, R.; Adhikari, R. Multi-hazard risk assessment of Kathmandu Valley, Nepal. *Sustainability* **2021**, *13*, 5369. [CrossRef]
6. Aly, A.M. Design of buildings for wind and earthquake. In Proceedings of the World Congress on Advances in Civil, Environmental, and Materials Research (ACEM'14), Busan, Korea, 24–28 August 2014.
7. Aly, A.M.; Abburu, S. On the design of high-rise buildings for multihazard: Fundamental differences between wind and earthquake demand. *Shock. Vib.* **2015**, *2015*, 148681. [CrossRef]
8. Indirli, M.; Valpreda, E.; Panza, G.; Romanelli, F.; Lanzoni, L.; Teston, S.; Rossi, G. Natural multi-hazard and building vulnerability assessment in the historical centers: The examples of San Giuliano di Puglia (Italy) and Valparaiso (Chile). In Proceedings of the 7th European Commission Conference "SAUVEUR", Heritage, Prague, 31 May 2006.
9. Venanzi, I.; Lavan, O.; Ierimonti, L.; Fabrizi, S. Multi-hazard loss analysis of tall buildings under wind and seismic loads. *Struct. Infrastruct. Eng.* **2018**, *14*, 1295–1311. [CrossRef]
10. Ettouney, M.M.; Alampalliz, S.; Agrawal, A.K. Theory of multihazards for bridge structures. *Bridge Struct.* **2005**, *1*, 281–291. [CrossRef]
11. García, H.J. J. Multi-Hazard Risk Assessment: An Interdependency Approach. Ph.D. Thesis, The University of British Columbia, Vancouver, BC, Canada, 2010.
12. Ettouney, M.M.; Alampalli, S. *Multihazard Considerations in Civil Infrastructure*; Taylor & Francis Group: Abingdon, UK, 2017; IRBS: 9781482208320.
13. Ardebili, M.A.H.; Saouma, V.E. Single and multi-hazard capacity functions for concrete dams. *Soil Dyn. Earthq. Eng.* **2017**, *101*, 234–249. [CrossRef]
14. Bodda, S.S. Multi-Hazard Risk Assessment of a Flood Defense Structure. Master's Theses, North Carolina State University, Raleigh, NC, USA, 2018.
15. Bessason, B.; Haflidason, E. Recorded and Numerical Strong Motion Response of a Base-Isolated Bridge. *Earthq. Spectra* **2004**, *20*, 309–332. [CrossRef]
16. Jónsson, M.H.; Bessason, B.; Haflidason, E. Earthquake response of a base-isolated bridge subjected to strong near-fault ground motion. *Soil Dyn. Earthq. Eng.* **2010**, *30*, 447–455. [CrossRef]
17. Jangid, R.S.; Datta, T.K. ; Datta, T.K. Seismic behavior of base isolated buildings: A state-of-the art-review. *Proc. ICE Struct. Build. Inst. Civ. Eng.* **1995**, *110*, 186–203. [CrossRef]
18. Kunde, M.C.; Jangid, R.S. Seismic behavior of isolated bridges: A state-of-the-art review. *Electron. J. Struct. Eng.* **2003**, *3*, 140–170.
19. Patil, S.J.; Reddy, G.R. State of art review—Base isolation systems for structures. *Int. J. Emerg. Technol. Adv. Eng.* **2012**, *2*, 438–453.
20. Buckle, I.G. Passive control of structures for seismic loads. In Proceedings of the 12th world conference on earthquake engineering, Auckland, New Zealand, 30 January–4 February 2000; pp. 2825–2838.
21. Soong, T.T.; Spencer, B.F. Supplemental energy dissipation: State-of-the-art and state-of-the-practice. *Eng. Struct.* **2002**, *24*, 243–259. [CrossRef]
22. Elias, S.; Matsagar, V. Research developments in vibration control of structures using passive tuned mass dampers. *Annu. Rev. Control* **2017**, *44*, 129–156. [CrossRef]
23. Henderson, P.; Novak, M. Response of base-isolated buildings to wind loading. *Earthq. Eng. Struct. Dyn.* **1989**, *18*, 1201–1217. [CrossRef]
24. Available online: https://reliefweb.int/report/world/hazard-definition-and-classification-review (accessed on 12 May 2022).
25. Padgett, J.E.; Kameshwar, S. Supporting Life Cycle Management of Bridges through Multi-Hazard Reliability and Risk Assessment. In *Multi-Hazard Approaches to Civil Infrastructure Engineering*; Springer: Berlin/Heidelberg, Germany, 2016; pp. 41–58.

26. Kameshwar, S.; Padgett, J.E. Multi-hazard risk assessment of highway bridges subjected to earthquake and hurricane hazards. *Eng. Struct.* **2014**, *78*, 154–166. [CrossRef]
27. Duthinh, D.; Simiu, E. Safety of structures in strong winds and earthquakes: Multihazard considerations. *J. Struct. Eng.* **2010**, *136*, 330–333. [CrossRef]
28. Kappes, M.S.; Keiler, M.; von Elverfeldt, K.; Glade, T. Challenges of analyzing multi-hazard risk: A review. *Nat. Hazards* **2012**, *64*, 1925–1958. [CrossRef]
29. Zaghi, A.E.; Padgett, J.E.; Bruneau, M.; Barbato, M.; Li, Y.; Mitrani-Reiser, J.; McBride, A. Establishing common nomenclature, characterizing the problem, and identifying future opportunities in multihazard design. *J. Struct. Eng.* **2016**, *142*, H2516001. [CrossRef]
30. Gardoni, P.; LaFave, J.M. Multi-Hazard Approaches to Civil Infrastructure Engineering: Mitigating Risks and Promoting Resilence. In *Multi-Hazard Approaches to Civil Infrastructure Engineering*; Springer: Berlin/Heidelberg, Germany, 2016; pp. 3–12.
31. Jalayer, F.; Asprone, D.; Prota, A.; Manfredi, G. Multi-hazard upgrade decision making for critical infrastructure based on life-cycle cost criteria. *Earthq. Eng. Struct. Dyn.* **2011**, *40*, 1163–1179. [CrossRef]
32. Fereshtehnejad, E.; Shafieezadeh, A. A multi-type multi-occurrence hazard lifecycle cost analysis framework for infrastructure management decision making. *Eng. Struct.* **2018**, *167*, 504–517. [CrossRef]
33. Available online: https://www.un-spider.org/risks-and-disasters/disaster-risk-management#:~{}:text=Exposure%20is%20defined%20as%20%E2%80%9Cthe,of%20assets%20in%20an%20area (accessed on 12 May 2022).
34. Barua, U.; Akhter, M.S.; Ansary, M.A. District-wise multi-hazard zoning of Bangladesh. *Nat. Hazards* **2016**, *82*, 1895–1918. [CrossRef]
35. Pourghasemi, H.R.; Gayen, A.; Edalat, M.; Zarafshar, M.; Tiefenbacher, J.P. Is multi-hazard mapping effective in assessing natural hazards and integrated watershed management? *Geosci. Front.* **2020**, *11*, 1203–1217. [CrossRef]
36. Pourghasemi, H.R.; Gayen, A.; Panahi, M.; Rezaie, F.; Blaschke, T. Multi-hazard probability assessment and mapping in Iran. *Sci. Total Environ.* **2019**, *692*, 556–571. [CrossRef]
37. Karaman, H. Integrated Multi-Hazard Map Creation by Using AHP and GIS. In *Recent Advances on Environmental and Life Science*; Geomatics Engineering Department, Istanbul Technical University: Istanbul, Turkey, 2015.
38. Bessason, B.; Rupakhety, R.; Bjarnason, J.Ö. Comparison and modelling of building losses in South Iceland caused by different size earthquakes. *J. Build. Eng.* **2022**, *46*, 103806. [CrossRef]
39. Thorvaldsdottir, S.; Bessason, B.; Rupakhety, R. Non-structural earthquake risk management for residential buildings. *Ann. Geophys.* **2021**, *64*, SE323. [CrossRef]
40. Ferreira, M.; Meroni, F.; Azzaro, R.; Musacchio, G.; Rupakhety, R.; Bessason, B.; Thorvaldsdottir, S.; Lopes, M.; Oliveira, C.S.; Solarino, S. What scientific information on non-structural elements seismic risk people need to know? Part 1: Compiling an inventory on damage to non-structural elements. *Ann. Geophys.* 2021. [CrossRef]
41. Nassirpour, A.; Galasso, C.; D'ayala, D. Multi-hazard physical vulnerability prioritization of school infrastructure in the Philippines. In Proceedings of the 11th US National Conference on Earthquake Engineering (11NCEE), Los Angeles, CA, USA, 25–29 June 2018; pp. 25–29.
42. Schwarz, J.; Maiwald, H.; Beinersdorf, S.; Kaufmann, C. Evaluation of the vulnerability of existing building stocks under single and Multi-Hazard impact. In Proceedings of the 16th European Conference on Earthquake Engineering (ECEE), Thessaloniki, Greece, 18–21 June 2018.
43. Grünthal, G.; Musson, R.; Schwarz, J.; Stucchi, M. *European Macroseismic Scale 1998*; Cahiers du Centre Européen de Geodynamique et de Seismologie: Luxembourg, 1998; Volume 15.
44. Gautam, D.; Dong, Y. Multi-hazard vulnerability of structures and lifelines due to the 2015 Gorkha earthquake and 2017 central Nepal flash flood. *J. Build. Eng.* **2018**, *17*, 196–201. [CrossRef]
45. D'Ayala, D.; Copping, A.; Wang, H. A conceptual model for multi-hazard assessment of the vulnerability of historic buildings. In Proceedings of the Fifth International Conference, Structural Analysis of Historical Constructions: Possibilities of Numerical and Experimental Techniques, New Delhi, India, 9–11 November 2006; pp. 121–140.
46. Julià, P.B.; Ferreira, T.M. From single-to multi-hazard vulnerability and risk in Historic Urban Areas: A literature review. *Nat. Hazards* **2021**, *108*, 93–128. [CrossRef]
47. Bhartia, B.K.; Vanmarcke, E.H. *Multi-Hazard Risk Analysis: Case of a Simple Offshore Structure*; National Center for Earthquake Engineering Research: Taipei, Taiwan, 1988; p. 80.
48. United States Federal Emergency Management Agency. *Multi-Hazard Identification and Risk Assessment: The Cornerstone of the National Mitigation Strategy*; Federal Emergency Management Agency: Washington, DC, USA, 1997.
49. Ciurean, R.; Gill, J.; Reeves, H.J.; O'Grady, S.; Aldridge, T. Review of Multi-Hazard Research and Risk Assessments. 2018. Available online: https://nora.nerc.ac.uk/id/eprint/524399/ (accessed on 12 May 2022).
50. Housner, G.W.; Bergman, L.A.; Caughey, T.K.; Chassiakos, A.G.; Claus, R.O.; Masri, S.F.; Skelton, R.E.; Soong, T.T.; Spencer, B.F.; Yao, J.T. Structural control: Past, present and future. *J. Eng. Mech. Am. Soc. Civ. Eng. ASCE* **1997**, *123*, 897–971. [CrossRef]
51. Kelly, J.M. Aseismic base isolation: Review and bibliography. *Soil Dyn. Earthq. Eng.* **1986**, *5*, 202–216. [CrossRef]
52. Buckle, I.G.; Mayes, R.L. Seismic isolation: History, application, and performance—A world view. *Earthq. Spectra* **1990**, *6*, 161–201. [CrossRef]
53. Saeed, T.E.; Nikolakopoulos, G.; Jonasson, J.-E.; Hedlund, H. A state-of-the-art review of structural control systems. *J. Vib. Control* **2013**, *21*, 919–937. [CrossRef]

54. Symans, M.D.; Constantinou, M.C. Semi-active control systems for seismic protection of structures: A state-of-the-art review. *Eng. Struct.* **1999**, *21*, 469–487. [CrossRef]
55. Spencer, B.F.; Nagarajaiah, S. State of the art of structural control. *J. Struct. Eng. Am. Soc. Civ. Eng. ASCE* **2003**, *129*, 845–856. [CrossRef]
56. List of Bridge Failures. Wikipedia. Available online: https://en.wikipedia.org/wiki/List_of_bridge_failures (accessed on 12 May 2022).
57. Okeil, A.M.; Cai, C.S. Survey of short-and medium-span bridge damage induced by Hurricane Katrina. *J. Bridge Eng.* **2008**, *13*, 377–387. [CrossRef]
58. Leech, T. The collapse of the Kinzua Viaduct: A combination of design oversight and material fatigue left a century-old railroad bridge vulnerable to an F-1 tornado. *Am. Sci.* **2005**, *93*, 348–354. [CrossRef]
59. Biezma, M.V.; Schanack, F. Collapse of steel bridges. *J. Perform. Constr. Facil.* **2007**, *21*, 398–405. [CrossRef]
60. Mylonakis, G.; Syngros, C.; Gazetas, G.; Tazoh, T. The role of soil in the collapse of 18 piers of Hanshin Expressway in the Kobe earthquake. *Earthq. Eng. Struct. Dyn.* **2006**, *35*, 547–575. [CrossRef]
61. Hanks, T.C.; Brady, A.G. The Loma Prieta earthquake, ground motion, and damage in Oakland, Treasure Island, and San Francisco. *Bull. Seismol. Soc. Am.* **1991**, *81*, 2019–2047. [CrossRef]
62. Nims, D.K. Collapse of the Cypress Street Viaduct as a result of the Loma Prieta Earthquake. No. UCB/EERC-89/16. 1991. Available online: https://trid.trb.org/view/337611 (accessed on 12 May 2022).
63. Kartal, H.; Soyluk, K. Dynamic Behaviour of a Cable-Stayed Bridge under Earthquake and Traffic Loads. In Proceedings of the 10th International Congress on Advances in Civil Engineering, Middle East Technical University, Ankara, Turkey, 17–19 October 2012.
64. Ghosh, J.; Caprani, C.C.; Padgett, J.E. Influence of traffic loading on the seismic reliability assessment of highway bridge structures. *J. Bridge Eng.* **2014**, *19*, 04013009. [CrossRef]
65. Franchin, P.; Pinto, P.E. Allowing traffic over mainshockdamaged bridges. *J. Earthq. Eng.* **2009**, *13*, 585–599. [CrossRef]
66. Terzić, V.; Stojadinović, B. Traffic Load Capacity of a Bridge Damaged in an Earthquake. 2009. Available online: https://www.caee.ca/10CCEEpdf/2010EQConf-001221.pdf (accessed on 12 May 2022).
67. Wang, Z.; Due~nas-Osorio, L.; Padgett, J.E. Seismic response of a bridge–soil–foundation system under the combined effect of vertical and horizontal ground motions. *Earthq. Eng. Struct. Dyn.* **2013**, *42*, 545–564. [CrossRef]
68. Moshirabadi, S.; Soltani, M.; Maekawa, K. Seismic interaction of underground RC ducts and neighboring bridge piers in liquefiable soil foundation. *Acta Geotech.* **2015**, *10*, 761–780. [CrossRef]
69. Ataei, N.; Stearns, M.; Padgett, J.E. Response sensitivity for probabilistic damage assessment of coastal bridges under surge and wave loading. Transportation Research Record. *J. Transp. Res. Board* **2010**, *2202*, 93–101. [CrossRef]
70. Ataei, N.; Padgett, J.E. Limit state capacities for global performance assessment of bridges exposed to hurricane surge and wave. *Struct. Saf.* **2013**, *41*, 73–81. [CrossRef]
71. Ataei, N.; Padgett, J.E. Fragility surrogate models for coastal bridges in hurricane prone zones. *Eng. Struct.* **2015**, *103*, 203–213. [CrossRef]
72. Ataei, N.; Padgett, J.E. Influential fluid–structure interaction modelling parameters on the response of bridges vulnerable to coastal storms. *Struct. Infrastruct. Eng.* **2015**, *11*, 321–333. [CrossRef]
73. Anarde, K.A.; Kameshwar, S.; Irza, J.N.; Nittrouer, J.A.; LorenzoTrueba, J.; Padgett, J.E.; Sebastian, A.; Bedient, P.B. Impacts of hurricane storm surge on infrastructure vulnerability for an evolving coastal landscape. *Nat. Hazards Rev.* **2018**, *19*, 04017020. [CrossRef]
74. Han, Z.; Ye, A.; Fan, L. Effects of riverbed scour on seismic performance of high-rise pile cap foundation. *Earthq. Eng. Eng. Vib.* **2010**, *9*, 533–543. [CrossRef]
75. Banerjee, S.; Ganesh Prasad, G. Seismic risk assessment of reinforced concrete bridges in flood-prone regions. *Struct. Infrastruct. Eng.* **2013**, *9*, 952–968. [CrossRef]
76. Wang, Z.; Due~nas-Osorio, L.; Padgett, J.E. Influence of scour effects on the seismic response of reinforced concrete bridges. *Eng. Struct.* **2014**, *76*, 202–214. [CrossRef]
77. Wang, S.C.; Liu, K.Y.; Chen, C.H.; Chang, K.C. Experimental investigation on seismic behavior of scoured bridge pier with pile foundation. *Earthq. Eng. Struct. Dyn.* **2015**, *44*, 849–864. [CrossRef]
78. Dong, Y.; Frangopol, D.M. Probabilistic time-dependent multihazard life-cycle assessment and resilience of bridges considering climate change. *J. Perform. Constr. Facil.* **2016**, *30*, 04016034. [CrossRef]
79. Yilmaz, T.; Banerjee, S. Impact spectrum of flood hazard on seismic vulnerability of bridges. *Struct. Eng. Mech.* **2018**, *66*, 515–529.
80. Yilmaz, T.; Banerjee, S.; Johnson, P.A. Performance of two real-life California bridges under regional natural hazards. *J. Bridge Eng.* **2016**, *21*, 04015063. [CrossRef]
81. Yilmaz, T.; Banerjee, S.; Johnson, P.A. Uncertainty in risk of highway bridges assessed for integrated seismic and flood hazards. *Struct. Infrastruct. Eng.* **2018**, *14*, 1182–1196. [CrossRef]
82. Deco, A.; Frangopol, D.M. Life-cycle risk assessment of spatially distributed aging bridges under seismic and traffic hazards. *Earthq. Spectra* **2013**, *29*, 127–153. [CrossRef]
83. Choe, D.E.; Gardoni, P.; Rosowsky, D.; Haukaas, T. Seismic fragility estimates for reinforced concrete bridges subject to corrosion. *Struct. Saf.* **2009**, *31*, 275–283. [CrossRef]
84. Kumar, R.; Gardoni, P.; Sanchez-Silva, M. Effect of cumulative seismic damage and corrosion on the life-cycle cost of reinforced concrete bridges. *Earthq. Eng. Struct. Dyn.* **2009**, *38*, 887–905. [CrossRef]

85. Choe, D.E.; Gardoni, P.; Rosowsky, D. Fragility increment functions for deteriorating reinforced concrete bridge columns. *J. Eng. Mech.* **2010**, *136*, 969–978. [CrossRef]
86. Gardoni, P.; Rosowsky, D. Seismic fragility increment functions for deteriorating reinforced concrete bridges. *Struct. Infrastruct. Eng.* **2011**, *7*, 869–879. [CrossRef]
87. Choine, M.N.; O'Connor, A.; Padgett, J.E. A seismic reliability assessment of reinforced concrete integral bridges subject to corrosion. *Key Eng. Mater.* **2013**, *569*, 366–373. [CrossRef]
88. Rokneddin, K.; Ghosh, J.; Due~nas-Osorio, L.; Padgett, J.E. Bridge retrofit prioritization for ageing transportation networks subject to seismic hazards. *Struct. Infrastruct. Eng.* **2013**, *9*, 1050–1066. [CrossRef]
89. Biondini, F.; Camnasio, E.; Palermo, A. Lifetime seismic performance of concrete bridges exposed to corrosion. *Struct. Infrastruct. Eng.* **2014**, *10*, 880–900. [CrossRef]
90. Martin, J.; Alipour, A.; Sarkar, P. Fragility surfaces for multi-hazard analysis of suspension bridges under earthquakes and microbursts. *Eng. Struct.* **2019**, *197*, 109169. [CrossRef]
91. Chen, S.; Zhou, Y.; Wu, J.; Chen, F.; Hou, G. Research of long-span bridge and traffic system subjected to winds: A system and multi-hazard perspective. *Int. J. Transp. Sci. Technol.* **2017**, *6*, 184–195. [CrossRef]
92. Ghosh, J.; Padgett, J.E. Aging considerations in the development of time-dependent seismic fragility curves. *J. Struct. Eng.* **2010**, *136*, 1497–1511. [CrossRef]
93. Simon, J.; Bracci, J.M.; Gardoni, P. Seismic response and fragility of deteriorated reinforced concrete bridges. *J. Struct. Eng.* **2010**, *136*, 1273–1281. [CrossRef]
94. Alipour, A.; Shafei, B.; Shinozuka, M. Performance evaluation of deteriorating highway bridges located in high seismic areas. *J. Bridge Eng.* **2011**, *16*, 597–611. [CrossRef]
95. Ghosh, J.; Padgett, J.E. Probabilistic seismic loss assessment of aging bridges using a component-level cost estimation approach. *Earthq. Eng. Struct. Dyn.* **2011**, *40*, 1743–1761. [CrossRef]
96. Sung, Y.C.; Su, C.K. Time-dependent seismic fragility curves on optimal retrofitting of neutralised reinforced concrete bridges. *Struct. Infrastruct. Eng.* **2011**, *7*, 797–805. [CrossRef]
97. Zhong, J.; Gardoni, P.; Rosowsky, D. Seismic fragility estimates for corroding reinforced concrete bridges. *Struct. Infrastruct. Eng.* **2012**, *8*, 55–69. [CrossRef]
98. Ou, Y.C.; Fan, H.D.; Nguyen, N.D. Long-term seismic performance of reinforced concrete bridges under steel reinforcement corrosion due to chloride attack. *Earthq. Eng. Struct. Dyn.* **2013**, *42*, 2113–2127. [CrossRef]
99. Akiyama, M.; Frangopol, D.M. Long-term seismic performance of RC structures in an aggressive environment: Emphasis on bridge piers. *Struct. Infrastruct. Eng.* **2014**, *10*, 865–879. [CrossRef]
100. Ni Choine, M.; Kashani, M.M.; Lowes, L.N.; O'Connor, A.; Crewe, A.J.; Alexander, N.A.; Padgett, J.E. Nonlinear dynamic analysis and seismic fragility assessment of a corrosion damaged integral bridge. *Int. J. Struct. Integr.* **2016**, *7*, 227–239. [CrossRef]
101. Shekhar, S.; Ghosh, J.; Padgett, J.E. Seismic life-cycle cost analysis of ageing highway bridges under chloride exposure conditions: Modelling and recommendations. *Struct. Infrastruct. Eng.* **2018**, *14*, 941–966. [CrossRef]
102. Ghosh, J.; Sood, P. Consideration of time-evolving capacity distributions and improved degradation models for seismic fragility assessment of aging highway bridges. *Reliab. Eng. Syst. Saf.* **2016**, *154*, 197–218. [CrossRef]
103. Thanapol, Y.; Akiyama, M.; Frangopol, D.M. Updating the seismic reliability of existing RC structures in a marine environment by incorporating the spatial steel corrosion distribution: Application to bridge piers. *J. Bridge Eng.* **2016**, *21*, 04016031. [CrossRef]
104. Rao, A.S.; Lepech, M.D.; Kiremidjian, A. Development of time-dependent fragility functions for deteriorating reinforced concrete bridge piers. *Struct. Infrastruct. Eng.* **2017**, *13*, 67–83. [CrossRef]
105. Alipour, A.; Shafei, B. Seismic resilience of transportation networks with deteriorating components. *J. Struct. Eng.* **2016**, *142*, C4015015. [CrossRef]
106. Ghosh, J.; Rokneddin, K.; Padgett, J.E.; Dueñas-Osorio, L. Seismic reliability assessment of aging highway bridge networks with field instrumentation data and correlated failures, I: Methodology. *Earthq. Spectra* **2014**, *30*, 795–817. [CrossRef]
107. Rokneddin, K.; Ghosh, J.; Due~nas-Osorio, L.; Padgett, J.E. Seismic reliability assessment of aging highway bridge networks with field instrumentation data and correlated failures, II: Application. *Earthq. Spectra* **2014**, *30*, 819–843. [CrossRef]
108. Gehl, P.; D'Ayala, D. Development of Bayesian Networks for the multi-hazard fragility assessment of bridge systems. *Struct. Saf.* **2016**, *60*, 37–46. [CrossRef]
109. Wang, Z.; Padgett, J.E.; Due~nas-Osorio, L. Risk-consistent calibration of load factors for the design of reinforced concrete bridges under the combined effects of earthquake and scour hazards. *Eng. Struct.* **2014**, *79*, 86–95. [CrossRef]
110. Guo, X.; Wu, Y.; Guo, Y. Time-dependent seismic fragility analysis of bridge systems under scour hazard and earthquake loads. *Eng. Struct.* **2016**, *121*, 52–60. [CrossRef]
111. Alipour, A.; Shafei, B.; Shinozuka, M. Reliability-based calibration of load and resistance factors for design of RC bridges under multiple extreme events: Scour and earthquake. *J. Bridge Eng.* **2013**, *18*, 362–371. [CrossRef]
112. Yilmaz, T. Risk assessment of highway bridges under multi-hazard effect of flood-induced scour and earthquake. Ph.D. Dissertation, The Pennsylvania State University, State College, PA, USA, 2015.
113. Chandrasekaran, S.; Banerjee, S. Retrofit optimization for resilience enhancement of bridges under multihazard scenario. *J. Struct. Eng.* **2016**, *142*, C4015012. [CrossRef]

114. Guo, X.; Chen, Z. Lifecycle multihazard framework for assessing flood scour and earthquake effects on bridge failure. *ASCE-ASME J. Risk Uncertain. Eng. Syst. Part A Civ. Eng.* **2016**, *2*, C4015004. [CrossRef]
115. Dong, Y.; Frangopol, D.M.; Saydam, D. Time-variant sustainability assessment of seismically vulnerable bridges subjected to multi-hazard. *Earthq. Eng. Struct. Dyn.* **2013**, *42*, 1451–1467. [CrossRef]
116. Asadi, P.; Hamed Ranjkesh, S.; Zeinal Hamedani, A. Life-Cycle Cost Analysis (LCCA) of RC Bridges Subjected to Multi-hazard. *Sci. Iran.* **2020**, *28*, 629–644.
117. Deco, A.; Frangopol, D.M. Risk assessment of highway bridges under multi-hazard. *J. Risk Res.* **2011**, *14*, 1057–1089. [CrossRef]
118. Banerjee, S.; Vishwanath, B.S.; Devendiran, D.K. Multihazard resilience of highway bridges and bridge networks: A review. *Struct. Infrastruct. Eng.* **2019**, *15*, 1694–1714. [CrossRef]
119. Kameshwar, S.; Padgett, J.E. Towards risk based multi-hazard resistant design of bridges. *ASCE Struct. Congr.* **2014**, *2014*, 2318–2329.
120. Gidaris, I.; Padgett, J.E.; Barbosa, A.R.; Chen, S.; Cox, D.; Webb, B.; Cerato, A. Multi-hazard fragility and restoration models of highway bridges for regional risk and resilience assessment in the United States: State-of-the-art review. *J. Struct. Eng.* **2017**, *143*, 04016188. [CrossRef]
121. Echevarria, A.; Zaghi, A.E.; Christenson, R.; Accorsi, M. CFFT bridge columns for multihazard resilience. *J. Struct. Eng.* **2016**, *142*, C4015002. [CrossRef]
122. Sun, D.; Chen, B.; Sun, B. Study based on bridge health monitoring system on multihazard load combinations of earthquake and truck loads for bridge design in the southeast coastal areas of China. *Shock Vib.* **2015**, *2015*, 829380. [CrossRef]
123. Nikellis, A.; Sett, K. Multihazard Risk Assessment and Cost–Benefit Analysis of a Bridge–Roadway–Levee System. *J. Struct. Eng.* **2020**, *146*, 04020050. [CrossRef]
124. Wang, Z.; Due~nas-Osorio, L.; Padgett, J.E. Influence of soilstructure interaction and liquefaction on the isolation efficiency of a typical multispan continuous steel girder bridge. *J. Bridge Eng.* **2014**, *19*, A4014001. [CrossRef]
125. Takewaki, I.; Murakami, S.; Fujita, K.; Yoshitomi, S.; Tsuji, M. The 2011 off the Pacific coast of Tohoku earthquake and response of high-rise buildings under long-period ground motions. *Soil Dyn. Earthq. Eng.* **2011**, *31*, 1511–1528. [CrossRef]
126. Takewaki, I.; Fujita, K.; Yoshitomi, S. Uncertainties in long-period ground motion and its impact on building structural design: Case study of the 2011 Tohoku (Japan) earthquake. *Eng. Struct.* **2013**, *49*, 119–134. [CrossRef]
127. Chen, E. Multi-Hazard Design of Mid-to High-Rise Structures. Master's Theses, University of Illinois Urbana-Champaign, Champaign, IL, USA, 2012.
128. Rasigha, J.; Neeladharan, C. Design of Structures to Resist Multi-hazard. *Int. J. Innov. Res. Sci. Eng. Technol.* **2016**, *5*, 1–6.
129. Huang, M. *High-Rise Buildings under Multi-Hazard Environment*; Springer: Berlin/Heidelberg, Germany, 2017.
130. Antoun, J.E.K. Multi-Hazard Performance Assessment of High-Rise Buildings. Master's Theses, Master of Science in Civil Engineering, The Department of Civil & Environmental Engineering, Louisiana State University, Baton Rouge, LA, USA, 2017.
131. Zheng, X.W.; Li, H.N.; Yang, Y.B.; Li, G.; Huo, L.S.; Liu, Y. Damage risk assessment of a high-rise building against multihazard of earthquake and strong wind with recorded data. *Eng. Struct.* **2019**, *200*, 109697. [CrossRef]
132. Li, Y.; Asce, M. Assessment of damage risks to residential buildings and cost–benefit of mitigation strategies considering hurricane and earthquake hazards. *J. Perform. Constr. Facil.* **2012**, *26*, 7–16. [CrossRef]
133. Chiu, G.L.F.; Chock, G.Y.K. Multihazard performance based objective design for managing natural hazards damage. In Proceedings of the IFAC, Control in Natural Disasters, Tokyo, Japan, 21–22 September 1998.
134. Asprone, D.; Jalayer, F.; Prota, A.; Manfredi, G. Proposal of a probabilistic model for multi-hazard risk assessment of structures in seismic zones subjected to blast for the limit state of collapse. *Struct. Saf.* **2010**, *32*, 25–34. [CrossRef]
135. Zhang, X.; Hao, H.; Li, C. Multi-hazard resistance capacity of precast segmental columns under impact and cyclic loading. *Int. J. Prot. Struct.* **2018**, *9*, 24–43. [CrossRef]
136. Chicchi, R.A. Multi-Hazard Resilience of Steel MFR Buildings. Ph.D. Dissertation, Purdue University, West Lafayette, IN, USA, 2017.
137. Shin, J. Multi-Hazard Performance Criteria for Non-Ductile Reinforced Concrete Frame Buildings Retrofitted with an FRP Column Jacketing System. Ph.D. Dissertation, Georgia Institute of Technology, Atlanta, GA, USA, 2017.
138. Unnikrishnan, V.U.; Barbato, M. Multihazard interaction effects on the performance of low-rise wood-frame housing in hurricane-prone regions. *J. Struct. Eng.* **2017**, *143*, 04017076. [CrossRef]
139. Chulahwat, A.; Mahmoud, H. A combinatorial optimization approach for multi-hazard design of building systems with suspended floor slabs under wind and seismic hazards. *Eng. Struct.* **2017**, *137*, 268–284. [CrossRef]
140. Djerouni, S.; Elias, S.; Abdeddaim, M.; Rupakhety, R. Optimal design and performance assessment of multiple tuned mass damper inerters to mitigate seismic pounding of adjacent buildings. *J. Build. Eng.* **2022**, *48*, 103994. [CrossRef]
141. Djerouni, S.; Abdeddaim, M.; Elias, S.; Rupakhety, R. Optimum double mass tuned damper inerter for control of structure subjected to ground motions. *J. Build. Eng.* **2021**, *44*, 103259. [CrossRef]
142. Djerouni, S.; Ounis, A.; Elias, S.; Abdeddaim, M.; Rupakhety, R. Optimization and performance assessment of tuned mass damper inerter systems for control of buildings subjected to pulse-like ground motions. *Structures* **2022**, *38*, 139–156. [CrossRef]
143. Marian, L.; Giaralis, A. Optimal design of a novel tuned mass-damper–inerter (TMDI) passive vibration control configuration for stochastically support-excited structural systems. *Probabilistic Eng. Mech.* **2014**, *38*, 156–164. [CrossRef]
144. Bedon, C.; Amadio, C. Numerical assessment of vibration control systems for multi-hazard design and mitigation of glass curtain walls. *J. Build. Eng.* **2018**, *15*, 1–13. [CrossRef]

145. Mahmoud, H.; Chulahwat, A. Multi-Hazard Multi-Objective Optimization of Building Systems with Isolated Floors under Seismic and Wind Demands. In *Multi-Hazard Approaches to Civil Infrastructure Engineering*; Springer: Berlin/Heidelberg, Germany, 2016; pp. 141–164.
146. Cao, L.; Laflamme, S.; Hong, J.; Dodson, J. Input space dependent controller for civil structures exposed to multi-hazard excitations. *Eng. Struct.* **2018**, *166*, 286–301. [CrossRef]
147. Dogruel, S.; Dargush, G.F. A framework for multi-hazard design and retrofit of passively damped structures. In Proceedings of the Architectural Engineering Conference (AEI), Denver, CO, USA, 24–27 September 2008; pp. 1–12.
148. Kleingesinds, S.; Lavan, O.; Venanzi, I. Life-cycle cost-based optimization of MTMDs for tall buildings under multi-hazard. *Struct. Infrastruct. Eng.* **2020**, *17*, 921–940. [CrossRef]
149. Roy, T.; Matsagar, V. Effectiveness of passive response control devices in buildings under earthquake and wind during design life. *Struct. Infrastruct. Eng.* **2019**, *15*, 252–268. [CrossRef]
150. Roy, T.; Matsagar, V. Probabilistic assessment of steel buildings installed with passive control devices under multi-hazard scenario of earthquake and wind. *Struct. Saf.* **2020**, *85*, 101955. [CrossRef]
151. Chapain, S.; Aly, A.M. Vibration attenuation in high-rise buildings to achieve system-level performance under multi-hazard. *Eng. Struct.* **2019**, *197*, 109352. [CrossRef]
152. Elias, S.; Matsagar, V. Optimum Tuned Mass Damper for Wind and Earthquake Response Control of High-Rise Building. In *Advances in Structural Engineering*; Springer: New Delhi, India, 2015; pp. 1475–1487.
153. Elias, S.; Rupakhety, R.; Olafsson, S. Analysis of a Benchmark Building Installed with Tuned Mass Dampers under Wind and Earthquake Loads. *Shock Vib.* **2019**, *2019*, 7091819. [CrossRef]
154. Gong, Y. Variable Friction Cladding Connection for Multi-hazard Mitigation. Ph.D. Dissertation, Iowa State University, Ames, IA, USA, 2019.
155. Maryam, M.R. Multi-Hazard Reliability Assessment of Offshore Wind Turbines. Ph.D. Thesis, Texas A&M University, College Station, TX, USA, 2012.
156. Mardfekri, M.; Gardoni, P. Multi-hazard reliability assessment of offshore wind turbines. *Wind Energy* **2015**, *18*, 1433–1450. [CrossRef]
157. Avossa, A.M.; Demartino, C.; Contestabile, P.; Ricciardelli, F.; Vicinanza, D. Some results on the vulnerability assessment of HAWTs subjected to wind and seismic actions. *Sustainability* **2017**, *9*, 1525. [CrossRef]
158. del Campo, J.O.M.; Estrada, A.P. Multi-hazard fragility analysis for a wind turbine support structure: An application to the Southwest of Mexico. *Eng. Struct.* **2012**, *209*, 109929. [CrossRef]
159. Katsanos, E.I.; Sanz, A.A.; Georgakis, C.T.; Thöns, S. Multi-hazard response analysis of a 5MW offshore wind turbine. *Procedia Eng.* **2017**, *199*, 3206–3211. [CrossRef]
160. Zuo, H.; Bi, K.; Hao, H.; Xin, Y.; Li, J.; Li, C. Fragility analyses of offshore wind turbines subjected to aerodynamic and sea wave loadings. *Renew. Energy* **2020**, *160*, 1269–1282. [CrossRef]
161. Zuo, H.; Bi, K.; Hao, H. Dynamic analyses of operating offshore wind turbines including soil-structure interaction. *Eng. Struct.* **2018**, *157*, 42–62. [CrossRef]
162. Asareh, M.A.; Schonberg, W.; Volz, J. Fragility analysis of a 5-MW NREL wind turbine considering aero-elastic and seismic interaction using finite element method. *Finite Elem. Anal. Des.* **2016**, *120*, 57–67. [CrossRef]
163. Xie, S.; Jin, X.; He, J. Structural vibration control for the offshore floating wind turbine including drivetrain dynamics analysis. *J. Renew. Sustain. Energy* **2019**, *11*, 023304. [CrossRef]
164. He, E.M.; Hu, Y.Q.; Zhang, Y. Optimization design of tuned mass damper for vibration suppression of a barge-type offshore floating wind turbine. *Proc. Inst. Mech. Eng. Part M J. Eng. Marit. Environ.* **2017**, *231*, 302–315. [CrossRef]
165. Stewart, G.M.; Lackner, M.A. The impact of passive tuned mass dampers and wind-wave misalignment on offshore wind turbine loads. *Eng. Struct.* **2014**, *73*, 54–61. [CrossRef]
166. Zhao, B.; Gao, H.; Wang, Z.; Lu, Z. Shaking table test on vibration control effects of a monopile offshore wind turbine with a tuned mass damper. *Wind Energy* **2018**, *21*, 1309–1328. [CrossRef]
167. Sun, C.; Jahangiri, V. Bi-directional vibration control of offshore wind turbines using a 3D pendulum tuned mass damper. *Mech. Syst. Signal Process.* **2018**, *105*, 338–360. [CrossRef]
168. Sun, C.; Jahangiri, V. Fatigue damage mitigation of offshore wind turbines under real wind and wave conditions. *Eng. Struct.* **2019**, *178*, 472–483. [CrossRef]
169. Sun, C.; Jahangiri, V.; Sun, H. Performance of a 3D pendulum tuned mass damper in offshore wind turbines under multiple hazards and system variations. *Smart Struct. Syst.* **2019**, *24*, 53–65.
170. Hu, Y.; Wang, J.; Chen, M.Z.; Li, Z.; Sun, Y. Load mitigation for a barge-type floating offshore wind turbine via inerter-based passive structural control. *Eng. Struct.* **2018**, *177*, 198–209. [CrossRef]
171. Zuo, H.; Bi, K.; Hao, H. Mitigation of tower and out-of-plane blade vibrations of offshore monopile wind turbines by using multiple tuned mass dampers. *Struct. Infrastruct. Eng.* **2019**, *15*, 269–284. [CrossRef]
172. Zuo, H.; Bi, K.; Hao, H. Using multiple tuned mass dampers to control offshore wind turbine vibrations under multiple hazards. *Eng. Struct.* **2017**, *141*, 303–315. [CrossRef]
173. Hussan, M.; Sharmin, F.; Kim, D. Multiple tuned mass damper based vibration mitigation of offshore wind turbine considering soil–structure interaction. *China Ocean Eng.* **2017**, *31*, 476–486. [CrossRef]

174. Altay, O.; Taddei, F.; Butenweg, C.; Klinkel, S. Vibration Mitigation of Wind Turbine Towers with Tuned Mass Dampers. In *Wind Turbine Control and Monitoring*; Springer: Berlin/Heidelberg, Germany, 2014; pp. 337–373.
175. Colwell, S.; Basu, B. Tuned liquid column dampers in offshore wind turbines for structural control. *Eng. Struct.* **2009**, *31*, 358–368. [CrossRef]
176. Dezvareh, R.; Bargi, K.; Mousavi, S.A. Control of wind/wave-induced vibrations of jacket-type offshore wind turbines through tuned liquid column gas dampers. *Struct. Infrastruct. Eng.* **2016**, *12*, 312–326. [CrossRef]
177. Bargi, K.; Dezvareh, R.; Mousavi, S.A. Contribution of tuned liquid column gas dampers to the performance of offshore wind turbines under wind, wave, and seismic excitations. *Earthq. Eng. Eng. Vib.* **2016**, *15*, 551–561. [CrossRef]
178. Sun, C. Semi-active control of monopile offshore wind turbines under multi-hazards. *Mech. Syst. Signal Process.* **2018**, *99*, 285–305. [CrossRef]
179. Hemmati, A.; Oterkus, E. Semi-active structural control of offshore wind turbines considering damage development. *J. Mar. Sci. Eng.* **2018**, *6*, 102. [CrossRef]
180. Rezaee, M.; Aly, A.M. Vibration control in wind turbines to achieve desired system-level performance under single and multiple hazard loadings. *Struct. Control Health Monit.* **2018**, *25*, e2261. [CrossRef]
181. Xie, F.; Aly, A.M. Structural control and vibration issues in wind turbines: A review. *Eng. Struct.* **2020**, *210*, 110087. [CrossRef]
182. Rezaee, M.; Aly, A.M. Vibration control in wind turbines for performance enhancement: A comparative study. *Wind. Struct.* **2016**, *22*, 107–131. [CrossRef]
183. Zhao, Z.; Dai, K.; Lalonde, E.R.; Meng, J.; Li, B.; Ding, Z.; Bitsuamlak, G. Studies on application of scissor-jack braced viscous damper system in wind turbines under seismic and wind loads. *Eng. Struct.* **2019**, *196*, 109294. [CrossRef]
184. Zuo, H.; Bi, K.; Hao, H. A state-of-the-art review on the vibration mitigation of wind turbines. *Renew. Sustain. Energy Rev.* **2020**, *121*, 109710. [CrossRef]
185. Rahman, M.; Ong, Z.C.; Chong, W.T.; Julai, S.; Khoo, S.Y. Performance enhancement of wind turbine systems with vibration control: A review. *Renew. Sustain. Energy Rev.* **2015**, *51*, 43–54. [CrossRef]
186. Rupakhety, R.; Sigurdsson, S.U.; Papageorgiou, A.S.; Sigbjörnsson, R. Quantification of ground-motion parameters and response spectra in the near-fault region. *Bull. Earthq. Eng.* **2011**, *9*, 893–930. [CrossRef]
187. Elias, S.; Rupakhety, R.; Ólafsson, S. Tuned mass dampers for response reduction of a reinforced concrete chimney under near-fault pulse-like ground motions. *Front. Built Environ.* **2020**, *6*, 92. [CrossRef]
188. Sigurðsson, G.Ö.; Rupakhety, R.; Rahimi, S.E.; Olafsson, S. Effect of pulse-like near-fault ground motions on utility-scale land-based wind turbines. *Bull. Earthq. Eng.* **2020**, *18*, 953–968. [CrossRef]
189. Jami, M.; Elias, S.; Rupakhety, R.; De Domenico, D.; Falsone, G.; Ricciardi, G. Are Bridges Safe Under Near-Fault Pulse-Type Ground Motions Considering the Vertical Component? In *International Conference of the European Association on Quality Control of Bridges and Structures*; Springer: Cham, Switzerland, 2021; pp. 1207–1215.

Paper 2

Jami, M., Rupakhety, R., Bessason, B., & Snæbjörnsson, J. T. (2023). Multimode Vibration Control Strategies of Long-Span Bridges Subjected to Multi-hazard: A Case Study of the Runyang Suspension Bridge. Journal of Vibration Engineering & Technologies.

Journal of Vibration Engineering & Technologies
https://doi.org/10.1007/s42417-023-01157-3

ORIGINAL PAPER

Multimode Vibration Control Strategies of Long-Span Bridges Subjected to Multi-hazard: A Case Study of the Runyang Suspension Bridge

Matin Jami[1] · Rajesh Rupakhety[1] · Bjarni Bessason[2] · Jonas Th. Snæbjörnsson[3]

Received: 24 May 2023 / Revised: 17 August 2023 / Accepted: 17 September 2023

Abstract

Purpose This study is an attempt to illustrate and discuss multi-hazard interactions in vibration control of long-span bridges subjected to wind and seismic loads. Such bridges, being flexible structures, are inherently vulnerable to wind loads. However, some response parameters of such bridges, for example, tower and deck acceleration, can be significant during large earthquakes which produce ground motions with low-frequency content.

Methods To illustrate this problem, a case study of the Runyang Suspension Bridge (RSB) is used. A finite element model of the bridge is created and verified against published literature. A set of ground motions from large worldwide earthquakes and spatially varying wind velocity time series, simulated as a realization of a random field, are used to evaluate the bridge's dynamic response with and without control devices. The control devices applied in this study are passive-tuned mass dampers (TMDs). Careful investigation of the uncontrolled response of the bridge shows that while wind load is mainly important for the displacement of the bridge deck, seismic loads can induce significant acceleration of the tower and the deck. Since the response of the tower and the deck are coupled at some higher modes of vibration, seismic action, although most critical for the tower, is also relevant for deck acceleration. These observations indicate the need for a multi-performance-based control strategy.

Results It is found that TMDs optimal for reducing seismic-induced deck acceleration can lead to amplification of wind-induced deck displacement. At the same time, TMDs optimal for reducing wind-induced displacement response are, in some cases, harmful to seismic-induced deck acceleration. These results clearly show multi-hazard interaction in control performance.

Conclusions To account for this problem, a control strategy for the deck and tower's seismic and wind responses is investigated. This consists of TMDs placed at the top of each tower and 4 TMDs placed on the deck. By tuning the TMDs to different vibration modes of the bridge, the system is shown to be effective for both seismic and wind actions.

Keywords Multi-hazard · Long-span bridge · TMD · Wind · Earthquake engineering

Rajesh Rupakhety, Bjarni Bessason and Jonas Th. Snæbjörnsson contributed equally to this work.

✉ Matin Jami
amj38@hi.is

✉ Rajesh Rupakhety
rajesh@hi.is

Bjarni Bessason
bb@hi.is

Jonas Th. Snæbjörnsson
jonasthor@ru.is

[1] Faculty of Civil and Environmental Engineering, School of Engineering and Natural Science, Earthquake Engineering Research Centre, University of Iceland, Selfoss, Iceland

[2] Faculty of Civil and Environmental Engineering, School of Engineering and Natural Science, University of Iceland, Selfoss, Iceland

[3] Department of Engineering, School of Technology, Reykjavik University, Reykjavik, Iceland

Published online: 19 October 2023

Introduction

Advances in science and technology make it increasingly feasible to build megastructures. Engineering ingenuity has made it possible to build many iconic structures around the world. Bridges across large crossing are not only of functional value but also important landmarks with aesthetic appeal showcasing engineering and architectural marvel. A few examples of such iconic bridge are the Golden Gate Bridge (San Francisco, USA), Çanakkale Bridge (Gelibolu, Turkey), Akashi Kaikyo Bridge (Kobe, Japan), Yangsigang Yangtze River Bridge (Wuhan, China), Great Belt Bridge (Korsør, Denmark), Humber Bridge (Hessle, UK), and the Rio-Antirrio Bridge (Patras, Greece). The history of bridge construction goes back centuries. The Arkadiko Bridge is claimed to be the oldest existing bridge in the world, built between 1300 and 1190 BC [31]. Functionality and complexity of bridges have grown with the development of transportation systems to the extent that today long-span bridges are considered one of its essential components.

The geometry of long-span bridges makes them vulnerable to dynamic forces induced by natural phenomena such as earthquakes and wind. The probability of simultaneous occurrence of large wind and seismic action on long-span bridges is low (see, e.g., [22]). However, during their useful life, such bridges may be exposed to these forces at different times with intensities that might pose threat to their safety and functionality. Such bridges therefore need to be robust against different hazards relevant to their sites. Multi-hazard consideration also becomes important because different natural forces might affect these bridges in different ways (see, [15], and references therein). Recently, Marić et al. [21] discussed multi-hazard considerations in cost, safety, reliability, and serviceability of long-span bridges.

Vibration suppression and energy dissipation methods have proven useful to enhance functionality and safety of large structures, including bridges [2, 9, 16, 24, 28, 33]. Such methods include base isolation, supplemental damping, and various types of passive/active/hybrid tuned dampers. Passive tuned mass dampers (TMDs) are one of the most common vibration control devices investigated in the literature. Several studies have confirmed their effectiveness is reducing vibrations of bridges. The Meiko Bridge, the Akashi Kaikyo Bridge, and the Trans-Tokyo Bay Bridge in Japan, the Kessock Bridge in the UK, and the Jindo Bridge in Korea are examples of long-span bridges where TMD is used as control devices [10, 11].

Several studies have investigated vibration control of long-span bridges. Xing et al. [38] studied the efficiency of TMDs in wind-induced vibration control of a long-span bridge. They report that a TMD-type counterweight placed at the mid-span of Sutong cable-stayed bridge is effective in reducing wind-induced vibrations of the deck. Chen et al. [6] present a procedure to optimize TMD parameters for multimode buffeting response control of long-span bridges. Wang et al. [36] presented a study on the optimal placement of dampers to control seismic vibrations of the Runyang Suspension Bridge. Experimental and theoretical studies on the performance of TMD in controlling wind-induced vibration of bridges are presented in Gu et al. [12] and Cai and Chen [5]. Analytical studies using TMD inerter to mitigate vortex-induced vibration of long-span bridges are reported in Xu et al. [39–41]. Gu et al. [13] and Tanida [34] studied the application of active and semi-active TMDs for wind-induced vibration control of long-span bridges. Soneji and Jangid [32], present effectiveness of elastomeric and sliding types of isolation systems for the seismic response control of cable-stayed bridges. Shum et al. [30] present wind-induced vibration control of long-span bridges using multiply pressurized tuned liquid column dampers. Zhu et al. [44] studied the effectiveness of fluid viscous damper (FVD) for mitigating seismic-induced vibrations of a cable-stayed bridge. Ha et al. [14] present a methodology for optimization of complex damper parameter for seismic response reduction of long-span bridges. The use of TMDs for controlling vibration of long-span bridges due to vertical component of ground motion is studied by Lavasani et al. [19] and Pourzeynali and Estaki [25].

The use of passive TMDs for vibration control of long-span bridges has so far been mostly concentrated on wind load. Wind-induced vibrations are, in most cases, the most critical consideration for long-span bridges. However, seismic excitations can also pose a threat to different components of such bridges, for example, the towers of suspension bridges. Wind and earthquake forces excite different vibration modes of long-span bridges. Wind loads are in general critical for displacement response of the deck, while seismic loads may excite vibration modes of the towers. For an overall performance enhancement of long-span bridges subjected to seismic and wind forces, vibration control strategies can be varied depending on the type of excitation, the structural component that is the most affected, and the response parameter to be controlled, for example, displacement or acceleration. As TMDs need to be tuned to certain vibration frequencies of the structure, for a complex structure excited by forces with drastically different frequency content, a multimode multi-performance strategy is necessary. Investigation of such scenarios for long-span bridges is lacking in the literature. This work is an attempt to shed light on important considerations in multi-performance, multi-hazard vibration control of long-span bridges using a case study of the RSB. The effect of ground motion and wind-induced force on the

super long-span bridge's two main parts (tower and deck) is evaluated, and implications of multi-hazard interactions in multi-performance control are investigated using various control strategies.

In the following, a summary of vibration mechanisms of long-span bridges is provided. It is followed by a case study of the RSB. The mathematical models of the bridge and the control devices are presented. Then, the wind and ground motion excitation used for evaluating the performance of control devices are presented. Different vibration control strategies with TMD placement and tuning are investigated for multi-performance control. Vibration control performance of these strategies is evaluated and discussed in detail, and the main findings are summarized.

Vibration Mechanisms of Long-Span Bridges

Vibrations can have adverse effects on long-span bridges, from bridge elements' fatigue to collapse under extreme cases. In addition, excessive vibration reduces the serviceability of bridges. Due to the unique dynamic characteristics of long-span bridges, namely low damping and high flexibility, they are susceptible to vibrations induced by many dynamic processes. A summary of different vibration mechanisms of long-span bridges is presented in the following.

Seismic-Induced Vibration

Ground acceleration causes vibration of different components of a bridge. The energy carried by earthquake ground motions usually has a higher frequency content than the fundamental natural frequencies of the deck vibrations. In general, displacement transmissibility is higher than acceleration transmissibility. Other elements of the bridge, for example, the towers, are stiffer and might be excited more than the deck by seismic ground motions.

Many big cities and their transportation routes, which include long-span bridges, have been built in earthquake-prone areas. However, very few have so far been damaged by earthquakes. For example, the Ji Da cable-stayed bridge in Taiwan was damaged by the Chi-Chi earthquake in 1999; Higashi-Kobe cable-stayed bridge was damaged during the Kobe earthquake in 1995. In general, the design of substructures and pylons mainly focuses on seismic load as the potential dynamic load, while wind load governs the design of the cables and girder [11].

Wind-Induced Vibration

Wind-induced force is a random dynamic process, and its effects on structures vary in space and time. In the design of long-span bridges, among various types of dynamic forces, wind-induced vibration is considered the most critical dynamic excitation. Oscillating components of a long-span bridge, such as towers, deck, and cables, shape the wind flow around the bluff body of the bridge result in a complex fluid–structure interaction. This interaction is studied under the title of resulting aerodynamic force and self-excited vibration. Wind-induced vibration processes are schematically summarized in Fig. 1.

Cables are the most flexible component of long-span bridges (cable-stayed bridges and suspension bridges). Low damping and high flexibility make cables susceptible to vibrations. Cable fatigue and damage to the anchorage are the most common problems caused by cable oscillations.

Traffic-Induced Vibration

Traffic-induced vibration is a common phenomenon that has been widely studied for long-span bridges. For example, Paultre et al. [23] presented a comprehensive review of traffic-induced vibration mechanisms. In design codes, moving traffic loads are considered through a dynamic amplification factor. This factor is based on bridge characteristics such as the geometry of the bridge, its natural frequencies, joints and support conditions, and vehicle characteristics such its dynamic specification, speed, weight, and pavement conditions.

One of the concerns for long-span bridges serving train traffic is the vehicle–structure interaction. The large moving load of the train passing at high speed along a long-span bridge produces forces and vibrations that can cause several problems such as train serviceability, passenger comfort and safety, fatigue of the bridge elements, and even resonance under certain circumstances.

Human-Induced Vibration

Events such as rallies or marathons passing a bridge can form human-induced vibrations. In fact, there have been many reports regarding human-induced vibration in bridges, especially footbridges. In some cases, human-induced vibrations have caused collapse, killed people, and resulted in economic loss. The Angers Bridge collapse in 1850 is an example of a bridge collapse due to human-induced vibration [4]. Many people walking in step generate periodic forces in horizontal and vertical directions, resulting in bridge vibrations. Therefore, resonance is a potential hazard for the bridge with natural frequencies close to human-induced vibration frequencies, which are considered in some design codes, as 2 Hz in the vertical direction and 1 Hz in the horizontal direction [11].

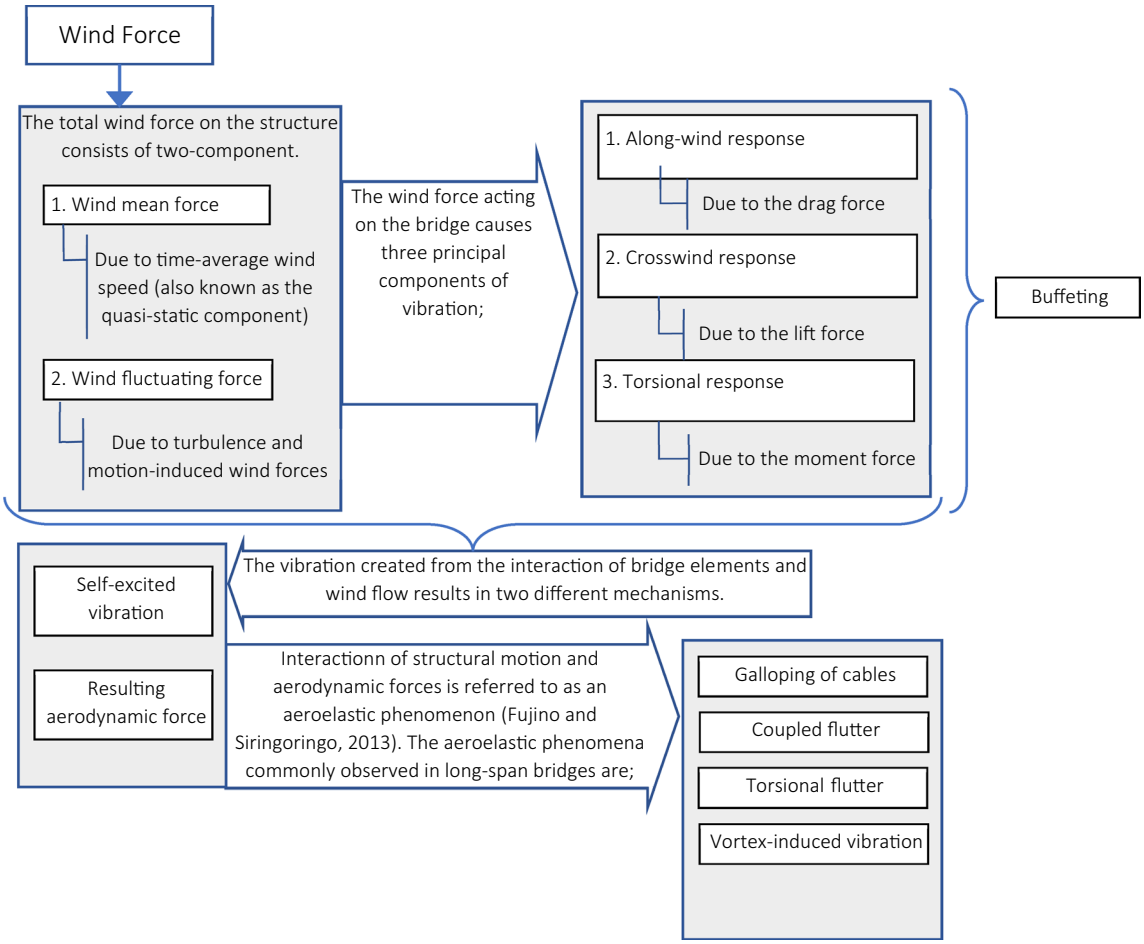

Fig. 1 Wind-induced vibration mechanisms (based on Fujino and Siringoringo [11])

Case Study of the Runyang Suspension Bridge (RSB)

This section provides a case study of the RSB to illustrate how wind and earthquake forces affect the bridge and its different components differently and what implications it has in selecting a proper vibration control strategy. The mathematical model of the bridge, the wind and seismic excitations used in the study, and the control systems being considered are described in the following sections.

Mathematical Models

The RSB crosses the Yangtze River in Jiangsu Province, China. The RSB is a super long-span suspension bridge with a main span of 1490 m (see Fig. 2). The main span of this bridge is suspended between two towers. Each tower is constructed from two steel–concrete columns with a height of 210 m and three prestressed concrete cross beams (see Fig. 2a, b). The main cables are 0.9 m in diameter, and each consists of 184 strands. Each strand contains 127 wires, 5.3 mm in diameter, made of steel with 1670 MPa yield strength. Each vertical suspender contains 109 steel wires of 5 mm diameter and 1670 MPa yield strength. The steel girder is 38.7 m wide and 3 m high, with a 2% slope on each side (see Fig. 2c). The main components of the deck are plates, longitudinal beams (U-ribs), and transverse beams (transverse diaphragms). The thickness of each part is as follows: 10 mm for the lower inclined web, 12 mm for the upper inclined web, 6 mm for longitudinal beams, 8 mm for transverse beams, and 14 mm for the deck. The distance between transverse beams is 3.22 m (see [17]). A finite element model (FEM) of the bridge was created in the computer program SAP2000. The model is based on specifications of the bridge available in the literature [17, 20]. Both the bridge and control device are assumed to remain in the elastic range. Three-dimensional frame elements are used to model the towers and the girder. Cable elements are used to model the main cables and the vertical suspenders. Connection between the girder and the suspender cables is assumed to be rigid. Masses of frame elements are lumped at their end nodes. Mass of nonstructural elements such as wearing

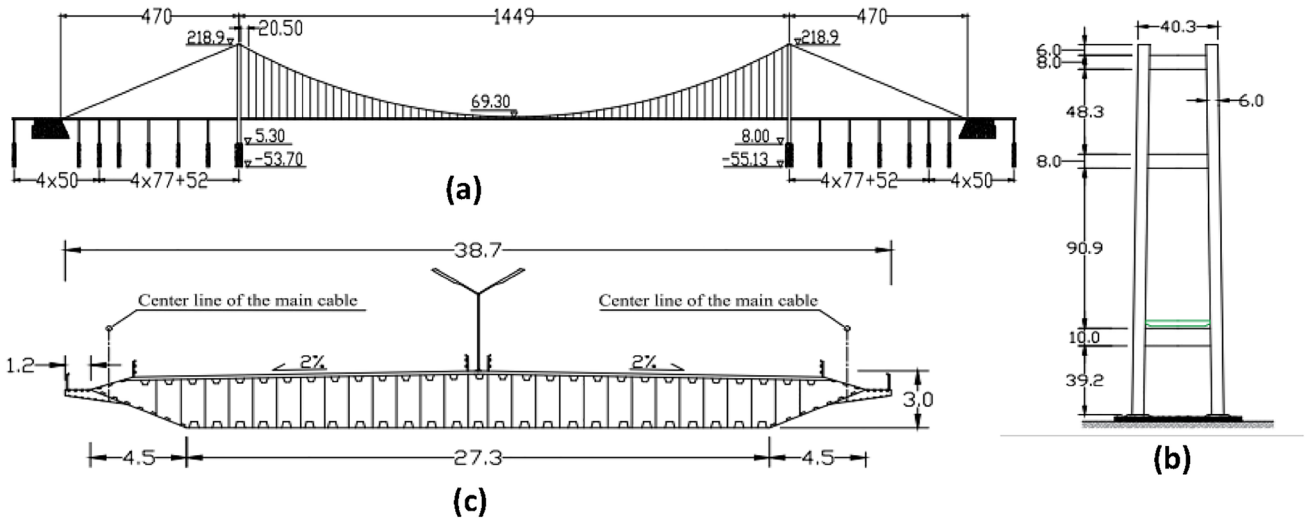

Fig. 2 RSB **a** elevation. **b** Geometry of the tower. **c** Cross-section girder. (Dimensions in m)

course and parapet walls are added to the model. Main cable anchors, abutments, and piers are assumed to be fixed in the foundation,i.e., soil–structure interaction is not considered.

The FEM of the RSB with a schematic representation of TMDs placed at different locations is shown in Fig. 3. The modal frequencies and mass participation ratios of the first ten modes of vibration of the RSB are presented in Table 1. The first horizontal symmetric mode corresponds to the transverse movement of the deck. The fifth mode is dominated by the movement of the tower in the *x*-direction. The shapes of the first horizontal symmetric mode and the fifth mode are shown in Fig. 4. We focus on these two modes because they contribute the most to the transverse response of the deck and the tower, respectively.

The modal properties of the RSB have been published by Wang et al. [36], which presented a finite element model updating the RSB using ambient vibration measurement data. The first horizontal symmetric mode of their FEM has a frequency of 0.054 Hz. Based on ambient vibration test, they identified the frequency of the mode to be 0.059 Hz. The frequency of the corresponding mode of our model is 0.05 Hz, which is close to the published results. Li et al. [20] report similar frequencies of the first tower mode, i.e., 0.05 Hz based on FEM and 0.051 based on ambient measurements. The frequency of the first vertical mode of the bridge based on FEM model of Li et al. [20] is 0.09 Hz and that of our model is also 0.09 Hz.

Wind and Seismic Loads

Linear time history analysis with earthquake ground motion and wind forces is used to evaluate the performance of several vibration control schemes for the case of the RSB. Details of ground motion and wind forces used for simulating the response of the bridge with and without control devices are given in the following. It is highlighted that this work is not a site-specific study but a general investigation of multi-performance vibration control of long-span bridges.

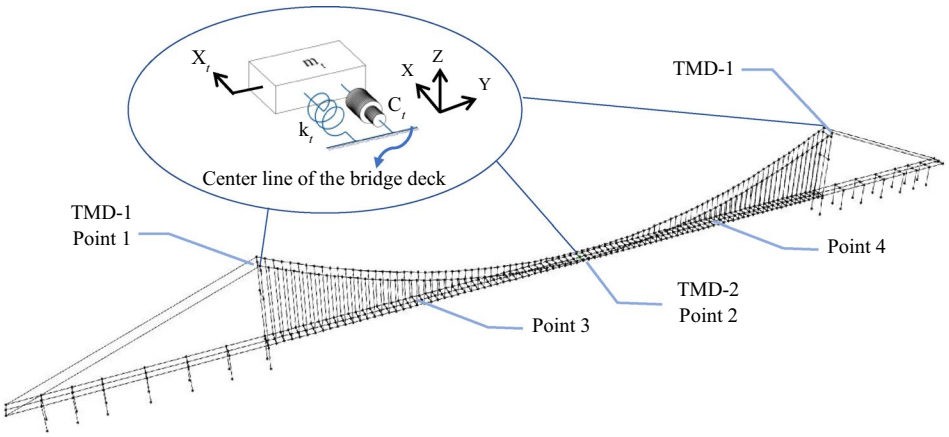

Fig. 3 A FE model of the RSB showing the locations of the TMDs investigated in subsequent sections. The TMDs move only in the transverse direction of the bridge

Table 1 Modal frequencies and modal participation mass ratio of RSB for Mode 1 and Mode 5 (U and R denote translation and rotation, respectively)

Mode #	Direction	Frequency (Hz)	Modal mass participation ratio						Location of max displacement
			Uy	Ux	Uz	Ry	Rx	Rz	
1	Transverse	0.0497	0	0.089	8.00E−11	0.00389	9.82E−20	0	Point 2
2	Vertical	0.0884	0.00017	3.77E−17	1.40E−20	4.21E−17	0.01231	2.99E−08	Points 3 and 4
3	Transverse	0.1365	8.67E−08	1.99E−18	2.92E−16	7.81E−19	1.59E−09	0.0207	Points 3 and 4
4	Vertical	0.1459	1.01E−19	8.23E−08	0.00414	1.97E−08	3.45E−20	7.78E−16	Points 2, 3, and 4
5	Transverse	0.2307	3.01E−14	0.41291	1.17E−07	0.8276	4.31E−13	6.31E−13	Point 1
6	Transverse	0.2313	3.69E−07	7.82E−13	3.94E−12	1.49E−12	9.11E−10	0.33106	Point 1
7	Vertical	0.2499	6.56E−17	2.91E−07	0.07077	7.84E−07	3.37E−17	1.06E−11	Points 3 and 4
8	Transverse	0.2669	2.29E−14	0.00209	2.56E−07	0.02602	6.94E−14	5.10E−15	Points 2, 3, and 4
9	Vertical	0.2681	0.00256	5.67E−14	5.60E−17	1.39E−12	0.00482	1.17E−08	Four points on the deck
10	Vertical	0.3914	1.85E−15	7.94E−07	0.01075	5.09E−07	1.59E−17	1.23E−13	Five points on the deck
11	Transverse	0.4367	2.20E−05	3.59E−14	4.48E−16	1.88E−14	8.21E−08	0.00487	Points 3 and 4
12	Torsion	0.4405	2.98E−13	5.80E−05	1.62E−08	0.00304	1.82E−13	2.50E−17	Point 2
13	Longitudinal	0.4785	0.43752	1.05E−14	4.44E−15	1.64E−12	0.00101	1.82E−05	Point 1

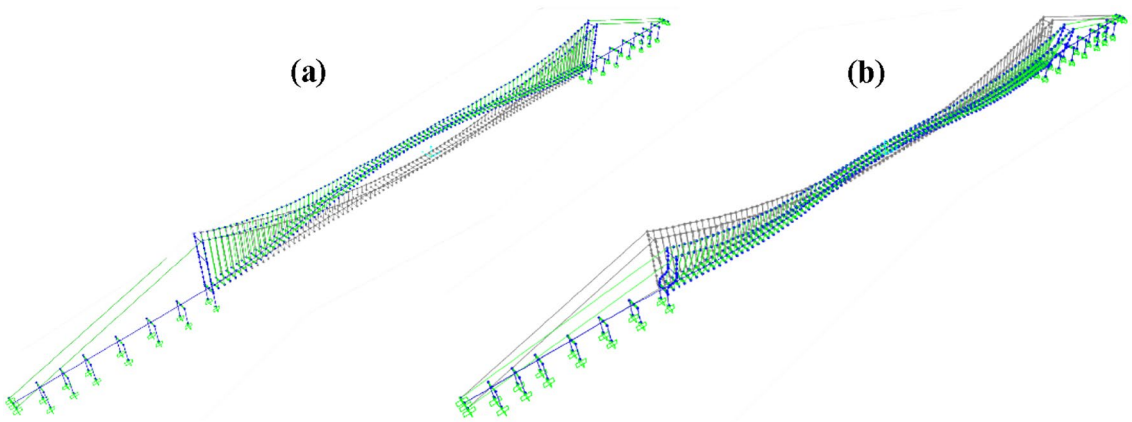

Fig. 4 Mode shapes of the RSB, **a** Mode 1, the first horizontal symmetric mode, and **b** Mode 5, the first tower transverse mode

Therefore, the seismic ground motion and wind force properties are not representative of the actual hazard at the RSB site. Both the seismic and wind action are only considered in the transverse direction of the bridge.

Ground Motions

In selecting ground motions, large earthquakes are given priority, as ground shaking from large earthquakes is richer in low-frequency content. By inspecting Fourier amplitude spectra of hundreds of ground motions from the PEER database [3], ten ground motions that had significant energy near the important vibration modes of the bridge were selected. Ground shaking is considered in the transverse direction of the bridge only. Some details of the selected ground motions are presented in Table 2. The ground acceleration time histories of the selected motions are shown in Fig. 5. The corresponding Fourier amplitude spectra (FAS) shown in Fig. 6 indicates that even for such large earthquakes, the spectral content at the first mode of the deck is insignificant. However, the ground motions contain significant energy at the tower vibration modes. Long-span structures such as the one studied here experience differential motion at their supports during earthquakes. The differential motion is a result of wave passage effect and random variability quantified by lagged coherency (see, e.g., [42]). Lagged coherency is a measure of similarity between motions at different measurement points. As the distance between the measurement points increases, the motions become more dissimilar and lagged coherency decreases. It also decreases with increasing frequency. Low-frequency motions are more coherent than high-frequency motion. Based on the SMART-1 array

Table 2 Ground motion time series used in this study (PGA = peak ground acceleration, R_{jb} = Joyner–Boore distance)

No.	Earthquake name	Year	Station name	Magnitude	Component	PGA (m/s^2)	R_{jb} (km)
1	Tabas Iran	1978	Tabas	7.35	N16° W	8.45	1.79
2	Imperial Valley-06	1979	El Centro Array #4	6.53	N40° W	3.63	4.9
3	Imperial Valley-06	1979	El Centro Array #7	6.53	N40° W	4.6	0.56
4	Chi-Chi Taiwan	1999	CHY101	7.62	E–W	3.9	9.94
5	Chi-Chi Taiwan	1999	TCU029	7.62	E–W	1.95	28.04
6	Chi-Chi Taiwan	1999	TCU031	7.62	E–W	1.22	30.17
7	Chi-Chi Taiwan	1999	TCU036	7.62	E–W	1.22	19.83
8	Chi-Chi Taiwan	1999	TCU039	7.62	E–W	1.36	19.89
9	Chi-Chi Taiwan	1999	TCU087	7.62	E–W	1.12	6.98
10	Chi-Chi Taiwan	1999	TCU128	7.62	E–W	1.63	13.13

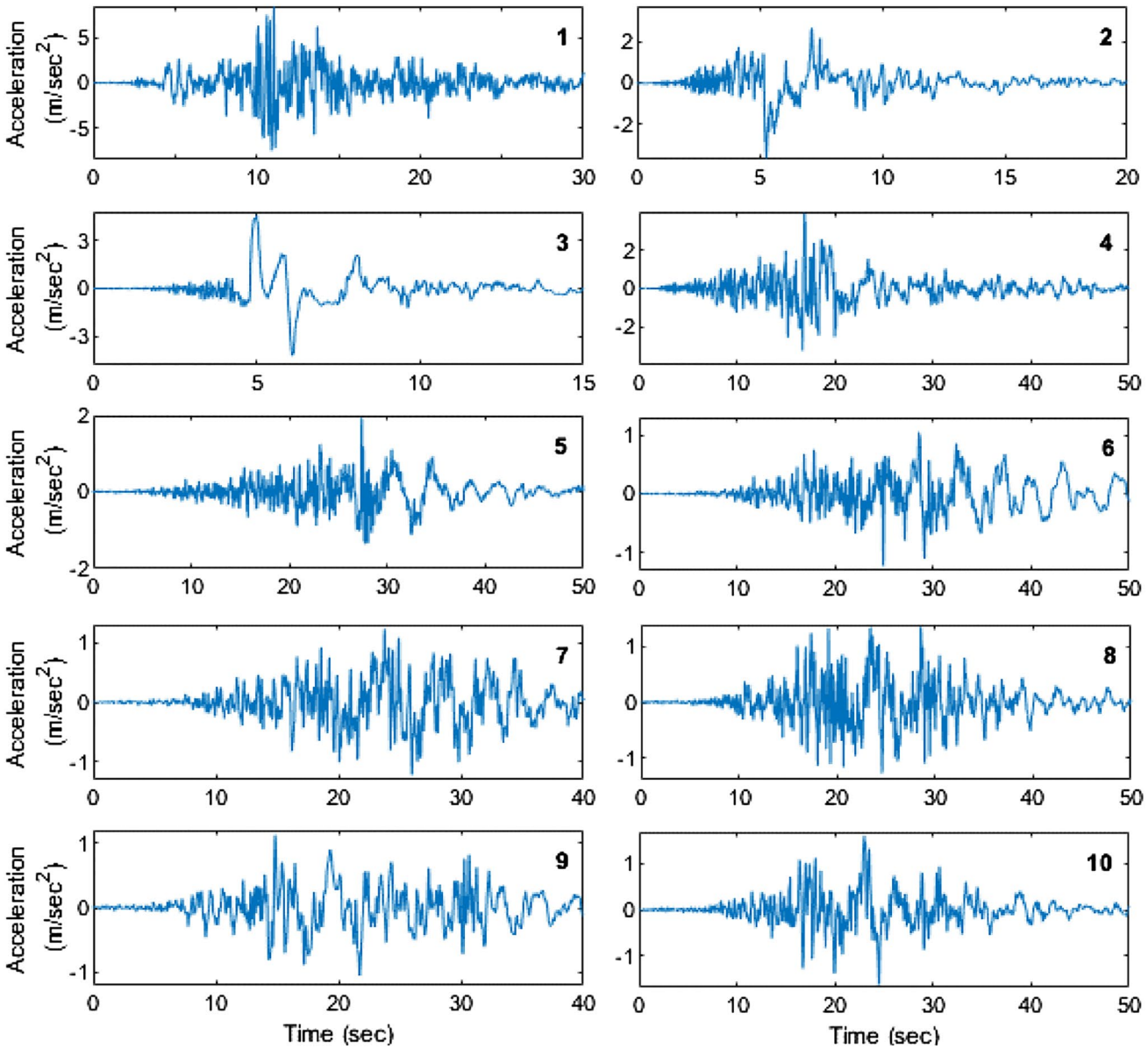

Fig. 5 Time histories of the ground accelerations listed in Table 2

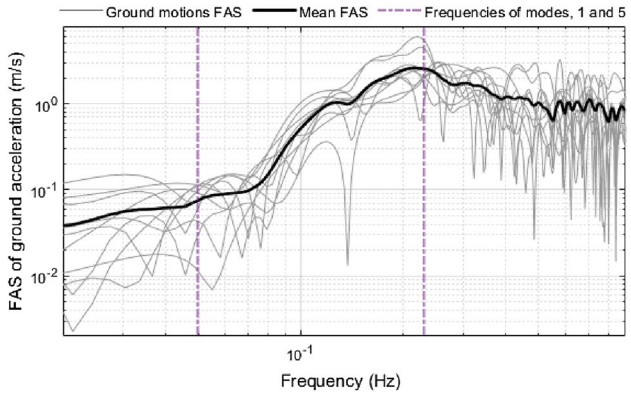

Fig. 6 Fourier amplitude spectra (FAS) of the selected horizontal ground motion time series are shown in Fig. 5. The gray lines correspond to individual ground motions, and the black line is the average FAS. The vertical lines correspond to the frequencies of the two modes listed in Table 1

data from Taiwan, Rupakhety and Sigbjörnsson [26] report that up to ~ 2 Hz, lagged coherency at 200 m separation distance is very close to 1. Zerva [42] reports similar results for a separation distance of 1000 m. Based on a case study of the El Asnam earthquake ground motion simulation, AfifChaouch et al. [1] report that at frequencies lower than 0.5 Hz, the lagged coherency is very close to 1 even for large separation distances. Based on these considerations, it is reasonable to ignore the effect of lagged coherency in the seismic response of the RSB because the frequencies of its modes that contribute to seismic response are well below 1 Hz. To account for wave passage effect, multi-support excitation was considered. Ground motion at one side of the main span was shifted in time by 0.6 s with respect to that at the other side. This is based on assumed apparent wave propagation velocity of 2.0 km/s and main span length of 1.5 km. The difference in peak response of the tower with uniform support excitation and multi-support excitation was found to be insignificant (less than 5%). Based on these results, it was decided to use uniform support excitation for evaluation of the control performance.

Wind Force

Wind force time series is applied on the deck and tower nodes. Turbulent wind field in two space dimensions is modeled as a random process. Realizations of the random process are simulated using the spectral representation method of Shinozuka and Deodatis [29]. Spatially correlated wind field is simulated in a 2D grid. The simulation is carried out using a toolbox provided by Cheynet [7]. The wind parameters used in the simulation are as follows: friction velocity, $u^* = 2.2$ m/s [35], von Karman constant = 0.4, roughness length $z_0 = 0.03$m, sampling interval $\Delta_t = 0.25$ s, and the co-coherence function decay coefficients, C_{ij}, correspond to velocity component i (u, v, w in x-, y-, and z-directions, respectively) and space dimension j. These coefficients are selected based on N400 [37], i.e., $C_{uy} = C_{uz} = 10, C_{vy} = C_{vz} = C_{wy} = 6.5$,and $C_{wz} = 3$.

The fluctuating wind forces are applied at several nodes in the tower and the deck. The force at a node is related to the wind velocity at the node as follows:

$$F(t) = \rho C_D A U u(t), \tag{1}$$

where ρ is the density of air (taken as 1.2 kg/m^3), A is the tributary area, U is the average wind velocity, $u(t)$ is the fluctuating wind velocity, and the drag coefficient C_D is taken as 1.2. The wind forces are calculated at 80.1 m separation along the length of the deck and 18 m along the height of the tower. It was found that a finer resolution in simulating the wind field did not have significant effect on the simulated response. Figures 7 and 8 show a realization of the wind velocity and its power spectrum at the center of the deck. Figure 9 shows the co-coherence of wind velocity in horizontal and vertical separations.

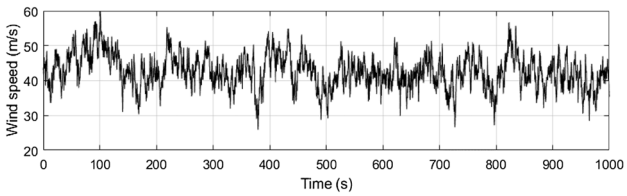

Fig. 7 A sample time history of along-wind velocity at the center of the deck

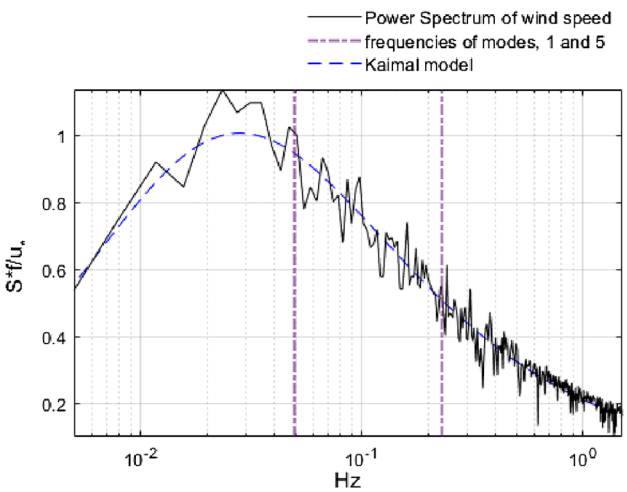

Fig. 8 Power spectrum of wind speed at the center pf the deck (see [18])

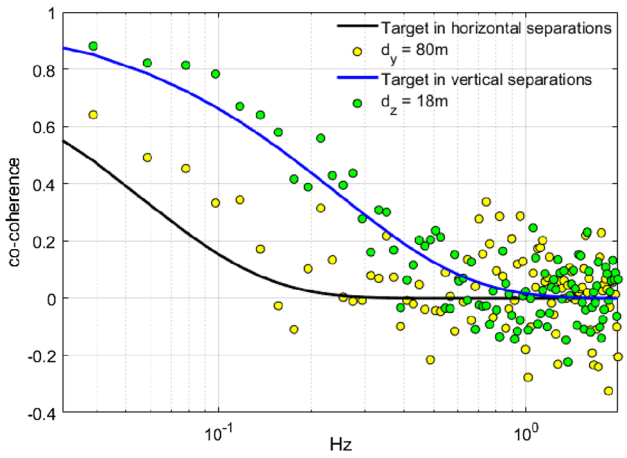

Fig. 9 Co-coherence of wind velocity in horizontal and vertical separations

Uncontrolled Response

The response of the bridge to ground motion and wind force was simulated using time history analysis. Wind forces and seismic loads are applied separately. Table 3 lists the peak displacement and acceleration response of the top of the south tower (Point 1) and the deck at mid-span (Point 2) for different ground motions and wind load. The effect of wind force on the displacement and acceleration response of the tower is negligible. Wind force is primarily relevant in terms of displacement response of the mid-span of the deck (Point 2). Seismic load is more relevant for the tower, both in terms of displacement and acceleration response. For deck acceleration, seismic load is much more relevant than wind load. Displacement response of the deck induced by ground motion is often much lower than that of wind load, but significant in some cases like ground motions 1 and 4. The peak displacement response of the deck induced by wind force is found to be 3.29 m. For the same bridge, Zhang [43] reports, from aero-static analysis, peak mid-span displacement of ~ 2.5 m at a wind speed of 45 m/s. For the same mean wind speed, our results are comparable although slightly higher than those of Zhang [43], which can be attributed to differences in wind loading parameters such as drag coefficient and the turbulence components in dynamic analysis. The peak wind speed at the deck mid-span in our analysis reaches 60 m/s, for which the aero-static mid-span displacement reported in Zhang [43] for spatially varying wind load is ~ 3.3 m, which is very close to our result. We performed response analysis with spatially uniform wind field and found that the peak response is significantly higher than for the case of a spatially variable wind field. Similar observations are reported in Zhang [43] for the same bridge.

Figure 10 presents the FAS of some of the key response parameters, i.e., displacement and acceleration at Point 1 and Point 2. For seismic load, displacement and acceleration at Point 1 and acceleration at Point 2 are presented, whereas for wind load only the displacement at Point 2 is presented. The energy in the wind force is concentrated at much lower frequencies than that in the seismic force. Wind force excites the first transverse mode but has limited energy at the vibration modes of the tower (see Fig. 8). For this reason, the wind force is primarily important for displacement (buffeting) response of the deck. Seismic motion, on the other hand, has significant energy at frequency corresponding to Mode 5 (see Fig. 6). This is reflected in the FAS of the tower-top response shown in Fig. 10. Mode 5, which is the first mode of the tower, contributes significantly to the acceleration response of the tower. The tower-top displacement is also primarily due to Mode 5. The fifth mode, although primarily related to the tower, also includes significant motion of the deck mid-span. Since the seismic load has significant energy at the frequency of this mode, it contributes to acceleration response of the deck mid-span. The contribution of the first mode in the overall acceleration response of the deck to seismic excitation is much smaller than that of the fifth mode.

Control Strategies

For multi-performance vibration control of the bridge response, passive tuned mass damper (TMD) systems are considered. The TMDs consist of a mass attached to the structure with an elastic spring and a viscous damper. It is schematically shown in Fig. 3. TMDs reduce the vibration of the structural modes they are tuned to by generating resisting inertia forces. The viscous dampers in the TMDs help to reduce the displacement of the TMD mass. Once the mass of the TMD is assigned, its stiffness and damping coefficient can be tuned for optimal vibration control. For a single TMD, the tuning is usually done to the most dominant mode

Table 3 Peak displacement and acceleration responses of tower (Point 1) and deck mid-span (Point 2)

Response	Location	Earthquake ground motion time history no										Wind force
		1	2	3	4	5	6	7	8	9	10	
Acc. (m/s^2)	Point 1 (tower)	5.44	3.01	3.36	4.50	3.17	2.60	2.49	2.17	2.23	2.67	0.02
	Point 2 (deck)	1.97	1.64	1.59	1.51	1.32	0.89	0.98	1.04	1.05	1.29	0.28
Displ. (m)	Point 1 (tower)	2.27	1.43	1.38	2.03	1.50	1.13	1.13	0.90	0.91	1.27	0.02
	Point 2 (deck)	1.95	1.15	0.88	1.31	0.84	0.56	0.78	0.88	0.70	0.81	3.29

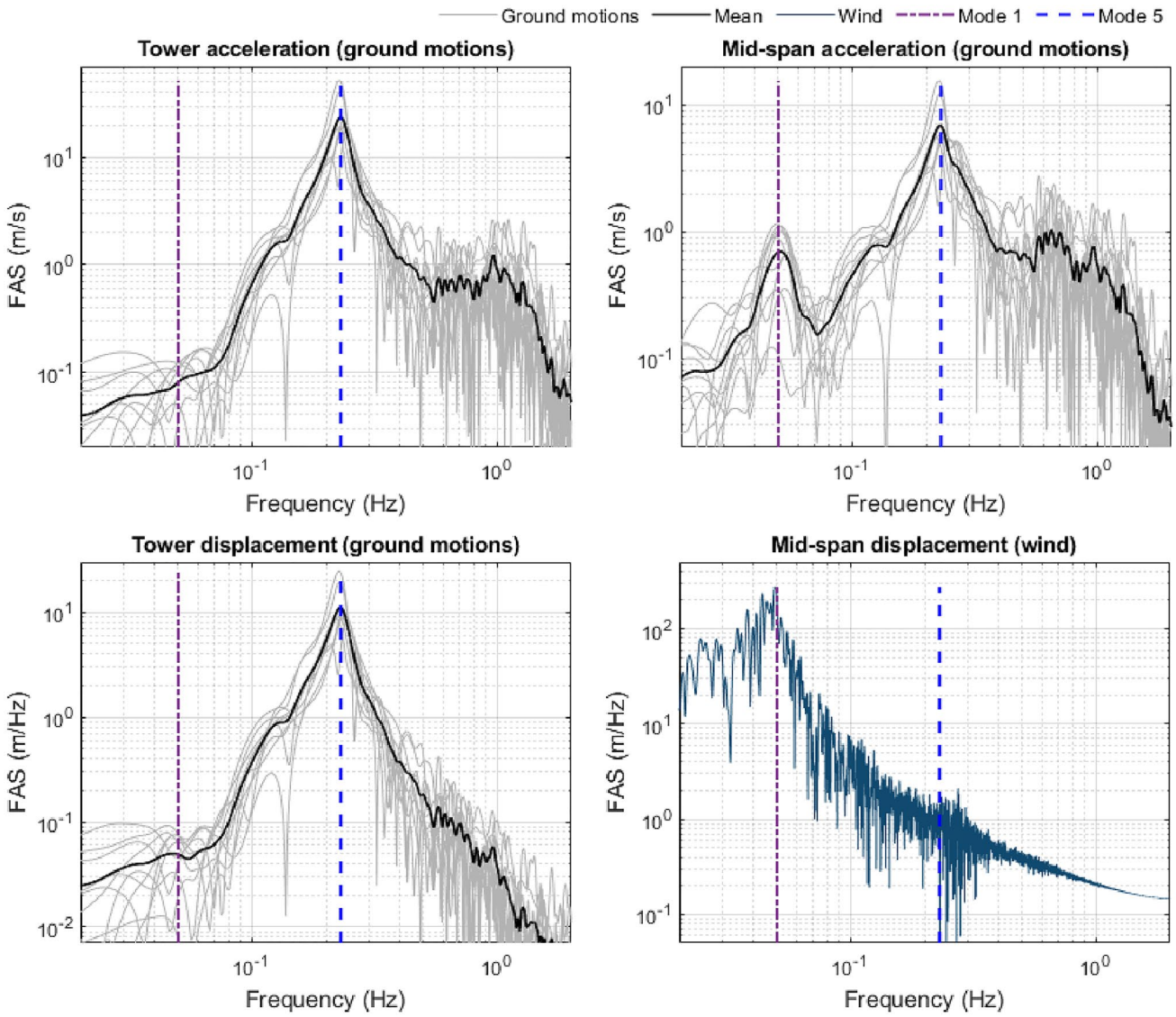

Fig. 10 FSA of tower and mid-span acceleration and displacement response in transverse direction due to wind-induced force and ground motions

of vibration on the structure. This mode, in many cases, is the fundamental mode. Multiple TMDs tuned to different modes are desirable when multiple modes of vibration contribute to the response.

In a multi-hazard scenario, the tuning of TMDs is not straightforward. Tuning in such cases depends on factors such as (i) the frequency content of excitation as it dictates which vibration mode is dominant in the response, (ii) the structural component whose response is being controlled, and (iii) the structural response to be controlled, i.e., acceleration and displacement. Factor (i) is related to the nature of the hazard, whereas factors (ii) and (iii) are linked to the location and characteristics of the TMD.

Different types of optimization methods can be used to tune TMDs for different performance objectives. One of the most used tuning methods for single TMDs is based on the Den Hartog's formulation [8]. This formulation has been adopted in this study for wind-induced vibration control. For base excited structures, such as those under seismic action, the formulation of Sadek et al. [27] is more appropriate and is therefore adopted in this study. The TMDs in this study are intended for reducing vibrations in the transverse directions of the bridge. They are therefore assumed to be fixed in the longitudinal and vertical directions. They are modeled as lumped masses attached to the structure with a two-node link element. Apart from different formulations for optimizing TMD parameters for seismic and wind actions, the properties of the TMDs vary based on which vibration mode they are tuned to.

Based on the analysis of the uncontrolled response of the bridge to ground motions and wind forces, performance objectives are identified as reduction in (i) wind-induced displacement of the deck, (ii) seismic-induced acceleration of the towers, and (iii) seismic-induced acceleration of the deck. Different combinations of TMD tuning and placements are investigated to achieve these objectives. The combinations and optimal TMD parameters are described below.

Case 1 The performance objective is reduction in seismic response of the towers. Two TMDs, one at the top of each tower, are used in this case. The TMDs are named TMD 1, with 1 indicating its location, i.e., the top of the tower. These TMDs are tuned to the fifth mode of the bridge, which is the first mode of the towers. Each TMD has a mass equal to 1% of the total mass of the bridge. The frequency and damping ratio of TMD 1 are 0.23 Hz and 6%, respectively.

Case 2 The performance objective is reduction in wind-induced displacement of the deck mid-span. The TMD is tuned to the first vibration mode of the bridge. The mass of the TMD is 1% of the total mass of the bridge. This TMD is named TMD 2, with 2 indicating its location, i.e., the mid-span of the deck. The frequency of the TMD is 0.049 Hz, and its damping ratio is 6%.

Case 3 The performance objective is reduction in seismic response of the deck. Since the seismic response is dominated by the fifth mode of vibration, the TMD is tuned to this mode. The TMD is placed at the mid-span of the deck and is named TMD 2. Its mass is 1% of the total mass of bridge. The frequency and damping ratio are 0.23 Hz and 6%, respectively, i.e., the same as in Case 1.

Case 4 Here, the control strategy is multi-hazard and multi-performance. Two subcases are investigated. Case 4a is combination of Case 1 and Case 2, i.e., to simultaneously control seismic response of the tower and wind-induced displacement of the deck. Case 4b is a combination of Case 1 and Case 3, with the objective of simultaneously controlling seismic response of the tower and the deck. To achieve this, TMDs are placed at the top of the towers and the mid-span of the deck.

Control Effectiveness

The effectiveness of the control devices is measured as percentage reduction in response. Table 4 presents a summary of control effectiveness of the different cases described above. For seismic response, maximum, minimum, and average reduction are presented. Case 1 results in reduction of tower acceleration by ~ 11–41%, with an average value of 24%. Reduction in tower displacement is also good, but slightly lower than that of tower acceleration. A single TMD placed at deck mid-span and tuned to the first mode of the bridge, i.e., Case 2, reduces the peak wind-induced acceleration and displacement by ~ 36 and 21%, respectively. Case 3 is effective in some cases, but results in amplification of deck acceleration during some of the ground motions. Case 4a is effective in seismic response control of the tower and wind response control of the deck, but not desirable for seismic response control of the deck. On the other hand, Case 4b is effective in controlling the response of the deck under most of the ground motions, but it greatly amplifies the wind-induced displacement. Comparison of Case 4a and Case 4b clearly show that a control system which is designed for seismic control of the deck amplifies wind response and vice versa. This is an important observation

Table 4 Response reduction (%) effectiveness of different cases of TMDs (negative numbers indicate amplification of response)

Case	Hazard	Performance		Ground motion			Wind
				Ave	Max	Min	
C-1	Earthquake	Towers	Accel	24.00	40.99	11.26	
			Displ	18.21	39.02	6.75	
C-2	Wind	Mid-span	Accel				35.82
			Displ				20.65
C-3	Earthquake	Mid-span	Accel	20.52	39.14	− 3.69	
			Displ	15.25	23.34	6.77	
C-4a	Earthquake and wind	Towers	Accel	24.01	41.00	11.26	18.88
			Displ	18.22	39.03	6.77	5.32
		Mid-span	Accel	0.60	8.92	− 5.79	35.75
			Displ	2.82	14.28	− 5.47	20.65
C-4b	Earthquake	Towers	Accel	24.14	41.54	11.13	24.68
			Displ	18.31	39.40	6.62	7.09
		Mid-span	Accel	21.28	39.86	− 4.08	1.98
			Displ	15.52	23.50	6.66	− 30.63
C-5	Wind and earthquake	Mid-span	Accel	18.80	41.12	− 1.27	37.33
			Displ	11.24	19.99	0.32	19.48

highlighting the multi-hazard interaction in vibration control of long-span bridges. If we consider that wind-induced displacement of the deck is more important to control than seismic-induced acceleration, we can conclude that Case 4a is the best solution.

In terms of acceleration of the deck, seismic response is much higher than the wind response. If we assume that both seismic and wind loads are relevant for the structure, although not acting simultaneously with high intensity, reducing seismic-induced acceleration of the deck might be important. But this reduction comes at a cost of amplified wind-induced displacement, which is clearly undesirable.

To overcome this problem and provide response reduction in multi-hazard scenario, we investigated an additional strategy which is called Case 5. Case 5 makes use of the TMDs as in Case 4a with three additional TMDs distributed along the deck. These additional TMDs are tuned to the fifth mode of vibration of the bridge because the seismic response of the deck is governed by this mode. The mass of each TMD is 0.33% of the total bridge mass, and damping ratio is 3.5%. The location of these TMDs is decided based on the deflected shape of the deck in this mode, which is shown in Fig. 4b. The deck deflects with two nodes and three peaks in the transverse direction. One of the peaks is located near the mid-span and the other two on either side of it. The distributed TMDs are therefore placed at quarter, half, and three quarter the length of the deck. The results corresponding to this case are also shown in Table 4. This case provides good reduction of deck response due to wind load. Unlike Case 4a, seismic response of the deck is also effectively controlled with only a minor amplification of acceleration response for one of the ground motions. It provides similar levels of seismic response reduction of the deck as Case 4b, but without amplification of the wind response. The reduction of seismic response of the towers is similar to in Case 1.

Conclusions

This study presents a case study of the Runyang Suspension Bridge (RSB) to illustrate multi-hazard and multi-performance considerations in vibration control of long-span bridges. Time history analysis of the bridge with and without tuned mass dampers (TMDs) is carried out, using a set of earthquake ground motions and spatially variable wind field simulated over a grid, to investigate the effects of wind and earthquake actions on the peak response of the deck and the towers of the bridge. The main conclusions that can be drawn from the results presented here are listed below.

(a) Wind load primarily excites the fundamental mode of the bridge and is important for deck displacement.
(b) Seismic load excites the first vibration mode of the tower and is important for its acceleration and displacement response. Since this mode is coupled with the transverse deflection of the deck, seismic load also induces significant acceleration of the deck.
(c) Tuned mass dampers (TMDs) can be effective in reducing seismic-induced and wind-induced response of the RSB when designed and placed appropriately. It was found that a TMD designed to reduce wind-induced displacement of the deck results in undesirable effects on its seismic response. Similarly, TMDs designed to control seismic response of the deck were found to amplify its wind-induced displacement by about 30%. Importance of multi-hazard and multi-performance considerations in passive vibration control is therefore clearly demonstrated.
(d) To control different response parameters such as displacement and acceleration of the different elements, i.e., the deck and the tower, multiple TMDs tuned in different ways are necessary. For example, of the solutions investigated here, a system with a TMD on each tower (tuned to the fifth mode), and three TMDs on the deck tuned to the first mode and one additional TMD on the deck mid-span tuned to the first mode provide the best solution in the multi-hazard and multi-performance consideration.

The results highlight the importance of multi-hazard considerations in vibration control of bridges, an area that has not been adequately addressed in the literature. This study does not provide a comprehensive framework for such work and has a limited scope. It does not formalize the uncertainties of the different loading types and their joint distributions, nor does it provide advanced optimization approaches. However, the study provides an illustration of some important issues in multi-hazard vibration control of structures affected by loads of different nature and frequency characteristics and is thus potentially a beginning of a more thorough and advanced future investigation in this area.

Funding Matin Jami is supported by a doctoral grant from the University of Iceland and a research grant from Vegagerðin, the Icelandic Road Administration. Rajesh Rupakhety acknowledges support from the University of Iceland Research Fund.

Data availability The data used in this study can be obtained by contacting the corresponding author.

References

1. AfifChaouch K, Tiliouine B, Hammoutene M, Sigbjörnsson R, Rupakhety R (2016) Estimating ground motion incoherence

through finite source simulation: a case study of the 1980 El-Asnam Earthquake. Bull Earthq Eng 14(4):1195–1217
2. Aly AM (2014) Vibration control of high-rise buildings for wind: a robust passive and active tuned mass damper. Smart Struct Syst 13(3):473–500
3. Ancheta TD, Darragh RB, Stewart JP, Seyhan E, Silva WJ, Chiou BS et al (2013) Peer nga-west2 database. Available online at http://peer.berkeley.edu/ngawest2/databases/. Last Accessed Dec 2021
4. Arioli G, Gazzola F (2013) Old and new explanations of the Tacoma Narrows Bridge collapse. In: Atti XXI Congresso AIMETA, Torino, p 10
5. Cai CS, Chen SR (2004) Wind vibration mitigation of long-span bridges in hurricanes. J Sound Vib 274(1):421–432
6. Chen SR, Cai CS, Gu M, Chang CC (2003) Optimal variables of TMDs for multi-mode buffeting control of long-span bridges. Wind Struct 6(5):387–402
7. Cheynet E (2020) Wind field simulation (the fast version). Zenodo. https://doi.org/10.5281/ZENODO.3774136
8. Den Hartog JP (1956) Mechanical vibrations, 4th edn. McGraw-Hill, New York
9. Elias S, Rupakhety R, De Domenico D, Olafsson S (2021) Seismic response control of bridges with nonlinear tuned vibration absorbers. Structures, vol 34. Elsevier, Amsterdam, pp 262–274
10. Fujino Y (2002) Vibration, control and monitoring of long-span bridges—recent research, developments and practice in Japan. J Constr Steel Res 58(1):71–97
11. Fujino Y, Siringoringo D (2013) Vibration mechanisms and controls of long-span bridges: a review. Struct Eng Int 23(3):248–268
12. Gu M, Chang CC, Wu W, Xiang HF (1998) Increase of critical flutter wind speed of long-span bridges using tuned mass dampers. J Wind Eng Ind Aerodyn 73(2):111–123
13. Gu M, Chen SR, Chang CC (2002) Control of wind-induced vibrations of long-span bridges by semi-active lever-type TMD. J Wind Eng Ind Aerodyn 90(2):111–126
14. Ha DH, Park JH, Park KS, Park W, Choo JF (2010) Optimization of complex dampers for the improvement of seismic performance of long-span bridges. KSCE J Civ Eng 14(1):33–40
15. Jami M, Rupakhety R, Elias S, Bessason B, Snæbjörnsson JT (2022) Recent advancement in assessment and control of structures under multi-hazard. Appl Sci 12(10):5118
16. Jangid RS (2022) Seismic performance assessment of clutching inerter damper for isolated bridges. Pract Period Struct Des Constr 27(2):04021078
17. Ji L, Zhong J (2006) Runyang Suspension Bridge over the Yangtze river. Struct Eng Int 16(3):194–199
18. Kaimal JC, Wyngaard JCJ, Izumi Y, Coté OR (1972) Spectral characteristics of surface-layer turbulence. Q J R Meteorol Soc 98(417):563–589
19. Lavasani SHH, Alizadeh H, Doroudi R, Homami P (2020) Vibration control of suspension bridge due to vertical ground motions. Adv Struct Eng 23(12):2626–2641
20. Li Z, Li A, Zhang J (2010) Effect of boundary conditions on modal parameters of the Run Yang suspension bridge. Smart Struct Syst 6(8):905–920
21. Marić MK, Ivanković AM, Srbić M, Skokandić D (2022) Assessment of performance indicators of a large-span reinforced concrete arch bridge in a multi-hazard environment. Buildings 12(7):1046
22. Padgett JE, Kameshwar S (2016) Supporting life cycle management of bridges through multi-hazard reliability and risk assessment. Multi-hazard approaches to civil infrastructure engineering. Springer, Cham, pp 41–58
23. Paultre P, Chaallal O, Proulx J (1992) Bridge dynamics and dynamic amplification factors—a review of analytical and experimental findings. Can J Civ Eng 19(2):260–278
24. Pisal AY, Jangid RS (2016) Vibration control of bridge subjected to multi-axle vehicle using multiple tuned mass friction dampers. Int J Adv Struct Eng (IJASE) 8:213–227
25. Pourzeynali S, Estaki S (2009) Optimization of the TMD parameters to suppress the vertical vibrations of suspension bridges subjected to earthquake excitations
26. Rupakhety R, Sigbjörnsson R (2012) Spatial variability of strong ground motion: novel system-based technique applying parametric time series modelling. Bull Earthq Eng 10(4):1193–1204
27. Sadek F, Mohraz B, Taylor AW, Chung RM (1997) A method of estimating the parameters of tuned mass dampers for seismic applications. Earthq Eng Struct Dynam 26(6):617–635
28. Saha P, Jangid RS (2009) Seismic control of benchmark cable-stayed bridge using passive hybrid systems. IES J Part A Civ Struct Eng 2(1):1–16
29. Shinozuka M, Deodatis G (1991) Simulation of stochastic processes by spectral representation
30. Shum KM, Xu YL, Guo WH (2008) Wind-induced vibration control of long span cable-stayed bridges using multiple pressurized tuned liquid column dampers. J Wind Eng Ind Aerodyn 96(2):166–192
31. Simpson RH (1998) The Mycenaean highways. Echos du monde classique Class views 42(2):239–260
32. Soneji BB, Jangid RS (2006) Effectiveness of seismic isolation for cable-stayed bridges. Int J Struct Stab Dyn 6(01):77–96
33. Soneji BB, Jangid RS (2007) Passive hybrid systems for earthquake protection of cable-stayed bridge. Eng Struct 29(1):57–70
34. Tanida K (2002) Progress in the application of active vibration control technologies to long-span bridges in Japan. Prog Struct Mat Eng 4(4):363–371
35. Wang H, Guo T, Tao TY, Li AQ (2016) Study on wind characteristics of Runyang Suspension Bridge based on long-term monitored data. Int J Struct Stab Dyn 16(04):1640019
36. Wang H, Li A, Jiao C, Spencer BF (2010) Damper placement for seismic control of super-long-span suspension bridges based on the first-order optimization method. Sci China Technol Sci 53(7):2008–2014
37. Wang J, Cheynet E, Snæbjörnsson JÞ, Jakobsen JB (2018) Coupled aerodynamic and hydrodynamic response of a long span bridge suspended from floating towers. J Wind Eng Ind Aerodyn 177:19–31
38. Xing C, Wang H, Li A, Xu Y (2014) Study on wind-induced vibration control of a long-span cable-stayed bridge using TMD-type counterweight. J Bridg Eng 19(1):141–148
39. Xu K, Bi K, Ge Y, Zhao L, Han Q, Du X (2020) Performance evaluation of inerter-based dampers for vortex-induced vibration control of long-span bridges: a comparative study. Struct Control Health Monit 27(6):e2529
40. Xu K, Bi K, Han Q, Li X, Du X (2019) Using tuned mass damper inerter to mitigate vortex-induced vibration of long-span bridges: analytical study. Eng Struct 182:101–111
41. Xu K, Dai Q, Bi K, Fang G, Zhao L (2022) Multi-mode vortex-induced vibration control of long-span bridges by using distributed tuned mass damper inerters (DTMDIs). J Wind Eng Ind Aerodyn 224:104970
42. Zerva A (2016) Spatial variation of seismic ground motions: modeling and engineering applications. CRC Press, Boca Raton
43. Zhang X (2007) Influence of some factors on the aerodynamic behavior of long-span suspension bridges. J Wind Eng Ind Aerodyn 95(3):149–164

44. Zhu J, Zhang W, Zheng KF, Li HG (2016) Seismic design of a long-span cable-stayed bridge with fluid viscous dampers. Pract Period Struct Des Constr 21(1):04015006

Paper 3

Jami, M., Rupakhety, R., Elias, Domenico, D., (2025). Reliability of Bridges Under Near-Fault Pulse-Type Ground Motions with Vertical Component Consideration.

Reliability of Bridges Under Near-Fault Pulse-Type Ground Motions with Vertical Component Consideration

Matin Jami[1], Said Elias[2,*] and Rajesh Rupakhety[1],
Dario De Domenico[3]

1 Earthquake Engineering Research Center, University of Iceland, Selfoss, Iceland
2 Marie Skłodowska-Curie Actions (MSCA), Institute for Risk and Reliability, Leibniz University Hannover (LUH), Hannover, Germany (elias.rahimi@irz.uni-hannover.de)
3 Department of Engineering, University of Messina, 98166 Messina, Italy

Abstract

Seismic waves from near-fault earthquakes often produce pronounced pulse effects, significantly influenced by vertical ground motion. This study investigates the seismic response of bridges under near-fault pulse-type ground motions (NFPTGMs), emphasizing the vertical component, and proposes a conceptual passive vibration control solution. A dataset of 100 NFPTGMs is used for three-dimensional nonlinear time history analyses of short/medium-span beam bridges and long-span suspension bridges. Plastic hinges are modeled in piers to simulate realistic damage, and seismic performance is evaluated by comparing peak moment responses to bending resistance derived from axial load-bending moment interaction domains. Statistical analysis produces fragility curves, revealing that the vertical component substantially increases the probability of exceeding damage thresholds. To mitigate seismic vulnerability, a 3D tuned mass damper (TMD) is proposed, positioned on the pier for beam bridges and the tower for suspension bridges. The TMD's parameters are optimized using a genetic algorithm to minimize lateral deformation while accounting for vertical excitation. Results demonstrate that the optimized 3D-TMD achieves over 60% reduction in peak moment responses for both bridge types. This solution offers a practical and effective approach to reduce seismic risk and enhance bridge resilience in near-fault regions, addressing the critical role of vertical ground motion.

Keywords: Bridges, Near-fault pulse-type ground motions, Vertical component, Tuned mass damper, Beam bridge, Suspension Bridge, Earthquake engineering, Fragility analysis

1. Introduction

Bridges are critical elements of the transportation network. The geometric configuration of bridges makes them particularly vulnerable to seismic hazard. Unseating failure and serious damage of the piers and foundations are among the most frequent causes of collapse of bridges under intense seismic excitation [1]. In addition to peculiar bridge structural elements contributing to their critical seismic response (e.g., defects in their supports, degradation of material parameters due to corrosion scenarios [2,3], curvilinear configuration amplifying deck torsion and risk of traction in the supports [4]), the level of seismic safety of existing bridges strongly depends on the earthquake specifications of the installation site [5]. A simplified dynamic analysis approach for evaluating suspension bridges under extreme blast loading is presented by Ali et al. [70]. Their method utilizes a bilayer solution with blast loads modeled as nodal loads and the structural response represented by a 3D fishbone skeleton finite-element model. The study identifies critical vulnerable locations, particularly the tower top node, where blast loads could lead to zipper-type progressive failure of the bridge. The paper emphasizes the importance of maintaining the demand-to-capacity ratio below 0.8 for all bridge components under medium- to large-sized explosives to ensure safety under extreme limit states. The challenging question arises whether bridges checked and constructed to comply with the so-called design earthquake, which is a conceptual principle summarizing the frequency content and amplitude of the earthquake excitation, are safe under any types of earthquakes.

During earthquake events, seismic waves propagate in three directions. These waves have different peculiarities depending on three factors: rupture mechanism, slip direction, and tectonic displacement causing a residual ground displacement. These source-related factors interact with ground layer properties crossed by the seismic waves before reaching the foundation level. Various methodologies have been proposed in the literature for classification of strong ground motion. The distance of the structure from the fault rupture represents one of the most popular and internationally recognized criteria for classification that directly influences the imposed peak displacement demand of a structure [6]. In particular, so-called near-fault pulse-type ground motions (NFPTGMs) are those affecting structures located in the vicinity of the fault rupture [7], whereas far-field records are those associated with rupture distance of 20 km or more. Ground motion records within 20 km from the fault are known to contain large velocity pulses [8], especially at sites which align with the direction of rupture propagation on the fault, the effect being known as forward directivity [9]. Long-period short-duration pulses and high ratios of peak ground velocity (PGV) to peak ground acceleration (PGA) are characteristics of such NFPTGMs [10]. Additionally, the tectonic deformation resulting from the fault rupture may be associated with a considerable residual (permanent) ground displacement termed fling-step effect [11].

Fragility models play a critical role in understanding and predicting the failure risks of infrastructure systems under natural hazards. For instance, spatiotemporal fragility models, such as those used in predicting lightning-related failures of overhead contact lines, demonstrate the value of probabilistic approaches to address uncertainties in external loads and system vulnerabilities [51]. Corrosion-induced degradation significantly affects the seismic performance of RC columns, reducing their drift and shear force capacities over time. Ghosh and Padgett [50] developed probabilistic models that integrate with fragility estimates to assess failure probability of aged bridges comprehensively. The construction of fragility curves (FCs) for assessing the seismic vulnerability of bridges is a widely recognized approach in earthquake engineering. Traditional methods often rely on site-specific parameters such as local stratigraphy and topography, which can introduce variability

in FCs. Recent advancements, such as spectrum-consistent transformation methods, allow for site-independent FCs that preserve consistency across diverse locations and soil conditions [52]. Incorporating soil spatial variability into the fragility assessment of bridges provides a more realistic evaluation of seismic vulnerabilities. For instance, Jiang et al. [53] demonstrated that neglecting soil spatial variability can lead to underestimation of both component and system-level fragility curves for cable-stayed bridges. Large-scale seismic risk assessments of bridge clusters are essential for understanding regional vulnerabilities. For example, Li et al. [54] employed artificial intelligence-based methodologies to evaluate the seismic risk of RC girder bridges, demonstrating the effectiveness of intelligent models in regional risk analysis. Time-dependent degradation of structural properties, such as corrosion in RC frames, has been shown to critically influence fragility estimates. Feng et al. [55] utilized a time-variant modeling strategy to simulate these effects, emphasizing their role in seismic risk assessment. The time-dependent seismic fragility and risk assessment methodology developed by Liljefors and Köhler [56] illustrated how aging and deterioration due to corrosion affect the seismic performance of bridge piers. Fragility estimates for flexible structures with outrigger systems were formulated using deep neural networks (DNNs) by Xing et al. [57], considering uncertainties in seismic input parameters. Chloride-induced corrosion significantly impacts the seismic performance of bridge piers, especially in marine environments. Guo et al. [58] develop a comprehensive framework to assess the life-cycle seismic resilience of sea-crossing bridges, incorporating the effects of corrosion and stochastic environmental conditions. Li et al. [54] address the challenges of inconsistent macroseismic intensity scales across different regions, proposing an updated macroseismic intensity measure (UCMS-20) that integrates instrument intensity and probabilistic seismic hazard models, thereby improving vulnerability assessments for structures. Recent studies on reliability analysis have proposed advanced models and methods for evaluating structural performance under various stochastic processes and seismic hazards. Dang et al. [60] introduced a loading contribution degree analysis-based strategy for time-variant reliability analysis of structures subjected to multiple loading processes, while Chen et al. [61] developed a probabilistic seismic capacity model of pier columns using a semiparametric regression approach. Furthermore, Monti et al. [62] have advanced risk-targeted seismic hazard models for Europe, contributing to a more refined understanding of seismic risk assessment. Kumbhojkar et al. [71] conduct a fragility analysis of a base-isolated integral bridge subjected to two-component far- and near-field earthquakes. Their study emphasizes the increased threat posed by near-field earthquakes, including directivity and fling-step effects, to the performance of base-isolated bridges. By using incremental dynamic analysis (IDA) with peak ground acceleration as the intensity measure, the study develops probabilistic seismic demand models and fragility curves based on maximum deck drift and shear strain in the isolator. The findings underscore the importance of carefully designing base isolators to account for the heightened risk from near-field earthquakes. Ahmed and Dasgupta [72] propose a novel methodology for assessing component-level fragility curves (FCs) for structures, particularly integral abutment bridges, under seismic loading. The authors develop a new approach for seismic demand assessment and a numerical technique for fragility computation, which enhances the reliability of the results by avoiding the complexities of dynamic analysis. Their method offers a more accurate and simplified alternative to traditional fragility formulations, which often rely on rough lognormal or normal fits. The study provides a practical and precise means of assessing the seismic vulnerability of bridge components, crucial for effective disaster mitigation strategies. Chen [73] presented an improved probabilistic seismic demand–intensity relationship that addresses heteroscedasticity in seismic demand models. The study systematically investigated the phenomenon

of nonconstant variance or covariance in seismic demand and proposes generalized methods for both univariate and multivariate cases. Using nonlinear time history analysis of a four-span simply supported girder bridge, the author develops Bayesian regression-based probabilistic seismic demand models. The results demonstrated that incorporating heteroscedasticity leads to better-calibrated predictions, offering a more accurate foundation for seismic fragility analysis and improved seismic risk assessment for decision-making. In addition to the previously discussed methodologies, Tabandeh et al. [74] offer an insightful review of importance sampling methods for reliability analysis. Their paper provides a comprehensive examination of the mathematical foundations of the technique and discusses two main approaches for constructing importance sampling densities. The authors highlight the advantages and challenges of implementing these methods, especially for time-variant reliability analysis, making their work a valuable contribution to the field of reliability assessment in structural engineering.

Yu et al. [63] emphasized the importance of statistical validation methods, including the Accuracy Likelihood and Distribution Match, for improving the robustness of regional risk models. Earthquake-induced damage to bridges can significantly affect their performance. Iannacone and Gardoni [64] develop a probabilistic model that accounts for both gradual deterioration and shock processes in seismic events, providing a more accurate estimate of bridge reliability under earthquake loading. In their study, Qin [65] proposed a reliability assessment framework for the seismic performance of highway bridge networks, considering failures due to traffic flow redistribution. Their work highlights the use of fragility curves and stochastic user equilibrium assignments to evaluate network efficiency and identify congestion-prone links in the aftermath of seismic events. Guidotti et al. [66] developed an efficient method for evaluating the connectivity probability of large-scale highway bridge networks by decomposing the network into smaller subnetworks. Their approach significantly improves computational efficiency by reducing running time compared to traditional methods while accurately assessing the network's reliability.

Jangid [67] conducted a performance analysis on a structure equipped with an inerter damper (TID) isolation layer under stochastic seismic excitations. Their work presents a comprehensive simulation-based dynamic response analysis and reliability assessment, demonstrating that the TID isolation layer significantly enhances the structural robustness and reliability by mitigating the effects of seismic randomness. Fadel Miguel and Beck [68] proposed a Reliability-Based Design Optimization (RBDO) procedure to determine the optimal track shape of Friction-based Track-Nonlinear Energy Sinks (T-NES II) in buildings subjected to seismic ground accelerations. Their approach aims to minimize life-cycle costs associated with various damage states, with results indicating that multimodal track profiles significantly reduce the oscillation of the host structure. Fadel Miguel et al. [69] proposed a Reliability-Based Design Optimization (RBDO) approach to determine the optimal track shape for supported Pendulum Tuned Mass Dampers (PTMDs) in buildings subjected to seismic excitation. Their method uses Padé approximants as design variables, reducing computational cost by 40% for circular track shapes. The optimized track shape significantly reduces the building's annual failure rate by 53%, with a track profile differing from the circular equation, showing a higher slope for moderate displacements.

Velocity pulses are extracted and examined from NFPTGMs using several time, frequency, and time-frequency methods. Several authors, among which Baker [12], Rupakhety et al. [13-17], Xie et al. [18], Panella et al. [19], Kohrangi et al. [20], Quaranta and Mollaioli [21], elaborated various procedures to identify NFPTGMs by collecting databases of recorded events and scrutinizing their peculiar characteristics. Among such peculiar characteristics, the vertical shaking of NFPTMGs was

found to be markedly higher than conventional far-field records. The reason for this is related to the fact that the number of wave refractions occurring in wave propagation from the hypocenter to the site is generally quite limited and, thus, not only the P waves but also the S waves (arriving at the surface with an inclined, not perfectly vertical, direction) contribute to the vertical seismic excitation. Some emblematic Italian cases of NFPTGMs showing such distinct feature, including L'Aquila 2009 and Casamicciola 2017 earthquakes, were recently discussed by Falsone et al. [22]. In most building codes the vertical action of ground motion is assumed assumed to be roughly 2/3 of the horizontal action [23]. Numerous studies from the literature, such as Chopra [24], Kalkan and Graizer [25], Piolatto [26], Abdollahiparsa [27], Langston and Hammer [28], and Shrestha [29], investigated the response of different types of structures when excited by ground motion in three directions with the aim to quantify the vertical-to-horizontal (V/H) ratio of the excitation and related seismic response. It was found that, due to the abovementioned reasons, NFPTGMs can have a vertical component that is comparable to, or even higher than, the horizontal component [30,31].

In a previous work, Falsone et al. [22] investigated the impact of the vertical component of NFPTGMs on one case study bridge structure, i.e., an ordinary beam bridge. In this work, interesting research findings were disclosed related to safety checks of bridge structures when the vertical component of NFPTGMs was included in the analysis, namely the reduction of bending moment capacity and ductility of piers. However, the numerical results reported in the previous work [22] were based on a simplified linear elastic model of the case study bridge, thus neglecting material nonlinear behavior that is experienced by damaged portions of bridges (e.g., piers) under severe seismic excitation. Moreover, only a couple (i.e., two in number) of near-fault records was considered, thus making it impossible to draw general (statistically valuable) conclusions. The seismic vulnerability of bridge structures to NFPTGMs and the prominent influence of the vertical component of such kind of excitation certainly deserves further investigation. To this end, this paper presents a more systematic study that expands and generalizes the previous work by Falsone et al. [22] by providing the following four novel contributions:

1) This study advances the current literature by incorporating the vertical component of Peak Ground Velocity (PGV) as an intensity measure (IM) in the fragility assessment of bridges. While most existing seismic fragility models predominantly focus on horizontal ground motions, our approach explicitly considers the vertical component, which has been shown to significantly impact the seismic response of bridge structures, particularly during strong ground shaking. In this study, 100 pulse-type ground motions are selected, with the intensity measure (PGV) varying up to 2 m/sec for short-span bridges and up to 3 m/sec for long-span bridges. This consideration of vertical PGV provides a more comprehensive evaluation of the seismic vulnerability of bridges, offering new insights into their behavior under earthquake-induced forces and improving the accuracy of fragility predictions.
2) Two representative existing bridge structures are comparatively analyzed, namely an ordinary short/medium-span girder beam bridge (BB) and a long-span suspension bridge, the Runyang Suspension Bridge (RSB), in order to cover a wider range of bridge structural behaviors.
3) Nonlinearity of structural response is considered to simulate the bridge seismic response (especially under severe earthquake excitations) more realistically than the previous work [22] that, as said above, adopted a simplified linear elastic model.
4) In addition to the two records previously considered in [22], the bridge structures are subjected to a set of further 98 NFPTGMs that are carefully selected based on Peak ground velocity (PGV) and other pulse indicators from the literature. The larger number of nonlinear time

history analyses has made it possible to draw more general conclusions by constructing bridge fragility curves accounting for and neglecting the vertical component of the seismic excitation.

5) A conceptual scheme of 3D tuned mass damper (TMD) is proposed to mitigate the bridge seismic response. Based on the selected group of 100 NFPTGMs, the tuning parameters of the 3D TMD are identified through genetic algorithm in the three directions independently, thus considering the mitigation of the bridge lateral deformation along with the effect of the vertical seismic excitation simultaneously. It is found that the proposed 3D-TMD reduces the peak moment responses by more than 60% in the piers and towers of the two bridges, respectively, thus proving to be a promising solution for mitigating the seismic risk of existing bridges located in near-fault regions.

This study builds upon and advances the work of Falsone et al. [22], who explored the impact of vertical near-fault pulse-type ground motions (NFPTGMs) on an ordinary beam bridge. While their study highlighted the reduction in bending moment capacity and ductility of piers under vertical excitations, it relied on a simplified linear elastic model and only considered a limited number of ground motion records. In contrast, this paper presents a more comprehensive investigation, incorporating a dataset of 100 NFPTGMs to provide a more robust and statistically significant analysis. Moreover, the study considers nonlinear material behavior, thus offering a more realistic representation of bridge performance under severe seismic conditions. One of the novel contributions of this work is the incorporation of vertical Peak Ground Velocity (PGV) as an intensity measure in the fragility analysis, which has been shown to significantly influence the seismic response of bridge structures, particularly in the presence of strong vertical ground shaking. Additionally, this paper proposes a novel 3D tuned mass damper (TMD) control strategy that addresses seismic effects in all three directions—vertical, horizontal, and longitudinal—simultaneously. The tuning parameters of the TMD are optimized using a genetic algorithm, ensuring that the bridge's lateral and vertical deformations are mitigated effectively. Through these innovative approaches, this study provides valuable insights into the seismic vulnerability of bridges under NFPTGMs and offers a promising solution for mitigating seismic risk in near-fault regions.

2. Methodology for fragility and reliability curve development

2.1. Nonlinear modeling

To investigate the seismic response of a bridge, researchers have used several methods, such as the frequency domain random vibration method, the response spectrum method, and the time-history analysis method [25]. In the frequency domain random vibration method, the system transfer function calculates the auto-spectral density functions for the input excitation. This method is sufficient only if the nonlinear effects are not expected to be significant. The response spectrum method is used to estimate the maximum values of response parameters. However, this method is generally used in design, and it is approximate and not an appropriate method for nonlinear analysis. The most preferred approach for investigating the response of the bridge subjected to ground excitation is time-history analysis. This method is an intensive computational method that can account for all nonlinearity sources. This study used a step-by-step nonlinear integration analysis in the time domain to obtain the bridges' seismic response. The mathematical modeling was made based on following assumptions:

- The bridges without or with the TMD are modeled by dividing the deck and piers into several small discrete elements interconnected at nodes. Three translational degrees of freedom and

three rotational degrees of freedom directions are considered at each node and the mass from each adjacent element is lumped at the node.

- Mass contribution from the nonstructural elements, such as wearing course, parapet walls, etc., are taken into account because they produce inertial forces. However, their stiffness is negligible in the dynamic behavior of the bridge.
- For nonlinear analysis, columns are modeled as nonlinear elements with lumped plasticity by defining plastic hinges at both ends of each column. The hinge's properties are based on FEMA-356 [32]. To define the plastic hinge's force–deformation behavior, five points are labeled as A, B, C, D, and E in Figure 1. Line AB presents the linear response and points B and C present the yield and ultimate capacity of the hinges. Beyond point C the degradation begins and from D to E the strength is significantly reduced. The component strength is essentially zero after point E. In this study, the modelled hinges incorporate P-M2-M3 interaction. Hinge properties are defined in terms of moment and rotation. The slope of line BC is 10% and the acceptance criteria Immediate Occupancy (IO), Life Safety (LS), and Levels of Collapse Prevention (CP) are selected based on FEMA-356 [32]. The hinge length was calculated based on ATC-32 [33].

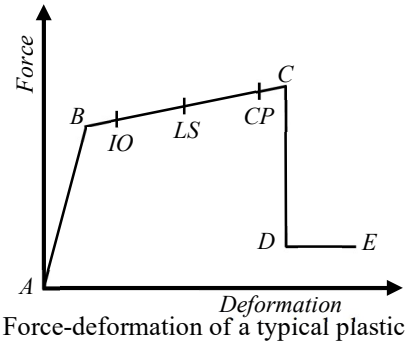

Figure 1. Force-deformation of a typical plastic hinge.

In this study, the incremental iteration strategy and Newmark's method with direct integration procedure are adopted for nonlinear analysis. This nonlinear inelastic dynamic analysis is presented as a flow chart in Fig. 8 to illustrate the details of the iteration strategy at each time step. In the nonlinear analysis, as in linear analysis, the inertial effects of lumped masses are considered at elements joints. The incremental equilibrium equation of motion is:

$$[M]\{\Delta\ddot{X}\} + [C]\{\Delta\dot{X}\} + [K]\{\Delta X\} = \{\Delta F\} \tag{1}$$

where $[M], [C]$, and $[K]$ are mass, damping and stiffness matrixes. $\{\Delta\ddot{X}\}, \{\Delta\dot{X}\}, \{\Delta X\}$, and $\{\Delta F\}$ are the incremental acceleration, velocity, displacement, and ground excitation force vector respectively, from time t to $t + \Delta t$. Also, the Newmark's method parameters γ and β are assumed as 0.5 and 0.25. The damping matrix is defined as:

$$[C] = \alpha_M[M] + \alpha_K[K] \tag{2}$$

where α_M is mass-proportional factor and α_K is stiffness-proportional factor. To estimate the incremental displacement we can use equation (3):

$$\Delta X = \Delta\hat{F}/[\hat{K}] \tag{3}$$

where $\Delta\hat{F}$ and $[\hat{K}]$ are incremental effective force vector and effective stiffness matrix obtained from the following equations (4) and (5)

$$\Delta\hat{F} = \{\Delta F\} + \left\{\frac{4}{\Delta t}[M] + 2[C]\right\}\{\dot{X}_n\} + 2[M]\{\ddot{X}_n\} \tag{4}$$

$$[\hat{K}] = \frac{4}{\Delta t^2}[M] + \frac{2}{\Delta t}[C] + [K] \tag{5}$$

then at the time $t + \Delta t$, the acceleration, velocity and displacement are updated based on ΔX as:

$$\{\ddot{X}_{n+1}\} = -\{\ddot{X}_n\} - \frac{4}{\Delta t}\{\dot{X}_n\} + \frac{4}{\Delta t^2}\{\Delta X\} \tag{6}$$

$$\{\dot{X}_{n+1}\} = -\{\dot{X}_n\} + \frac{2}{\Delta t}\{\Delta X\} \tag{7}$$

$$\{X_{n+1}\} = \{X_n\} + \{\Delta X\} \tag{8}$$

then for each subsequent time steps the effects of Residual Force $\{R_f\}$ are considered for structural system. The residual forces are calculated from the damping force, inertial force, total external force $\{F\}$ and updated internal force $\{F_{int}\}$ form equation (9)

$$\{\Delta R_f\} = \{F_{n+1}\} - [M]\{\ddot{X}_{n+1}\} - [C]\{\dot{X}_{n+1}\} + \{F_{int}\} \tag{9}$$

then for the subsequent time step the structural response is updated as follows:

$$\{\Delta\Delta X\} = \{\Delta R_f\}/[\hat{K}] \tag{10}$$

$$\{\Delta X^{k+1}\} = \{\Delta X^k\} + \{\Delta\Delta X\} \tag{11}$$

$$\{\ddot{X}_{n+1}\} = -\{\ddot{X}_n\} - \frac{4}{\Delta t}\{\dot{X}_n\} + \frac{4}{\Delta t^2}\{\Delta X^{k+1}\} \tag{12}$$

$$\{\dot{X}_{n+1}\} = -\{\dot{X}_n\} + \frac{2}{\Delta t}\{\Delta X^{k+1}\} \tag{13}$$

$$\{X_{n+1}\} = \{X_n\} + \{\Delta X^{k+1}\} \tag{14}$$

This direct integration time history analysis is applied to all 3-directions simultaneously. The axial load and base moment for the pier are calculated in the time domain. Then, for evaluating the effect of the vertical component of ground motion on the moment capacity of columns, an approach for the axial force-bending moment interaction diagram for circular reinforced concrete columns proposed by Quaranta et al. [34] has been used. This interaction diagram is based on the following formula:

$$M_{R\,(h+v)}(P_E) \approx \psi(P_E) M_R^{max} \tag{15}$$

where, $M_{R\,(h+v)}$ is design bending moment resistance for applied axial load for each time step (P_E), M_R^{max} is the maximum bending capacity of the column, and $\psi(P_E)$ is calculated based on the following formulation:

$$\psi(P_E) = 1 - \left|\frac{2\frac{P_E}{\pi R_{ce}^2 f_{cd}(1-\rho_c^2)}+1}{2\omega+1}\right|^{\alpha} \tag{16}$$

where R_{ce} is the outer radius in circular elements, f_{cd} is the strength of the concrete, ω is the total mechanical ratio of longitudinal reinforcement, ρ_c is the ratio between the outer and inner radius of the circular section, α is an exponent determined through an optimization process suggested by

Quaranta et al. [34]. For calculating the moment capacity of rectangular sections, at each time step, the following formula is used:

$$M_{R\,(h+v)} = A_s f_y \left(d - \frac{P_E - A_s f_y}{2\alpha_1 f'_c b}\right) \tag{17}$$

where f'_c is the concrete compressive strength, f_y is the steel yield strength, A_s the area of steel reinforcement, b is the width of the section, d is effective depth of reinforcement, and α_1 typically ranges from 0.65 to 0.85 depending on the design codes (e.g., 0.85 for ACI 318), [35].

2.2. Fragility analysis

The influence of the vertical component of NFPTGMs on the seismic response of bridge structure is investigated by comparing the bending moment capacity, meant as the flexural capacity of bridge pier, and the bending moment demand, meant as the maximum absolute value induced by seismic time-history analysis. Nonlinear three-dimensional finite element analyses on the two bridges are performed under the three components of the earthquake excitation concurrently acting. Spatial variability of the earthquake excitation is ignored in the numerical analyses. Upon neglecting shear (brittle) failure mechanisms for simplicity, bridges are deemed to be in safe conditions provided the bending moment demand obtained from the numerical analysis is less than the bending moment capacity. The variation of the vertical load (primarily caused by the vertical component of the seismic excitation) is considered to affect the fluctuations of the bending moment capacity of bridge piers through simplified axial load-bending moment interaction domains [34]. In this way, the influence of the vertical component on the safety conditions of the bridge can be directly analyzed. The methodology for fragility curve development is as follows;

For the construction of the fragility curves, the value of PGV is assumed as Intensity Measure (IM). Total number of IM samples and the range of IM values are defined. The observed PGV values from real earthquakes data are given by;

$$IM_{existing} = \{PGV_1, PGV_1, \dots, PGV_{100}\} \tag{18}$$

These values are read and processed to form an array. The Probabilistic Data (PD) is provided as

$$PD = \{PD_1, PD_1, \dots, PD_{100}\} \tag{19}$$

for each earthquake record, where M is the number of data points per earthquake. For each PD dataset, scaling factors are calculated to interpolate the probabilistic displacement across the new IM range (FEMA P695 2009):

$$scaling\ factor_{i,j} = \frac{IM_i}{IM_{existing,j}} \tag{20}$$

where i indexes the IM samples and j indexes the existing PD values. The scaled PD values PD_{new} for each earthquake record are then computed as:

$$PD_{new,i,j} = PD_j \cdot scaling\ factor_{i,j} \tag{21}$$

where PD_j is the original probabilistic displacement for a given earthquake.
To categorize the damage states of a bridge pier in terms of moment demand relative to its moment capacity, the states are typically defined using empirical and analytical studies in seismic and structural engineering. Drawing from existing research (FEMA 2008 [50]; Chen [45]; Karim and Yamazaki [46]; Pang and Li [47]; Uenaga et al. [48]; and Chen and Li [49]), the damage states are classified into four categories: slight, moderate, extensive, and complete. Table 1 summarizes the relationship between these damage states and the corresponding moment demands.

Table 1. Damage state

Damage State	Moment Demand (% of Capacity)	Description
Slight Damage	> 25%	Minor cracking or superficial damage, no significant structural impairment.
Moderate Damage	> 50%	Noticeable cracking, spalling, or minor structural damage, but still functional.
Extensive Damage	> 75%	Severe structural damage, stability threatened, close to collapse.
Complete Damage	> 100%	Pier collapse or failure, structure cannot support any further load.

Limit states LS_k are defined as thresholds for damage, derived from a Base value B:

$$LS_k = \frac{B}{f_k}, \quad f_k \in \{0.25M_R, 0.5M_R, 0.75M_R, M_R\} \tag{22}$$

where k indexes the limit states, representing different levels of structural damage and M_R is the moment capacity of tower/pier.
For each limit state LS_k and each IM sample IM_i , the exceedance count $C_{k,j}$ is determined by:

$$C_{k,j} = \sum_{j=1}^{M} \mathbb{I}(PD_{new,i,j} > LS_k) \tag{23}$$

where $\mathbb{I}(\cdot)$ is the indicator function, returning 1 if the condition is true and 0 otherwise.
The Probability Density Function (PDF) of absolute peak moment response of the bridges is computed. To this end, a normal PDF is fitted to the discrete peak moment results obtained from the numerical analyses according to following formula:

$$f_{(m)} = \frac{1}{\sqrt{2\pi}a} exp\left(\frac{-(m-\mu)^2}{2\sigma^2}\right), \quad \sigma > 0 \tag{24}$$

where (m) is the peak moment response, assumed as random variable, μ is the mean of the peak moment distribution, and σ^2 is the related variance. The PDF of the bending demand in Eq. (24) is compared with that of the capacity (bending resistance) of the bridge piers/towers, under the two distinct hypotheses of accounting for and neglecting the vertical component of the seismic excitation. This check has been performed at the base of piers.

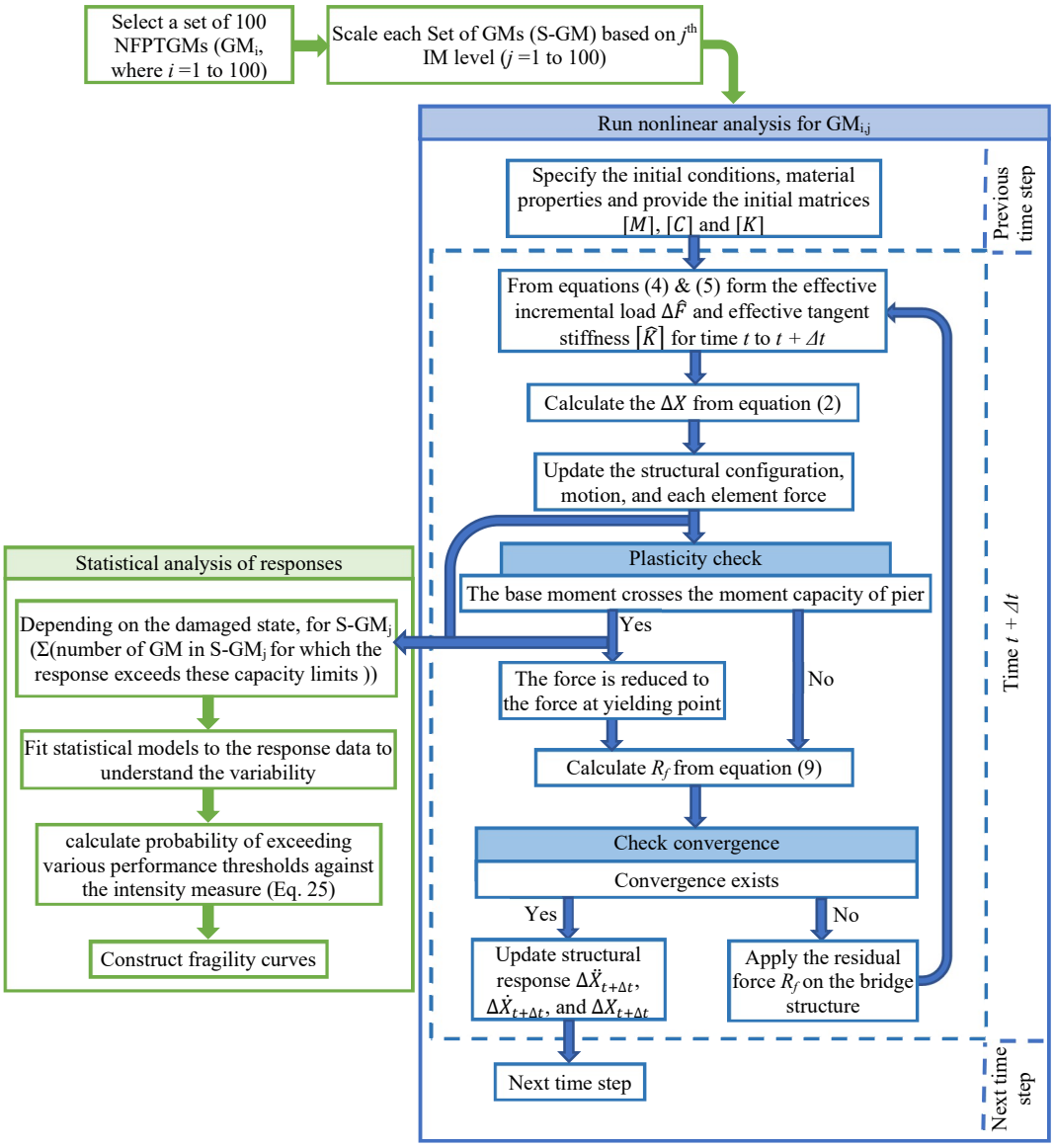

Figure 2. Flowchart for fragility analysis of bridge structures.

For fragility analysis, it is assumed that the *IM* levels causing the collapse of the bridge (i.e., the exceedance of moment capacity in the most critical pier) are lognormally distributed. According to this hypothesis, the fragility function is defined as follows:

$$P(C|IM = x) = \Phi\left(\frac{\ln {}^{x}/_{\theta}}{\beta}\right) \tag{25}$$

where $P(C|IM = x)$ is the probability that a NFPTGM associated with $IM = x$ will cause structural failure, Φ is the the standard normal cumulative distribution function (CDF), θ and β are the two parameters of the fragility function, representing the median (i.e., the IM level with 50% probability of collapse) of the fragility function and the standard deviation of $\ln IM$ (dispersion of IM), respectively.

Calibrating Eq. (25) for the considered bridge structures implies estimating θ and β from the seismic analysis results. For parameter estimation of the fragility function, the maximum likelihood estimation (MLE) is used. Multiple Stripe Analysis (MSA) approach is adopted by computing the

fraction of NFPTGMs at each stripe (the IM level) causing the bridge collapse [36]. The fragility analysis of the bridge structure is visually outlined in the flowchart depicted in Figure 2.

3. Selection of near-fault pulse-type ground motions

To investigate the structural response of bridges under NFPTGMs and to draw more general and statistically significant conclusions than those reported in the previous study by Falsone et al. [22], in addition to the two near-fault records considered in ref. [22] (i.e., L'Aquila (2009) and Casamicciola Terme (2007)) a further set of 98 NFPTGMs having a variety of frequency characteristics and seismological properties were selected from the Pacific Earthquake Engineering Research (PEER) database [37]. Therefore, a total number of 100 NFPTGMs are considered in this numerical study, whose seismological characteristics are summarized in Table 1 of Appendix A.
Three components (two horizontal and one vertical) of each earthquake event were collected, including the time history of acceleration, velocity and displacement. The classification framework proposed by Baker [12] is adopted in this work. Continuous wavelet transform of the velocity time history is performed, the largest pulse in the record is extracted and subtracted from the ground motion so as to obtain a residual record in addition to the original (source) record. Three criteria are taken into consideration in accordance with this classification framework:

i. PGV must be higher than 30 cm/sec in order to exclude low-amplitude records.
ii. Pulse indicator PI, calculated according to Eq. (26) and representing the likelihood that a record is actually pulse-like, must be higher than a threshold $PI_{\min} = 0.85$, that is:

$$PI = \frac{1}{1+\exp\left(-23.3+14.6\rho_{PGV}+20.5\rho_{E_v}\right)} \geq PI_{\min} = 0.85 \tag{26}$$

where ρ_{PGV} represents the PGV ratio, i.e., the PGV of the residual record divided by that of the original record, while ρ_{E_v} is the energy ratio, i.e., the energy calculated as cumulative squared velocity (CSV) of the residual record divided by that of the original record.
iii. Only early-arriving pulses are considered through a criterion based on the time variation of the CSV of original record and extracted pulse comparatively, i.e., $t_{20\%,\text{orig}} > t_{10\%,\text{pulse}}$ according to Baker [12], in order to selectively limit the analysis to records with directivity effects.

In the selected group of 100 NFPTGMs, each record satisfies the above-mentioned three criteria.

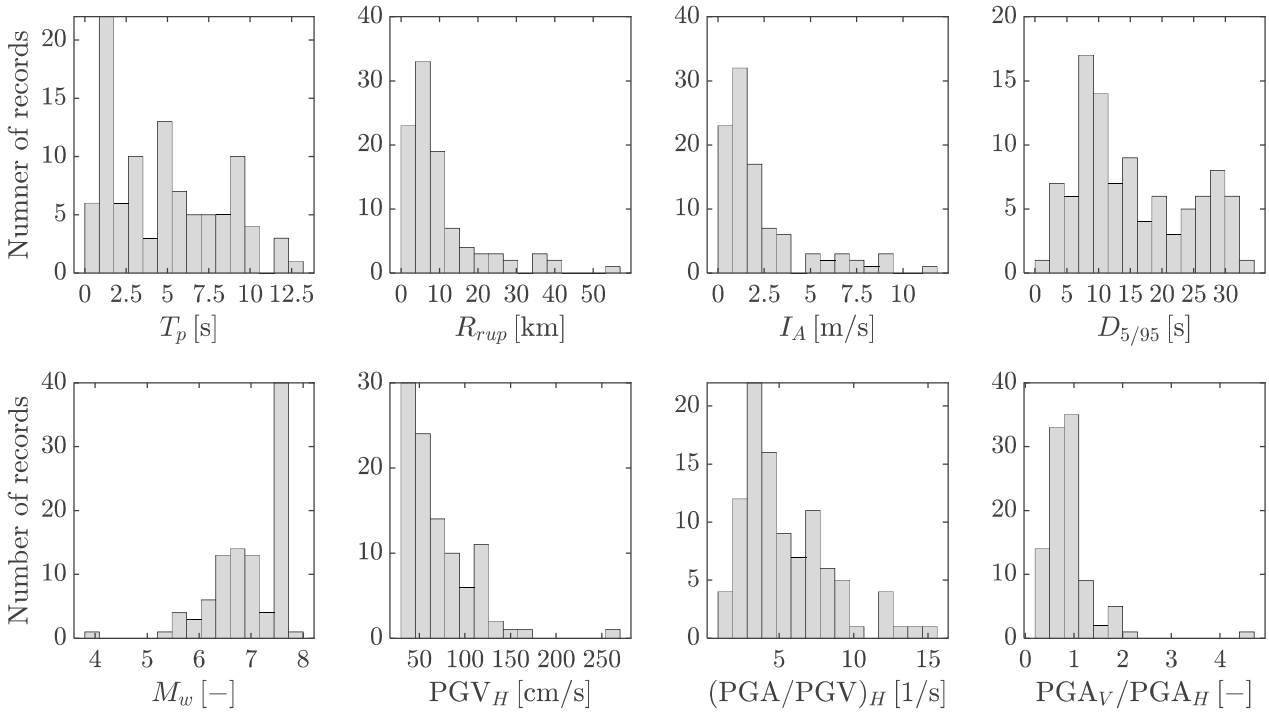

Figure 3. Distribution of main seismological parameters for the 100 NFPTGMs selected in this study.

The distribution of the main seismological parameters is shown in the histograms of Figure 3, based on which the following critical considerations can be drawn. First, the pulse periods (T_p) span a wide range from 0.59 s to 13.12 s, with a mean value of 4.85 s and a fairly uniform distribution. This implies that the considered set of ground motions are representative of different frequency contents of the seismic excitation. Most of the rupture distances (R_{rup}) of the selected events fall into the interval 0-15 km, which confirms that the pulse-like feature of the selected ground motions is generally correlated with relatively low epicentral distances (although the epicentral distance has not been taken into consideration as an explicit criterion for selecting the NFPTGMs according to the above-described classification framework [12]). The significant duration of the ground motion, meant as the time duration between the 5% and 95% of the Arias intensity and denoted as $D_{5/95}$, is relatively short for the majority of the events (10-15 s), which confirms the short duration characteristic of the selected NFPTGMs. By carefully analyzing the PGV and PGA values and ratios between the horizontal and vertical components, it emerges that a large number of selected records are characterized by high values of PGV_H (horizontal PGV), even larger than 80 cm/s, associated with a low value of the $(\mathrm{PGA/PGV})_H$ ratio (which is correlated to pulse duration of the ground motion [38]). Moreover, a markedly high ratio between the PGA in the vertical and horizontal direction is observed, much larger than the conventional value of 2/3 assumed in building codes and the literature [23] and even exceeding the unity, which means that the PGA of the vertical component is higher than that of the horizontal component. The latter result confirms the extreme importance of including the vertical component of the seismic excitation to perform seismic analysis of bridges subject to NFPTGMs.

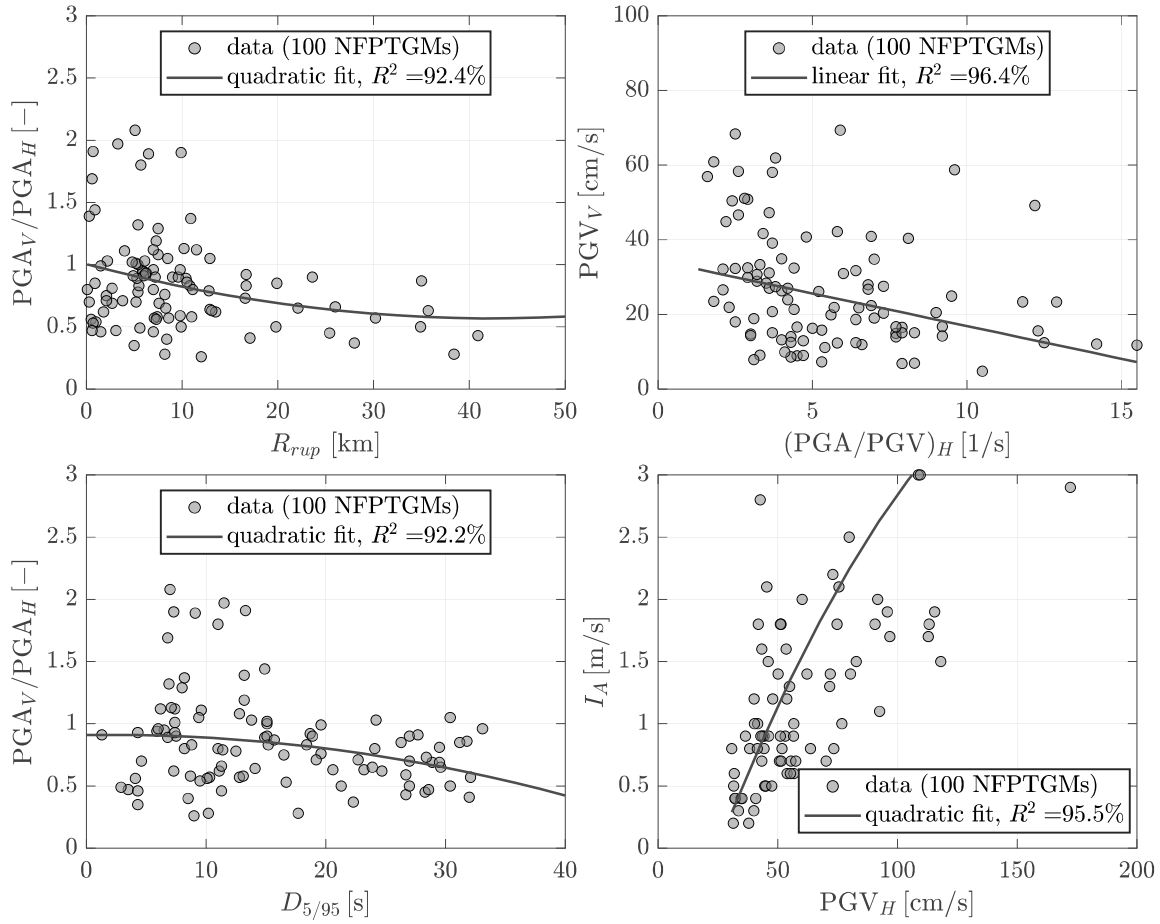

Figure 4. Correlation trends of seismological parameters for the 100 NFPTGMs selected in this study.

It is interesting to analyze some correlation trends between the seismological parameters of the 100 NFPTGMs selected in this study, as depicted in Figure 4. In general, low values of the rupture distance (R_{rup}) are associated with a higher value of the $\mathrm{PGA}_V/\mathrm{PGA}_H$ ratio, which confirms that, as explained in the introductory section 1, for near-fault earthquake events (i.e., $R_{rup} < 15 - 20$ km) the limited number of wave refractions occurring along the short traveling path of the seismic waves from the hypocenter to the site contribute to prominent effects of the vertical seismic excitation related not only to the P waves, but also to oblique S waves. The contribution of the vertical seismic excitation is more marked for those NFPTGMs having a low $(\mathrm{PGA/PGV})_H$ ratio and a low value of the significant duration $D_{5/95}$, which are two parameters somehow related to the short pulse duration of near-fault events. On the other hand, the horizontal value of the PGV (i.e., PGV_H) is a characteristic parameter correlated very well with the severity of the earthquake excitation represented by the Arias intensity I_A; hence, PGV_H can be considered a measure of the strength of NFPTGMs and is, in fact, selected as intensity measure in the construction of fragility curves discussed in the next section.

The pseudo-acceleration response spectrum, calculated as square root of sum of squares (SRSS) of the three components (two horizontal and one vertical), is depicted in Figure 5a in terms of arithmetic mean and mean ± standard deviation (std). In Figure 5b the mean pseudo-acceleration response spectrum of the three components independently considered ($S_{pa,H1}$, $S_{pa,H2}$ and $S_{pa,V}$) is illustrated along with the fundamental periods of vibration of the beam bridge (superscript BB) and of the Runyang Suspension Bridge (RSB) in the horizontal (subscript H) and vertical (subscript V) direction. It can be clearly seen that the value of the PGA in the vertical direction (PGA_V) is higher than $2/3 \cdot$

PGA_H (marked as horizontal dashed line in Figure 5b for comparison purposes), a ratio commonly referred to in the literature [23].

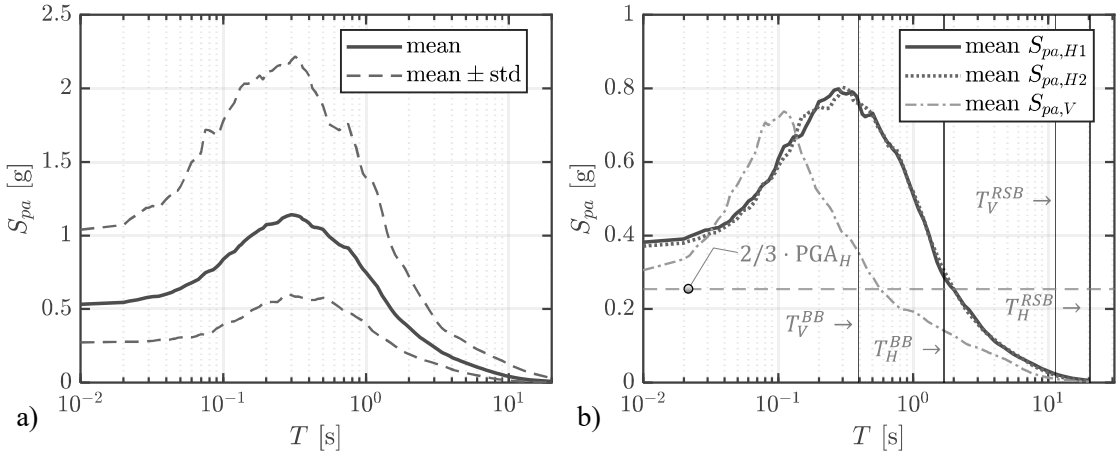

Figure 5. a) Pseudo-acceleration response spectrum (SRSS of the three components); b) comparison of horizontal and vertical mean pseudo-acceleration spectra of the 100 selected NFPTGMs.

In accordance with the Alaska Earthquake Center (AEC) classification [39], the 100 NFPTGMs were subdivided into subgroups to assess the seismic performance in a more critical and systematic manner. Three different categorization methods were used. The first categorization method classifies records into different classes depending on the moment magnitude M_w: the first group corresponds to light-to-moderate earthquakes having magnitude less than 6, the second group is representative of moderate-to-strong earthquakes with magnitude between 6 and 7, while the third and last group concerns major and severe earthquakes associated with magnitude higher than 7.

Since the peak ground velocity represents a key feature for identifying NFPLGMs, as confirmed by the observation of the previous correlation trends, the value of this parameter (PGV_H, hereinafter denoted simply as PGV) is assumed as basis for the second categorization method of earthquakes, including again three different subgroups. As said above, PGV values higher than 30 cm/sec represents a criterion for identifying pulse-type ground motions; additionally, some statistical research has indicated that the destructive force of earthquake considerably increased when PGV reached or exceeded 60 cm/sec [40]. Based on these considerations, the first group is associated with PGV less than 30 cm/sec, the second group corresponds to PGV between 30 cm/sec to 60 cm/sec, and the third group includes ground motions with PGV higher than 60 cm/sec (corresponding to strong pulse-type earthquakes).

Another factor that governs the seismic response of structures under NFPTGMs is the ratio between the period of the dominant pulse T_p of the excitation and the fundamental period of the structure T_n. Therefore, in the third categorization method, the ground motions were divided into three groups for each bridge, based on the T_p/T_n ratio, where T_p is calculated as follows [41]:

$$\ln T_p = -6.55 + 1.12 \cdot M_w \tag{27}$$

and T_n is the natural period of the bridge (T_n is 1.03sec for beam bridge and 20sec for the Rungyang suspension bridge). Table 2 indicates the number of ground motions falling in each category.

Table 2. Number of NFPTGMs falling in each category out of the 100 selected records.

Magnitude	$M < 6$	$6 < M < 7$	$7 < M$
No. of earthquakes	9	44	47
PGV	PGV<30cm/sec	30cm/sec<PGV<60cm/sec	60cm/sec<PGV
No. of earthquakes	12	54	34
T_p/T_n for beam bridge	$T_p/T_n < 0.8$	$0.8 < T_p/T_n < 1.5$	$1.5 < T_p/T_n$
No. of earthquakes	4	15	81
T_p/T_n for RSB	$T_p/T_n < 0.2$	$0.2 < T_p/T_n < 0.5$	$0.5 < T_p/T_n$
No. of earthquakes	44	48	8

4. Control Strategies

TMD systems are considered for vibration control of bridge responses. The application of TMDs to bridge structures has been extensively researched. For instance, Jami et al. [42] assessed the effectiveness of multiple distributed TMDs for RSB. Their study considered different natural vibration sources and various TMD system configurations to determine the optimal TMD design for multi-hazard vibration control.

The study introduces a novel framework aimed at optimizing the parameters of 3D-TMDs and assessing their performance in both vibration control and their impact on the moment capacity of bridge columns, considering the vertical component. First, modal frequencies and mode shapes of the considered bridges are determined. For this system, the equation of motion in matrix form is:

$$[M_s]\{\ddot{u}(t)\} + [C_s]\{\dot{u}(t)\} + [K_s]\{u(t)\} = -[M_s]\{r\}\{\ddot{u}_g\} \tag{28}$$

where the stiffness, damping, and mass matrices of the bridge are indicated as $[K_\mathrm{s}]$, $[C_\mathrm{s}]$, and $[M_\mathrm{s}]$ respectively of order $(3N + 3n) \times (3N + 3n)$; N and n indicate the degrees of freedom of the bridge and the TMD. Also, $\{u\} = \{X_1, X_2, \dots X_N, x_1 \dots x_n, Y_1, Y_2, \dots Y_N, y_1 \dots y_{n,}, Z_1, Z_2, \dots Z_N, z_1 \dots z_n\}^T$, $\{\dot{u}\}$, and $\{\ddot{u}\}$ are the displacement, velocity, and acceleration vectors, respectively. $\{\ddot{u}_\mathrm{g}\}$ is the earthquake ground acceleration vector, including $\ddot{x}_g$, $\ddot{y}_g$, and $\ddot{z}_g$ as the earthquake ground acceleration in the longitudinal, transverse, and vertical directions, and $\{r\}$ is the vector of influence coefficients. Further, $\{X_i\}$, $\{Y_i\}$, and $\{Z_i\}$ are the displacements of the i^{th} node of the bridge in the longitudinal, transverse, and vertical directions, respectively. Figures 6 presents the sketch of 3D-TMD installed in the bridges.

A computer program is developed specifically to optimize the TMD parameters based on a selected set of seismic records. Leveraging the Genetic Algorithm's (GA) capability, speed, and flexibility for multi-objective optimization, it efficiently identifies the optimal values for the TMD parameters. The parameters under optimization, based on setting the TMD mass at 1% of the total bridge mass, include the frequency ω_T and damping ratio ζ_T in three dimensions. To minimize the analysis time, we considered a single mass and stiffness system in three dimensions, matching the mass and stiffness of the bridge structure for our primary system. Then, a TMD was added to this system, resulting in a 6-degree of freedom system with the TMD. The combined equations of motion for the 6 DOF system with the TMD can be written as:

$$\begin{bmatrix} M_s & 0 \\ 0 & M_T \end{bmatrix}\begin{bmatrix} \ddot{u}_s(t) \\ \ddot{u}_T(t) \end{bmatrix} + \begin{bmatrix} C_s + C_T & -C_T \\ -C_T & C_T \end{bmatrix}\begin{bmatrix} \dot{u}_s(t) \\ \dot{u}_T(t) \end{bmatrix} + \begin{bmatrix} K_s + K_T & -K_T \\ K_T & K_T \end{bmatrix}\begin{bmatrix} u_s(t) \\ u_T(t) \end{bmatrix} = \begin{bmatrix} -M_s\{r\}\ddot{u}_g(t) \\ 0 \end{bmatrix} \tag{29}$$

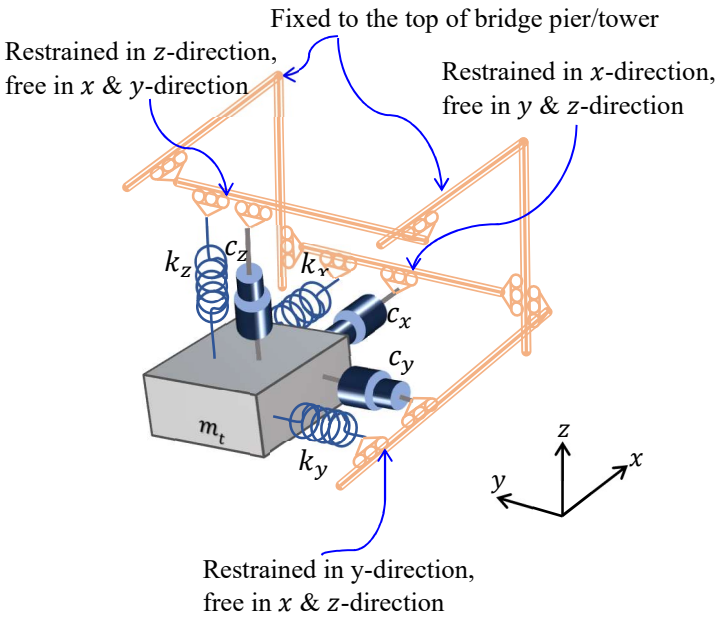

Figure 6. Schematic model of the 3D-TMD.

where M_T, K_T, and C_T are mass stiffness and damping of the TMD respectively, and u_T, $\dot{u}_T$, and $\ddot{u}_T$ are the displacement, velocity, and acceleration of TMD for the three directions x, y, and z. The damping of this structure has been calculated based on the frequency of the bridge with 5% of damping. The procedure used for optimization process involves the following steps:

- The TMD parameters to be optimized are frequencies ($\omega_{Tx}, \omega_{Ty}, and\ \omega_{Tz}$) and damping ratios ($\zeta_{Tx}, \zeta_{Ty}, and\ \zeta_{Tz}$) along the x, y, and z directions.
- The objective is to minimize the maximum base moment in the horizontal directions (x and y) and optimize the TMD's frequency and damping ratio in the vertical direction (z) so as to increase the moment capacity of the columns. So, the objective function can be written as:

$$min_{\{\omega_{Tx},\omega_{Ty},\omega_{Tz},\zeta_{Tx},\zeta_{Ty},\zeta_{Tz}\}} \left[\max(M_x(t), M_y(t)), \left(1 - \frac{\sqrt{(M_{x,max})^2 + (M_{y,max})^2}}{M_R} \right) \right] \quad (30)$$

  where $\max(M_x(t), M_y(t)$ are the base moments in the x and y directions, respectively. $M_{x,max}$, and $M_{y,max}$ are the maximum base moments in the x and y directions over the time history.
- The initial population $C = [\omega_T;\ \zeta_T\ ]$ has been built based on the following ranges in all three directions for restricting the variables.
  $0.5 \leq \omega_{Tx}, \omega_{Ty}, \omega_{Tz} \leq 1.5$ & $0.001 \leq \zeta_{Tx}, \zeta_{Ty}, \zeta_{Tz} \leq 0.7$ for Beam Bridge
  $0.1 \leq \omega_{Tx}, \omega_{Ty}, \omega_{Tz} \leq 3$ & $0.001 \leq \zeta_{Tx}, \zeta_{Ty}, \zeta_{Tz} \leq 0.3$ for RSB
- Also, the following parameters have been used; Constraint Tolerance = 1e-6, Population Size = 200, Stalls Generations = 200, and Generations = 200. For the optimization process, three-degree-of-freedom structure with a single mass equal to the total mass of the bridge is considered.

The optimization process is visually outlined in the flowchart depicted in Figure 7. This flowchart provides a clear depiction of the GA optimization process.

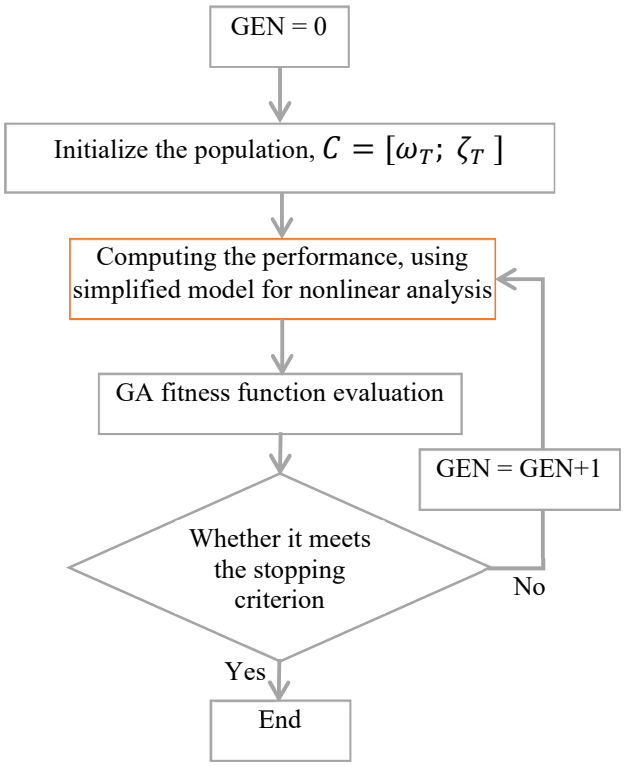

Figure 7. Flowchart of the GA optimization.

To properly evaluate the effects of earthquake vertical components and the effectiveness of the 3D-TMD system on bridges, two bridges with distinct dynamic characteristics are considered. Due to these differing characteristics, each bridge requires an individual evaluation approach. Consequently, the responses of each bridge are analyzed separately in the following sections.

5. Response mitigation of beam bridge

5.1. Probabilistic analysis of beam bridge

The first bridge model chosen for this study is an ordinary six-span simply supported beam bridge. The deck of this bridge has three prestressed concrete I-shaped girders and an overlying 22 cm thick reinforced concrete slab, with an overall width (including curbs) of 9.5 m. The bridge can be representative of a short/medium-span bridge, as its span length is 30 m, and a static scheme of simply support girders on neoprene bearings reinforced with steel shims is adopted. The piers have variable height, ranging from 8 m (side pier) to around 20 m (central pier), a circular hollow cross section. The reinforcement layout comprises 32 + 32ϕ20 (20 mm diameter) longitudinal bars arranged in two layers and stirrups ϕ12 at constant spacing of 200 mm. The foundation of each pier consists of a square pier cap (side 7.20 m, depth 2.00 m) on which five deep-type piles are attached. Abutments and pier caps are made of reinforced concrete. Pier (C) represents the tallest structure within this bridge (see Figure 8). Consequently, this study focuses on assessing the performance of Pier (C). The finite element model of the beam bridge is realized with the structural analysis and design software SAP2000 [43], in which piers and girders are modeled through beam elements, self-weight and dead load is combined with seismic action according to Eurocode 8 provisions [44], supports are modeled accounting for different horizontal and vertical stiffness, left-side abutment is of fixed type, whereas right-side abutment is modeled with a simple roller support. Plastic hinges are defined at either ends

of each pier. The fundamental lateral vibration frequency of the beam bridge identified from modal analysis is 0.98 Hz (period equal to 1.02 s), while the fundamental vertical vibration frequency is 2.67 Hz (period equal to 0.37 s). The geometrical sketch of the beam bridge along with the finite element model are sketched in Figure 8.

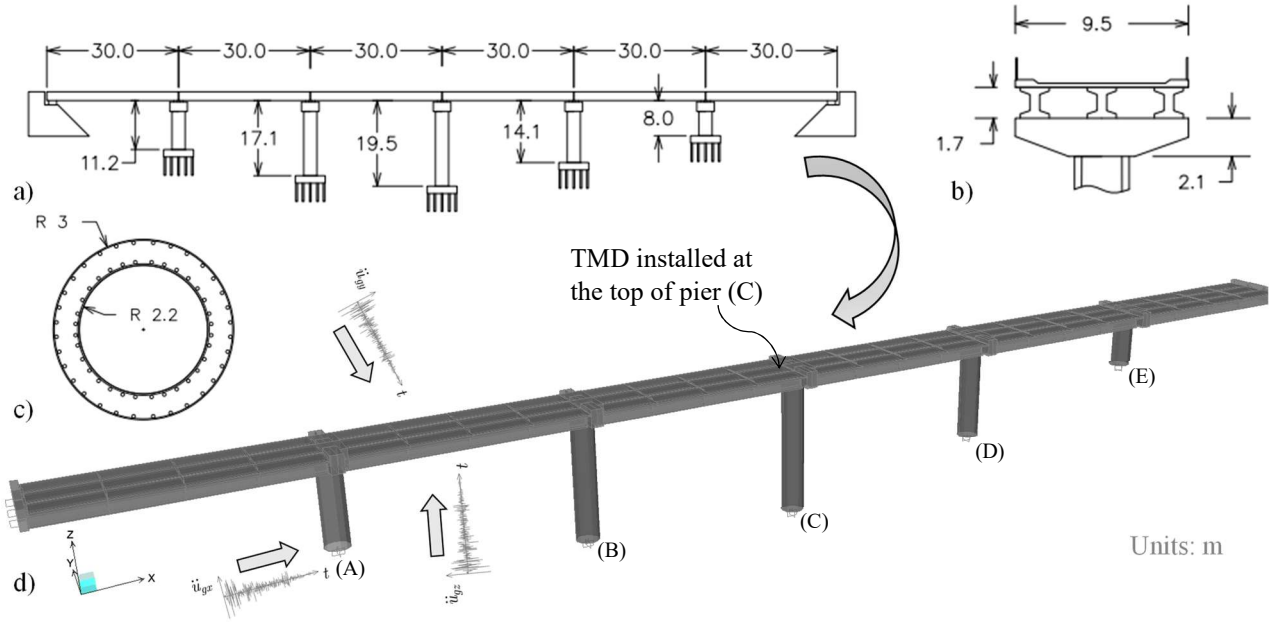

Figure 8. Geometrical data of the beam bridge: a) elevation view, b) deck cross section, c) pier cross section, d) finite element model.

The set of 100 ground motions encompasses a wide range of intensities across all seismological parameters such as Magnitude, PGV, or PGA. To better understand the impact of the vertical component, the ground motions are scaled so that the bridge's response to the horizontal component approaches the pier's capacity (C), while ensuring that the structure remains within safe limits due to the horizontal excitation of ground motion and then evaluate the effect of the vertical component of ground motion (see Figure 9). For this study, only results (axial force-bending moment response) concerning the most critical pier of the beam bridge (i.e., the middle pier (C) with the greatest height) are shown and discussed. Moreover, rather than focusing on moment in the transverse or longitudinal direction, we consider and calculate the resultant moment using the following approach:

$$M_{(t)} = \sqrt{\left(M_{x(t)}\right)^2 + \left(M_{y(t)}\right)^2} \tag{31}$$

where, $M_{(t)}$ is the resultant moment, $M_{x(t)}$ and $M_{y(t)}$ are moments in longitudinal and transverse direction respectively. The resultant moment has been chosen due to the circular cross-section of columns, which offers uniform moment capacity in any direction and features plastic hinges. These hinges interact as (P-M2-M3), meaning that if they are in a plastic state due to a moment in one direction, they exhibit plastic behavior in another direction as well. In this model, the demand moment in the transverse direction reaches the yielding point first during almost all earthquakes. Consequently, the demand moment in the longitudinal direction is determined based on plastic behavior. However, the response in the longitudinal direction has not reached the yielding point. To better illustrate this concept, the moment response of the bridge to the Northridge 1994 earthquake, specifically at the Rinaldi Receiving Station, is presented as an example in Figure 9. It is important

to note that the variation in moment capacity is negligible when only the horizontal component of ground motion is considered in the analysis. Therefore, in such cases, a constant value for the pier's moment capacity is used. For pier (C) the moment capacity is $M_R = 19900\ kNm$. The variation of moment capacity of the pier (C) subjected to the vertical component of ground motion is calculated based on equations (15) and (16).

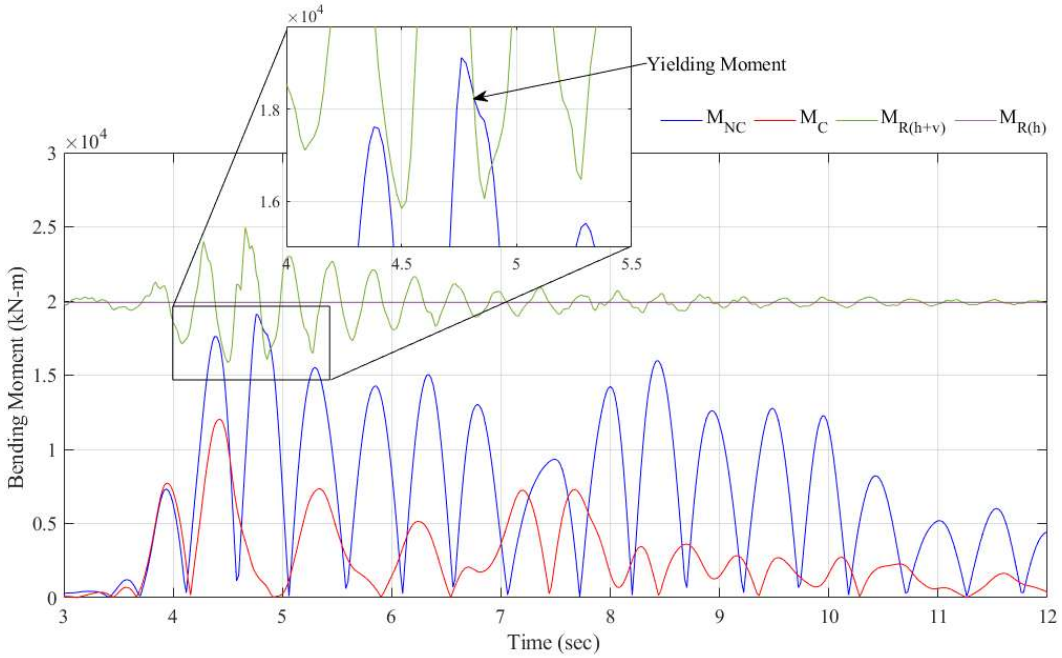

Figure 9. Bending moment response of the pier C to Northridge 1994 earthquake, Rinaldi Receiving Station; M_{NC} is the moment without control device, M_C is the moment with control device, $M_{R(h)}$ and $M_{R(h+v)}$ are the moment capacity of the column neglecting and considering the vertical component of the earthquake, respectively.

As depicted in this figure, the maximum moment demand from the horizontal ground excitations is less than the moment capacity of the column. However, upon considering the effect of the vertical component of ground motion, the capacity of the column changes in the time domain. At a specific time, the induced moment by ground motion surpasses the moment capacity of the column, demonstrating nonlinear behavior in this case.

Results from the probabilistic analysis of the beam bridge are presented in Figure 10. This figure illustrates the probability density function of the peak moment responses from the scaled set of 100 ground motions. As we can see in this figure most peak responses are less than M_R, However, the inclusion of the vertical component results in an average reduction of moment capacity by approximately 6%.

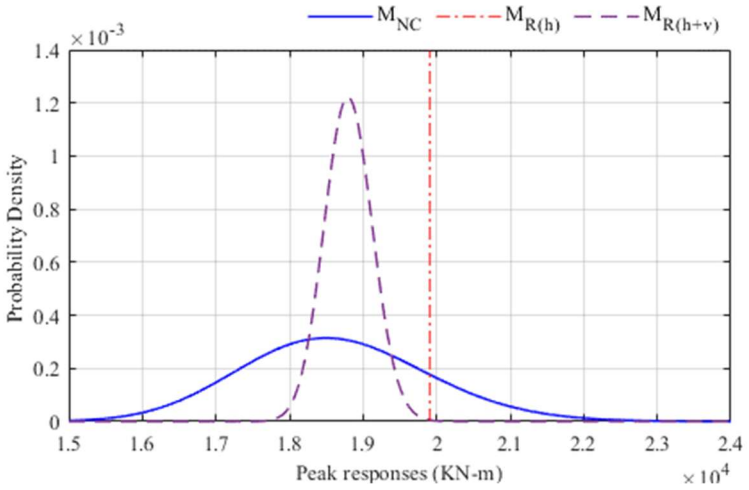

Figure 10. Probability density of peak moment responses of beam bridge to the set of 100 NFPTGMs. M_{NC} is the peak of resultant moment responses of the pier (C) without control devices. $M_{R(h)}$ is the moment capacity of pier (C). $M_{R(h+v)}$ is the moment capacity of pier (C) considering the vertical component of ground motion.

5.2. Control system evaluation for beam bridge

The optimization prosses described in section 4 is used to obtain the optimum parameters for TMDs. The TMD is placed at the top of pier (C). The results of the optimization process are presented in Table 3.

Table 3. TMD parameters for beam bridge

Direction	Mass ratio (%)	Bridge fundamental frequency (Hz)	Tuning frequency (Hz)	Damping ratio (%)
Longitudinal	1	0.97	0.97	0.06
Transverse	1	0.98	0.92	0.06
Vertical	1	2.67	2.63	0.069

In the beam bridge, Pier (C) is identified as the critical pier due to its height, thus the TMD is positioned at the top of this pier (see Figure 8). SAP2000 software [43] was used to analyze the nonlinear models of beam bridge with no control, and with 2D-TMD and 3D-TMD. The difference between 2D-TMD and 3D-TMD is that 2D-TMD is considered fixed in the vertical direction, whereas 3D-TMD is tuned to the vertical direction based on the parameters in Table 3. The analysis results of the beam bridge highlight the advantage of 3D-TMD compared to 2D-TMD. Figure 11 not only underscores the efficacy of the 3D-TMD in reducing moments but also highlights its beneficial impact on column moment capacity. Table 4 presents a summary of the analyses conducted for beam bridge.

Table 4. Percentage of moment reduction and of moment capacity increase obtained from non-linear analysis of beam bridge.

Direction	Moment reduction (%)		Moment capacity increase (%) (3D-TMD)	
	Max	Median	Max	Median
Resultant Moment	61	12.2	13.8	1.8

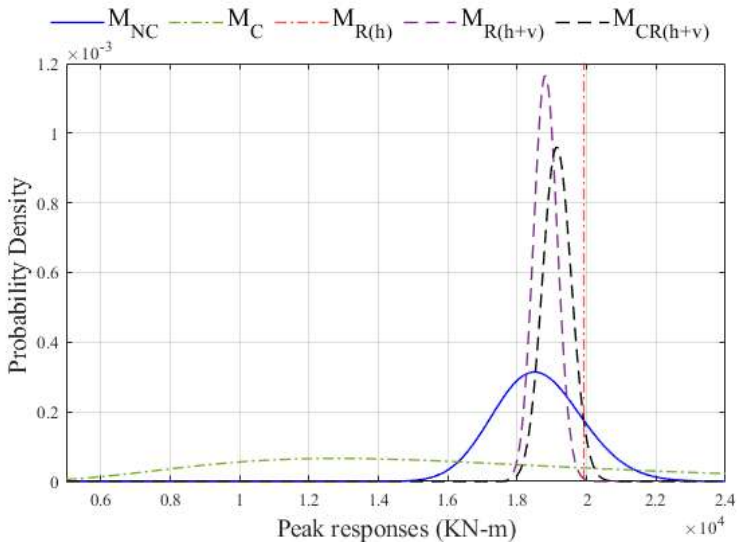

Figure 11. Probability density of peak moment responses of beam bridge to the set of 100 NFPTGMs. M_{NC} and M_C are the peak of resultant moment responses of the pier (C) without control devices and with control devices respectively. $M_{R(h)}$ is the moment capacity of pier (C). $M_{R(h+v)}$ is the moment capacity of pier (C) considering the vertical component of ground motion. $M_{CR(h+v)}$ is the moment capacity of pier (C) with 3D-TMD considering the vertical component of ground motion.

5.3. Fragility analysis of beam bridge

To gain a comprehensive grasp of the findings from this study and the impact of 3D-TMDs on enhancing the resilience of bridge columns, fragility analysis was conducted for the both bridges based on description in section 2.2. For the construction of fragility curves, the value of PGV is assumed as intensity measure (IM). For fragility analysis, it is assumed that the IM levels causing the collapse of the bridge (i.e., the attainment of the bending moment capacity in pier C) are lognormally distributed. The damage states are classified into four categories: slight, moderate, extensive, and complete (see Table 1).

The results of the fragility analysis reveal a notable influence of the vertical component on the probability of reaching the limit state condition. It becomes evident that the seismic vulnerability of bridges increases with the inclusion of the vertical excitation component. However, the presence of a 3D-TMD can notably increase the bridge's reliability. Specifically, the analysis results imply that the considered 3D-TMD exhibits positive effects compared to 2D-TMD, particularly for strong ground motion with high PGV. Figures 12, and 13 showcases the outcomes of the fragility analysis for different damage states described in Table 4.8 for both bridges (Beam bridge and RSB).

In Figures 12 and 13, the NC(h+v) presents the probability of collapse when considering the vertical component of ground motion without TMD. NC(h) presents the probability of collapse without considering the vertical component of ground motion. 2DC(h+v) presents the probability of collapse with 2D-TMD considering the vertical component of ground motion. 3DC(h+v) presents the probability of collapse of column with 3D-TMD when considering the vertical component of ground motion.

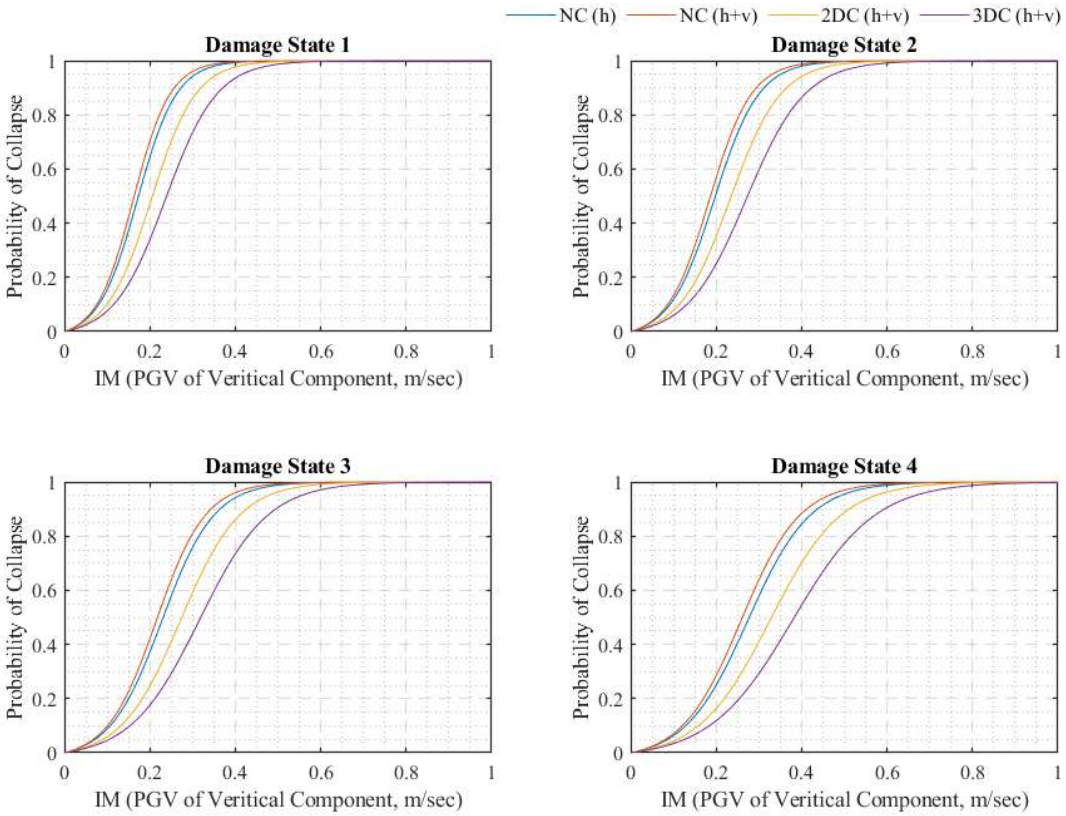

Figure 12. Bending moment simplified fragility curves for Beam Bridge in longitudinal direction.

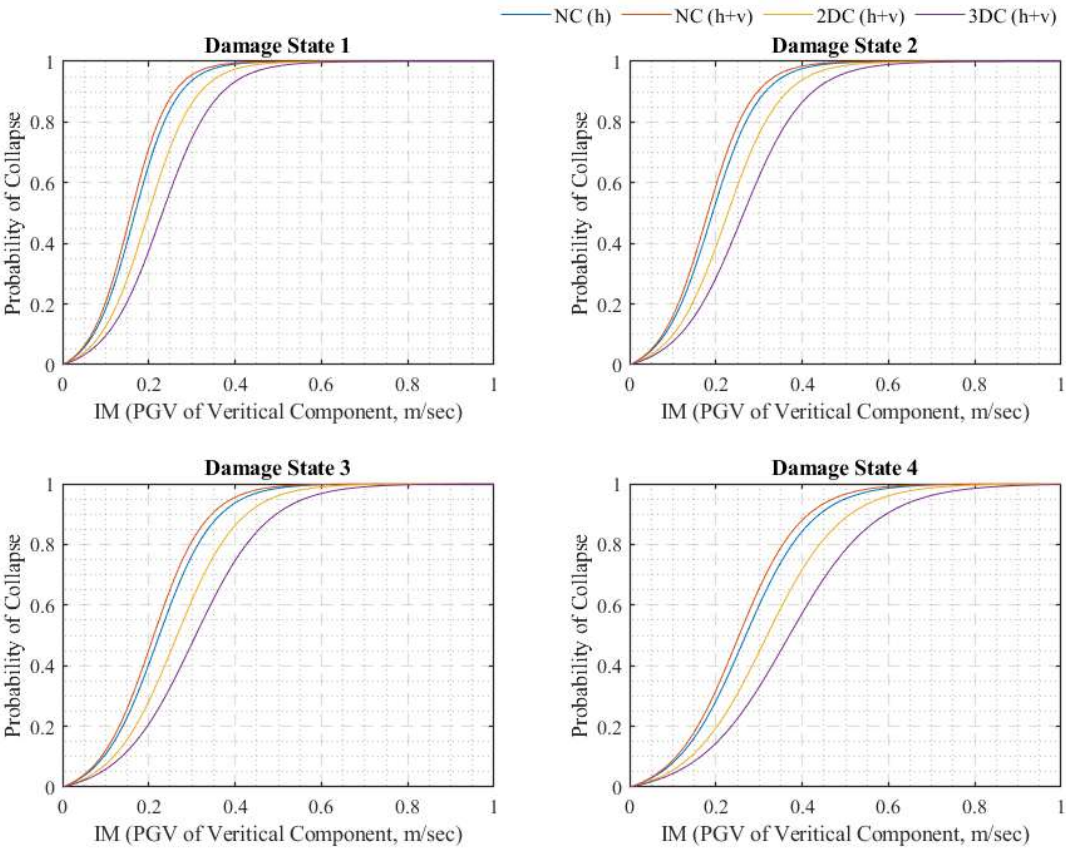

Figure 13. Bending moment simplified fragility curves for Beam Bridge in transverse direction

6. Response mitigation of Runyang Suspension Bridge (RSB)

6.1. Probabilistic analysis of RSB

The second bridge considered for this study is the Runyang Suspension Bridge (RSB), a long-span suspension bridge in China that has been open for traffic since April 2005. The main span is 1490m long and hung through towers on each side. Each tower consists of two steel-concrete columns 210 m in height connected by three prestressed concrete cross beams. The diameter of the main cable is 0.9m made of steel with 1670 MPa strength. The deck is connected to the main cable through two vertical suspenders at each suspension point. The steel girder has a 3 m height and 38.7 m width with a 2% slope on each side (for more details, see Jami et al. [42]). Plastic hinges are defined at the base of each tower. Figure 14 presented geometrical data along with the FE model of RSB. The SAP2000 platform [43] is used to prepare the FE model of RSB. The first lateral and vertical frequencies of the RSB are 0.049 Hz and 0.088 Hz, respectively. The RSB has symmetric geometry, so one tower was chosen for performance evaluation in this study.

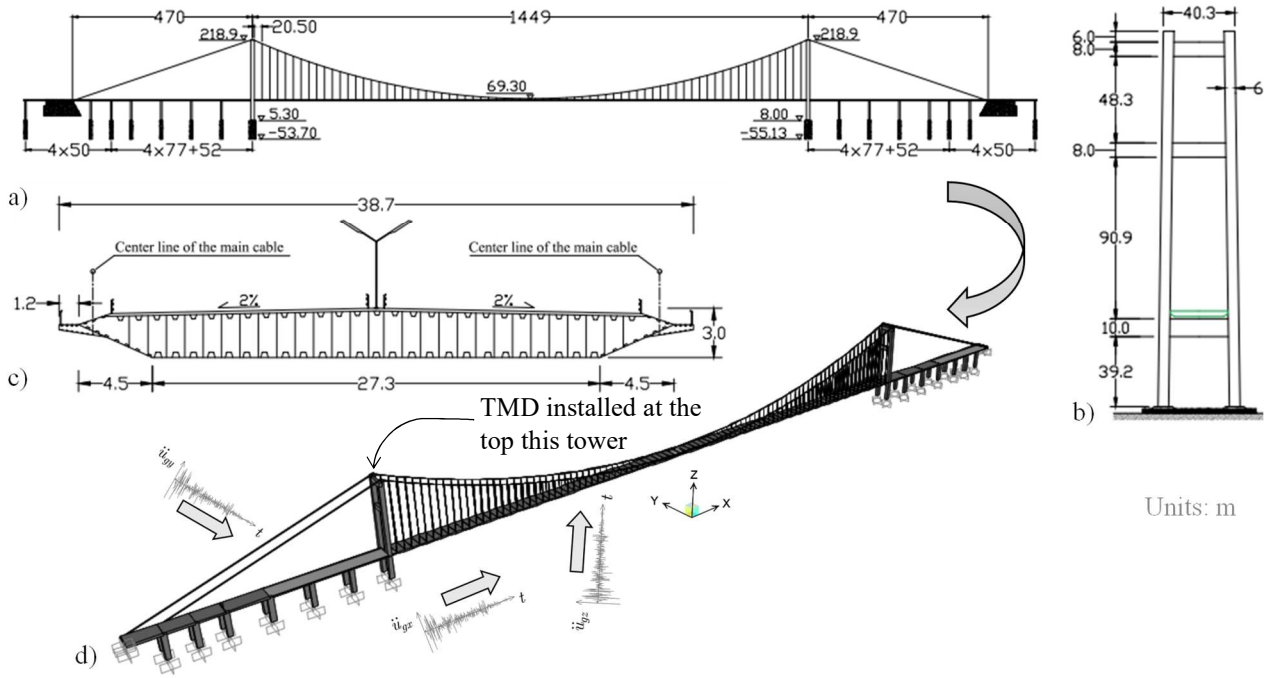

Figure 14. Geometrical data of the RSB: a) elevation view, b) suspension tower, c) deck cross section, d) finite element model.

The same set of 100 NFPTGMs records described in section 3 is used for nonlinear analysis of RSB. The results are categorized based on ground motion records categorization in section 3. Also based on control strategies described in section 4, TMD parameters for this case are indicated in Table 5. The RSB frequencies considered for the design of TMD are based on frequencies of the RSB's tower in longitudinal, transverse, and vertical directions (see Table 5). RSB has symmetric geometry, so one tower was chosen to evaluate its response. The 3D-TMD is installed at the top of the selected tower (see Figure 14).

Table 5. TMD parameters for RSB

Direction	Mass ratio (%)	Bridge fundamental frequency (Hz)	Tuning frequency (Hz)	Damping ratio (%)
Longitudinal	1	0.47	0.462	0.061
Transverse	1	0.23	0.223	0.059
Vertical	1	0.52	0.525	0.067

The same procedure described in the previous section for the beam bridge was also used for the probabilistic analysis of the RSB. Results are presented in Figure 15 illustrating the probability density function of response to different categories of ground motions. It vividly demonstrates the significant impact of the vertical component of ground motions on the capacity of the towers, especially during strong earthquakes. While there are instances where the capacity of towers increases, in most cases, strong ground motions have adverse effects, leading to a reduction in tower capacity by up to 19%. Furthermore, the results highlight another observation. Despite RSB being a flexible structure with a high fundamental period, the vertical component of ground motion, with higher pulse period exhibits a more noticeable impact on tower capacities.

To delve into the results stemming from the analysis of the RSB, Figure 15 and Table 6 present the outcomes derived from nonlinear analysis under various categories of ground excitations. These results distinctly showcase the efficacy of the installed TMD for the RSB, displaying notable reductions in peak moment responses. The installed TMD mitigates peak moment responses by up to 68% in the longitudinal direction and 50% in the transverse direction. In Figure 15, since we have more control with the 3D-TMD in the vertical oscillations, the capacity is tending to the dashed vertical lines corresponding to the cases without vertical component; correspondingly, we have a reduction of the bending moment demand for the cases with the 3D-TMD.

Table 6. Percentage of moment reduction and moment capacity of column increase contacted from non-linear analysis of RSB.

Direction	Moment reduction (%)		Moment capacity increase (%)	
	Max	Median	Max	Median
Longitudinal	68	34	19	3
Transverse	50	28	19.2	2.6

The significant impact of TMDs on seismic reduction in bridges has been widely acknowledged in prior studies. However, what deserves particular attention in this study is the observed influence of TMDs on enhancing the moment capacity of bridge columns, particularly when tuned in the vertical direction. This is a consequence of reduction in vertical forces experienced by the columns. Results illustrate that under intense ground motions characterized by higher magnitudes, PGV, and the ratio of T_p to T_n approaching the unity, the 3D-TMD exhibits excellent performance in increasing column capacity. While the effect of 2D-TMD on column moment capacity is deemed negligible, the 3D-TMD demonstrates remarkable efficiency, yielding up to a 19% enhancement in moment capacity in both horizontal directions.

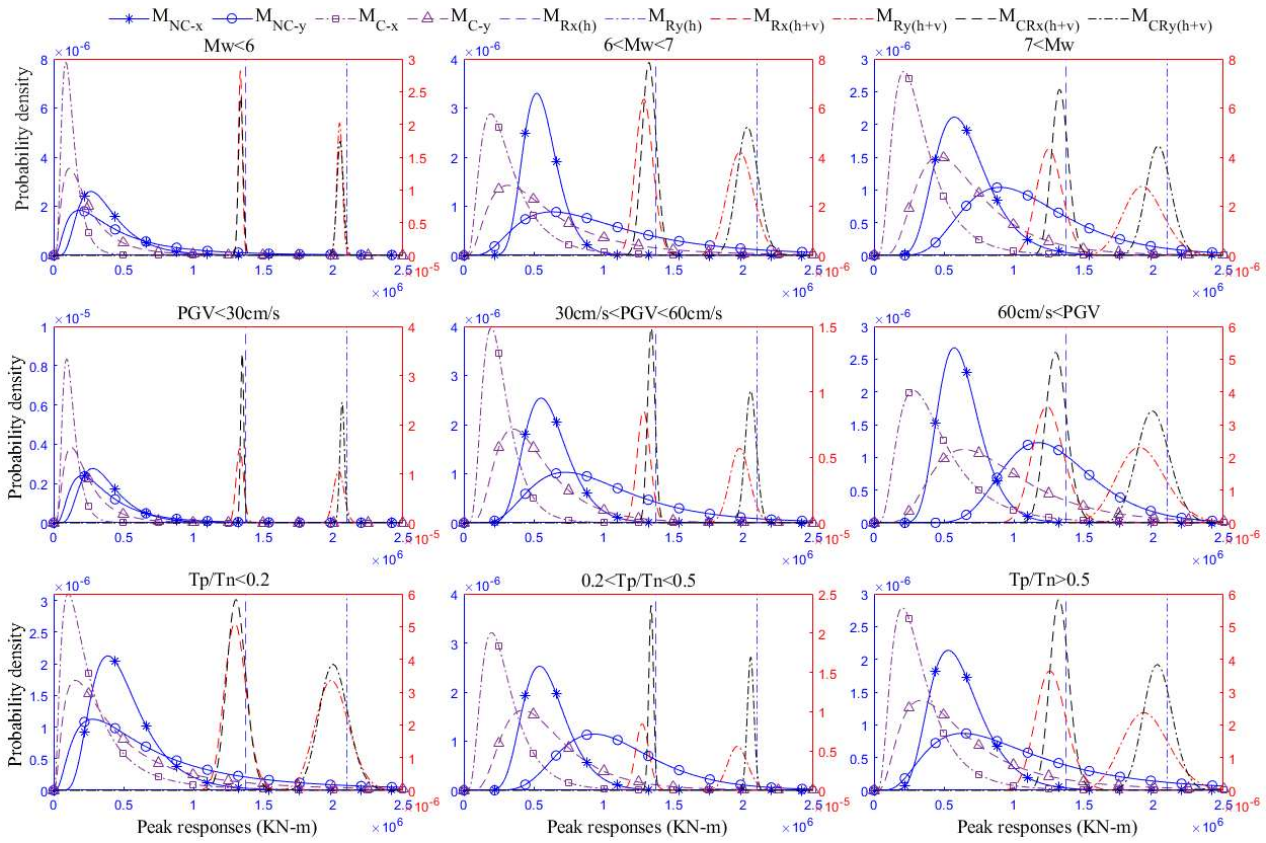

Fig. 15. Probability density of peak moment responses of RSB to the different categories of ground motion. $M_{NC\text{-}x}$ and $M_{NC\text{-}y}$ are the peak moment responses of the RSB's tower in the longitudinal and transverse direction without control devices. $M_{C\text{-}x}$ and $M_{C\text{-}y}$ are the peak moment responses of the RSB's tower in the longitudinal and transverse direction with control devices. $M_{Rx(h)}$ and $M_{Ry(h)}$ is the moment capacity of RSB's tower in the longitudinal and transverse direction without considering the vertical component of ground motion. $M_{Rx(h+v)}$ and $M_{Ry(h+v)}$ are the moment capacity of RSB's tower without TMD and in the longitudinal and transverse direction considering the vertical component of ground motion. $M_{CRx(h+v)}$ and $M_{CRy(h+v)}$ are the moment capacity of RSB's tower with 3D-TMD in the longitudinal and transverse direction considering the vertical component of ground motion.

6.2. Fragility analysis of RSB

For fragility analysis of RSB, we employ the same procedure that was conducted for beam bridge fragility analysis. It is assumed that the IM levels causing the bridge collapse are lognormally distributed, and the fragility function is defined as in section 2.2. Furthermore, the multiple stripe analysis approach is adopted by computing the fraction of the set of ground motions at each stripe that causes the bridge to collapse.

Figures 16 and 17 display the results of the fragility analysis in both longitudinal and transverse directions, respectively for different damage states described in Table 1. These findings distinctly highlight how the vertical component of ground motion influences the probability of collapse in each direction. Additionally, the positive impact of control systems on enhancing bridge performance is demonstrated. The results further reveal that the 3D-TMD outperforms the 2D-TMD, particularly under ground motions with high PGVs.

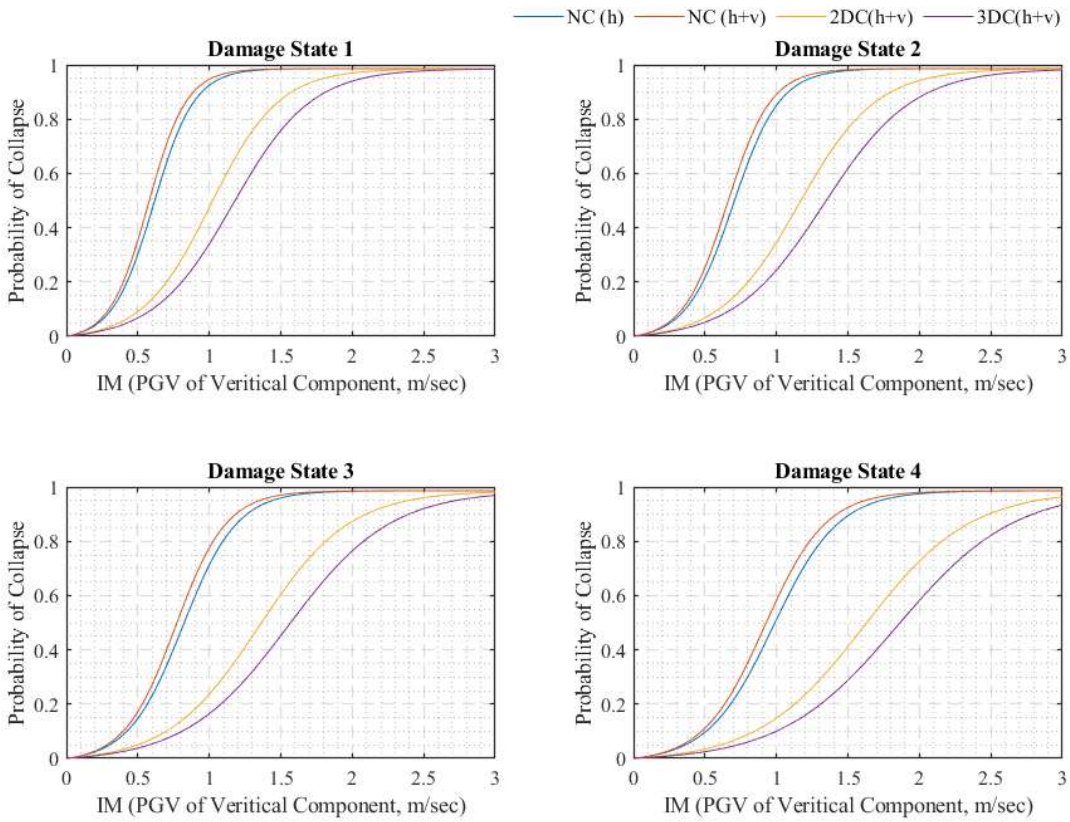

Figure 16. Bending moment simplified fragility curves for RSB in longitudinal direction

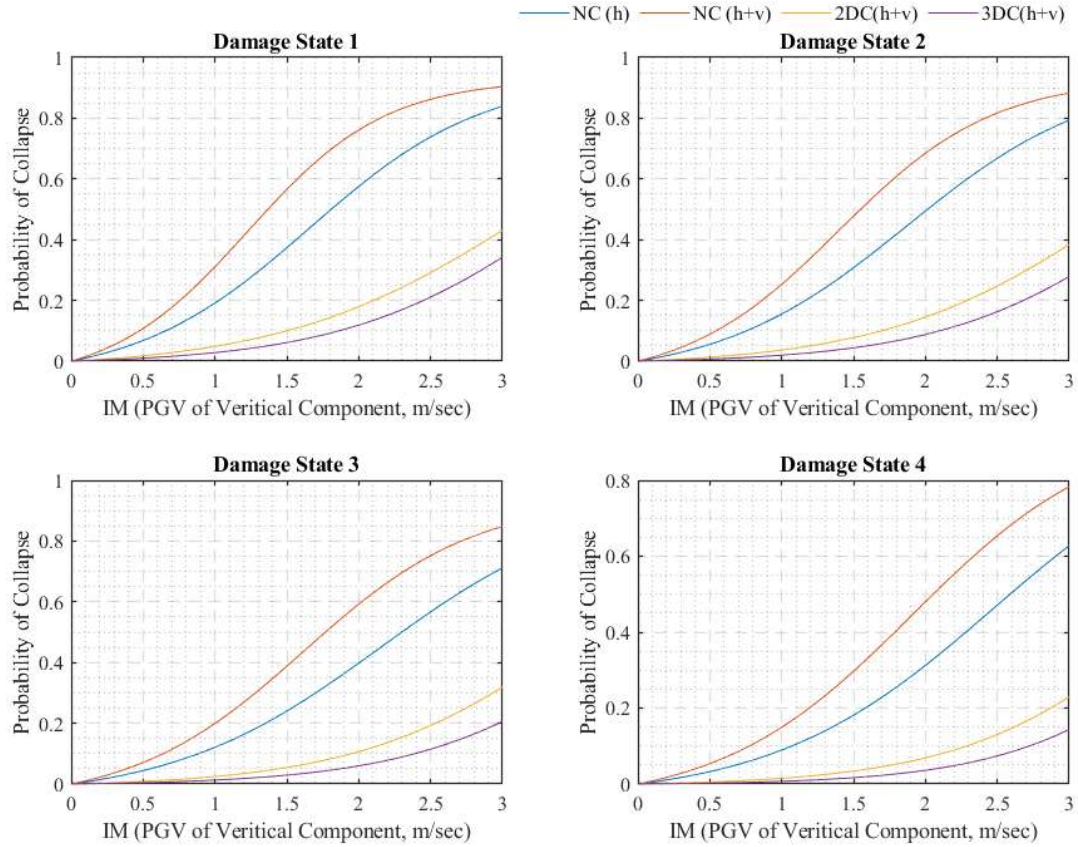

Figure 17. Bending moment simplified fragility curves RSB in transverse direction.

In Figures 16 and 17, the NC(h+v) presents the probability of collapse when considering the vertical component of ground motion without TMD. NC(h) presents the probability of collapse without

considering the vertical component of ground motion. 2DC(h+v) presents the probability of collapse with 2D-TMD considering the vertical component of ground motion. 3DC(h+v) presents the probability of collapse of column with 3D-TMD when considering the vertical component of ground motion.

7. Reliability analysis of RSB and Beam bridge

The reliability analysis of the Beam bridge and RSB, as presented in Figures 17, 18, 19, and Table 7, offers insight into how each bridge responds to various seismic conditions and damage states.
The PGV values for 50% reliability indicate the ground motion intensity each bridge can withstand, with a 50% probability of avoiding collapse.
The reliability analyses of the Beam Bridge and the RSB, as illustrated in Figures 18 - 21 and presented in Table 7, make it clear that vertical ground motion plays a key role in evaluating seismic performance and that installing tuned mass damper (TMD) systems can significantly reduce the likelihood of collapse. Focusing on the Beam Bridge first, we see that when the vertical component is ignored (in the "NC(h)" scenario), the resulting reliability estimates appear higher than they really are once vertical excitations are accounted for ("NC(h+v)"). In other words, not considering vertical motion can lead to an overestimation of how safely the Beam Bridge will perform during a strong earthquake. Fortunately, the introduction of TMDs provides a meaningful improvement. According to Table 4.9, the 2D-TMD arrangement consistently boosts the ability of the Beam Bridge to handle higher PGV levels, particularly in moderate to extensive damage ranges, while the 3D-TMD setup goes even further by controlling vibrations in multiple directions simultaneously.
The RSB demonstrates a similar pattern. Comparing "NC(h)" with "NC(h+v)" reveals that leaving out the vertical component overestimates how well the RSB can handle seismic loading. Even so, the RSB tends to maintain a higher PGV capacity in moderate damage states than the Beam Bridge, pointing to factors like increased stiffness or more robust structural framing. Table 4.9 underlines this observation by showing a clear shift to greater reliability when either 2D-TMD or 3D-TMD systems are applied to the RSB. Notably, the 3D-TMD configuration provides the biggest leap in reliability at higher damage levels, stressing how critical it is to keep both lateral and vertical motions under control in strong earthquakes.For extensive or complete damage, the PGV values required for 50% reliability are very high, particularly for the RSB. Although the beneficial effects of TMDs remain evident, the unrealistically high PGV values suggest that it may not be necessary to evaluate the performance of TMD systems or the impact of the vertical component of ground motion in such severe damage states. These extreme conditions suggest that further analysis might not yield practical insights regarding TMD effectiveness.
All things considered, the data in Table 4.9 confirm that ignoring vertical ground motion can lead to an overly optimistic—and potentially unsafe assessment of seismic reliability for both bridges. At the same time, both 2D-TMD and 3D-TMD setups help mitigate the chances of severe damage, although the 3D-TMD system shows the broadest benefits over a wider range of intensities. These results underscore that, for both the Beam Bridge and the RSB, a three-dimensional perspective on seismic loads, combined with a well-conceived TMD strategy, is essential for achieving greater resilience when earthquakes strike.

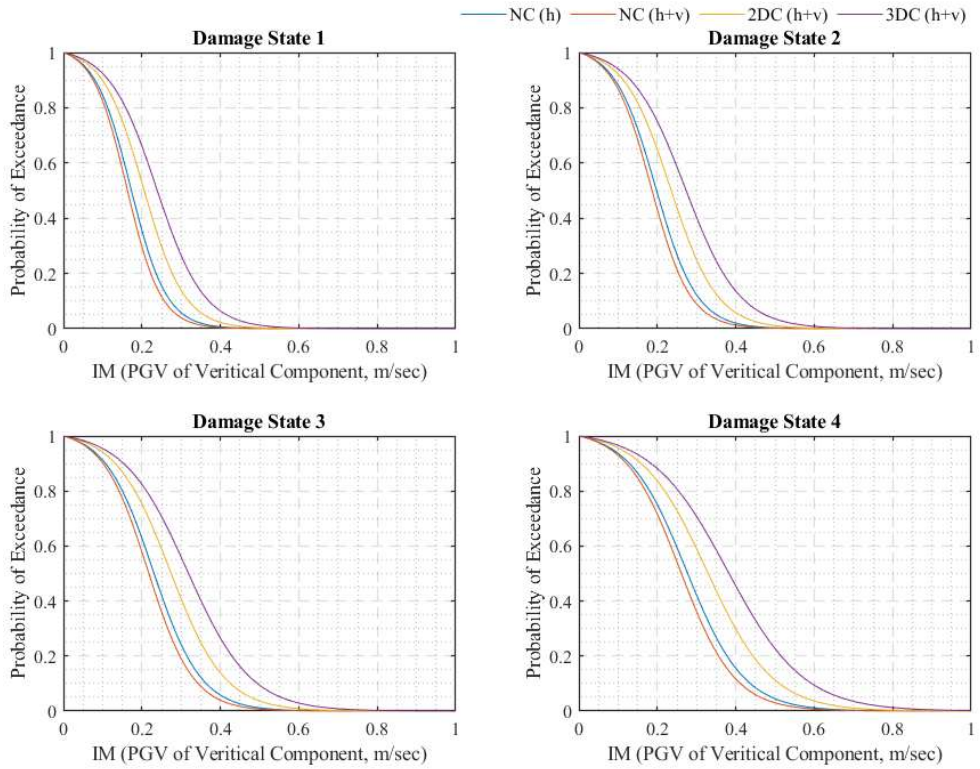

Figure 18. Bending moment simplified reliability curves for Beam Bridge in longitudinal direction.

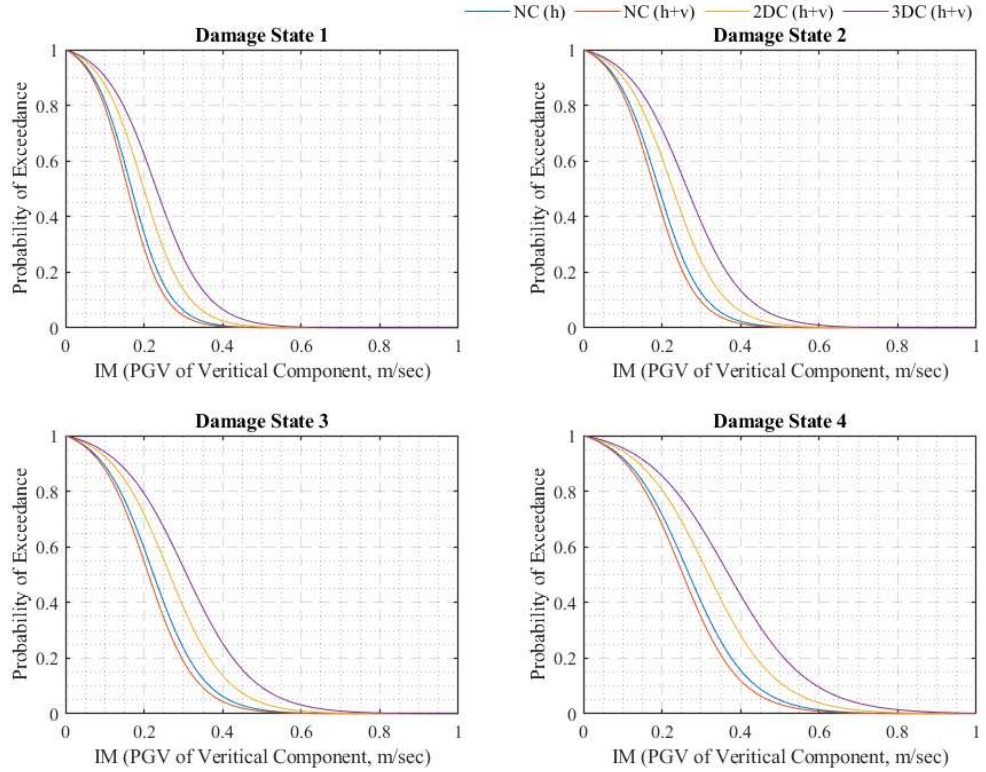

Figure 19. Bending moment simplified reliability curves for Beam Bridge in transverse direction.

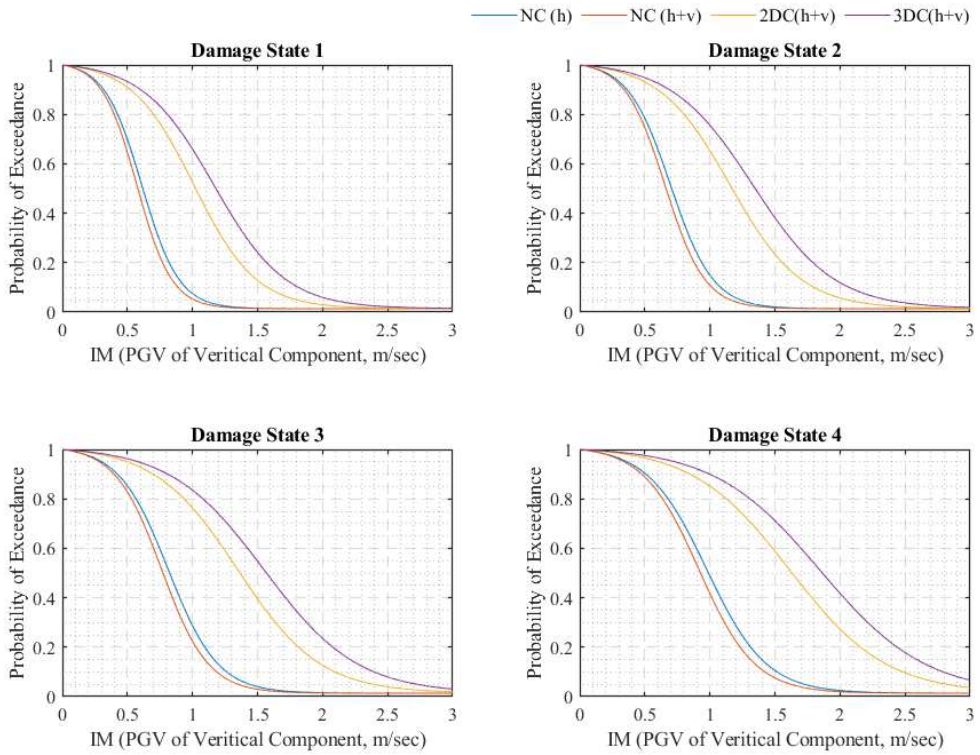

Figure 20. Bending moment simplified reliability curves for RSB in longitudinal direction.

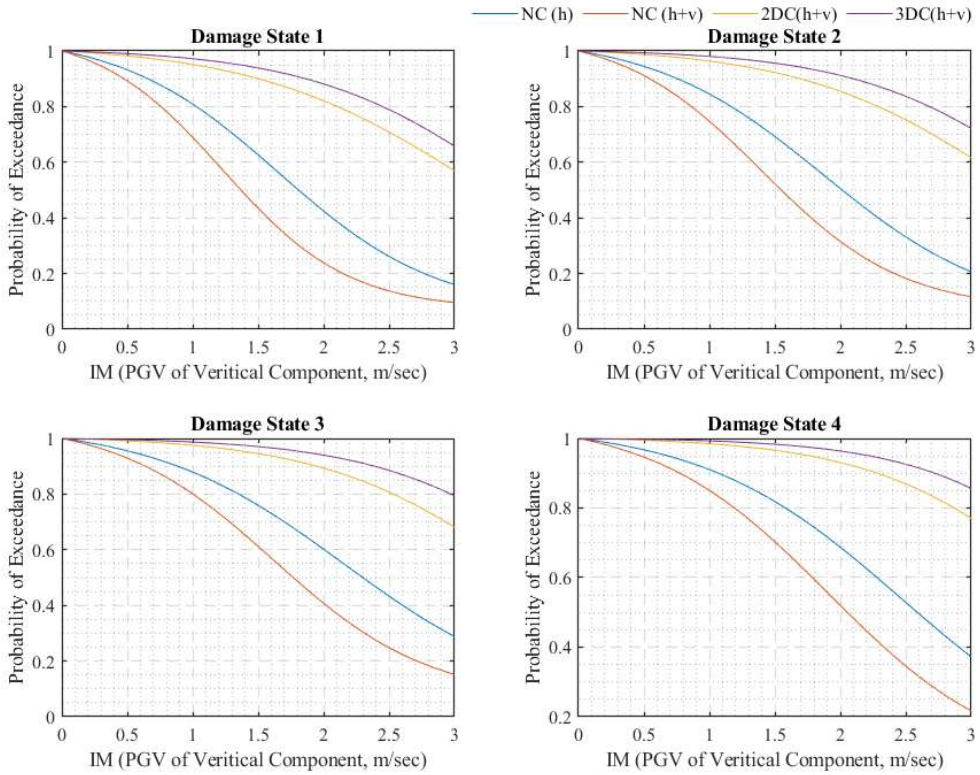

Figure 21. Bending moment simplified reliability curves for RSB in transverse direction.

In Figures 18 – 21, and Table 7, the NC(h+v) presents the probability of collapse when considering the vertical component of ground motion without TMD. NC(h) presents the probability of collapse

without considering the vertical component of ground motion. 2DC(h+v) presents the probability of collapse with 2D-TMD considering the vertical component of ground motion. 3DC(h+v) presents the probability of collapse of column with 3D-TMD when considering the vertical component of ground motion.

Table 7. PGV (m/s) for 50% reliability of RSB and Beam bridge.

Bridge	Direction	Damage State	PGV (m/s) for 50% Reliability			
			$NC_{(h)}$	$NC_{(h+v)}$	$2DC_{(h+v)}$	$3DC_{(h+v)}$
Beam bridge	longitudinal direction	Slight Damage	0.17	0.16	0.2	0.24
		Moderate Damage	0.2	0.9	0.24	0.27
		Extensive Damage	0.23	0.22	0.28	0.32
		Complete Damage	0.28	0.26	0.33	0.38
	transverse direction	Slight Damage	0.17	0.16	0.19	0.23
		Moderate Damage	0.19	0.18	0.23	0.26
		Extensive Damage	0.22	0.21	0.26	0.31
		Complete Damage	0.27	0.25	0.32	0.37
RSB	longitudinal direction	Slight Damage	0.6	0.58	1.02	1.18
		Moderate Damage	0.7	0.66	1.17	1.35
		Extensive Damage	0.82	0.77	1.36	1.58
		Complete Damage	0.99	0.92	1.63	1.84
	transverse direction	Slight Damage	1.81	1.37	3.21	3.51
		Moderate Damage	2.01	1.55	3.58	3.86
		Extensive Damage	2.3	1.77	3.84	4.01
		Complete Damage	2.6	2.06	4.3	4.51

8. Conclusions

The objective of the present study is to examine the effect of the vertical component of earthquake ground motions on the safety of bridges. An ordinary beam bridge and a long-span suspension bridge are modelled through a three-dimensional finite element model, and its seismic response is assessed under a set of pulse-like ground records. The axial load and bending moment are the critical response indicators checked to assess the design safety requirements of the bridges. In the numerical analysis, for obtaining the responses of the bridges, nonlinear analysis is used. For nonlinear analysis, plastic hinges are considered for bridges columns/towers. In this study, bridges are considered to be safe if the moment induced by the ground motion is lower than the corresponding bending resistance.

For the considered bridges and for the given set of pulse-type ground motions including the vertical component, fragility curves are constructed to show the probability of exceeding the limit state threshold representative of the safety of the bridges. The peak ground velocity is considered to be the intensity measure for developing fragility curves. A critical comparison of fragility curves accounting for and neglecting the vertical component of the seismic excitation is illustrated. It is observed that the probability of crossing the limit state condition is affected by the consideration of the vertical component.

For enhancement of the safety of the bridges, TMD was used as a control device for reducing the bridge response from ground excitation. The results indicated that installing a 3D TMD (i.e., a TMD

tuned to three directions concurrently) could be efficient for reducing the bridge's response in both horizontal and vertical directions. Results of this numerical study indicated that the TMD reduces the peak moment responses up to 68% for RSB and 62% for beam bridge. The results also illustrate that under intense ground motions characterized by higher magnitudes, PGV, and ratios of T_p to T_n approaching the unity, the 3D-TMD exhibits excellent performance in increasing the column capacity. While the effect of 2D-TMD on column moment capacity is deemed negligible, the 3D-TMD demonstrates remarkable efficiency, yielding up to a 19% enhancement in moment capacity in both horizontal directions of RSBs tower, and 13% enhancement in moment capacity of beam bridges column. Table 7 further illustrates how adding TMD systems, especially the 3D-TMD configuration, dramatically reduces the chances of severe damage by controlling multi-directional vibrations. Overall, these results highlight the importance of a comprehensive, three-dimensional approach to seismic design and the need for robust vibration-control solutions to keep our bridges safer and more resilient under real-world earthquake conditions.

The reliability analysis of the Beam Bridge and the RSB makes it clear that disregarding vertical ground motion can lead to overly optimistic and potentially unsafe estimates of how each structure will perform under seismic loading. Incorporating the vertical component demonstrates a realistic view of lower reliability for both bridges, with the RSB tending to withstand moderate damage states better than the Beam Bridge.

Although the results of this study seem encouraging and offer a general view of the effects of the vertical component, the diversity of earthquake characteristics requires further investigation to develop novel technological solutions and appropriate structural control strategies.

References

1. Xiang, N., Goto, Y., Obata, M., & Alam, M. S. (2019). Passive seismic unseating prevention strategies implemented in highway bridges: a state-of-the-art review. Engineering Structures, 194, 77-93.
2. De Domenico, D., Messina, D., & Recupero, A. (2023). Seismic vulnerability assessment of reinforced concrete bridge piers with corroded bars. Structural Concrete, 24(1), 56-83.
3. Deng, P., Zhang, C., Pei, S., & Jin, Z. (2018). Modeling the impact of corrosion on seismic performance of multi-span simply-supported bridges. Construction and Building Materials, 185, 193-205.
4. Aviram, A.; Mackie, K.R.; Stojadinovic, B. (2008). Guidelines for Nonlinear Analysis of Bridge Structures in California; Pacific Earthquake Engineering Research Center: Berkeley, CA, USA.
5. Castaldo, P., & Amendola, G. (2021). Optimal DCFP bearing properties and seismic performance assessment in nondimensional form for isolated bridges. Earthquake Engineering & Structural Dynamics.
6. Nabid, N., Hajirasouliha, I., & Petkovski, M. (2021). Simplified method for optimal design of friction damper slip loads by considering near-field and far-field ground motions. Journal of Earthquake Engineering, 25(9), 1851-1875.
7. Chopra, A. K., & Chintanapakdee, C. (2001). Comparing response of SDF systems to near-fault and far-fault earthquake motions in the context of spectral regions. Earthquake engineering & structural dynamics, 30(12), 1769-1789.
8. Xie, L., Xu, L., & Adrian, R. M. (2005). Representation of near-fault pulse-type ground motions. Earthquake Engineering and Engineering Vibration, 4(2), 191-199.
9. Bray, J. D., & Rodriguez-Marek, A. (2004). Characterization of forward-directivity ground motions in the near-fault region. Soil Dynamics and Earthquake Engineering, 24(11), 815-828.
10. Somerville, P. G., Smith, N. F., Graves, R. W., & Abrahamson, N. A. (1997). Modification of empirical strong ground motion attenuation relations to include the amplitude and duration effects of rupture directivity. Seismological research letters, 68(1), 199-222.
11. Somerville, P. G. (2002). Characterizing near fault ground motion for the design and evaluation of bridges. In Proceedings of the 3rd National Seismic Conference and Workshop on Bridges and Highways (Vol. 28, pp. 137-148).
12. Baker, J. W. (2007). Quantitative classification of near-fault ground motions using wavelet analysis. Bulletin of the Seismological Society of America, 97(5), 1486-1501.
13. Rupakhety, R., & Sigbjörnsson, R. (2011). Can simple pulses adequately represent near-fault ground motions? Journal of Earthquake Engineering, 15(8), 1260-1272.
14. Rupakhety R, Sigbjörnsson R. Three-dimensional characteristics of strong-ground motion in the near-fault area. In Proceedings of the Second European Conference on Earthquake Engineering and Seismology 2014 Aug (pp. 25-29).
15. Rupakhety R, Sigurdsson SU, Papageorgiou AS, Sigbjörnsson R. Quantification of ground-motion parameters and response spectra in the near-fault region. Bulletin of Earthquake Engineering. 2011 Aug 1;9(4):893-930.
16. Sigurðsson SU, Rupakhety R, Sigurðsson TG. Elastic response spectra of near Elastic response spectra of near-fault ground motions fault ground motions.
17. Rupakhety, R., Sigurðsson, S. U., & Sigbjörnsson, R. (2012). Response spectral model for forward-directivity ground motion in the near-fault area. In 15th World Conference on Earthquake Engineering, Lisbon.
18. Xie, L., Xu, L., & Adrian, R. M. (2005). Representation of near-fault pulse-type ground motions. Earthquake Engineering and Engineering Vibration, 4(2), 191-199.
19. Panella, D. S., Tornello, M. E., & Frau, C. D. (2017). A simple and intuitive procedure to identify pulse-like ground motions. Soil Dynamics and Earthquake Engineering, 94, 234-243.
20. Kohrangi, M., Vamvatsikos, D., & Bazzurro, P. (2019). Pulse-like versus non-pulse-like ground motion records: Spectral shape comparisons and record selection strategies. Earthquake Engineering & Structural Dynamics, 48(1), 46-64.
21. Quaranta, G., & Mollaioli, F. (2019). Analysis of near-fault pulse-like seismic signals through Variational Mode Decomposition technique. Engineering Structures, 193, 121-135.
22. Falsone, G., Recupero, A., & Spinella, N. (2020). Effects of near-fault earthquakes on existing bridge performances. Journal of civil structural health monitoring, 10(1), 165-176.

23. Bozorgnia, Y., & Campbell, K. W. (2004). The vertical-to-horizontal response spectral ratio and tentative procedures for developing simplified V/H and vertical design spectra. Journal of Earthquake Engineering, 8(02), 175-207.
24. Chopra, A. K. (1966). The importance of the vertical component of earthquake motions. Bulletin of the Seismological Society of America, 56(5), 1163-1175.
25. Kalkan, E., & Graizer, V. (2007). Multi-component ground motion response spectra for coupled horizontal, vertical, angular accelerations and tilt. ISET J. Earthq. Technol, 44(1), 259-284.
26. Piolatto, A. (2009). Structural Response Including Vertical Component of Ground Motion (Doctoral dissertation, Southern Illinois University Carbondale).
27. Abdollahiparsa, H., Homami, P., & Khoshnoudian, F. (2016). Effect of vertical component of an earthquake on steel frames considering soil-structure interaction. KSCE Journal of Civil Engineering, 20(7), 2790-2801.
28. Langston, C. A., & Hammer, J. K. (2001). The vertical component P-wave receiver function. Bulletin of the Seismological Society of America, 91(6), 1805-1819.
29. Shrestha, B. (2009). Vertical ground motions and its effect on engineering structures: a state-of-the-art review. In Proceeding of international seminar on hazard management for sustainable development in Kathmandu, Nepal (pp. 29-30).
30. Li, X., Dou, H., & Zhu, X. (2007). Engineering characteristics of near-fault vertical ground motions and their effect on the seismic response of bridges. Earthquake Engineering and Engineering Vibration, 6(4), 345-350.
31. Elnashai, A. S., & Papazoglou, A. J. (1997). Procedure and spectra for analysis of RC structures subjected to strong vertical earthquake loads. Journal of Earthquake Engineering, 1(01), 121-155.
32. FEMA 356, F. E. (2000). Prestandard and commentary for the seismic rehabilitation of buildings. FEMA Publication No, 356.
33. Nutt, R. V. (1996). Improved seismic design criteria for California bridges: provisional recommendations (No. ATC-32, Final Report).
34. Quaranta, G., Trentadue, F., & Marano, G. C. (2017). Closed-form approximation of the axial force-bending moment interaction diagram for hollow circular reinforced concrete cross-sections. Engineering Structures, 153, 516-524.
35. James, K., Wight, and James, G., MacGregor, (2016). Reinforced Concrete: Mechanics and Design. 7th Edition.
36. Baker, J. W. (2015). Efficient analytical fragility function fitting using dynamic structural analysis. Earthquake Spectra, 31(1), 579-599.
37. Ancheta, T. D., Darragh, R. B., Stewart, J. P., Seyhan, E., Silva, W. J., Chiou, B. S., ... & Donahue, J. L. (2013). Peer nga-west2 database, available online at http://peer.berkeley.edu/ngawest2/databases/ (last accessed December 2021).
38. Castaldo, P., & Tubaldi, E. (2018). Influence of ground motion characteristics on the optimal single concave sliding bearing properties for base-isolated structures. Soil Dynamics and Earthquake Engineering, 104, 346-364.
39. https://earthquake.alaska.edu/earthquake-magnitude-classes
40. Wu, Y. M., Hsiao, N. C., Teng, T. L., & Shin, T. C. (2002). Near real-time seismic damage assessment of the rapid reporting system. Terrestrial Atmospheric and Oceanic Sciences, 13(3), 313-324.
41. Shahi, S. K., & Baker, J. W. (2014). An efficient algorithm to identify strong-velocity pulses in multicomponent ground motions. Bulletin of the Seismological Society of America, 104(5), 2456-2466.
42. Jami, M., Rupakhety, R., Bessason, B., & Snæbjörnsson, J. T. (2023). Multimode Vibration Control Strategies of Long-Span Bridges Subjected to Multi-hazard: A Case Study of the Runyang Suspension Bridge. Journal of Vibration Engineering & Technologies, 12(3), 4867-4880.
43. CSI, SAP2000: Integrated software for structural analysis and design, Computer and Structures 2009, Inc., Berkeley, CA, USA.
44. Eurocode 8: Design of structures for earthquake resistance - Part 3: Assessment and retrofitting of buildings, European Committee for Standardization, 2005.

45. Chen, X. (2020). System fragility assessment of tall-pier bridges subjected to near-fault ground motions. Journal of Bridge Engineering, 25(3), 04019143.
46. Karim, K. R., & Yamazaki, F. (2001). Effect of earthquake ground motions on fragility curves of highway bridge piers based on numerical simulation. Earthquake engineering & structural dynamics, 30(12), 1839-1856.
47. Pang, Y., & Li, L. (2018). Seismic collapse assessment of bridge piers constructed with steel fibers reinforced concrete. PLoS one, 13(7), e0200072.
48. Uenaga, T., Omidian, P., George, R. C., Mirzajani, M., & Khaji, N. (2023). Seismic resilience assessment of curved reinforced concrete bridge piers through seismic fragility curves considering short-and long-period earthquakes. Sustainability, 15(10), 7764.
49. Chen, X., & Li, J. (2021). Seismic fragility analysis for tall pier bridges with rocking foundations. Advances in Bridge Engineering, 2(1), 7.
50. Ghosh, J., & Padgett, J. E. (2010). Aging considerations in the development of time-dependent seismic fragility curves. Journal of Structural Engineering, 136(12), 1497-1511.
51. Li, X., Yan, X., Ma, L., Li, H., Wang, H., Cai, L., ... & Wei, X. (2025). Probabilistic Risk Analysis for Catenary System of Heavy-Haul Railway Based on Casual Inference. Concurrency and Computation: Practice and Experience, 37(3), e8368.
52. Barrile, V., Candela, G., Demartino, C., Monti, G., Bernardo, E., & Bilotta, G. (2022, June). Rapid Seismic Risk Assessment of Bridges Using UAV Aerial Photogrammetric Survey. In Italian Conference on Geomatics and Geospatial Technologies (pp. 355-367). Cham: Springer International Publishing.
53. Jiang, H., Bai, X., Song, G., Wang, L., Zeng, C., Xue, Z., & Zhao, X. (2024). Fragility assessment of sea-crossing cable-stayed bridge subjected to multi-hazard action via TKC and R-vine copula. Engineering Structures, 307, 117874.
54. Li, S. Q., Zhang, C., Zheng, L. L., Chen, P. C., & Qin, P. F. (2025). Comparison of vulnerability models for masonry building portfolios considering different macroseismic intensity scales. Journal of Building Engineering, 112066.
55. Feng, D. C., Xie, S. C., Li, Y., & Jin, L. (2021). Time-dependent reliability-based redundancy assessment of deteriorated RC structures against progressive collapse considering corrosion effect. Structural safety, 89, 102061.
56. Liljefors, F., & Köhler, J. (2023). Decision support and structural assessment of a corroding reinforced concrete bridge considering new information. Structure and Infrastructure Engineering, 1-16.
57. Xing, L., Gardoni, P., Song, G., & Zhou, Y. Deep Learning-Based Surrogate Capacity Models and Multi-Objective Fragility Estimates for Reinforced Concrete Frames. Available at SSRN 5043813.
58. Guo, H., Feng, R., Dong, Y., & Gardoni, P. (2024). Life-cycle seismic resilience prediction of sea-crossing bridge piers exposed to chloride-induced corrosion in marine environments. Structural Safety, 111, 102523.
59. Omidian, P., Khaji, N., & Aghakouchak, A. A. (2025). An integrated decision-making approach to resilience–LCC Bridge network retrofitting using a genetic algorithm-based framework. Resilient Cities and Structures, 4(1), 16-40.
60. Dang, C., Valdebenito, M. A., & Faes, M. G. (2025). Towards a single-loop Gaussian process regression based-active learning method for time-dependent reliability analysis. Mechanical Systems and Signal Processing, 226, 112294.
61. Chen, L., Chen, L., Zheng, Z., Guo, Z., & Gardoni, P. (2023). Probabilistic seismic capacity model of pier columns: A semiparametric regression approach. ASCE-ASME Journal of Risk and Uncertainty in Engineering Systems, Part A: Civil Engineering, 9(3), 04023021.
62. Monti, G., Demartino, C., & Gardoni, P. (2023). Towards risk-targeted seismic hazard models for Europe. Scientific reports, 13(1), 10717.
63. Yu, Y. C., Sharma, N., & Gardoni, P. (2024). Protocol for the Validation of Models for Regional Risk Analysis. ASCE-ASME Journal of Risk and Uncertainty in Engineering Systems, Part A: Civil Engineering, 10(4), 04024069.
64. Iannacone, L., & Gardoni, P. (2024). Probabilistic modeling of bridge deterioration due to earthquakes. In Bridge Maintenance, Safety, Management, Digitalization and Sustainability (pp. 1946-1954). CRC Press.

65. Qin, J. (2018). Information-dependent seismic reliability assessment of bridge networks based on a correlation model. Engineering Structures, 176, 314-323.
66. Guidotti, R., Gardoni, P., & Chen, Y. (2017). Network reliability analysis with link and nodal weights and auxiliary nodes. Structural Safety, 65, 12-26.
67. Jangid, R. S. (2024). The role of a simple inerter in seismic base isolation. Applied Sciences, 14(3), 1056.
68. Miguel, L. F. F., & Beck, A. T. (2024). Optimal path shape of friction-based Track-Nonlinear Energy Sinks to minimize lifecycle costs of buildings subjected to ground accelerations. Reliability Engineering & System Safety, 248, 110172.
69. Miguel, L. F. F., Elias, S., & Beck, A. T. (2024). Reliability-based optimization of supported pendulum TMDs' nonlinear track shape using Padé approximants. Engineering Structures, 306, 117861.
70. Ali, K., Saleem, A., Javed, A., Khadim, B., & Quadri, A. I. (2024). A Simplified Approach for Dynamic Analysis of Suspension Bridges under Extreme Limit State. Practice Periodical on Structural Design and Construction, 29(4), 04024046.
71. Kumbhojkar, K. R., Shrimali, M. K., Bharti, S. D., & Datta, T. K. (2025). Fragility Analysis of a Base-Isolated Integral Bridge under Two-Component Far-and Near-Field Excitation. Journal of Structural Design and Construction Practice, 30(2), 04024114.
72. Ahmed, B. F., & Dasgupta, K. (2023). A Methodology for Assessing the Component-Level Fragility Curves and Its Application to a Class of Integral Abutment Bridges. ASCE-ASME Journal of Risk and Uncertainty in Engineering Systems, Part A: Civil Engineering, 9(1), 04022056.
73. Chen, L. (2025). Improved Probabilistic Seismic Demand–Intensity Relationship: Heteroscedastic Approaches. ASCE-ASME Journal of Risk and Uncertainty in Engineering Systems, Part A: Civil Engineering, 11(1), 04024089.
74. Tabandeh, A., Jia, G., & Gardoni, P. (2022). A review and assessment of importance sampling methods for reliability analysis. Structural Safety, 97, 102216.

Appendix A

Table 1 Seismological parameters of the 100 near-fault pulse-like ground motions considered in this study.

Record ID	RSN	Event name	Recording station	Year	T_p [sec]	R_{rup} [km]	I_A [m/s]	$D_{5/95}$ [s]	M_w	PGV_H [cm/s]	$\left(\frac{\mathrm{PGA}}{\mathrm{PGV}}\right)_H$ [$1/s$]	$\frac{\mathrm{PGA_V}}{\mathrm{PGA}_H}$ [$-$]
1	77	San Fernando	Pacoima Dam	1971	1.6	1.8	8.9	7.3	6.6	114.2	9.6	0.62
2	143	Tabas Iran	Tabas	1978	6.2	2.1	11.8	16.5	7.4	123.3	6.9	0.75
3	147	Coyote Lake	Gilroy Array #2	1979	1.5	9.0	0.5	7.5	5.7	31.6	7.9	0.90
4	148	Coyote Lake	Gilroy Array #3	1979	1.2	7.4	0.4	8.7	5.7	32.3	8.3	0.58
5	149	Coyote Lake	Gilroy Array #4	1979	1.4	5.7	0.6	11.0	5.7	31.8	7.7	1.80
6	150	Coyote Lake	Gilroy Array #6	1979	1.2	3.1	0.8	3.5	5.7	44.3	9.2	0.47
7	159	Imperial Valley-06	Agrarias	1979	2.3	0.7	1.0	13.3	6.5	41.6	4.5	1.91
8	161	Imperial Valley-06	Brawley Airport	1979	4.4	10.4	0.4	14.9	6.5	40.8	4.3	0.89
9	170	Imperial Valley-06	EC County Center FF	1979	4.4	7.3	0.8	13.2	6.5	73.4	3.1	1.19
10	171	Imperial Valley-06	El Centro - Meloland Geot. Array	1979	3.4	0.1	1.1	8.2	6.5	92.5	3.2	0.80
11	173	Imperial Valley-06	El Centro Array #10	1979	4.5	8.6	0.7	12.8	6.5	50.7	3.3	0.57
12	178	Imperial Valley-06	El Centro Array #3	1979	4.5	12.9	1.2	14.1	6.5	47.9	4.7	0.64
13	179	Imperial Valley-06	El Centro Array #4	1979	4.8	7.1	1.4	10.3	6.5	80.4	4.5	0.57
14	180	Imperial Valley-06	El Centro Array #5	1979	4.1	4.0	1.7	9.6	6.5	96.8	3.7	1.11
15	181	Imperial Valley-06	El Centro Array #6	1979	3.8	1.4	1.8	11.5	6.5	113.2	3.7	4.57
16	182	Imperial Valley-06	El Centro Array #7	1979	4.4	0.6	1.7	6.8	6.5	112.9	4.0	1.69
17	184	Imperial Valley-06	El Centro Differential Array	1979	6.3	5.1	2.1	7.0	6.5	75.5	4.4	2.08

18	185	Imperial Valley-06	Holtville Post Office	1979	4.8	7.5	0.9	12.8	6.5	53.1	4.1	1.08
19	285	Irpinia Italy-01	Bagnoli Irpinio	1980	1.7	8.2	0.4	19.6	6.9	34.7	5.3	0.76
20	292	Irpinia Italy-01	Sturno (STN)	1980	3.3	10.8	1.4	15.2	6.9	71.9	4.2	0.83
21	316	Westmorland	Parachute Test Site	1981	4.4	16.7	0.7	18.7	5.9	55.5	4.0	0.92
22	451	Morgan Hill	Coyote Lake Dam - SW Abutment	1984	1.1	0.5	3.9	4.1	6.2	78.5	12.3	0.56
23	459	Morgan Hill	Gilroy Array #6	1984	1.2	9.9	0.9	7.3	6.2	36.5	7.7	1.90
24	566	Kalamata Greece-02	Kalamata (bsmt) (2nd trigger)	1986	0.8	5.6	0.3	2.9	5.4	33.6	10.5	0.49
25	568	San Salvador	Geotech Investig Center	1986	0.8	6.3	2.5	4.3	5.8	79.8	6.6	0.93
26	569	San Salvador	National Geografical Inst	1986	1.1	7.0	2.2	6.2	5.8	73.0	7.0	1.12
27	764	Loma Prieta	Gilroy - Historic Bldg.	1989	1.6	11.0	0.7	13.9	6.9	43.3	6.4	0.58
28	766	Loma Prieta	Gilroy Array #2	1989	1.7	11.1	1.2	11.0	6.9	40.1	7.9	0.80
29	767	Loma Prieta	Gilroy Array #3	1989	2.6	12.8	2.1	13.1	6.9	45.4	7.9	0.79
30	802	Loma Prieta	Saratoga - Aloha Ave	1989	4.6	8.5	1.5	11.0	6.9	46.0	6.8	1.05
31	828	Cape Mendocino	Petrolia	1992	3.0	8.2	3.8	11.4	7.0	88.5	7.3	0.28
32	838	Landers	Barstow	1992	9.1	34.9	0.2	9.4	7.3	31.4	5.3	0.50
33	879	Landers	Lucerne	1992	5.1	2.2	7.0	11.1	7.3	131.8	4.8	1.03
34	900	Landers	Yermo Fire Station	1992	7.5	23.6	0.9	17.7	7.3	51.1	4.7	0.90
35	982	Northridge-01	Jensen Filter Plant Adm. Building	1994	3.2	5.4	5.3	21.3	6.7	111.4	3.6	0.78
36	983	Northridge-01	Jensen Filter Plant Gen. Building	1994	3.5	5.4	6.5	13.8	6.7	76.1	7.3	1.32
37	1004	Northridge-01	LA - Sepulveda VA Hospital	1994	0.9	8.4	7.0	18.9	6.7	77.5	9.5	0.40
38	1013	Northridge-01	LA Dam	1994	1.6	5.9	1.8	12.5	6.7	74.8	5.6	0.95
39	1044	Northridge-01	Newhall - Fire Sta	1994	1.4	5.9	5.7	6.9	6.7	96.5	6.0	0.94

40	1045	Northridge-01	Newhall - W Pico Canyon Rd.	1994	3.0	5.5	1.5	8.5	6.7	118.1	3.5	0.83
41	1050	Northridge-01	Pacoima Dam (downstr)	1994	0.6	7.0	0.9	6.5	6.7	44.3	9.2	0.46
42	1051	Northridge-01	Pacoima Dam (upper left)	1994	0.8	7.0	8.7	5.9	6.7	103.3	12.2	0.96
43	1052	Northridge-01	Pacoima Kagel Canyon	1994	0.7	7.3	1.8	8.8	6.7	51.4	8.3	0.56
44	1054	Northridge-01	Pardee - SCE	1994	1.2	7.5	3.1	4.3	6.7	76.1	5.4	1.29
45	1063	Northridge-01	Rinaldi Receiving Sta	1994	1.2	6.5	7.5	6.0	6.7	147.5	5.8	1.89
46	1084	Northridge-01	Sylmar - Converter Sta	1994	3.0	5.4	6.0	10.1	6.7	116.1	5.2	1.00
47	1085	Northridge-01	Sylmar - Converter Sta East	1994	3.5	5.2	4.8	8.0	6.7	120.8	6.8	1.01
48	1086	Northridge-01	Sylmar - Olive View Med FF	1994	2.4	5.3	5.0	9.1	6.7	129.3	6.4	0.89
49	1106	Kobe Japan	KJMA	1995	1.1	1.0	8.4	15.1	6.9	91.1	8.1	0.54
50	1114	Kobe Japan	Port Island (0 m)	1995	2.8	3.3	1.8	7.4	6.9	90.6	3.8	1.97
51	1119	Kobe Japan	Takarazuka	1995	1.8	0.3	3.9	6.8	6.9	85.9	7.0	0.70
52	1120	Kobe Japan	Takatori	1995	1.6	1.5	8.7	9.5	6.9	122.8	5.0	0.46
53	1148	Kocaeli Turkey	Arcelik	1999	7.8	13.5	0.3	11.5	7.5	40.0	3.1	0.62
54	1161	Kocaeli Turkey	Gebze	1999	6.0	10.9	0.5	4.6	7.5	44.6	4.3	1.37
55	1165	Kocaeli Turkey	Izmit	1999	5.4	7.2	0.8	11.3	7.5	38.3	5.8	0.90
56	1176	Kocaeli Turkey	Yarimca	1999	4.9	4.8	1.3	11.1	7.5	71.7	3.2	1.02
57	1182	Chi-Chi Taiwan	CHY006	1999	2.6	9.8	2.0	8.2	7.6	60.2	5.7	0.59
58	1193	Chi-Chi Taiwan	CHY024	1999	6.7	9.6	1.8	15.1	7.6	51.1	3.6	0.90
59	1244	Chi-Chi Taiwan	CHY101	1999	5.3	9.9	3.0	15.1	7.6	108.7	3.6	0.50
60	1402	Chi-Chi Taiwan	NST	1999	7.9	38.4	0.8	26.7	7.6	30.8	12.9	0.28
61	1475	Chi-Chi Taiwan	TCU026	1999	8.4	56.1	0.2	27.0	7.6	37.9	3.0	0.62

62	1476	Chi-Chi Taiwan	TCU029	1999	5.3	28.0	0.8	30.4	7.6	51.8	3.7	0.37
63	1477	Chi-Chi Taiwan	TCU031	1999	5.9	30.2	0.6	10.2	7.6	53.9	2.1	0.57
64	1478	Chi-Chi Taiwan	TCU033	1999	9.0	40.9	0.8	24.7	7.6	41.5	3.7	0.43
65	1479	Chi-Chi Taiwan	TCU034	1999	8.9	35.7	0.9	22.3	7.6	43.6	4.3	0.63
66	1480	Chi-Chi Taiwan	TCU036	1999	5.4	19.8	0.7	32.1	7.6	57.5	2.3	0.50
67	1481	Chi-Chi Taiwan	TCU038	1999	9.6	25.4	1.0	26.7	7.6	56.7	2.5	0.45
68	1482	Chi-Chi Taiwan	TCU039	1999	9.3	19.9	0.9	23.2	7.6	56.6	2.4	0.85
69	1483	Chi-Chi Taiwan	TCU040	1999	6.4	22.1	0.6	27.0	7.6	56.7	2.5	0.65
70	1485	Chi-Chi Taiwan	TCU045	1999	9.3	26.0	1.4	28.3	7.6	50.1	9.0	0.66
71	1486	Chi-Chi Taiwan	TCU046	1999	8.0	16.7	0.4	26.3	7.6	32.1	4.4	0.83
72	1487	Chi-Chi Taiwan	TCU047	1999	12.3	35.0	1.8	29.6	7.6	41.9	6.9	0.87
73	1489	Chi-Chi Taiwan	TCU049	1999	10.2	3.8	1.4	11.3	7.6	62.2	3.8	0.71
74	1491	Chi-Chi Taiwan	TCU051	1999	10.4	7.6	1.2	18.4	7.6	53.8	2.9	0.69
75	1492	Chi-Chi Taiwan	TCU052	1999	12.0	0.7	2.9	15.7	7.6	172.2	2.3	0.53
76	1493	Chi-Chi Taiwan	TCU053	1999	13.1	6.0	0.9	22.7	7.6	46.2	2.9	0.91
77	1496	Chi-Chi Taiwan	TCU056	1999	8.9	10.5	0.9	28.9	7.6	42.9	3.4	0.86
78	1498	Chi-Chi Taiwan	TCU059	1999	7.8	17.1	1.6	16.7	7.6	53.5	3.0	0.41
79	1501	Chi-Chi Taiwan	TCU063	1999	6.6	9.8	1.5	27.7	7.6	82.8	1.6	0.96
80	1502	Chi-Chi Taiwan	TCU064	1999	8.5	16.6	0.6	31.8	7.6	55.3	2.1	0.73
81	1503	Chi-Chi Taiwan	TCU065	1999	5.7	0.6	7.7	32.0	7.6	125.3	5.9	0.47
82	1505	Chi-Chi Taiwan	TCU068	1999	12.3	0.3	3.3	33.1	7.6	264.0	1.3	1.39
83	1510	Chi-Chi Taiwan	TCU075	1999	5.0	0.9	3.0	28.4	7.6	109.5	2.9	0.85

84	1511	Chi-Chi Taiwan	TCU076	1999	4.7	2.7	3.7	28.6	7.6	59.6	6.4	0.69
85	1515	Chi-Chi Taiwan	TCU082	1999	8.1	5.2	1.3	13.2	7.6	54.9	4.0	0.70
86	1519	Chi-Chi Taiwan	TCU087	1999	10.4	7.0	0.5	31.2	7.6	45.0	2.6	0.80
87	1528	Chi-Chi Taiwan	TCU101	1999	10.3	2.1	1.0	29.5	7.6	76.8	2.6	0.71
88	1529	Chi-Chi Taiwan	TCU102	1999	9.6	1.5	2.0	27.0	7.6	91.7	2.5	0.99
89	1530	Chi-Chi Taiwan	TCU103	1999	8.7	6.1	0.7	24.1	7.6	70.2	1.8	1.03
90	1531	Chi-Chi Taiwan	TCU104	1999	7.2	12.9	0.5	19.2	7.6	47.5	1.8	1.05
91	1548	Chi-Chi Taiwan	TCU128	1999	9.0	13.1	0.8	19.6	7.6	63.7	2.2	0.63
92	1550	Chi-Chi Taiwan	TCU136	1999	8.9	8.3	0.7	24.2	7.6	51.4	3.3	0.65
93	1602	Duzce Turkey	Bolu	1999	0.9	12.0	3.7	30.4	7.1	65.7	11.8	0.26
94	2114	Denali Alaska	TAPS Pump Station #10	2002	3.2	2.7	1.9	20.6	7.9	115.5	2.8	0.81
95	2734	Chi-Chi Taiwan-04	CHY074	1999	2.4	6.2	1.6	23.9	6.2	43.3	7.7	0.93
96	3473	Chi-Chi Taiwan-06	TCU078	1999	4.2	11.5	1.0	9.0	6.3	40.3	6.5	1.12
97	3475	Chi-Chi Taiwan-06	TCU080	1999	1.0	10.2	3.1	29.5	6.3	36.0	14.2	1.13
98	3548	Loma Prieta	Los Gatos - Lexington Dam	1989	1.6	5.0	1.9	7.4	6.9	95.8	4.2	0.35
99†	-	L'Aquila	AQV	2009	0.7	4.9	2.8	7.4	6.1	42.7	12.5	0.91
100†	-	Tyrrhenian Sea	IOCA (Casamicciola Terme)	2017	0.9	0.9	0.4	7.1	3.9	35.1	15.5	1.44

R_{rup} is the closest distance to the rupture surface; I_A is the Arias intensity; $D_{5/95}$ is the significant duration estimated between 5% and 95% of I_A;
$(\cdot)^{\dagger}$ ≔ these two records were taken from Ref. as examples of NFPTGMs with strong vertical component.

Paper 4

Jami, M., Rupakhety, R., Bessason, B., & Snæbjörnsson, J. T. (2024). Fragility of long-span bridges to near-fault pulse-like ground motions.

FRAGILITY OF LONG-SPAN BRIDGES TO NEAR-FAULT PULSE-LIKE GROUND MOTIONS

Matin Jami[1], Rajesh Rupakhety[1], Bjarni Bessason[2], Jonas Th. Snæbjörnsson[3]

[1*] Earthquake Engineering Research Centre, Faculty of Civil and Environmental Engineering, School of Engineering and Natural Science, University of Iceland, Selfoss, Iceland.

[2] Faculty of Civil and Environmental Engineering, School of Engineering and Natural Science, University of Iceland, Selfoss, Iceland.

[3] Department of Engineering, School of Technology, Reykjavik University, Reykjavik, Iceland.

Abstract;

This study investigates the impact of near-fault ground motions on cable-stayed bridges. For a case study, we focus on the new bridge planned for construction over the Ölfus River in Selfoss. This bridge is designed as a cable-stayed structure and exhibits significant mass participation in vibration modes with periods ranging from 0.6 to 2 seconds. Consequently, there is a likelihood that specific vibration modes of the bridge will resonate with the low-frequency near-fault ground motion velocity pulses, imposing substantial demands on the structure. To address these challenges, non-linear finite element models were developed using OpenSees. The bridge will be equipped with Lead Rubber Bearings (LRBs) to enhance its seismic resilience. For the Lead Rubber Bearing (LRB) design, we have used the set of near-fault ground motions to optimize LRB parameters. Subsequently, a set of near-fault ground motions, collected and processed by Rupakhety et al. (2011), was employed for response history analysis. To better understand the impact of Near-Fault Pulse-Type Ground Motions (NFPTGMs) on the bridge structure, a set of 27,600 PTGMs was simulated and applied in the longitudinal and transverse directions to the bridge structure for nonlinear analysis. This simulation was conducted using a set of 69 PTGMs as seeds to generate 27,600 pulse type ground motins. The study further investigates the bridge's fragility for both near-fault pulse-type ground motions. The fragility analysis highlights the significant seismic vulnerability of bridge bearings. It is crucial to establish a meticulous post-earthquake monitoring system for these bearings, and their design should incorporate the capability for replacement when necessary to ensure the long-term safety and functionality of the bridge.

Keywords: Cable-stayed Bridge, Probabilistic Analysis, fragility, LRB, Near-Fault Pulse-Type Ground Motions and Earthquake Engineering.

1. Introduction

In today's world, bridges stand as vital infrastructures for the modernization of countries. Bridges come in various shapes, including arch bridges, suspension bridges, and cable-stayed bridges, each with unique characteristics. It is essential to note that each type of bridge has its own advantages and disadvantages, and the choice of bridge type depends on several factors, such as construction techniques, project-specific requirements, available materials, and the local climate. Cable-stayed bridges offer several advantages, including efficient material usage, aesthetic appeal, relatively low

maintenance costs, improved structural performance, fast construction, and design flexibility (Troitsky 1988).

The concept of the cable-stayed bridge was first conceived in 1595 (Zahrai and Froozanfar, 2019), but it took more than two centuries for this idea to materialize. After two cable-stayed bridges collapsed in 1818 and 1824 (Birnstiel, 2013), this bridge type fell out of favour for an extended period. However, over time, cable-stayed bridge construction has evolved significantly, and today, advancements in computing technology enable the construction of more complex cable-stayed bridges.

During seismic events, seismic energy propagates in the form of waves. Ground motions are categorized based on factors such as rupture mechanism, slip direction, and tectonic displacement. Various authors (including Baker, 2007; Rupakhety and Sigbjörnsson, 2011 and 2014; Rupakhety et al., 2011; Rupakhety et al., 2012; Xie et al., 2005; Panella et al., 2017; Kohrangi et al., 2019; and Quaranta and Mollaioli, 2019) have outlined procedures to identify near-fault velocity pulse-type ground motions by collecting databases of recorded events and analysing their distinctive characteristics. The distance of a structure from the fault rupture is a widely recognized criterion that directly affects the imposed peak displacement demand on a structure. Ground motion records within 20 kilometres of the fault often exhibit significant velocity pulses (Xie et al., 2005). Specifically, NFPTGMs are those that affect structures located close to the fault rupture, typically within 12 kilometres (Chopra and Chintanapakdee, 2001), while far-field records are associated with epicentral distances of 20 kilometres or more.

The destructive potential of NFPTGMs has garnered the attention of bridge engineers, leading to extensive research on assessing the performance of cable-stayed bridges subjected to NFPTGMs. Among the studies conducted in this regard, the following can be mentioned; Yi (2023), Xie and Sun (2021), Li et al. (2017), Tochaei et al. (2020), Soyluk and Karaca (2017), Gautam et al. (2023), and Wang et al. (2017). These studies utilize numerical simulations, physical testing, and real-world observations to evaluate the impact of NFPTGMs on cable-stayed bridges. They consider factors such as bridge geometry, ground motion characteristics, and the behaviour of bridge components under these excitation forces. Key findings from these studies have highlighted the vulnerability of cable-stayed bridges to damage and failure during NFPTGMs, emphasizing the need to account for NFPTGM characteristics in the design and construction of such bridges to ensure their safety and performance.

Based on the existing literature, it becomes evident that earthquake induced forces can excite distinct modes of vibration within cable-stayed bridges. To study the overall performance of cable-stay bridges, it is imperative to evaluate the vulnerability of the bridge structure and tailor vibration control and/or mitigation strategies according to the excitation, the structural components most susceptible, and the targeted response parameter (e.g., displacement or acceleration).

This study, is set against the backdrop of Iceland's unique environmental and geological conditions, as we evaluate the Ölfus Cable-Stayed Bridge (OCSB) response when subjected to near-field ground motion. Our approach entails the creation of a nonlinear model for the OCSB using the OpenSees

platform. Subsequently, we apply a series of NFPTGMs , ultimately generating fragility curves for a comprehensive probabilistic analysis.

2. Case study of the Ölfus Cable-Stayed Bridge

This section presents the case study of the Ölfus cable-stayed bridge (OCSB) to illustrate how NFPTGMs affect the bridge and its components in distinct ways. The findings are statistically detailed to formulate bridge fragility curves for assessing bridge reliability in Near-fault zone. The subsequent sections outline the mathematical model of the bridge, and the seismic excitations employed in the study.

2.1. Selection of near-field velocity pulse type ground motions

To investigate the structural responses of bridges when subjected to NFPTGMs and derive broader, statistically significant insights, we curated a collection of 106 NFPTGMs. This selection encompasses a diverse range of frequency characteristics and seismological attributes drawn from the University of Iceland's Earthquake Engineering Research Centre database. This study focused only on the horizontal component containing the velocity pulse. This collection of NFPTGMs was assembled by Rupakhety et al. (2011), following the methodology outlined in their earlier work (Rupakhety et al., 2010). The properties of these ground motions, including aspects such as amplitude and frequency content, were examined thoroughly in Rupakhety et al. (2011) study.

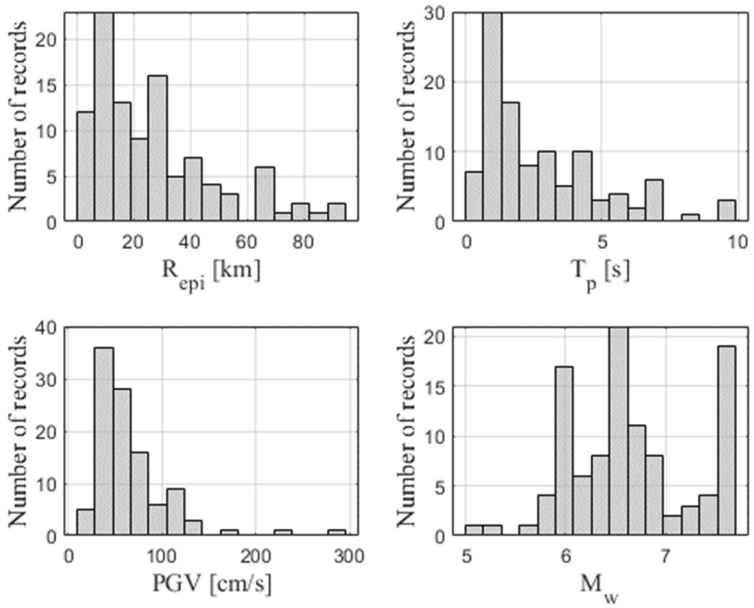

Figure 1. Distribution of main seismological parameters for the 106 NFPTGMs selected in this study.

The distribution of the main seismological parameters is depicted in histograms (Figure 1), from which critical considerations emerge. Most of the selected events' rupture distances (R_{epi}) fall within the 0-30 km interval, confirming that the pulse-like feature of the chosen ground motions generally correlates

with relatively short epicentral distances. The velocity pulse periods (T_p) span a wide range, ranging from 0.42s to 14s, with a mean value of 3.37s and a relatively uniform distribution. This implies that the considered set of ground motions represents various frequency contents of seismic excitation. These ground motions' peak ground velocity (PGV) ranges from 10.6 to 294.2 cm/s, encompassing a broad spectrum of amplitude variations. Correspondingly, these ground motions are associated with earthquake magnitudes (M_w) ranging from 5 to 7.6 on the moment magnitude scale. A comprehensive summary of the seismological properties of this ground motion dataset is provided in Appendix A. The corresponding Fourier Amplitude Spectra (FAS) shown in Figure 2 indicates that for selected earthquakes, the spectral content at the first mode of the bridge in both the longitudinal and transverse directions is significant.

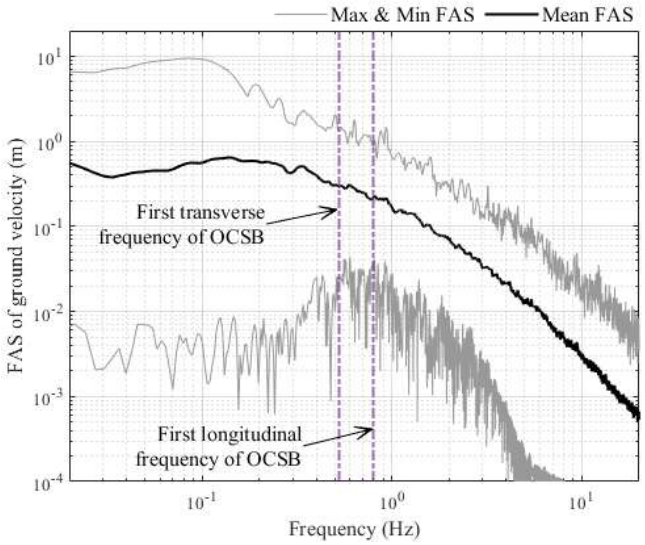

Figure 2. FAS of the selected horizontal ground motion time series shown in Appendix A. The grey lines correspond to Minimum and Maximum, and the black line is the average FAS. The vertical lines correspond to the frequencies of the two modes listed in Table 2.

2.2. Description of numerical model of OCSB

2.2.1. Description of the OCSB

For this case study, a single-tower cable-stayed bridge has been selected (refer to Figure 3). This cable-stayed bridge is planned for construction over the Ölfus River in Selfoss. It's important to note that the Ölfus Cable-Stayed Bridge (OCSB) is asymmetric, with a span length of 145 m on the western side and 155 meters on the eastern side. The deck measures 23 meters in width and is composed of two steel girders on the sides, a central steel beam, cross beams, and a concrete slab (see Figure 3(c)). Material details and cross-section specifications for the deck elements can be found in Table 1.

In this model, a 55 m tall steel tower is considered (see Figure 3(b)), featuring a rectangular cross-section with side lengths of 3.5 meters and a thickness of 40 mm. Additionally, there are four struts on

each side, each 40 cm in length and 2 cm thick (see Figure 3, section A-A). The tower's two legs are anchored on a 4-meter by 4-meter concrete block (see Figure 3(b)). The cables are connected to the tower at intervals of 1.5 meters and with an interval of 9.0 meters to the bridge floor on the west side and 9.5 meters on the east side. The cables proposed for the preliminary design are constructed from parallel wires with a cross-sectional area of 150 mm. The number of wires in the cables varies due to the cable's length, ranging from 31 to 37. The bridge is equipped with LRBs to enhance its seismic resilience. Six LRBs are used, two at each end and two aligned with the tower (see Figure 4).

Table 1. *OCSB deck elements details*

Elements	Material	Cross-section				
		Section	Height (mm)	Width (mm)	Flange thickness (mm)	Web thickness (mm)
Girder at the tower side	Steel S355	Box	1540	800	70	30
Girder at the abutment side	Steel S356	Box	1270	800	35	20
Middle beam	Steel S357	Box	440	600	20	15
Cross beam	Steel S358	Box	1140	600	20	15
slab west side	concrete		300	20000		
slab East side	concrete		270	20000		

It's worth noting that the bridge is situated in an active seismic zone known as the South Icelandic Seismic Zone (SISZ). According to a study by Ragnar et al. (2014), the OCSB is approximately 2 km away from the fault. The database from the Earthquake Engineering Research Center (EERC) indicates that two significant earthquakes occurred in the Southern Fault Zone in 2000 and 2008, both registering magnitudes between 6.3 and 6.5. The bridge exhibits substantial mass participation in vibration modes with periods in the range of 0.6 to 2 seconds. It is, therefore, likely that some modes of vibration of the bridge will resonate with the near-fault ground motion pulses, resulting in large demands on the structure. On the other hand, the geographical location of Iceland in the middle of the North-Atlantic ocean, requires that wind-induced force be considered as a potential hazard in the design of the bridge.

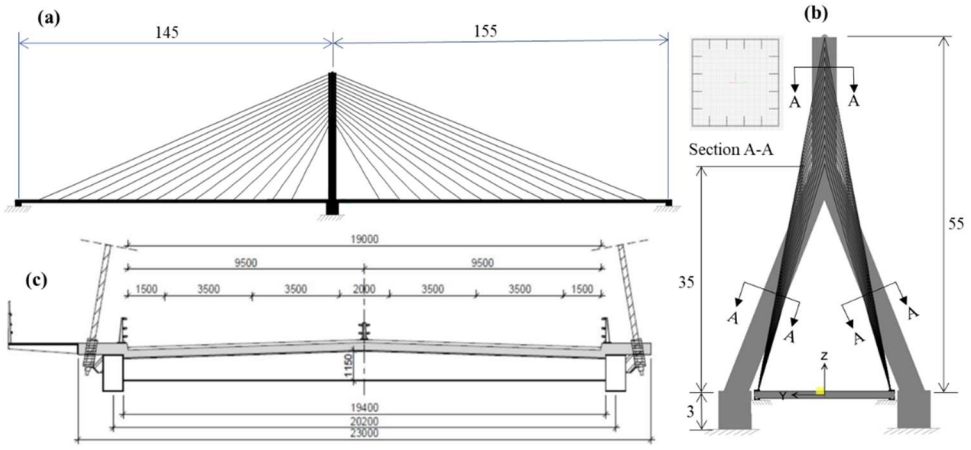

Figure 3. The OCSB (a) elevation. (b) Geometry of the tower. (c) Cross-section girder. (Dimensions in m)

2.2.2. Numerical model of OCSB

A nonlinear three-dimensional Finite Element (FE) model of the bridge has been developed within the OpenSees platform (as depicted in Figure 4). This model is constructed based on the bridge specifications available from the preliminary design and literature sources (Ingvar Hjartarson, 2019). The modal shapes, frequencies, and mass participation ratios for the first four vibration modes of the OCSB are presented in Figure 5 and summarized in Table 2. In this model, the bridge deck is represented using linear elastic beam-column elements that pass through its shear center. The stiffness properties and mass of the deck section are primarily concentrated in the spine beams. The inclined stay cables are assumed to maintain their elasticity throughout their entire service life, with the capacity to resist tensile forces exclusively. Consequently, the cable forces are applied to the bridge via truss elements constructed from tension-only materials with initial strain. It is anticipated that the tower elements may experience plastic deformation when subjected to extreme loads, such as strong earthquakes or wind-induced forces. As a result, two plastic hinges have been incorporated into the connection of the tower legs to the concrete foundation blocks. These plastic hinges are modeled using zero-length elements with uniaxial Bilin material properties (OpenSeesWiki-Command Manual). The connection of the bridge deck to the abutments is facilitated by bearings. Lead-rubber-X elements have been employed for modelling the behaviour of these bearings. To determine the optimal parameters for the lead-rubber-X element, a novel methodology, which is detailed in the following section of this study, has been proposed.

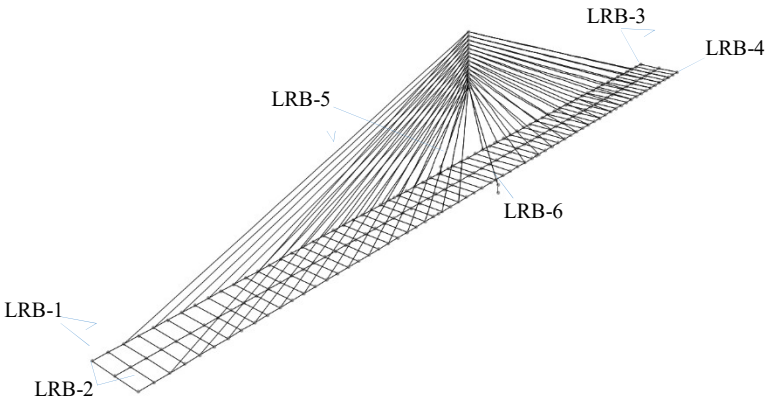

Figure 4. 3D Finite Element Model of the OCSB.

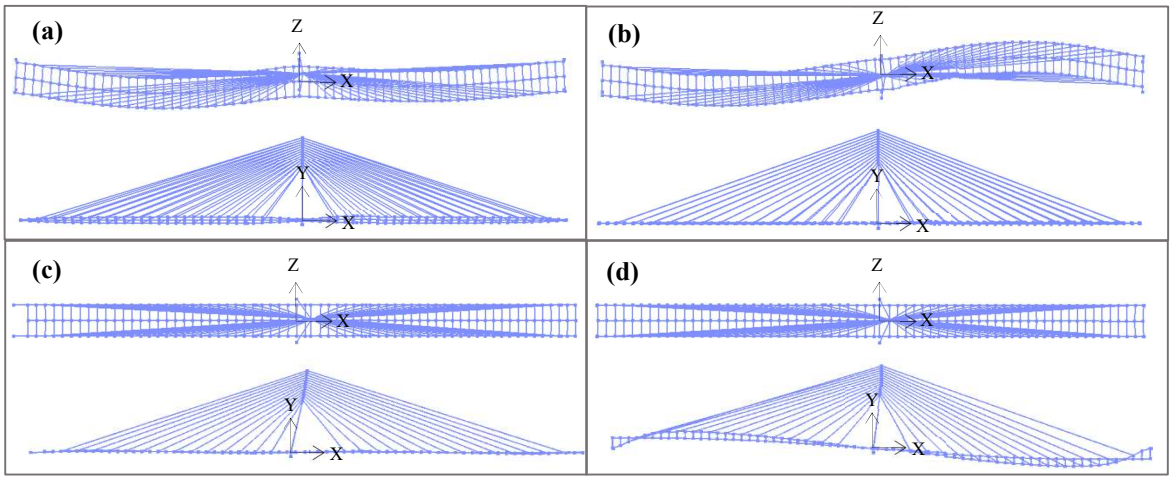

Figure 5. First 4 modes of vibration of the OCSB (a) first mode shape (horizontal), bridge deck moves symmetrically in the transverse direction; (b) second mode shape (horizontal), the bridge deck moves asymmetrically in the transverse direction; (c) third mode shape (horizontal) the bridge deck and tower both move in the longitudinal direction, and; (d) forth mode shape (rotational, vertical, and horizontal), the tower moves horizontal in the longitudinal direction pulling the bridge deck asymmetrically in the vertical direction

***Table 2**. Modal frequencies, and modal participation mass ratio of OCSB for modes 1 to 4 (U and R denote translation and rotation, respectively)*

Mode #	Direction	Frequency (Hz)	Modal mass participation ratio (%)					
			Ux	Uy	Uz	Rx	Ry	Rz
1	Transverse	0.53	0	0	79.69	3.75	3.13	0
2	Rotational and Transverse	0.60	0	0	3.88	0.18	70.39	0
3	Longitudinal	0.80	96.81	0	0	0	0	0.04
4	Rotational	0.86	0.06	0.27	0	0	0	95.19

2.2.3. Optimization of bearings lead diameter.

A lead rubber bearing consists of several materials, including sealing steel plates, a steel shim layer, a lead core, and cover rubber (see Figure 6). Several procedures have been used for designing lead rubber bearings (see references include Lee, 1994; Turkington et al., 1989; Hameed et al., 2008; Li et al., 2018; and Cao et al., 2020). However, finding the optimum parameters for a lead rubber bearing in a nonlinear structural model is a challenging task. In such cases, genetic algorithms (GA) can be a suitable method which has been employed in various research endeavours to optimize control device parameters.

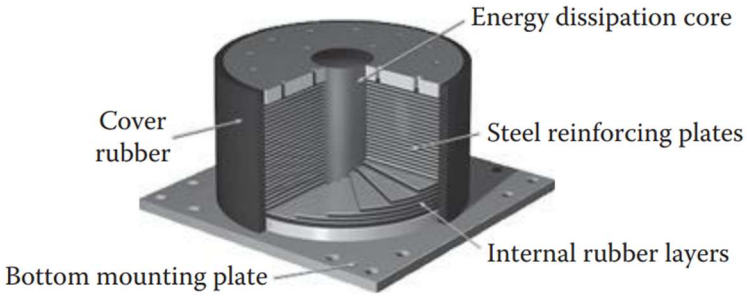

Figure 6. LRB, (Chen and Duan, 2014).

In this study, the lead rubber bearing in the Opensees platform, is modelled using the "LeadRubberX" command. This command constructs a three-dimensional LeadRubberX bearing element within a 12 DOF, 2-node discrete element framework. Designed to replicate the 3D continuum geometry of a lead rubber bearing, this model expands upon the ElastomericX formulation by integrating strength degradation effects resulting from lead-core heating. The LeadRubberX command requires several geometric and material properties of the elastomeric bearing as input parameters. All the parameters listed in Table 3 are required inputs for this command, including shear modulus, bulk modulus, rubber layer thickness, lead yield stress, and thermal conductivity. These parameters define the six-directional material behavior of the bearing within OpenSees (OpenSeesWiki) .

***Table 3**. parameters of Lead Rubber bearing (Units are in N, m, s)*

Post-elastic stiffness ratio in shear	0.05
Shear modulus of rubber obtained from testing of elastomeric bearings at large shear strains	6.50E+05 Pa
Bulk modulus of rubber	2.00E+09 Pa
Thickness of steel shim plates	6.00E-03 m
Thickness of a single rubber layer	1.00E-02 m
Number of rubber layers	25
Outer diameter of lead rubber bearing	1.00E+00 m
Bearing cover	1.20E-02 m
Yield stress of lead initially	1.30E+07 Pa
Thermal conductivity of steel	5.00E+01 W/(m.K)

In this study, most design parameters are based on established references (see Lee, 1994; Turkington et al., 1989; Hameed et al., 2008; Li et al., 2018; and Cao et al., 2020), except for the lead diameter. Since the lead core is the primary component responsible for energy dissipation in the bearing, we conducted an optimization process to determine the optimal lead diameter. To balance accuracy and computational efficiency, we opted not to use the Genetic Algorithm (GA) approach for optimizing the lead diameter. Instead, we predefined 20 different lead diameters for the LRBs, ranging from 10 cm to 70 cm, and modelled each case individually. The analysis was then performed for all 106 sets of ground motions for each model. All six LRBs share the same geometry and material properties. To evaluate their performance, the mid-span displacement response in the transverse direction for a 145-meter span, which is relatively stiffer was considered. This displacement was chosen as the key output parameter to determine the optimal lead diameter.

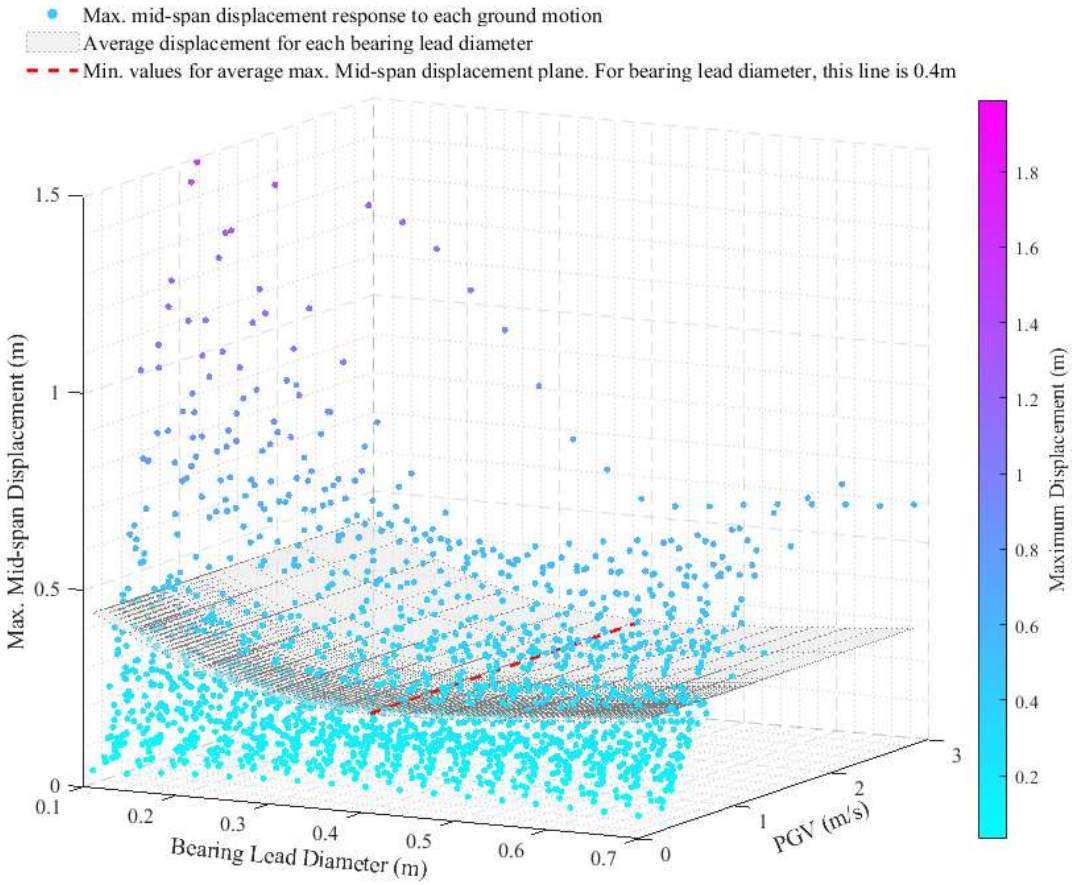

Figure 7. The scatter plot shows individual data points (Max. mid-span displacement). The transparent plane represents the average maximum displacement across bearing diameters. The red dashed line highlights the optimal bearing diameter of 0.4 m, spanning all PGV values.

Figure 7, present the 3D scatter plot illustrates the relationship between bearing lead diameter (m), peak ground velocity (PGV, m/s), and maximum mid-span displacement (m) for a set of 106 ground motion records. Each scatter point represents the maximum displacement for a specific bearing lead diameter and PGV combination. The semi-transparent plane highlights the average maximum displacement

across all bearing lead diameters, providing a visual representation of overall structural performance. The red dashed line at a bearing lead diameter of 0.4 m highlights the trend of maximum mid-span displacements across different PGV values. This specific diameter is identified as optimal based on structural performance, as it consistently results in lower displacement values compared to other diameters. To better understand this effect, we analysed the results in Figure 8, where the relationship is further clarified by evaluating the mean peak mid-span displacement. This helps highlight how different bearing lead diameters contribute to structural response and identify the most effective diameter for minimizing displacement. Based on Figure 8, it is clear that the lead diameter of 0.4m has the best performance.

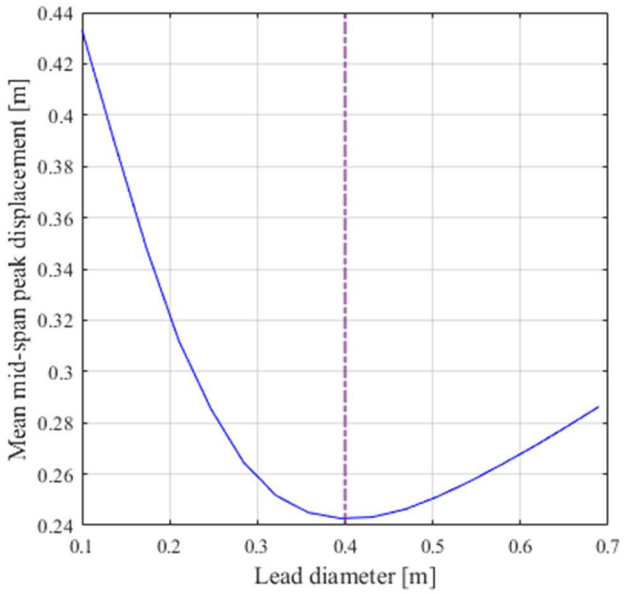

Figure 8. variation of mean values of OCSB peak mid-span response in the transvers direction to a set of 106 ground motions for LRBs with different bearing lead diameter.

However, it should be noted that changing the lead diameter has a direct effect on dynamic characteristics of bridge system. As an explanation of the contributing factors, we can mention the following:

- A smaller diameter (less than 0.4m) may lack sufficient stiffness, causing excessive deformation, which leads to higher mid-span displacements and structural instability.
- A larger diameter (greater than 0.4m) may be overly stiff, reducing the bearing's ability to dissipate seismic energy, resulting in higher force transmission to the structure (see Figure 9).
- The 0.4 m bearing lead diameter provides sufficient deformation capacity to absorb seismic energy without excessive displacement (see Figure 9).
- The 0.4 m bearing lead diameter likely optimizes the hysteretic behaviour of the bearing material, ensuring an efficient energy dissipation (see Figure 9).
- A bearing lead diameter of 0.4 m yields the best structural performance, as Figure 7 and 8 demonstrates, since it consistently achieves lower maximum displacements across a wide range

of PGV values. This suggests that a 0.4 m lead diameter of bearing optimally balances flexibility and stability under seismic loading.

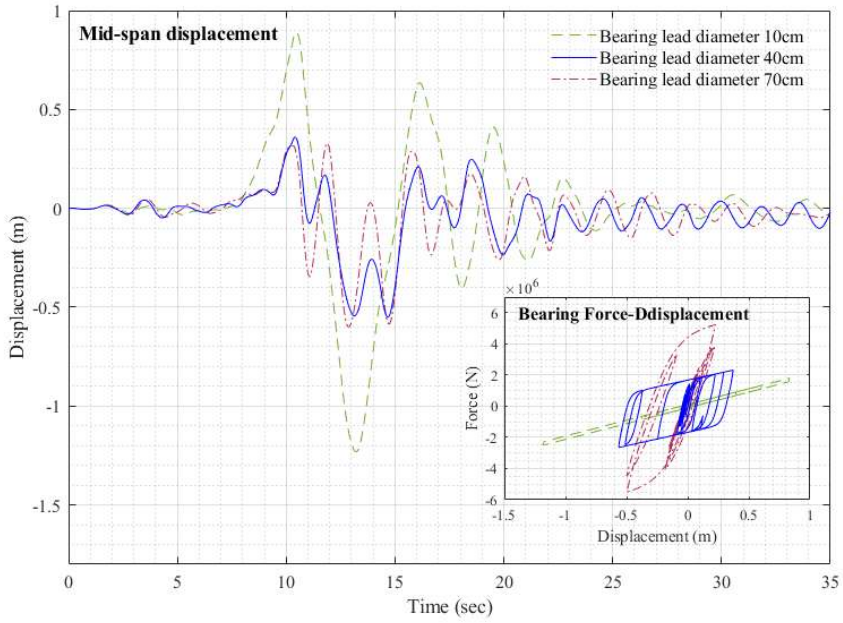

Figure 9. Mid-span displacement and bearing force-displacement responses for an extreme ground excitation case (Chi-Chi Earthquake, 1999), considering cases with bearing lead diameters of 10 cm, 40 cm, and 70 cm.

To better understand the effects of pulse-type ground motions on bridge response, a new set of 69 pulse-type ground motions, as addressed by Sigurðsson et al. (2020), was considered. Based on the specifications of this dataset, a total of 125 time series of seismic motion containing a velocity pulse were simulated using the procedure explained in the following paragraphs.

The mean and standard deviation of PGV and T_p were extracted from the original dataset. Using these statistical parameters, a MATLAB program was developed based on Eq. 1 to simulate the pulse velocity wave.

$$v_g = \begin{cases} \frac{A}{2}\left[1 + cos\left(\frac{2\pi f_p}{\gamma}(t - t_0)\right)\right] cos\left[2\pi f_p(t - t_0) + v\right], & t_0 - \frac{\gamma}{2f_p} \le t \le t_0 + \frac{\gamma}{2f_p} \\ 0 & Otherwise \end{cases} \quad (1)$$

Where v_g is velocity waveform, A and f_p are the amplitude and frequence of the pulse; v is the phase angle; t_0 is indicated the time location of the pulse and γ controls the zero crossings the pulse (Mavroeidis and Papageorgiou, 2003).

The simulation range for PGV and T_p was defined as the mean ± one standard deviation. Within these ranges, five variations of T_p and five variations of PGV were considered, generating a grid of 25 combinations. For each combination, five ground motions were simulated with random phase angles (v) and oscillatory characteristics (γ), resulting in a total of 125 ground motion time series.

For each of the 125 ground motions simulated, structural analysis was conducted seven times, with the lead diameter of the bearing changing in each analysis. This resulted in a total of 875 analyses.

The same procedure as described in Section 3.3.3 for determining the optimal lead diameter was applied here. For each lead diameter, the mean value of the maximum mid-span displacement was extracted and plotted in Figure 10. The figure illustrates the relationship between the lead diameter and the average Maximum Mid-span Displacement (MSDmax) of the structure under varying ground motion conditions. Each point on the plot represents the average MSDmax for a specific lead diameter across all combinations of PGV and T_p . The results indicate that the optimal lead diameter for mitigating the effects of velocity pulse energy is 0.5 m.

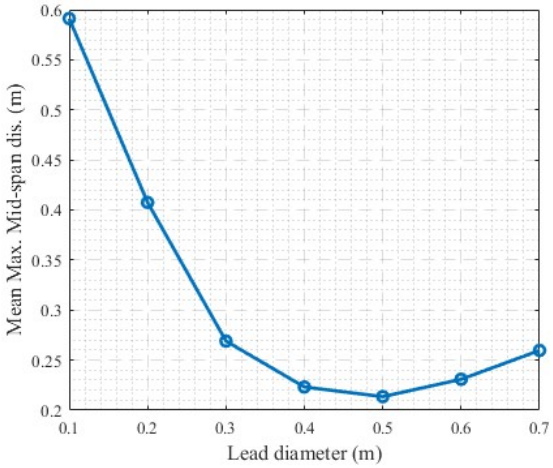

Figure 10. The mean peak mid-span response in the transvers direction of the OCSB as a function bearing lead diameter for a set of 125 near-field seismic pulses.

For a better perspective of the velocity pulse effects on different bearing lead diameters, the results are plotted up in Figure 11, which illustrates the relationship between PGV, T_p, and the MSDmax of a bridge structure for various bearing lead diameters. The scatter points in the figure represent the computed average MSDmax values across multiple combinations of PGV and T_p, with the lead diameters color-coded, as shown in the colour bar. These points provide a detailed visualization of how the structural response varies with ground motion characteristics. Two smooth surfaces are overlaid to represent the mean MSDmax response for lead diameters of 0.4 m (green) and 0.5 m (orange). These surfaces interpolate the MSDmax values across the ranges of PGV and Tp, providing insight into the performance of each lead diameter under different conditions. The dashed black vertical line in the figure highlights the specific ground motion parameters of PGV = 0.5431 m/s and T_p = 1.43 s, which correspond to the Ölfus South Iceland 2008 earthquake. The intersection points of this line with the planes are marked by red and blue stars, indicating the MSDmax response for lead diameters of 0.4 m and 0.5 m, respectively.

For T_p values in the range of 1.0 to 2.0 s, which covers the natural period range of the lowest modes of vibration of the bridge, the 0.4 m lead diameter surface shows lower MSDmax values compared to the 0.5 m plane. This suggests that a 0.4 m lead diameter performs better in mitigating displacements under these conditions. However, for PGV values greater than 0.4 m/s or T_p values exceeding 2 s, the 0.5 m lead diameter demonstrates lower MSDmax values, making it more effective in handling higher-intensity pulse motions. In conclusion, the choice of lead diameter depends on the specific ground motion parameters chosen for design. For moderate pulse intensities and excitation periods closer to the bridge's natural period, a 0.4 m lead diameter is more effective. In contrast, for higher PGV or longer T_p, a 0.5 m lead diameter provides better performance in reducing mid-span displacements.

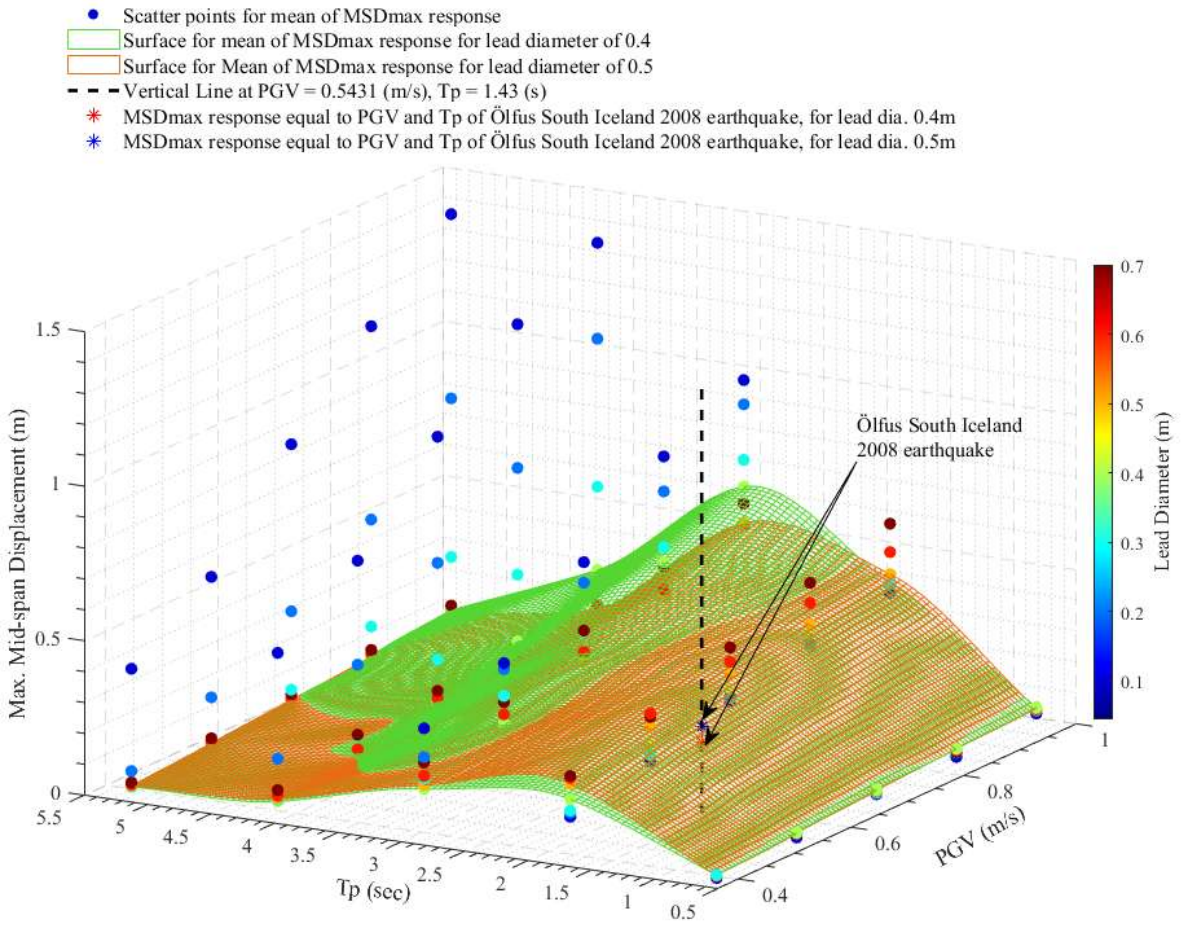

Figure 11. 3D-Scatter plot for the mean peak mid-span response in the transvers direction for the OCSB as function of the period and PGV of near-fault pulsed seismic motion for a range of bearing lead diameters. A surface is drawn for bearing lead diameters of 0.4 m and 0.5 m.

2.3. Evaluating the bridge responses

In this section, the response of the OCSB to a set of ground motions is evaluated, with a focus on highlighting key aspects of the bridge's behaviour under seismic loading. To achieve this, the results from the analysis are used to generate figures that illustrate the relationship between T_p, PGV, and structural response, as well as the FAS of the displacement responses (see Figures 12 and 13).

Figure 12 shows how the displacement response at both the mid-span (transverse direction) and the top of the tower (longitudinal direction) is strongly influenced by the ratio of the excitation period and the natural period, T_p/T_n. The figure highlights that peak displacements occur when T_p approaches or slightly exceeds T_n, which results in intensified structural demands due to resonance effects.

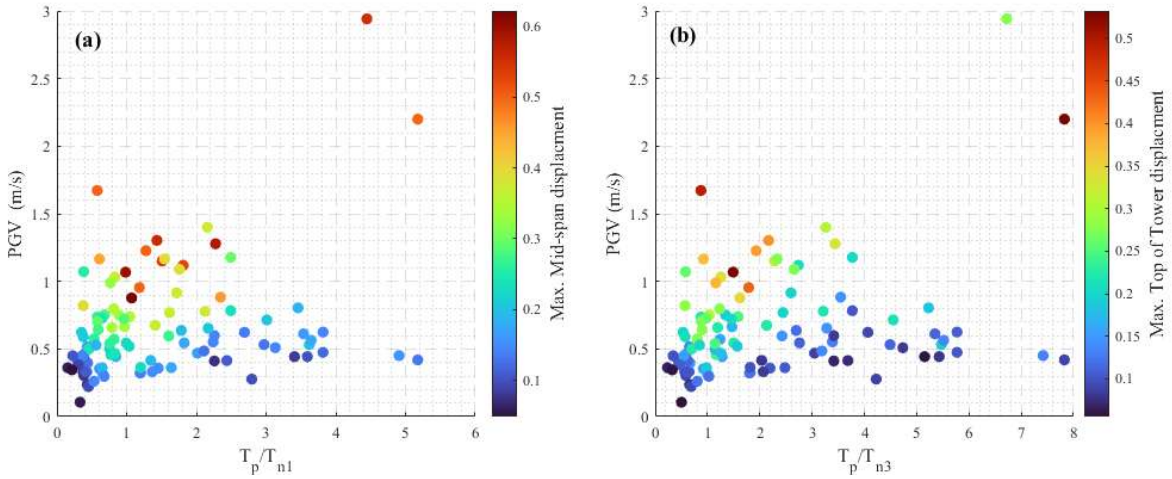

Figure 12. 2D Scatter plot of PGV and displacement of as a function of the period ratio T_p/T_n. (a) Max. mid-span in transvers-direction and the first natural period in transvers direction T_{n1}. (b) Max. displacement of the tower in longitudinal-direction and the first natural period in longitudinal direction, T_{n3}.

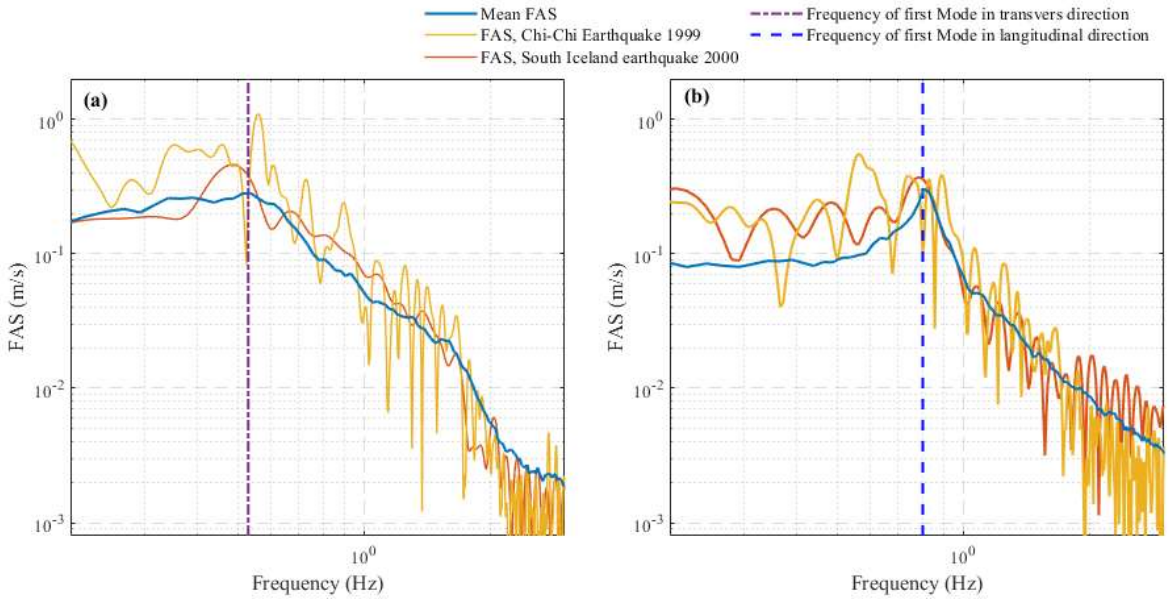

Figure 13. Fourier amplitude spectra (FAS) of displacement response at (a) mid-span in transvers-direction and (b) top of the tower in longitudinal-direction.

Figure 13 presents the Fourier amplitude spectra (FAS) of the displacement responses. It reveals that the first natural frequencies of the bridge align with significant energy components of certain seismic events, such as the Chi-Chi Earthquake and the South Iceland Earthquake in 2008. This alignment amplifies structural responses, particularly at the mid-span in the transverse direction and at the tower top in the longitudinal direction. The spectral response also demonstrates that the severity of the bridge's displacement is event-specific, with certain earthquakes inducing higher energy excitation at frequencies close to the bridge's natural modes. This variability underscores the importance of adopting tailored seismic design strategies that consider the unique characteristics of the local seismic environment.

These findings form the basis for the subsequent Fragility Analysis, which provides a more comprehensive and probabilistic evaluation of the bridge's vulnerability to NFPTGMs scenarios. By quantifying the likelihood of structural damage or failure, fragility analysis offers deeper insights into the bridge's performance. Transitioning from response analysis to fragility analysis bridges the gap between deterministic modelling and probabilistic risk assessment, ensuring a holistic approach to enhancing the resilience and safety of the OCSB.

2.4. Fragility analysis

To evaluate the structural integrity of a cable-stayed bridge under the influence of natural hazards, specifically NFPTGMs, fragility analysis is employed. During strong near-fault ground motion, the most susceptible component of the bridge is the bearing. This is because the primary purpose of the bearing elements is to dissipate the energy generated by earthquakes, and their functionality during the entirety of the event is of key importance. Therefore, when conducting a fragility analysis of a bridge subjected to near-fault ground motion, it is crucial to assess the strength capacity of these bearing elements. In this study, the shear strain of the bearings serves as a parameter for evaluating their damage state.

Damage models are typically derived from experimental data, where observed damage and the measured capacity of specimens are correlated with the level of applied demand. For fragility analysis in the context of near-fault ground motion, different damage states are considered based on studies conducted by Zhang and Hou (2009) and Billah and Todorov (2019):

Level 1 - Slight Damage: The shear strain of the bearing exceeds 100%.

Level 2 - Moderate Damage: The shear strain of the bearing surpasses 150%.

Level 3 - Extensive Damage: The shear strain of the bearing exceeds 200%.

Level 4 - Collapse: The shear strain of the bearing is greater than 250%

To develop fragility curves, we adopted the Multiple Stripe Analysis (MSA) approach by calculating the fraction of NFPTGMs at each stripe (Intensity Measure level) that caused bridge collapse (Baker, 2015). A set of 106 pulse-type ground motions, described in the previous section, was scaled based on each Intensity Measure (IM) level. We calculated the absolute peak bearing displacement response in

the longitudinal direction (D_x) and transverse direction (D_z) of the bridge and then statistically analysed the results to construct the bridge fragility curves. The PGV was considered as the *IM* for the fragility analysis. It was assumed that the *IM* levels corresponding to different damage states of the bridge follow a lognormal distribution. Based on this assumption, the fragility function is defined as follows:

$$P(C|IM = x) = \Phi\left(\frac{\ln\left(x/\theta\right)}{\beta}\right) \quad (2)$$

In this equation, $P(C|IM = x)$ represents the probability that a NFPTGM associated with $IM = x$ will cause structural damage. Φ is the standard normal cumulative distribution function (CDF), and θ and β are the two parameters of the fragility function. θ represents the median of the fragility function, and β represents the standard deviation of $\ln(IM)$ which characterizes the dispersion of *IM*. Calibrating Equation 2 for the considered bridge structures involves estimating and θ and β from the results of seismic analysis. For parameter estimation of the fragility function, we used the Maximum Likelihood Estimation (MLE) method.

The fragility curves for earthquake hazard are indicated in Figure 14. To better understand the resilience of the OCSB in the Icelandic environment, the PGV of the nearest earthquake to the bridge location (the Selfoss earthquake of 2008). The fragility analysis highlights that the seismic vulnerability of bearings is quite significant, especially in the longitudinal direction. This is because the bridge is more flexible in the transverse direction, allowing part of the ground excitation to be absorbed by the deck. However, in the longitudinal direction, the deck remains almost rigid, and all the ground motion energy is absorbed by the bearings. This requires that after each earthquake, the bearings are carefully examined, and the bearings should be designed in such a way that they can be replaced if necessary.

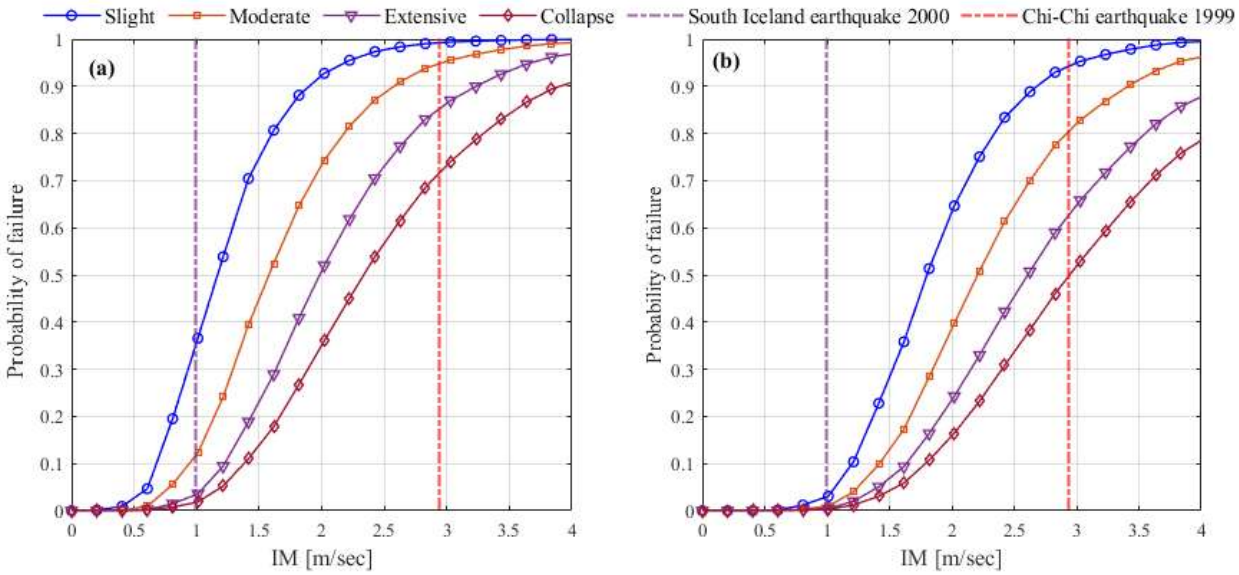

Figure 14. Shear strain fragility curves for OCSB, using the maximum likelihood approach. (a) for longitudinal direction, (b) for transverse direction.

2.5. Near-field velocity pulse response analysis

The evaluation of the near-field seismic velocity pulse response is a crucial factor for gaining a deeper understanding of the impact of NFPTGMs on bridge structures. While the velocity pulse in an earthquake alone may not encompass all the earthquake characteristics, it is anticipated that the peak response of a structure to a NFPTGM is influenced by the velocity pulse within that ground motion.

To delve into this matter, we conducted a nonlinear analysis using a set of 106 velocity pulses (PTGMs) that were extracted from NFPTGMs records by Rupakhety et al. (2011). The results were then compared with the original NFPTGMs responses.

Figure 15 shows the ratio of peak mid-span displacement response in the longitudinal and transverse directions for the original NFPTGMs plotted as a function of the ratio of the natural period of bridge structure divided by the pulse period. In both directions, for $\frac{T_s}{T_p} \geq 1$, the peak displacement responses for the original NFPTGMs and the pulse are closely aligned. This indicates that the extracted pulses from the NFPTGMs effectively captures the primary characteristics of the ground motion influencing the structural response, particularly when the structural period aligns with the pulse period. In the longitudinal direction, for smaller values of $\frac{T_{sL}}{T_p}$, there are slight deviations in the response, but the variation remains relatively constrained. This suggests that the extracted pulses (PTGMs) successfully represent the dominant features of the NFPTGMs for longitudinal responses. Overall, there is stronger alignment in the longitudinal direction compared to the transverse direction. This difference is likely due to variations in the dynamic characteristics or sensitivity of the structure in these two directions.

In the transverse direction, when the ratio $\frac{T_{sT}}{T_p}$ is smaller than 0.5 (indicating a stiffer structure in this direction), the pulse response is significantly lower than the original response. This happens for several reasons: The pulse energy is delivered at a much lower frequency compared to the stiffness dominated response in the transverse direction, leading to poor resonance. Or we can say that the pulse energy is less efficiently transferred to the structure when the structural period is much shorter than the pulse period. This mismatch results in a lower response to the pulse compared to the original NFPTGM, which contains higher-frequency components that can excite the transverse direction more effectively. Additionally, the transverse response might be influenced by other high-frequency content present in the original NFPTGM but absent in the extracted pulse. This could explain why the original response is higher than the pulse-only response for smaller values of $\frac{T_{sT}}{T_p}$.

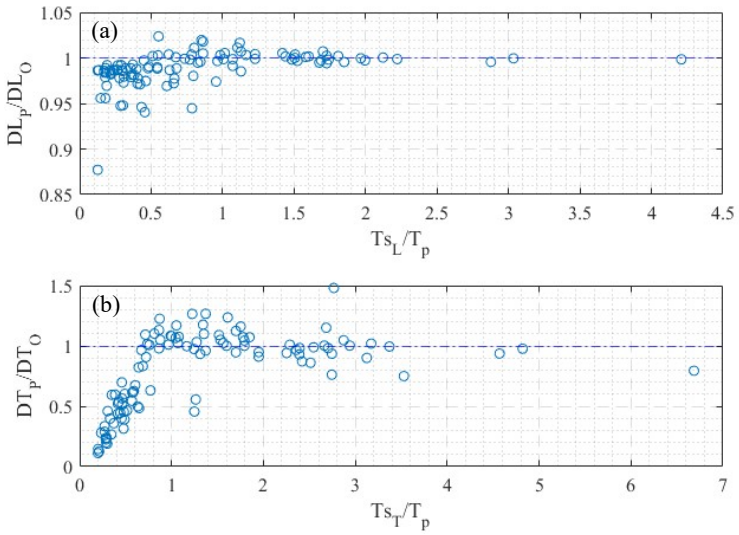

Figure 15. Comparison of mid-span displacement response to the the original NFPTGMs and the corresponding extracted pulsein (a) longitudinal and (b) transverse direction. DL_o and DT_o, are peak mid-span displacement response to original NFPTGMs in longitudinal and transverse direction, respectively. DL_p, and DT_p are peak mid-span displacement response to the extracted velocity pulse in longitudinal and transverse direction, respectively. Tp is the pulse period, and Ts_L and Ts_T are the first natural periods of the structure in longitudinal and transverse direction.

To better understand the impact of NFPTGMs on the bridge structure, a set of 27,600 PTGMs was simulated and applied in longitudinal and transverse direction to the bridge structure for nonlinear analysis. This simulation was conducted using a set of 69 PTGMs as seeds to generate 27,600 PTGMs. Figure 16 provides a flowchart summarizing the main steps of the simulation procedure.

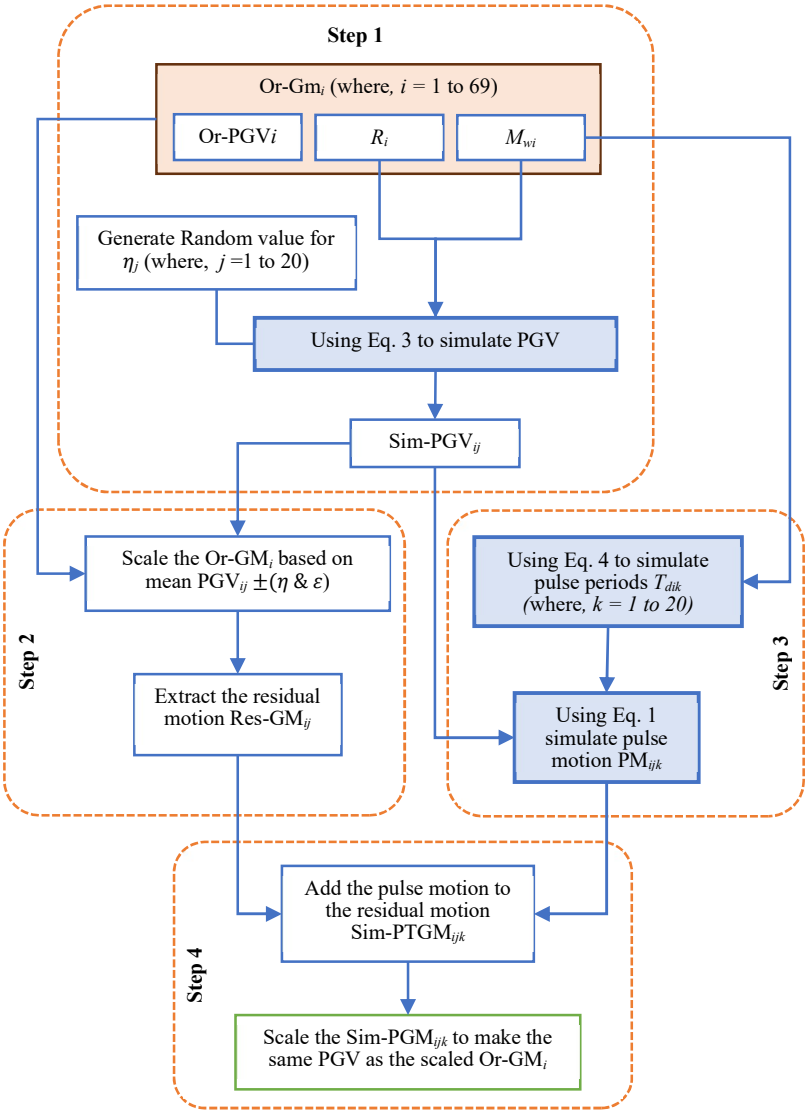

Figure 16. Flowchart summarizing steps of simulation of PTGMs.

Step 1, Simulating PGVs;

For the i^{th} Original Ground Motion (Or-GMi) from the set of 69 NFPTGMs, the parameters R_i and Mw_i are used with Eq. 3 to simulate PGVs. In this process, random values for η_j $(where, j = 1\ to\ 20)$ are used. Based on these random η values, PGV$_{ij}$ is simulated (Sim-PGV$_{ij}$).

$$\log(PGV_{ij}) = \begin{cases} a + bM_w + cM_w^2 + dlog(R^2 + e^2) + \eta_j + \varepsilon & if\ \ M_w \le M_{sat} \\ a + bM_{sat} + cM_{sat}^2 + dlog(R^2 + e^2) + \eta_j + \varepsilon & otherwise \end{cases} \quad (3)$$

Regression coefficients for the model of Eq. 3 are presented in Table 4. For description of Eq. 3 see Rupakhety et al. (2011).

Table 4. *Regression coefficients*

A	b	*c*	d	e	M_{sat}	ε
-5.17	1.98	-0.14	-0.1	0.75	7.0	0.16

Step 2, Scaling and Residual Extraction:

The Or-GM$_i$ is scaled based on the $mean\ PGV_{ij} \pm (\eta\ \&\ \varepsilon)$, and the residual part of the motion is extracted (Res-GM$_{ij}$).

Step 3, Simulating Pulse Periods and Motion:

Using M_{wi} in Eq. 3, pulse periods (T_{dik}, where k = 1 to 20) simulated. a MATLAB program based on Eq. 1 (Mavroeidis and Papageorgiou, 2003) has been developed using T_{dik} and Sim-PGV$_{ij}$ to simulate Pulse Motions (PM_{ijk}).

$$\log(T_d) = \alpha M_w + \beta + \varepsilon \quad (4)$$

where α,and β are model coefficients determined by regression analysis; and ε is a Gauss ian-distributed random variable with zero mean and standard deviation σ (see Rupakhety et al., 2011).

Step 4, Generating Simulated PTGMs:

The PM_{ijk} are added to the Res-GM$_{ij}$ to generate simulated pulse-type ground motions (Sim-PTGM$_{ij}$). Finally, Sim-PTGM$_{ij}$ is scaled to ensure it has the same PGV as the scaled Or-GM$_i$.

Figures 17 and 18 provide a visual representation of the nonlinear analysis conducted on the OCSB using a dataset of 27,600 pulse-type ground motions. These 2D contour plots depict the bridge's seismic response in both transverse and longitudinal directions, highlighting the relationship between *PGV*, T_p, and the maximum mid-span displacement during simulated earthquake scenarios. The color-coded contours indicates the ratio of maximum bearing displacement to the limit state, offering a clear depiction of damage levels under varying seismic conditions. The contour lines represent the levels of maximum mid-span displacement under varying PGV and T_p. However, it is important to note that the results beyond the collapse level may not be entirely accurate due to the nonlinear behaviour of the structure under extreme conditions.

The connection between maximum mid-span displacement and damage levels, as influenced by T_p and *PGV*, offers valuable insight into the bridge's seismic behaviour. As *PGV* increases, the intensity of ground shaking grows, leading to greater mid-span displacements and higher damage levels, reflected in the rise of bearing displacements. Similarly, T_p, which captures the duration and frequency characteristics of seismic pulses, plays a significant role. Longer T_p values often align with the natural period of the bridge, causing amplified displacements and heightened susceptibility to extensive or collapse-level damage. This interaction between T_p and *PGV* underscores the need to account for both the intensity and duration of ground motion when analysing seismic performance. By doing so, engineers can better predict potential structural damage and develop more resilient designs and retrofitting strategies.

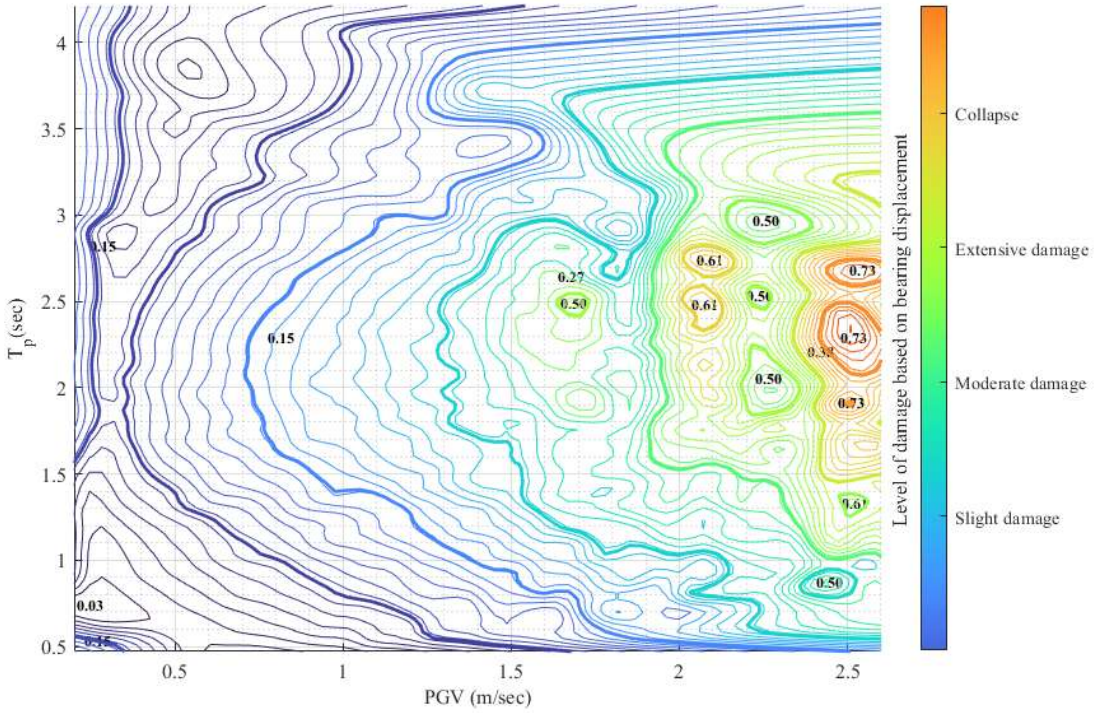

Figure 17. 2D contour plot of transverse seismic response: relationship between *PGV*, T_p , and maximum mid-span displacement of OCSB with damage levels.

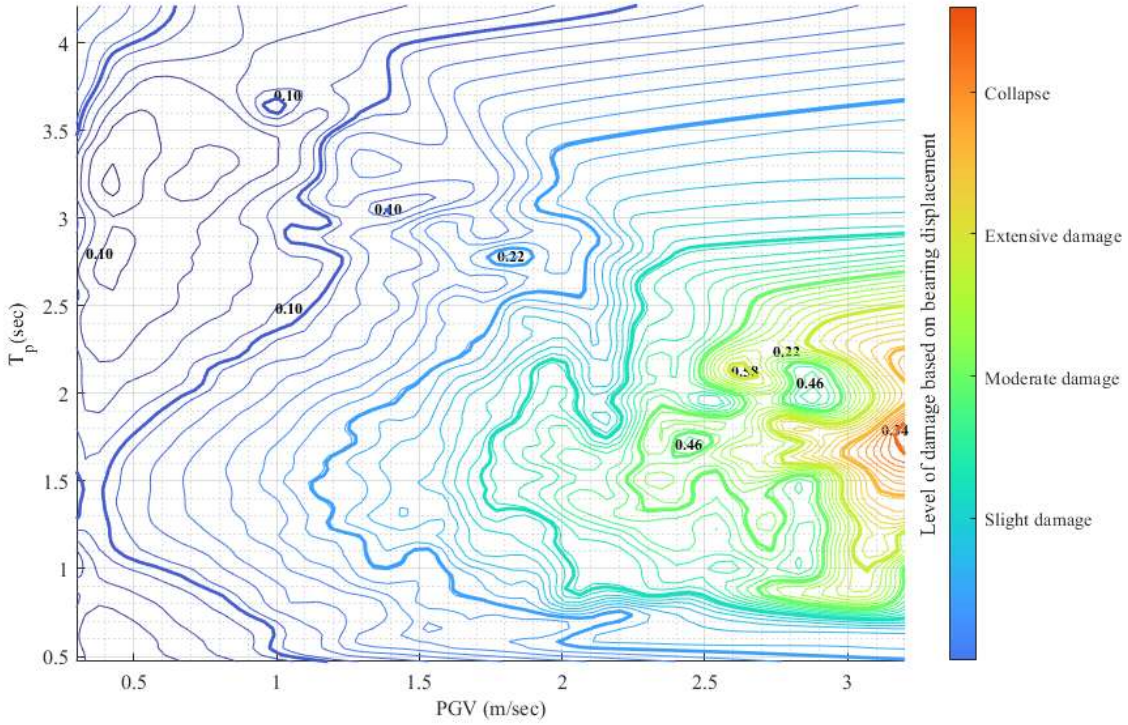

Figure 18. 2D contour plot of longitudinal seismic response: relationship between *PGV*, T_p , and maximum mid-span displacement of OCSB with damage levels.

3. Conclusions

This study evaluates the seismic vulnerability of the OCSB under NFPTGMs, with a focus on probabilistic fragility assessment. A detailed nonlinear finite element model of the bridge was developed using OpenSees, and LRBs were implemented as seismic isolation devices. The LRB design was optimized by evaluating the structural response under various lead core diameters using multiple sets of NFPTGMs. To explore the effects of velocity pulse characteristics on bridge response, both recorded and simulated PTGMs were utilized. A robust ground motion simulation framework was applied, generating 27,600 PTGMs based on 69 seed motions. These simulations accounted for variability in PGV and Tp, enabling an extensive analysis of structural behaviour under a broad range of seismic input conditions.

The key conclusions drawn from the study's results are outlined below.

- Given the historical seismic activity in Iceland, with fault lines close to urban areas, particular attention should be directed towards NFPTGMs in the design and construction of infrastructure. The study highlights their significance in ensuring the structural integrity of critical infrastructure such as CSBs.
- The fragility analysis reveals that the seismic vulnerability of the bridge bearings is a key factor in the performance of the bridge. It is essential to implement careful post-earthquake examination of the bearings, and their design should allow for replacement when necessary to ensure the bridge's long-term safety and functionality.
- The comparison of peak mid-span displacement response suggests that the response of the bridge to the velocity pulse of the near-field motion, closely corresponds to the response induced by the original NFPTGMs, both in the longitudinal and transverse directions. Consequently, it can be inferred that the velocity pulse within the near-field ground motion are indeed a key influence on the overall peak structural response to a NFPTGM.
- The analysis shows that an increase in amplitude and period simultaneously increases the velocity pulse's destructive potential, reaching a critical point at a specific pulse frequency. It is expected that as the pulse period approaches the structural period, the likelihood of damage will increase.
- The choice of bearing lead diameter depends on the specific ground motion parameters. For moderate pulse intensities and periods closer to the bridge's natural period, a 0.4 m lead diameter is found to be most effective for the case studied. In contrast, for higher PGV and/or longer T_p, a 0.5 m lead diameter provides better performance in reducing mid-span displacements.

References

1. Baker, J. W. (2007). Quantitative classification of near-fault ground motions using wavelet analysis. Bulletin of the Seismological Society of America, 97(5), 1486-1501.
2. Baker, J. W. (2015). Efficient analytical fragility function fitting using dynamic structural analysis. Earthquake Spectra, 31(1), 579-599.
3. Barker, R. M., & Puckett, J. A. (2013). Design of Highway Bridges: An LRFD Approach. John Wiley & Sons.
4. Billah, A. M., & Todorov, B. (2019). Effects of subfreezing temperature on the seismic response of lead rubber bearing isolated bridge. Soil Dynamics and Earthquake Engineering, 126, 105814.
5. Birnstiel, C. (2013). Collapse of a cable-stayed road bridge in Germany in 1825. Proceedings of the Institution of Civil Engineers-Engineering History and Heritage, 166(4), 207-226.
6. Camara, A., Astiz, M. A., & Ye, A. J. (2014). Fundamental mode estimation for modern cable-stayed bridges considering the tower flexibility. Journal of Bridge Engineering, 19(6), 04014015.
7. Cao, S., Ozbulut, O. E., Wu, S., Sun, Z., & Deng, J. (2020). Multi-level SMA/lead rubber bearing isolation system for seismic protection of bridges. Smart Materials and Structures, 29(5), 055045.
8. Chen, W. F., & Duan, L. (Eds.). (2014). *Bridge engineering handbook: construction and maintenance*. CRC press.
9. Cheynet, E. (2020). Wind Field Simulation (the Fast Version). Zenodo, doi:10.5281/ZENODO.3774136.
10. Cheynet, E., Jakobsen, J. B., & Snæbjörnsson, J. (2016). Buffeting response of a suspension bridge in complex terrain. Engineering Structures, 128, 474-487.
11. Cheynet, E., Jakobsen, J. B., Snæbjörnsson, J., Mann, J., Courtney, M., Lea, G., & Svardal, B. (2017). Measurements of surface-layer turbulence in a wide Norwegian fjord using synchronized long-range Doppler wind LiDARs. Remote Sensing, 9(10), 977.
12. Chopra, A. K., & Chintanapakdee, C. (2001). Comparing response of SDF systems to near-fault and far-fault earthquake motions in the context of spectral regions. Earthquake engineering & structural dynamics, 30(12), 1769-1789.
13. Daniotti, N., Jakobsen, J. B., Snæbjörnsson, J., Cheynet, E., & Wang, J. (2021). Observations of bridge stay cable vibrations in dry and wet conditions: A case study. Journal of Sound and Vibration, 503, 116106.
14. Elias, S., Djerouni, S., De Domenico, D., Abdeddaim, M., & El Ouni, M. H. (2023). Seismic response control of building structures under pulse-type ground motions by active vibration controller. Journal of Low Frequency Noise, Vibration and Active Control, 42(1), 345-367.
15. Fan, L., Zhou, W., & Xue, S. (2014). "Seismic Performance and Vibration Control of Cable-Stayed Bridges: A State-of-the-Art Review". Journal of Bridge Engineering, 19(3), 04013021.
16. Gautam, D., Adhikari, R., Olafsson, S., & Rupakhety, R. (2023). Dynamic identification of an aging prestressed concrete bridge using heavy vehicle excitation. *Soil Dynamics and Earthquake Engineering*, *173*, 108127.
17. Gu, Y., Huang, W., & Fan, L. (2010). The assessment method of safety performance of cable-stayed bridge under multi-hazard based on structure vulnerability. In ICCTP 2010: Integrated Transportation Systems: Green, Intelligent, Reliable (pp. 3261-3271).
18. Hameed, A., Koo, M. S., Do, T. D., & Jeong, J. H. (2008). Effect of lead rubber bearing characteristics on the response of seismic-isolated bridges. KSCE Journal of Civil Engineering, 12, 187-196.
19. Hassan, M., & Matsumoto, T. (2013). "Corrosion Protection and Monitoring of Stay Cables". Journal of Bridge Engineering, 18(2), 109-117.
20. Hjartason, I. (2019) Jarðskjálftavarnir fyrir stagbrú á Ölfusá við Efri Laugardælaeyju. MS thesis, University of Iceland, https://skemman.is/handle/1946/32539.
21. *Icelandic weather records. Icelandic Met Office (in Icelandic). Retrieved 2017-03-20.*

22. Jami, M., Rupakhety, R., Bessason, B., & Snæbjörnsson, J. T. (2023). Multimode Vibration Control Strategies of Long-Span Bridges Subjected to Multi-hazard: A Case Study of the Runyang Suspension Bridge. Journal of Vibration Engineering & Technologies, 1-14.
23. Jami, M., Rupakhety, R., Elias, S., Bessason, B., & Snæbjörnsson, J. T. (2022). Recent Advancement in Assessment and Control of Structures under Multi-Hazard. Applied Sciences, 12(10), 5118.
24. Kaimal, J. C., Wyngaard, J. C. J., Izumi, Y., & Coté, O. R. (1972). Spectral characteristics of surface-layer turbulence. Quarterly Journal of the Royal Meteorological Society, 98(417), 563-589.
25. Kohrangi, M., Vamvatsikos, D., & Bazzurro, P. (2019). Pulse-like versus non-pulse-like ground motion records: Spectral shape comparisons and record selection strategies. Earthquake Engineering & Structural Dynamics, 48(1), 46-64.
26. Kong, M. S., Ka, H., Son, S. H., & Yhim, S. S. (2006). Damage Detection in Cable-Stayed Bridges Using Vibration Modes. Journal of the Korea institute for structural maintenance and inspection, 10(6), 113-123.
27. Kumarasena, S., Jones, N. P., Irwin, P., & Taylor, P. (2007). Wind-induced vibration of stay cables (No. FHWA-RD-05-083).
28. Kwasniewski, L., & Chandrasekaran, S. (2015). "Advanced Computational Models for Bridge Assessment Under Combined Hazards" in Computational Structural Engineering: Recent Developments and Applications. Springer.Lee, D. J. (1994). Bridge bearings and expansion joints. CRC Press.
29. Li, D., Ou, J., Lan, C., & Li, H. (2012). Monitoring and failure analysis of corroded bridge cables under fatigue loading using acoustic emission sensors. Sensors, 12(4), 3901-3915.
30. Li, H. N., & Ou, J. P. (2009). "Innovative Seismic Design of Cable-Stayed Bridges". Earthquake Engineering and Engineering Vibration, 8(1), 87-98.
31. Li, S., Dezfuli, F. H., Wang, J. Q., & Alam, M. S. (2018). Longitudinal seismic response control of long-span cable-stayed bridges using shape memory alloy wire-based lead rubber bearings under near-fault records. Journal of Intelligent Material Systems and Structures, 29(5), 703-728.
32. Li, S., Zhang, F., Wang, J. Q., Alam, M. S., & Zhang, J. (2017). Seismic responses of super-span cable-stayed bridges induced by ground motions in different sites relative to fault rupture considering soil-structure interaction. Soil Dynamics and Earthquake Engineering, 101, 295-310.
33. Markogiannaki, O. (2019). Climate change and natural hazard risk assessment framework for coastal cable-stayed bridges. Frontiers in built environment, 5, 116.
34. Martin, J., Alipour, A., & Sarkar, P. (2019). Fragility surfaces for multi-hazard analysis of suspension bridges under earthquakes and microbursts. Engineering Structures, 197, 109169.
35. Mavroeidis, G. P., & Papageorgiou, A. S. (2003). A mathematical representation of near-fault ground motions. Bulletin of the seismological society of America, 93(3), 1099-1131.
36. Mavroeidis, G. P., & Papageorgiou, A. S. (2003). A mathematical representation of near-fault ground motions. *Bulletin of the seismological society of America*, *93*(3), 1099-1131.
37. Oliveira Pedro, J. J., & Reis, A. J. (2016, March). Composite cable-stayed bridges: state of the art. In *Proceedings of the Institution of Civil Engineers-Bridge Engineering* (Vol. 169, No. 1, pp. 13-38). Thomas Telford Ltd.
38. OpenSeesWiki, https://opensees.berkeley.edu/wiki/index.php/Command_Manual
39. Panella, D. S., Tornello, M. E., & Frau, C. D. (2017). A simple and intuitive procedure to identify pulse-like ground motions. Soil Dynamics and Earthquake Engineering, 94, 234-243.
40. Pang, B., & Li, J. (2015). "Multi-Hazard Risk Assessment of Cable-Stayed Bridges Using Bayesian Networks". Structural Safety, 55, 12-23.
41. Pedro, J. J. O., & Reis, A. J. (2016). Simplified assessment of cable-stayed bridges buckling stability. *Engineering Structures*, *114*, 93-103.
42. Quaranta, G., & Mollaioli, F. (2019). Analysis of near-fault pulse-like seismic signals through Variational Mode Decomposition technique. Engineering Structures, 193, 121-135.

43. Rupakhety R, Sigbjörnsson R. Three-dimensional characteristics of strong-ground motion in the near-fault area. In Proceedings of the Second European Conference on Earthquake Engineering and Seismology 2014 Aug (pp. 25-29).
44. Rupakhety R, Sigurdsson SU, Papageorgiou AS, Sigbjörnsson R. (2011). Quantification of ground-motion parameters and response spectra in the near-fault region. Bulletin of Earthquake Engineering. 9(4):893-930.
45. Rupakhety, R., & Sigbjörnsson, R. (2011). Can simple pulses adequately represent near-fault ground motions? Journal of Earthquake Engineering, 15(8), 1260-1272.
46. Rupakhety, R., Sigurðsson, S. U., & Sigbjörnsson, R. (2012). Response spectral model for forward-directivity ground motion in the near-fault area. In 15th World Conference on Earthquake Engineering, Lisbon.
47. Shinozuka, M., & Deodatis, G. (1991). Simulation of stochastic processes by spectral representation.
48. Sigbjörnsson, R., Rupakhety, R., Halldórsson, B., & Snæbjörnsson, J. T. (2014). On the modelling of incoherence of strong-motion: a study of the May 2008 Ölfus earthquake. In Proceedings of the second European conference on earthquake engineering and seismology, Istanbul.
49. Sigurðsson, G. Ö., Rupakhety, R., Rahimi, S. E., & Olafsson, S. (2020). Effect of pulse-like near-fault ground motions on utility-scale land-based wind turbines. *Bulletin of Earthquake Engineering*, *18*, 953-968.
50. Soyluk, K., & Karaca, H. (2017). Near-fault and far-fault ground motion effects on cable-supported bridges. Procedia engineering, 199, 3077-3082.
51. Tochaei, E. N., Taylor, T., & Ansari, F. (2020). Effects of near-field ground motions and soil-structure interaction on dynamic response of a cable-stayed bridge. Soil Dynamics and Earthquake Engineering, 133, 106115.
52. Troitsky, M. S. (1988). Cable-stayed bridges: theory and design.
53. Turkington, D. H., Cooke, N., Moss, P. J., & Carr, A. J. (1989). Development of a design procedure for bridges on lead-rubber bearings. Engineering Structures, 11(1), 2-8.
54. Wang, H., Tao, T., Gao, Y., & Xu, F. (2018). Measurement of wind effects on a kilometer-level cable-stayed bridge during Typhoon Haikui. Journal of Structural Engineering, 144(9), 04018142.
55. Wang, X., Zhu, B., & Cui, S. (2017). Research on collapse process of cable-stayed bridges under strong seismic excitations. Shock and Vibration, 2017.
56. Wu, Z., & Wang, T. (2018). "Fatigue Reliability Assessment of Steel Cables in Cable-Stayed Bridges Considering Environmental Effects". Engineering Structures, 156, 365-373.
57. Xie, L., Xu, L., & Adrian, R. M. (2005). Representation of near-fault pulse-type ground motions. Earthquake Engineering and Engineering Vibration, 4(2), 191-199.
58. Xie, L., Xu, L., & Adrian, R. M. (2005). Representation of near-fault pulse-type ground motions. Earthquake Engineering and Engineering Vibration, 4(2), 191-199.
59. Xie, W., & Sun, L. (2021). Assessment and mitigation on near-fault earthquake wave effects on seismic responses and pile-soil interactions of soil-pile-bridge model. Soil Dynamics and Earthquake Engineering, 143, 106596.
60. Xu, Y. L., & Xia, Y. (2012). Structural Health Monitoring of Long-Span Suspension Bridges. Spon Press.
61. Yi, J. (2023). Modeling and analysis of cable vibrations in cable-stayed bridges under near-fault ground motions. Engineering Structures, 277, 115443.
62. Yin, S. H., & Tang, C. Y. (2011). Identifying cable tension loss and deck damage in a cable-stayed bridge using a moving vehicle.
63. Yu, H., & Wilamowski, B. M. (2018). Levenberg–marquardt training. In Intelligent systems (pp. 12-1). CRC Press.
64. Zahrai, S. M., & Froozanfar, M. (2019). Performance of passive and active MTMDs in seismic response of Ahvaz cable-stayed bridge. Smart Structures Syst, 23(5), 449-466.
65. Zhang, J., & Huo, Y. (2009). Evaluating effectiveness and optimum design of isolation devices for highway bridges using the fragility function method. Engineering Structures, 31(8), 1648-1660.

66. Zhou, Y., & Chen, Y. (2012). "Probabilistic Multi-Hazard Risk Assessment Framework for Highway Bridges". Journal of Risk and Uncertainty in Engineering Systems, Part A: Civil Engineering, 24(3), 150-160.

Appendix A

Seismological parameters of the 106 near-fault pulse-like ground motions considered in this study.

Location	Date	Mw	Station	Component	PGV (cm/s2)	EpiD (km)	Tp
San Fernando, CA, USA	09 February 1971	6.61	PCD	SN	116.5	11.9	1.47
Coyote lake, CA, USA	08 June 1979	5.74	GA6	SN	51.5	4.4	1.06
Imperial Valley, CA, USA	15 October 1979	6.53	Aeroporto Mexicalli	SN	44.3	2.5	1.85
Imperial Valley, CA, USA	15 October 1979	6.53	Agrarias	SN	54.4	2.6	2.37
Imperial Valley, CA, USA	15 October 1979	6.53	Brawley airport	SN	36.12	43.2	3.78
Imperial Valley, CA, USA	15 October 1979	6.53	EC county center FF	SN	54.5	29.1	4.50
Imperial Valley, CA, USA	15 October 1979	6.53	EC Meloland Overpass FF	SN	115	19.4	2.90
Imperial Valley, CA, USA	15 October 1979	6.53	E10	SN	46.9	26.3	4.20
Imperial Valley, CA, USA	15 October 1979	6.53	E0 3	SN	41.1	28.7	4.50
Imperial Valley, CA, USA	15 October 1979	6.53	E04	SN	77.9	27.1	4.32
Imperial Valley, CA, USA	15 October 1979	6.53	E05	SN	91.5	27.8	4.10
Imperial Valley, CA, USA	15 October 1979	6.53	E06	SN	111.9	27.5	4.00
Imperial Valley, CA, USA	15 October 1979	6.53	E07	SN	108.9	27.6	4.20
Imperial Valley, CA, USA	15 October 1979	6.53	E08	SN	48.5	28.1	4.00
Imperial Valley, CA, USA	15 October 1979	6.53	El Centro Differential Array	SN	59.6	27.2	3.85
Imperial Valley, CA, USA	15 October 1979	6.53	Holtville Post Office	SN	55.2	19.8	3.90
Mammoth Lake-06	25 May 1980	5.94	Long Valley Dam (Upper L Abut)	SN	33.1	14.0	1.07
Irpinia, Italy-01	23 November 1980	6.9	Sturno	SN	41.5	30.4	2.70
Westmorland	26 April 1981	5.9	Parachute test site	SN	35.8	20.5	2.70
Coalinga-05	22 July 1983	5.77	Oil City	SN	41.2	4.6	0.57
Coalinga-05	22 July 1983	5.77	Transmitter hill	SN	46.1	6.0	0.74
Coalinga-07	25 July 1983	5.21	Coalinga 14th & Elm (Old CHP)	SN	36.1	9.6	0.42
Morgan Hill, CA, USA	24 April 1984	6.19	Gilroy Array # 6	SN	35.4	36.3	1.05
Taiwan SMART1 (40)	20 May 1986	6.3	SMART1 C00	SN	31.2	68.2	1.42
Taiwan SMART1 (40)	20 May 1986	6.3	SMART1 M07	SN	36.1	67.2	1.40
Palm Springs, CA, USA	08 July 1986	6.06	NPS	SN	73.64	10.6	1.35
San Salvador	10 October 1986	5.8	Geotech Investigation center	SN	62.3	7.9	0.80
Whittier Narrows, CA, USA	10 October 1987	5.99	DOW	SN	30.4	16.0	0.80
Whittier Narrows, CA, USA	10 October 1987	5.99	LB Orange Eve	SN	32.9	20.7	0.82
Superstition Hills, CA, USA	24 November 1987	6.54	PTS	SN	106.8	16.0	2.38
Loma Prieta, CA, USA	17 October 1989	6.93	Alameda Naval Air Stn Hanger	SN	32.2	90.8	1.90
Loma Prieta, CA, USA	17 October 1989	6.93	Gilroy Array #2	SN	45.7	29.8	1.74
Loma Prieta, CA, USA	17 October 1989	6.93	Oakland Outer Harbor Wharf	SN	49.9	94.0	1.84
Erzincan, Turkey	13 March 1992	6.69	ERZ	SN	95.4	9.0	2.40
Cape Mendocino	25 April 1992	7	Petrolia	SN	82.1	4.5	3.10
Landers, CA, USA	28 June 1992	7.28	LUC	SN	140	44.0	6.50
Landers, CA, USA	28 June 1992	7.28	Yermo Fire Station	SN	53.2	86.0	6.70
Northridge, CA, USA	17 January 1994	6.7	JFA	SN	67.42	13.0	3.00
Northridge, CA, USA	17 January 1994	6.7	JFA generator	SN	67.4	13.0	3.00
Northridge, CA, USA	17 January 1994	6.7	LA Wadsworth VA hospital North	SN	32.4	19.6	2.50

Northridge, CA, USA	17 January 1994	6.7	LA Dam (LDW)	SN	75.21	11.8	1.75
Northridge, CA, USA	17 January 1994	6.7	NWS	SN	87.75	21.6	2.92
Northridge, CA, USA	17 January 1994	6.7	Pacoima dam (upper left)	SN	107.1	20.4	0.95
Northridge, CA, USA	17 January 1994	6.7	RRS	SN	167.2	10.9	1.35
Northridge, CA, USA	17 January 1994	6.7	SCG	SN	130.3	13.1	3.00
Northridge, CA, USA	17 January 1994	6.7	SCH	SN	116.6	13.6	3.12
Northridge, CA, USA	17 January 1994	6.7	Sylmar Olive View Medical FF	SN	122.7	16.8	2.23
Kobe, Japan	19 January 1995	6.9	Takarazuka	SN	72.6	38.6	1.73
Chi-Chi, Taiwan	20 September 1999	7.6	CHY006	SN	66.4	40.5	2.40
Chi-Chi, Taiwan	20 September 1999	7.6	TCU031	SN	59.8	80.1	5.00
Chi-Chi, Taiwan	20 September 1999	7.6	TCU036	SN	62.3	67.8	5.50
Chi-Chi, Taiwan	20 September 1999	7.6	TCU038	SN	50.9	73.1	7.50
Chi-Chi, Taiwan	20 September 1999	7.6	TCU040	SN	53.2	69.0	6.00
Chi-Chi, Taiwan	20 September 1999	7.6	TCU042	SN	47.5	78.4	7.00
Chi-Chi, Taiwan	20 September 1999	7.6	TCU046	SN	44.33	68.9	7.40
Chi-Chi, Taiwan	20 September 1999	7.6	TCU049	SN	45.1	38.9	10.50
Chi-Chi, Taiwan	20 September 1999	7.6	TCU053	SN	41.9	41.2	12.00
Chi-Chi, Taiwan	20 September 1999	7.6	TCU054	SN	61.2	37.6	8.00
Chi-Chi, Taiwan	20 September 1999	7.6	TCU065	SN	127.8	26.7	5.00
Chi-Chi, Taiwan	20 September 1999	7.6	TCU075	SN	88.3	20.7	5.60
Chi-Chi, Taiwan	20 September 1999	7.6	TCU076	SN	63.7	16.0	4.10
Chi-Chi, Taiwan	20 September 1999	7.6	TCU082	SN	56.4	36.2	8.00
Chi-Chi, Taiwan	20 September 1999	7.6	TCU103	SN	62.5	52.4	7.90
Chi-Chi, Taiwan	20 September 1999	7.6	TCU128	SN	78.3	63.3	5.80
Yountville	03 September 2000	5	Napa Fire Station #3	SN	42.93	9.9	0.70
Chi-Chi, Taiwan aftershock	20 September 1999	6.2	CHY024	SN	33.1	25.5	3.00
Chi-Chi, Taiwan aftershock	20 September 1999	6.2	CHY080	SN	70.31	29.5	1.18
Chi-Chi, Taiwan aftershock	20 September 1999	6.2	TCU076	SN	58.9	20.8	1.02
Chi-Chi, Taiwan aftershock	25 September 1999	6.3	CHY101	SN	36.4	50.0	2.45
Parkfield, CA, USA	27 June 1966	6.19	CO2	SN	75.1	31.0	2.20
Gazli, USSR	17 March 1976	6.80	KAR	SN	65.3	12.8	4.20
Bucharest, Romania	04 March 1977	7.27	BRI	Rad	73.9	NA	2.00
Tabas, Iran	16 September 1978	7.11	TAB	SP	117.7	55.2	5.38
Mexicalli Valley, Mexico	09 June 1980	6.33	VCT	SN	76.9	11.8	3.72
Morgan Hill, CA, USA	24 April 1984	6.19	HAL	SN	39.7	3.9	0.87
Palm Springs, CA, USA	08 July 1986	6.06	DSP	SN	29.7	10.4	1.74
Superstition Hills, CA, USA	24 November 1987	6.54	ELC	SN	52.0	35.8	2.40
Loma Prieta, CA, USA	17 October 1989	6.93	LGP	SN	103.2	18.5	2.60
Loma Prieta, CA, USA	17 October 1989	6.93	STG	SN	57.2	27.2	4.90

Sierra Madre, CA, USA	28 June 1991	5.56	COG	Rad (filt)	10.6	NA	1.20
Izmit, Tukey	17 August 1999	7.51	ARC	SN	44.3	53.7	7.14
Izmit, Tukey	17 August 1999	7.51	SKR	SP	80.4	33.2	9.52
Izmit, Tukey	17 August 1999	7.51	GBZ	SN	41.4	47.0	4.76
Izmit, Tukey	17 August 1999	7.51	GBZ	SP	27.7	47.0	6.10
Chi-Chi, Taiwan	20 September 1999	7.60	TCU052	SN	220.0	39.6	14.00
Chi-Chi, Taiwan	20 September 1999	7.60	TCU068	SN	294.2	47.9	12.00
Chi-Chi, Taiwan	20 September 1999	7.60	TCU129	SN	71.5	14.2	7.70
South Iceland	17 June 2000	6.57	Flagbjarnarholt	SN	72.2	5.3	2.20
South Iceland	21 June 2000	6.49	Thorsarbru	SN	79.7	5.3	1.80
South Iceland	21 June 2000	6.49	Thorsartun	SN	65.8	5.6	1.73
South Iceland	21 June 2000	6.49	Solheimar	SN	98.9	11.0	1.73
Ölfus, South Iceland	25 May 2008	6.30	EERC, Basement	SN	41.1	8.0	1.23
Ölfus, South Iceland	25 May 2008	6.30	Selfoss City Hall	SN	33.0	8.0	1.58
Ölfus, South Iceland	25 May 2008	6.30	Hveragerdi Retirement House	SN	54.0	3.0	2.00
L'Aquila, Italy	06 April 2009	6.30	AQK	SN	46.7	4.0	1.74
Parkfield, CA, USA	28 September 2004	6.00	Parkfield fault zone 12	SN	57.5	11.1	1.23
Parkfield, CA, USA	28 September 2004	6.00	Parkfield Cholame 2 west	SN	50.0	11.5	1.28
Parkfield, CA, USA	28 September 2004	6.00	Parkfield Cholame 2 east	SN	23.7	11.6	1.15
Parkfield, CA, USA	28 September 2004	6.00	Parkfield fault zone 1	SN	64.2	8.4	1.29
Parkfield, CA, USA	28 September 2004	6.00	Parkfield Cholame 3 west	SN	45.0	11.9	1.03
Parkfield, CA, USA	28 September 2004	6.00	Parkfield Cholame 4 west	SN	38.4	12.4	0.82
Parkfield, CA, USA	28 September 2004	6.00	Parkfield Cholame 4A west	SN	22.2	13.0	1.22
Parkfield, CA, USA	28 September 2004	6.00	Parkfield Stone Corral 1 east	SN	45.0	7.2	0.74
Parkfield, CA, USA	28 September 2004	6.00	Parkfield fault zone 9	SN	26.1	10.0	1.28
Parkfield, CA, USA	28 September 2004	6.00	Parkfield Cholame 3 east	SN	34.5	11.9	0.50
Parkfield, CA, USA	28 September 2004	6.00	Parkfield Cholame 1 east	SN	52.8	11.6	1.25